Role of *Mitf in* melanocyte development as determined by a conditional hypomorphic mutation

Romain Lasseur

Thesis for the degree of Philosophiae Doctor

April 2024

School of Health Sciences

FACULTY OF MEDICINE

UNIVERSITY OF ICELAND

Role of *Mitf in* melanocyte development as determined by a conditional hypomorphic mutation

Romain Lasseur

Thesis for the degree of Philosophiae Doctor

Supervisor

Eiríkur Steingrímsson, PhD

Doctoral committee

Margrét Helga Ögmundsdóttir, PhD
Guðrún Valdimarsdóttir, PhD
Lionel Larue, PhD
Pétur Henry Petersen, PhD

April 2024

School of Health Sciences

FACULTY OF MEDICINE

UNIVERSITY OF ICELAND

Áhrif skilyrtrar stökkbreytingar í *Mitf* geni músar á þroskun og starfsemi litfruma

Romain Lasseur

Ritgerð til doktorsgráðu

Leiðbeinandi

Eiríkur Steingrímsson, PhD

Doktorsnefnd

Margrét Helga Ögmundsdóttir, PhD
Guðrún Valdimarsdóttir, PhD
Lionel Larue, PhD
Pétur Henry Petersen, PhD

Apríl 2024

Heilbrigðisvísindasvið

LÆKNADEILD

HÁSKÓLI ÍSLANDS

Thesis for a doctoral degree at the University of Iceland. All right reserved. No part of this publication may be reproduced in any form without the prior permission of the copyright holder.

© Romain Lasseur 2024

ISBN 978-9935-9732-5-2

ORCID: 0000-0003-0729-4841

Reykjavik, Iceland 2024

Ágrip

Litfrumur eru meðal frumugerða sem eiga uppruna sinn í taugakambi snemma í þroskun hryggdýra. Forverafrumur litfruma, sem nefnast melanoblast-frumur, myndast í taugakambi en fjölga sér áður en þær ferðast til að þekja allt yfirborð húðarinnar. Þessar frumur fara inn í þekju húðarinnar áður en hinar eiginlegu litfrumur verða til og hefja myndun litarefnis. Í músum enda flestar litfrumur í hársekknum þar sem þær flytja litarefni í hárið. Þetta flókna ferli kallar á ýmis stjórnprótein og umritunarþætti. Einn mikilvægasti umritunarþátturinn í litfrumum er MITF eða *Microphthalmia-associated Transcription Factor* en hann er nauðsynlegur fyrir frumufjölgun, lifun og frumufar í myndun litfruma. Hlutverk *Mitf* hefur einkum verið rannsakað í sortuæxlisfrumum en þótt þær eigi uppruna sinn í litfrumum hafa frumurnar breyst við æxlismyndunina og því ekki ljóst að hið sama eigi við í litfrumunum eða forverum þeirra. Stökkbreytingar í *Mitf* geni músa leiða oftast til þess að litfrumurnar og forvera þeirra vantar alveg og því hefur reynst erfitt að skilgreina *in vivo* hlutverk gensins í hinum ýmsu skrefum litfrumuþroskunar.

Hér lýsum við skilyrtri stökkbreytingu í *Mitf* geni músar þar sem táknanum fyrir amínósýru 243 er breytt úr lýsin í arginín. Þegar þessi breyting var kölluð fram í litfrumum urðu einungis til mýs með mislit svæði þar sem skiptust á svört, grá og hvít svæði. Þrátt fyrir $Mitf^{K243R}$ stökkbreytinguna hafa einhverjar starfhæfar litfrumur orðið til (svört svæði), einhverjar eru vanstarfhæfar (grá svæði) og enn aðrar eru óstarfhæfar eða vantar alveg (hvít svæði). Með því að rekja litfrumurnar í þroskun sýndum við að mun færri litfrumur verða til og íferð þeirra inn í þekjuna gerist sjaldnar. Frumulínur voru útbúnar úr litfrumum músanna og notaðar til að skoða áhrif stökkbreytingarinnar *in vitro*. Niðurstöðurnar sýna að þegar $Mitf^{K243R}$ stökkbreytingin er virkjuð í frumulínunum fækkar frumuskiptingum og lifun frumanna minnkar. Raðgreining RNA sameinda sýndi að stökkbreytingin hefur sértæk áhrif á tjáningu markgena og að þau áhrif útskýra að hluta áhrif stökkbreytingarinnar á þroskun litfruma.

Lykilorð:

MITF, litfrumur, þroskun, tíglun, stjórnun umritunar

Abstract

Establishment of melanocytes, the pigment-producing cells, starts from the multipotent neural crest cells. Melanoblasts, the melanocyte precursor cells, follow a tight schedule during their development requiring proliferation, migration, and invasion of the epidermis before they form the pigment producing melanocytes. In the mouse, most melanocytes localize to the hair bulb where they deliver melanin to the hair, which gives mice their coat color. As melanocyte development is complex, this process involves many regulatory proteins and transcription factors. *Microphthalmia-associated Transcription Factor* (*Mitf*) is required for proliferation, survival and migration during the formation of melanocytes, and has therefore been suggested as the key regulator of their development. The role of *Mitf* has been largely studied in melanoma cells, but little is known about its role in the generation of the melanocytes. In mice, mutations in *Mitf* lead in most cases to the absence of melanocytes, making it difficult to observe melanoblasts during the development in *vivo*. We have generated an inducible mutation in MITF in the mouse by changing lysine in position 243 into an arginine. We induced this mutation in melanocytes resulting in mice with alternating areas of black, grey and white areas. This means that despite the $Mitf^{K243R}$ mutation, some melanocytes have grown, migrated and differentiated, while others did not (hypomorphic phenotype), displaying heterogeneity for the fate of melanocytes during development upon the $Mitf^{K243R}$ mutation. We found that in these mice, fewer melanoblasts develop and they are not able to invade the epidermis to reach the hair follicle. We generated melanocyte primary cell lines from the mice and used those to perform *in vitro* studies. The results revealed that upon activation of the $Mitf^{K243R}$ mutation, the cells exhibited reduced proliferation and survival. RNAseq analysis revealed genes that are differentially regulated by MITF upon induction of the $Mitf^{K243R}$ mutation that might explain how this conditional mutation dysregulates the development of melanocytes.

Keywords:

MITF, melanocyte, development, mosaicism, transcription regulation

Acknowledgements

"Our greatest glory is, not in never falling, but in rising every time we fall."

Confucius

This sentence by the Chinese philosopher sum up all the gratitude and thankfulness I feel towards my supervisor Prof. Eiríkur Steingrímsson, my colleagues and friends, and my family, who all were of a priceless help for me to rise again after this long and tough journey this Ph.D has been.

It started thanks to an unbelievable scientist, Prof. Eiríkur Steingrímsson, who has introduced me into real and beautiful science, and then supported and guided me throughout my project. He has been incredibly patient, attentive, always providing me with the best advice, and sharing his invaluable knowledge and expertise. I would like to particularly thank him for the faithful support, especially in the tough moments when everything seems to be over, and for his unbelievable patience with a student like me. No other supervisor would have been better than how he has been, and I feel lucky that I have been part of his lab. I want to thank him particularly for all the help he provided me during this Ph.D and help me grow as a scientist. The MITF and melanocyte community also lucky to have someone like him to make things moving in the field.

I would also like to thank the members of my Ph.D committee for being part of the project by assisting me with their knowledge and advice, that have been more than valuable in many ways. Thanks to you, I have been able to get different point of view, ideas and directions to follow. This has provided valuable tools for my advancement and that I benefited a lot from. I would like to particularly thank Prof. Lionel Larue for his great help, resources and time that he has been involved in this project, but also for his innumerable but always on-target comments which have been more than helpful. Profs. Margrét Helga Ögmundsdóttir, Guðrún Valdimarsdóttir, and Pétur Henry Petersen, thank you so much for your substantial input!

Many people from the Department of Biochemistry and Molecular Biology at the BioMedical Center of the University of Iceland in Reykjavik, have been incredibly helpful. I would like to thank especially Dr. Sara Sigurbjörnsdóttir, Berglind Ósk Einarsdóttir and Adrian de Lomana, who are all incredible scientists and kind persons.

I am also grateful to the people who founded and run the animal facility ArcticLAS for their advice, help and support for all the mouse work I had to do. Bergþóra Eiríksdóttir and Þóra Dagbjartsdóttir, thank you so much for everything.

This journey would also not have been the same without all the people I got to meet and known throughout these years, with a special thanks to Thejus, Nhung, Abbi, Teitur, Sara, Tinna, Clem, Kristrún and Marta, Evangeline, Kevin, Laura, Maria, Eyvindur, Halla, Clara, Fatich, Hilmar, Valerie, Marie, Marjorie, Matti, Máney, Parinaz, and all the others. Thank you so much for being nice persons and helpful at any time.

I would like to thank my family for being my support, including my parents, my grandparents, my sisters. Thanks for asking me about what I am doing even though you are not really interested in it, you were always there for me.

Thanks also to all my friends in France: Loris, Romain, Sam, Tanguy, Mathieu, Julien et bien-sûr mon Petibon, merci for being the incredible friends you are.

Finally, to my incredible wife Mathilde, and to my two lovely children Lyra and Nino, thanks for being in my life and being besides me, giving me all the strength and the love.

Je vous aime.

The day I started this PhD, I did not know how, almost five years, a COVID pandemic, after becoming a husband and a father, I would have changed so much as a human being and as a scientist. To all the persons that have been part of my life during these many years, thanks for being here, I hope that I brought the same light you brought to me in my life.

Romain.

Contents

Ágrip ..... **iii**
Abstract ..... **v**
Acknowledgements ..... **vii**
Contents ..... **ix**
List of Abbreviations ..... **xii**
List of Figures ..... **xv**
List of Tables ..... **xvii**
Declaration of Contribution ..... **xviii**
1 Introduction **1**
1.1 Development and biology of melanocytes 1
1.1.1 From neural crest cells to melanoblasts 1
1.1.2 Migration of melanoblasts 2
1.1.3 Invasion of the epidermis 3
1.1.4 Localization of melanocytes 4
1.1.5 Hair follicle 5
1.1.6 Hair cycle 5
1.1.7 Hair renewal 6
1.2 Signaling pathways involved in melanocyte development 8
1.2.1 G-protein-couple receptor pathways 8
1.2.2 Single-pass receptors 9
1.2.3 Transcription factors downstream of RTKs signaling 11
1.3 Phenotypes associated with defective melanocytes 12
1.3.1 Albinism and white spotting 12
1.3.2 Progressive graying (mouse vitiligo) 13
1.3.3 White spotting mouse models 14
1.3.4 Pigmentary mosaicism 15
1.4 *Microphthalmia-associated Transcription Factor* 17
1.4.1 Isoforms and Post-Translational Modifications of MITF 18
1.4.2 *Mitf* mutations in humans 19
1.4.3 *Mitf* mutations in mice 19

1.4.4 Role of MITF 22
1.4.5 Melanoma and MITF 23
1.4.6 Role of *Mitf* during development 25
1.4.7 Regulation of *Mitf* expression 26
1.5 Acetylation and *Mitf*^{K243R} mutation 27
2 Aims 29
2.1 Characterization of an inducible *Mitf*^{K243R} mutant mouse model 29
2.2 Effects of the *Mitf*^{K243R} mutation in primary melanocyte cell lines *in vitro* ... 29
3 Materials and Methods 31
3.1 Generation of mice carrying the *Mitf*^{K243R} mutation 31
3.2 Genotyping of the transgenic mice 31
3.3 Hair preparation 32
3.4 Quantification of the optical absorbance of melanin in mouse hairs 32
3.5 Whole mount β-galactosidase staining of embryos and melanoblast quantification 33
3.6 Cryopreservation and sectioning of embryos 33
3.7 Primary cell line generation and cell culture 34
3.8 Induction of the *Mitf*$^{K243R/K2432R}$ mutation 34
3.9 Sanger sequencing 35
3.10 Growth assay 35
3.11 Apoptosis assay 35
3.12 Immunostaining 36
3.13 Single cell migration assay 36
3.14 Transwell invasion assay 36
3.15 Flow cytometry 37
3.16 RNA extraction for sequencing 37
3.17 RNA sequencing analysis 38
4 Results 39
4.1 Characterization of the *Mitf*^{K243R} mutant mice 39
4.1.1 Generation of the constructs 39
4.1.2 Generation of the *Mitf*^{K243R} mouse 43
4.1.3 Generation of triple transgenic mice also carrying the Dct::LacZ reporter 44
4.1.4 *Mitf*^{K243R} mice have altered coat color 47
4.1.5 Genotyping strategy of the *Mitf*^{K243R} mutant mice 48
4.1.6 Characterization of hair from the differently pigmented areas 50

4.1.7 Effects of the *Mitf*^{K243R} mutation on melanocyte development 53
4.1.8 Generation of the 4-OHT inducible *Mitf*$^{K243R/K243R}$ mutation mouse strain 60
4.2 Effects of the *Mitf*$^{K243R/K243R}$ mutation in *vitro* 63
4.2.1 Generation of the primary melanocyte cell lines 63
4.2.2 Induction of the *Mitf*^{K243R} mutation in the cell lines 65
4.2.3 Phenotypic characterization of the *Mitf*^{K243R} mutant cell lines 65
4.2.4 Effects of the *Mitf*^{K243R} mutation on gene expression 80
5 Discussion and conclusion 97
5.1 Effects of the *Mitf*^{K243R} mutation *in vivo* 97
5.1.1 The *Mitf*^{K243R} mutant phenotype affects melanoblast development 98
5.1.2 Timing of the induction of the *Mitf*^{K243R} mutation creates the coat color pattern 100
5.2 Effects of the *Mitf*^{K243R} mutation in *vitro* 102
5.2.1 The *Mitf*^{K243R} mutation has a strong effect on the phenotype of the *Mitf*^{K243R} mutant cells 102
5.2.2 The *Mitf*^{K243R} mutation affects gene expression 104
References 109
Appendix A 131

List of Abbreviations

4-OHT	4-Hydroxytamoxifen
7-AAD	7-aminoactinomycin D
ADAMTS20	ADAM Metallopeptidase With Thrombospondin Type 1 Motif 20
ASP	Agouti signal protein
ATF4	Activating transcription factor 4
BCL2	B-cell leukemia/lymphoma 2 protein
BIRC7	Baculoviral IAP Repeat Containing 7
BMP	Bone morphogenetic protein
BRAF	V-raf murine sarcoma viral oncogene homolog B1
POU3F2	POU Class 3 Homeobox 2
cAMP	Cyclic adenosine monophosphate
CREBBP	CREB binding protein
CCND1	Cyclin D1
CDK2	Cyclin-dependent kinase 2
CDKN2A	Cyclin Dependent Kinase Inhibitor 2A
cPM	Conditional point mutation
CREB1	CAMP responsive element binding protein 1
DCT	Dopachrome Tautomerase
DEG	Differentially expressed genes
DLL	Delta-like
DNA	Deoxyribonucleic acid
Dom	*Dominant megacolon*
ECM	Extra cellular matrix
EDN3	Endothelin 3
EDNRB	Endothelin receptor type B
EMT	Epithemlial-to-mesenchymal transition
ERG	Electro retinography
ERK	Extracellular signal-regulated kinase
FGF	Fibroblast growth factor
FOXD3	Forkhead Box D3
FSC	Forward scattered
FZD	Frizzled
GLI2	Glioma associated oncogene family member 2

GO	Gene ontology
GPR143	G protein-coupled receptor 143
GWAS	Genome wide associated study
HAT	Histone acetyltransferase
HES1	Hairy/enhancer of split 1
HGF	Hepatocyte growth factor
ID2	Inhibitor Of DNA Binding 2
ID3	Inhibitor Of DNA Binding 3
LEF1	Lymphoid enhancer-binding factor 1
Ls	*Lethal spotting*
MAPK	Mitogen-activated protein kinase
MAX	Myc-associated factor X
MC1R	Melanocortin 1 receptor
MCOLN3	Mucolipin TRP Cation Channel 3
mi	*microphthalmia*
mi-OR	*Mi-Oak ridge*
MiT/TFE	Microphthalmia/transcription factor E
MITF	Microphthalmia-associated transcrition factor
mi-vit	*Mi-Vitiligo*
Mi-Wh	*Mi-White*
MLANA	Melanoma antigen recognized by T cells 1
MSA	Migration staging area
MSC	Melanocyte stem cell
MSH	Melanocyte-stimulating hormone
NCC	Neural crest cells
NF1	Neurofibromin 1
NOTCH	Neurogenic locus notch homolog protein 1
NRAS	Neuroblastoma ras viral oncogene homolog
OC-2	Onecut-2
OCT	Optimal cutting temperature
OCT	Optical coherence tomography
p53	Tumor protein 53
PAX3	Paired box 3
PCA	Principal component analysis
PCR	Polymerase chain reaction
PDGF	Platelet-derived growth factor
PFA	Paraformaldehyde
PI3K	Phosphoinositide 3-kinase
PKC	Protein kinase C

PM	Point mutation
PMEL	Premelanosome protein
PND	Post-natal day
PTM	Post translational modification
RNA	Ribonucleic Acid
RPE	Retinal pigment epithelial
RTK	Receptor tyrosine kinase
S	*Piebald*
Sl	*Steel*
SLC45A2	Solute carrier family 45 member 2
SNAI1	Snail family transcriptional repressor 1
SNAI2	Snail family transcriptional repressor 2
SNP	Single nucleotide polymorphism
SOX10	SRY-box transcription factor 10
SOX9	SRY-box transcription factor 9
SSC	Side scattered
TBX2	T-box transcription factor 2
TF	Transcription factor
TFE3	Transcription factor E3
TFEB	Transcription factor EB
TFEC	Transcription factor EC
tg	transgene
TGF-β	Transforming growth factor β
TPA	12-O-Tetradecanoylphorbol-13-acetate
TYR	Tyrosinase
TYRP-1	Tyrosinase related protein 1
USF	Upstream stimulatory factor
W	*White*
WNT	Wingless-related integration site
WS2A	Waardenburg syndrome type 2A
WT	Wild-type
ZEB2	Zinc finger E-box binding homeobox 2
β-cat	β-catenin

List of Figures

Figure 1. Model of development of neural crest and melanocytes to their final localization. 2

Figure 2. Role of MSC and melanocyte in the hair cycle. 4

Figure 3. Signaling pathways involved in melanocyte development. 7

Figure 4. MITF mouse isoforms.. 16

Figure 5. MITF rheostat model. 21

Figure 6. The *Mitf*^{K243} amino acid is highly conserved between bHLH transcription factor and species. 26

Figure 7. Knockout and transgenic constructs used in this work and the strategy of inducing the *Mitf*^{K243R} mutation *in vivo*. 40

Figure 8. Generation of the *Mitf*^{K243R} mutant mice *in vivo*.. 42

Figure 9. The Dct::LacZ transgene, principle and integration into the *Mitf*^{K243R} model. 44

Figure 10. The effects of the *Mitf*^{K243R} mutation on mouse phenotype. 46

Figure 11. Genotyping of the MitfK243R mutant mice and of the Tyr::Cre and Dct::LacZ transgenes. 49

Figure 12. Mouse hair from grey areas have less eumelanin and white areas none.. 52

Figure 13. The *Mitf*^{K243R} mutation reduces melanoblast numbers.. 55

Figure 14. Pattern of melanoblast distribution in *Mitf*^{K243R} mice at developmental stage E14.5. 57

Figure 15. The *Mitf*^{K243R} mutation affects invasion of melanoblast into the epidermis. 59

Figure 16. Generation of mice carrying the *Mitf*^{K243R} construct with Dct::LacZ and Tyr::CreER^{T2} transgenes. 62

Figure 17. Genetic construct and strategy of the conditional induction of the *Mitf*^{K243R} mutation in *vitro through the Tyr::CreER*^{T2} *system*. 63

Figure 18. *Mitf*^{K243R} mutant cells fail to grow. 67

Figure 19. *Mitf*^{K243R} mutant cell population stops to grow and start dying. 69

Figure 20. Cell cycle profiles of WT and *Mitf*^{K243R} mutated cells. 71

Figure 21. Quantification of cell cycle profiles exhibit a reduced number of *Mitf*^{K243R} mutant cells entering S-phase. 73

Figure 22. *Mitf*^{K243R} mutants cells die after 48h of 4-OHT treatment. 75

Figure 23. The *Mitf*^{K243R} mutation reduces the size of the nucleus of cell lines 4774 and 4775. 77

Figure 24. WT and *Mitf*^{K243R} mutant melanocytes show no difference in single-cell migration. 79

Figure 25. 4-OHT treatment affects gene expression. 82

Figure 26. Gene expression profile upon 4-OHT treatment. 84

Figure 27. GSEA profiles of the cell lines upon 4-OHT induction. 85

Figure 28. Gene expression profile upon 4-OHT treatment of the *Mitf*^{K243R} mutant cell lines with the DEGs of the WT MITF cell line removed. 86

Figure 29. GSEA profiles of the *Mitf*^{K243R} cell lines after removal of the effects of the 4-OHT treatment. 87

Figure 30. *Mitf*^{K243R} mutation changes expression of genes involved in WNT signaling pathway and transcription. 90

Figure 31. Many DEGs in the 3922 WT MITF cell line do not change expression in *Mitf*^{K243R} mutants. Volcano plots showing only the DEGs in the WT cell line that are not differentially expressed in the *Mitf*^{K243R} mutant cell lines (A) 4774, (B) 4775 and (C) 4776. 91

Figure 32. *Mitf*^{K243R} do not regulate cell cycle genes while WT MITF does. 93

Figure 33. Effects of the *Mitf*^{K243R} mutation on gene expression. 96

Figure 34. Model illustrating the timeline of establishment of melanocytes in WT MITF and *Mitf*^{K243R} mutant mice. 101

Figure 35. Montage of *Mitf*^{K243R} phenotype and WT MITF mice. 131

Figure 36. Genotyping strategy to separate Tyr::CreER^{T2} positive mice from Tyr::Cre. 132

Figure 37. Non-dying cells do not cycle normally. 133

Figure 38. Transwell invasion assay. 134

Figure 39. Quality control for the RNA sequencing. 135

List of Tables

Table 1: Primers used for PCR amplification of genomic DNA..... 32

Table 2. Primary melanocytes cell lines generated. * tg = transgene, ** = HG is Hilmar Gunnlaugsson, RL is Romain Lasseur. 64

Declaration of Contribution

The *Mitf*^{K243R} project presented here in this thesis is a continuation of work performed by my former colleagues Dr. Kristin Bergsteinsdóttir and Hilmar Gunnlaugsson. I took over this work and led it under the supervision and assistance of Prof. Eirikur Steingrímsson. I have been in charge of the animal husbandry and performed all the matings to generate the mouse strains for investigating the role of MITF during melanocyte development. This has involved mouse maintenance, genotyping, and all subsequent experiments. Hilmar Gunnlaugsson and Kristin Bergsteinsdóttir generated and characterized the E15.5 embryos whereas I generated and characterized the E13.5 and E14.5 embryos. Hilmar Gunnlaugsson created 14 of the primary melanocytes cell lines, and I created an additional 15. I performed all the phenotypic assays on the cell lines, extracted RNA from the cells, and prepared the samples for RNA-sequencing. Adrián López García de Lomana assisted me with the bioinformatics analysis of the RNA sequencing results. All figures and tables in this thesis were generated by me except Figures 2, 3 and 4.

1 Introduction

1.1 Development and biology of melanocytes

Pigmentation is one of the first traits we are looking at in the living world. Whether it is for plants or mushrooms and mainly for animals, pigmentation offers a wide spectrum of colors. For scientists, it is even more interesting than just the look because it is an accessible system to study, as a single mutation can be responsible for a big phenotypical change already visible to the naked eye. Moreover, despite being an important system in the living kingdom, lack of pigmentation is rarely lethal, thus allowing scientists to study pigmentary genetics and system extensively. In the case of mammals, the main responsible factor for pigmentation is the pigment melanin (red/yellow or black/brown), a molecule that can be delivered in the skin, hairs or eyes through melanosomes which results in the coloration of these systems. For example, Golden Retriever is a good example of a dog breed colored by the red/yellow pigment, when black cats are for pigmentation by the black pigment. But color phenotype does not only depend on the pigment produced, but also location, which results in color patterns, as for the tiger for example that produces yellow and black pigment making stripes. The cells responsible for the pigmentation are the pigment-producing cells called melanocytes.

1.1.1 From neural crest cells to melanoblasts

The journey to the establishment of mouse melanocytes starts at the very beginning of the formation of the neural tube during development (Figure 1A). The neural plate invaginates, giving rise to two ridges (called neural folds) on each side at embryonic day 7.5 (E7.5). When the neural tube closes at E8 of mouse development, a few cells will not take part in the formation of the neuroepithelium of the neural tube but will escape between these two structures and be called Neural Crest Cells (NCC). The NCCs will become highly migratory and will reach the Migration Staging Area (MSA) located between the neural tube, the somites, and the ectoderm (Figure 1B). Around stage E9, cells are multipotent but have already started expressing important NCC markers. Some NCCs start migrating between the neural tube and the somites, a path called the ventral pathway, (Henion and Weston, 1997). Those are considered to represent a neurogenic population of cells, such as neurons or glial cells. Later, other NCCs will migrate between the somites and the ectoderm in the dermis, a pathway known as the dorso-lateral pathway (Wehrle-Haller and Weston, 1995). These cells will give rise to the melanocyte precursor cells called melanoblasts.

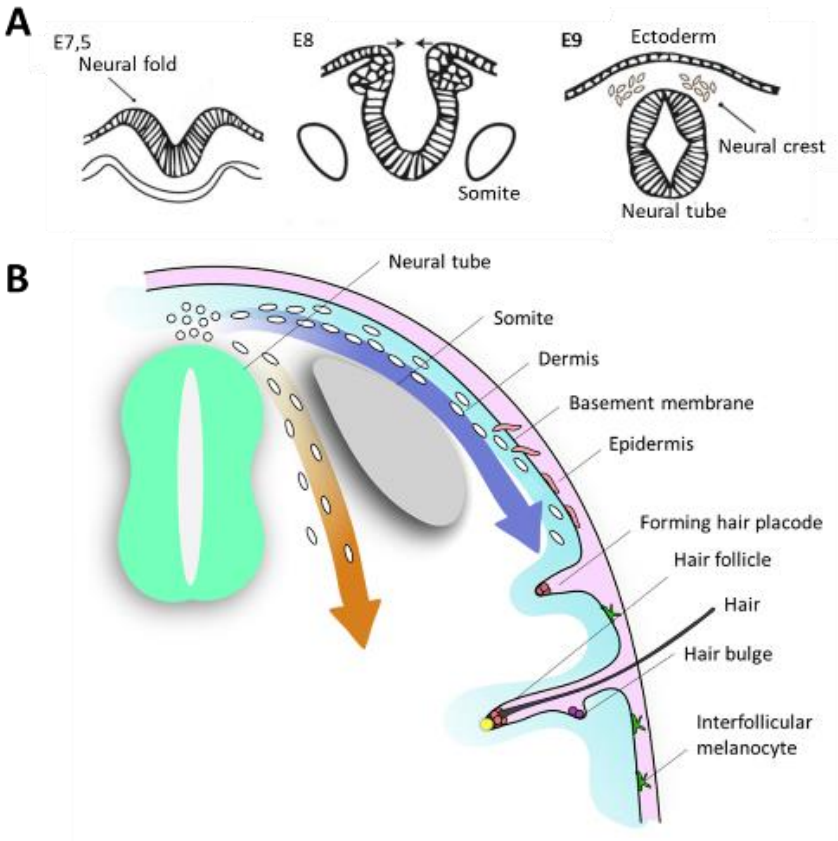

Figure 1. Model of development of neural crest and melanocytes to their final localization. (A) Neural crest specification and delamination. Adapted from Vandamme and Berx, TBD. (B) Mouse melanoblast model for migration during development. The blue arrow represents the dorso-lateral pathway and the orange one the ventral pathway.

1.1.2 Migration of melanoblasts

Some of the NCCs will express genes such as *Mitf* and *Kit* (see later) both of which are essential for the establishment of the melanoblasts (Opdecamp et al., 1997). This happens around stage E10.5 when the cells have started migrating along the dorso-lateral pathway. *Mitf* has been shown to be a key regulator of the specification of NCCs into melanoblasts (Baxter et al., 2010)) Upregulation of WNT3A induces expression of *Mitf* (Takeda et al., 2000), as well as PAX3 and SOX10, that have been shown to act synergistically (Bondurand et al., 2000; Potterf et al., 2000; Watanabe et al., 2002). Later, after the MITF-driven melanoblast specification, other melanocytic specific genes will be expressed such as the gene encoding the *Dopachrome Tautomerase* (*Dct)* (Steel et al., 1992). The migration of the melanoblasts starts during the NCC state in the MSA and continues until E15. The migration first starts in the dermis where the melanoblasts

proliferate while they migrate dorso-laterally to colonize the whole embryo (Figure 1). The mesenchymal dermis is the compartment that has been shown to be optimal for melanoblast migration (Erickson et al., 1992).

Recently, it has been shown that some melanoblasts arise from cells migrating through the ventral pathway (reviewed in (Ernfors, 2010)). Indeed, the Schwann cell precursors have been shown to be able to change their fate to become melanoblasts (Adameyko et al., 2009). To reinforce this, some studies show that it is possible *in vitro* to differentiate Schwann cell precursors into glial or melanocytic progenitors and then into melanocytes (Dupin et al., 2003). It has been suggested that FOXD3 is responsible for the fate of NCC to go into the ventral pathway by indirectly repressing MITF through repression of PAX3, such that the cells do not follow the dorso-lateral pathway (Thomas and Erickson, 2009).

1.1.3 Invasion of the epidermis

From E11.5, some melanoblasts start to invade the epidermis from the dermis through the basement membrane (Luciani et al., 2011). Dermis and epidermis are separated by the basement membrane which is a barrier mainly composed of laminins, type-IV collagen, integrins and proteoglycans (Paulsson, 1992). It has been shown that the process of crossing the basement membrane is active but degradation of the ExtraCellular Matrix (ECM) is not involved (Li et al., 2011). Invasion of the epidermis has been previously reviewed (Larue et al., 2013). In normal conditions, the number of epidermal melanoblasts increases faster than the number of dermal melanoblasts. Larue et al. (2013) thus developed a mathematical model to simulate the proliferation and invasion of the epidermis of the melanoblasts. This model suggested an asymmetric division of melanoblasts in the dermis with one daughter cell becoming able to invade the epidermis straight after the division, and the other cell remaining in the dermis. They also suggested that the proliferation was faster in the epidermis and that half the melanoblasts have already transmigrated to the epidermis at E12.5. Interestingly, the way melanoblasts migrate in the epidermis is neither directed nor by repulsion but rather by dispersion (Mort et al., 2016). Moreover, this dispersion of melanoblasts is dependent on the density of the cells, meaning that slower proliferating cells will show less dispersion and thus the resulting phenotype would be a belly spot, the belly being one of the last part of the embryo to be colonized by the melanoblasts. In KIT mutant mice, whose phenotype is a belly spot, the melanoblasts not show differences in migration, but rather show a reduced proliferation, suggesting the density-dependent dispersion of the melanoblasts. These data suggest that the fate of melanoblasts is dependent on their location,on the timing of the events and on their density and dispersal. However, how their fate is determined, and what other cell types and molecules are involved remains unclear.

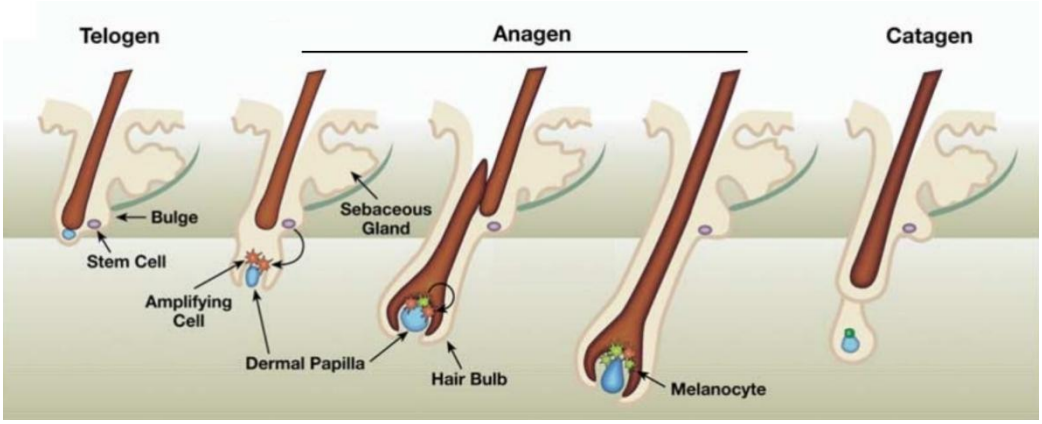

Figure 2. Role of MSC and melanocyte in the hair cycle. The three stages of the development of the hair with the repopulation of melanocytes needed for the anagen phase in the bulb made by the MSCs in the hair bulge. Figure from Steingrimsson et al, 2005 presented with permission from Elsevier Inc., permit number TBD.

1.1.4 Localization of melanocytes

The final step of melanocyte development is finding their final location, starting from E15.5. Melanoblasts that have reached the epidermis can go in three different places in mouse skin. Two of these locations are in the forming hair follicle. First, some of the melanoblasts will go to the lower part of the hair follicle where they will differentiate into mature melanocytes and be able to start producing melanin in hair. The localization of melanoblasts in the hair follicle can take place through attracting them with the chemokines SDF1 and CXCL12 to their receptor CXCR4 (Belmadani et al., 2009), in combination with KITLG on the KIT receptor of melanoblasts that acts as an accelerator of the localization into the follicle (Jordan and Jackson, 2000). There is also a switch in the expression of the calcium-dependent cadherins for the melanoblasts to localize in the hair follicle, with the suppresion of E-cadherin concomitant to the increased expression of P-cadherin (Nishimura et al., 1999). Later, during the first post-natal day (PND), some of the melanoblasts will reach the bulge of the hair follicle and become Melanocyte Stem Cells (MSC). These cells are characterized by low levels of MITF and KIT expression, and are slow-cycling undifferentiated melanoblasts, in a quiescent state but which still express *Dct* (Nishimura et al., 2002). The third location for melanocytes is in the interfollicular epidermis, but this population of melanocytes is minor compared to the ones in the hair follicle, as it is only located in the skin of the tail and ears, but not in hairy skin (Hirobe, 1984). Indeed, few days after the birth of the mouse, the other interfollicular melanocytes located in hairy skin decrease in number as a consequence of loss of KITLG expression by the surrounding keratinocytes.

Melanocytes in mice can be categorized into two types: classical, which are located in the skin and non-classical, which are located in other body parts. Melanocytes that populate different organs such as the eye, the inner ear, the heart, olfactory bulb,

meninges and bones (reviewed in (Colombo et al., 2011)), are called non-classical melanocytes and are rare. However, most of the melanocytes are classical and are located in the skin. Therefore, here, we will focus on classical melanocytes. Mouse adult skin is composed of two main compartments namely the epidermis (top layer) and the dermis (middle layer) and lies on subcutaneous tissue. Dermis is derived from the mesoderm whereas the epidermis is derived from the ectoderm. The epidermis is composed of keratinocytes distributed in layers and has structures such as glands (sebaceous and sweat) and hair follicles. Classical melanocytes are mostly located in the hair follicle, but a few are also present in the interfollicular epidermis of specific non-hairy parts such as the tail, ears and paws, where they are in charge of producing melanin for skin pigmentation. In humans, the so-called classical melanocytes are located in the skin, in the basal layer of the epidermis where they are in contact with 30 to 40 keratinocytes within the same compartment, forming the pigmentary unit (Cichorek et al., 2013). Epidermal melanocytes are involved in response to UV radiation by transferring the pigment melanin to neighboring keratinocytes where it protects the skin from further damage. Melanocytes are also present in hair follicles in the ratio of one melanocyte for five keratinocytes and they participate in the formation of the hair by delivering melanin to the growing hair shaft.

1.1.5 Hair follicle

In mouse hairy skin, mature melanocytes are located in the lower part of the hair, close to the dermal papilla. The hair follicle is a structure that goes deep in the dermis and into the hypodermis. Three main structures compose the hair follicle: the hair bulb, the dermal papilla and the bulge area. The dermal papilla is a dermal structure made of specific fibroblasts having the role of attracting epidermal melanoblasts down the hair to structure the hair follicle. The bulge area is where the melanocyte stem cells (MSCs) reside (see below). The mature melanocytes at the bottom of the hair follicle produce melanin and deliver it to the hair.

1.1.6 Hair cycle

The hair cycle leads to the production of a new hair (Alonso and Fuchs, 2006; Müller-Röver et al., 2001). Unlike interfollicular melanocytes which deliver melanin to the keratinocytes through melanosomes, in the hair melanogenesis only happens in the first of three stages, called anagen (Figure 2). In this long phase that lasts approximatively 17 days (Lavker et al., 2003), melanocytes located in the hair bulb deliver melanin to the growing hair shaft while the hair follicle is growing deep into the dermis and below in the hypodermis. The hair shaft is produced in the lower part of the hair bulb, by the flow of keratinocytes that go into the hair shaft. At the same time, in the upper part of the hair follicle, the melanocytes produce melanin and transfer it to the keratinocytes entering the hair shaft. The final result of the production of the hair shaft is a ladder-like formation of medullary segments containing the melanin, and that are surrounded by a

structure called cortex (Ellis et al., 1958). The melanin contained in the keratinocytes of the hair determines the pigmentation phenotype of the hair and thus the coat color of the mouse. Melanocytes are only involved at this stage. The next phase is the one-day-long catagen phase. It corresponds to the regression of the "cycling" part of the hair in the anagen phase, with the melanocytes dying by apoptosis (Tobin et al., 1998). The role of the hair club is to anchor the hair shaft to the hair follicle (Lindner et al., 1997). Finally, the hair cycle goes into the resting phase called telogen, which can last longer, from a few to several months, depending on the age of the mouse.

1.1.7 Hair renewal

The hair bulge is formed during the first Post-Natal Day (PND) and is a reservoir niche which repopulates hair follicles with new differentiated melanocytes and keratinocytes during each hair renewal (Nishimura et al., 2002). This crucial mechanism has been shown by using Dct::LacZ mice as an early marker for melanoblasts (Mackenzie et al., 1997). Nishimura et al. (2002) have used an antibody directed against KIT (a marker of melanocytic lineage, see below) in newborn mouse pups that results in the specific depletion of the amplifying population of melanoblasts but leaves the resting cells unchanged (Nishikawa et al., 1991). Interestingly, the first hairs produced by the newborn pups after the antibody injection were almost all unpigmented, whereas during the next hair cycles the hairs were pigmented, which indicated that undifferentiated cells were able to repopulate the hair follicle to produce melanocytes in the new hair cycle. Moreover, they showed that these cells, later called MSCs, were located in the hair bulge of the hair follicle, and that they were slow-cycling, which indicated a stem cell-potential state of these cells. However, the maintenance of the MSCs is considered incomplete as with ageing the pool of MSCs is reduced and therefore less capable of renewing the melanocyte population needed to pigment the hairs (Nishimura et al., 2005). The lack of maintenance of the MSCs due to ageing results in hair graying. Mutations in *Mitf* or *Bcl2* (see below), genes involved in survival of melanoblasts and MSCs, are also responsible for early hair graying (Nishimura et al., 2005; Steingrimsson et al., 2004).

1.1.7.1 Pigment synthesis

The pigment-granule melanin that is delivered to the hair during each anagen step of the hair cycle is delivered in an organelle called melanosome. The production of a melanosome is the result of the combination of successive processes in the melanocytes. If any of these steps is deficient, the coat color of the mouse might result in loss of pigmentation, alteration in color or hypopigmentation (see below). Melanosomes are an organelle related to the lysosome-family of organelles and are meant to be secreted. Mouse melanocytes can produce two different types of melanin pigment: the dark black or brown eumelanin and the yellow pheomelanin in mice (Ozeki et al., 1997). The act of producing melanin is called melanogenesis. It is a

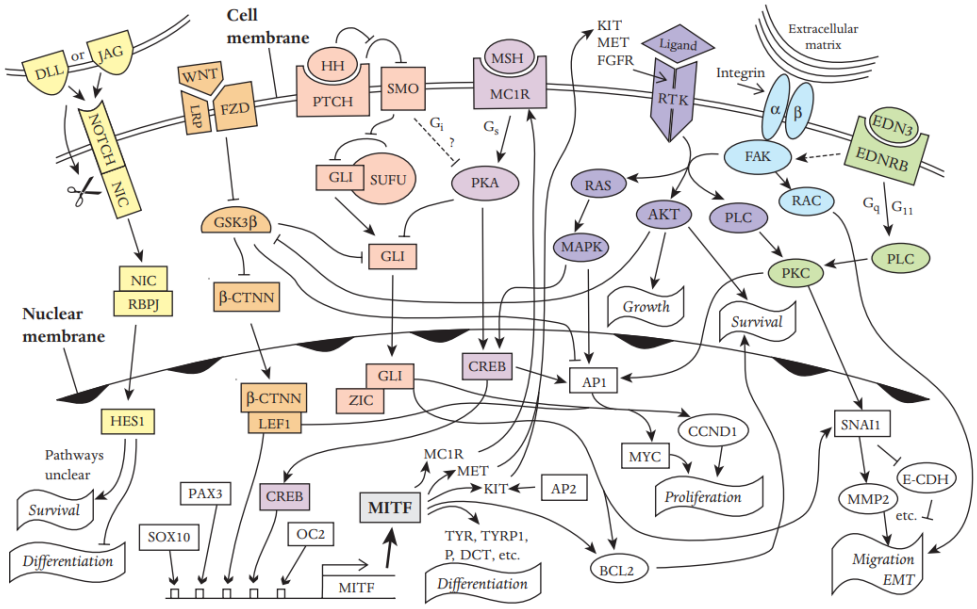

Figure 3. Signaling pathways involved in melanocyte development. Schematic represention of the different signaling pathways known to be involved in the regulation of mechanisms such as survival, diffenrentiation, proliferation and migration of melanocytes. Figure obtained with permission from John Wiley & Sons Ltd, according to permit number TBD (Lamoreux et al., 2010).

tightly regulated mechanism as it can be toxic for the cell if not in the melanosome. The process goes from an early melanosome in stage I to a mature melanosome in stage IV, ready to be delivered to the forming hair.

Here, we will detail the formation of a melanosome containing eumelanin. The first stage of the formation of melanosomes is the creation of a multivesicular body from the Endoplasmic Reticulum (ER) of the melanocyte. Then, the immature melanosome goes to stage II called eumelanosome when a matrix formed by the protein PMEL is generated (Harper et al., 2008). PMEL organizes the eumelanosome in an elongated shape made of the so-called fibrils. Once the melanosomes are structured, at least three enzymes will be transported from the cytoplasm to be included in the membrane of the melanosome: Tyrosinase (TYR), Tyrosinase Related Protein 1 (TYRP1) and Dopachrome tautomerase (DCT). As transmembrane proteins, they are located in the membrane of melanosomes, with their active domain directed toward the inside of the vesicle. From this moment and onward, these enzymes become competent for the melanogenesis of the eumelanin pigment (Yasumoto et al., 2004). Briefly, synthesis of eumelanin starts from hydroxylation of tyrosine or Dopa into Dopaquinone, a reaction catalyzed by TYR. In absence of Cysteine, the Dopaquinone is oxidized into Dopachrome and then converted into 5,6-dihydroxyindole (DHI) and 5,6-dihydroxyindole-2-carboxylic acid (DHICA). These two molecules can both be oxidatively polymerized to eumelanin. However, in presence of Cysteine, the Dopaquinone is converted to Cysteinyldopa and

then to Benzothiazole intermediates to finally give pheomelanin. The melanosomes thus enter stage III, with the pigment melanin accumulating. Finally, when the melanosome is mature and completely filled with melanin, it will be transported alongside microtubules in direction of the dendrites to be delivered to the neighboring cells, the keratinocytes via either exocytosis or phagocytosis. Keratinocytes can then produce the hair with pigmentation. There are many proteins that help during this process. For example, GPR143 (Schiaffino and Tacchetti, 2005) and ATP7A (Mercer, 1998) are involved in the regulation of internal processes of the melanosome, OCA2 (Potterf et al., 1998) and SLC45A2 (Costin et al., 2003) in maturing and processing the melanosomal proteins, and proteins involved in the trafficking of the proteins towards the melanosomes. Thus, melanogenesis is a complex mechanism involving many different proteins and needs to be tightly regulated.

1.2 Signaling pathways involved in melanocyte development

Many different signaling pathways are involved in the development of melanocytes (Lamoreux et al., 2010). This chapter will give a general overview of the forces involved in this process. A synthesis of all the pathways discussed in this thesis are shown in Figure 3.

1.2.1 G-protein-couple receptor pathways

G-protein-coupled receptors (GPCRs) are important in melanocyte development and function. G-protein-coupled receptors are GTPase-binding proteins which, when stimulated by the associated ligand, release a G subunit molecule that will activate a downstream signaling cascade. Four GPCRs are of interest for this thesis.

The Proopiomelanocortin protein/Agouti signal protein/Melanocortin 1 receptor (POMC/ASIP/MC1R) pathway is involved in survival and differentiation of melanoblasts in mouse development (Herraiz et al., 2017). MC1R is a GPCR that can be bound by the agonist MSH that stimulates production of cAMP resulting in the production of the black/brown pigment eumelanin (Suzuki et al., 1996). On the contrary, ASP is an antagonist of MC1R, and the blockade of the signaling cascade results in the production of cinnamon-colored pigment pheomelanin (Abdel-Malek et al., 2001). This cascade is involved in "pigment-type switching" (Abdel-Malek and Supp, 2008), a mechanism that results in the agouti coat color of mice where each hair has a band of eumelanin, then a band of phaeomelanin and finally a band of eumelanin. This pathway will not be discussed further here.

The Endothelin 3/ Endothelin receptor type B (EDN3/EDNRB) ligand/receptor pair has been shown to be important for the development of the NCC (Opdecamp et al., 1997; Pavan and Tilghman, 1994b; Pla and Larue, 2003). EDNRB is a GPCR that EDN3 binds to and activates. This pathway activates the Protein Kinase C (PKC) pathway (see

below), a crucial factor for proliferation of the melanocyte lineage (Alberts, 2017). It has been shown to be effective in melanocyte development between E10 and E12.5, when melanoblasts migrate along the dorso-lateral pathway, suggesting that the EDN3/EDNRB pathway is involved in the migration of melanoblasts, when they start migrating from the MSA, but also in their survival during the initiation of migration (Shin et al., 1999).

The WNT/frizzled-1 canonical signaling pathway has been shown to be important for melanocyte development. The secreted glycoprotein WNT can bind to the GPCR called Frizzled (FZD) eventually resulting in the repression of the degradation of β-catenin (β-cat). The two WNT ligands encoded by the *Wnt1* and *Wnt3a* genes are required for the development of melanoblasts (Ikeya et al., 1997). Both are important for melanocyte development, and the lack of one or the other or both lead to absence of melanoblasts, suggesting that they activate survival and differentiation of neural crest-derived cells at different stages of development, alongside other factors like EDN3 and KITLG (Dunn et al., 2005). The downstream effect is to prevent the degradation of β-cat, a protein that interacts with a nuclear protein complex to regulate gene transcription. In the case of melanoblasts, if β-cat is knocked out, MITF and DCT positive cells do not develop, suggesting the important role of β-cat in this pathway (Hari et al., 2002). WNT signaling has also been shown to transcriptionally activate Lymphoid enhancer-binding factor 1 (LEF1), a protein from the LEF1/TCF family that interacts with β-cat to regulate MITF expression in melanocytes, and thus in the differentiation into the melanocytic lineage (Takeda et al., 2000).

1.2.2 Single-pass receptors

1.2.2.1 Notch signaling pathway

Another type of signaling pathway involves single-pass transmembrane receptors, that are composed of a ligand-binding domain on the outside of the membrane and an effector domain inside. Neurogenic locus Notch homolog protein 1 (NOTCH1) receptors are proteins of this type that form heterodimers that can be bound by either Delta-like (DLL) or Jagged protein ligands. Hairy/Enhancer of Split 1 (HES1) is a transcription factor of the bHLH family and is directly targeted by the Notch signaling pathway. The Notch pathway is important for the delamination and formation of the NCC during early development as its conditional ablation results in a defect of pigmentation (Hari et al., 2002) and later in the maintenance of the melanocyte stem cells in the hair bulge. It has been shown to be necessary for development of melanoblasts, and establishment and maintenance of MSCs as its inactivation leads to hair graying (Aubin-Houzelstein et al., 2008), through activation of *Hes1*. *Hes1* is involved in this mechanism by inhibiting apoptosis and differentiation of MSCs (Schouwey et al., 2007). Also, the expression of *Hes1* in NOTCH knock-out mice rescued the phenotype (Moriyama et al., 2006). Interestingly, NOTCH signaling has

been shown to inhibit the WNT and β-cat signaling pathways (De Strooper and Annaert, 2001), suggesting again the complex regulation during melanocyte development.

1.2.2.2 TGF-β and BMP signaling pathways

The Transforming Growth Factor β (TGF- β) can bind to a superfamily of single-pass serine/threonine kinases receptor called TGF-β receptors (TGF-βRs). All TGF-β cytokines (1, 2 and 3), bind to the TGF-βR2 which will bind to TGF-βR1 and activate the kinase activity of the SMAD proteins, named after the combination of the homology between the *Caenorhabditis elegans* SMA ("SMAll body size") protein and the *Drosophila* MAD ("Mother Against Decapentaplegic"). protein. The activated SMAD proteins can enter the nucleus to regulate transcription of target genes and are thus involved in the regulation of many processes such as cell growth, proliferation, differentiation and apoptosis (Alberts, 2017).

Another similar family of ligands is the BMP family that interact with the single-pass BMP receptors (BMPRs), which subsequently transduce the signal in the cell through the SMAD signaling pathway (different from the mentioned above, with SMAD1, 5 and 9). Studies in chick inhibiting BMP activity have shown that NCC migration was impaired, meaning that the BMP signaling pathway is involved in NCC development and migration (Goldstein et al., 2005).

1.2.2.3 Receptor Tyrosine Kinase (RTK)

The single-pass Receptor Tyrosine Kinase (RTK) receptors are molecules that dimerize to initialize a phosphorylation cascade. Among the cascades that are involved in the signaling are the Mitogen-Activated Protein Kinase (MAPK) and Phosphoinositide 3-kinase (PI3K) pathways. The MAPK pathway is conserved in almost all eukaryotes and has been shown to be responsible for cell proliferation, migration, differentiation and apoptosis (Wilkinson and Millar, 2000). The PI3K pathway activates the serine/threonine kinase AKT to promote cell survival and growth (Hemmings and Restuccia, 2012). The PKC proteins can also be activated by the RTKs. The PKCs are involved in the phosphorylation of serine/threonine residues and thus in the regulation of gene expression (Newton, 2001). These proteins have been shown to be important for cellular proliferation and differentiation (Nishizuka, 1992).

There are many different RTKs that can induce the signaling cascade previously described. One of the first expressed in melanocyte development is KIT which can be bound by its ligand, KITLG. Interestingly, mutations in KIT result in semidominant white spotting characterized by a diluted coat color with white spots on the belly and head and a reduced pigmentation in the tail and the skin (Mackenzie et al., 1997), while KITLG semidominant mutations result in a diluted coat color with occasional spotting (copeland, 1990). They are some of the first genes expressed during melanoblast specification from NCC. Mutations of KITLG and KIT revealed that KITLG is

involved in the survival of the melanoblasts in the MSA and in their dispersion in the dorso-lateral pathway, while KIT has been shown to be important for survival of melanoblast precursors when they are migrating and proliferating in the dermis (Wehrle-Haller and Weston, 1995). Thus, these factors are crucial for survival, proliferation and migration of the melanocytic lineage (Price et al., 1998).

Hepatocyte Growth Factor (HGF) can bind to the RTK receptor MET. It has been shown to be important for the mesenchymal-epithelial interactions in the hair follicle growth that starts taking place late in development at E14 and during hair cycling (Lindner et al., 1997). Some other RTKs are the Platelet-Derived Growth Factor Receptors (PDGFRs) and their ligands PDGFs, the Human EGF Receptor (HER) and their ligands Epidermal Growth Factors (EGFs), and FGF Receptors (FGFRs) and their ligands Fibroblast Growth Factors (FGFs). Mice having a deletional mutation in the PDGFRA subunit display the white spotting *Patch* phenotype but the effect on melanocytes development have been suggested to be due to rearrangemment in the regulatory region for *Kit*, resulting in ectopic expression of KIT (Wehrle-Haller et al., 1996). EGFR-null mice display a darker non-hairy skin, but it has been suggested as a secondary event from the increased keratinocytes proliferation (Fitch et al., 2003). Particularly, FGF has been shown to be involved in NCC development, and later for melanoblasts (Sviderskaya et al., 1995) and melanocytes (Halaban et al., 1987).

1.2.3 Transcription factors downstream of RTKs signaling

There are many different TFs that are regulated downstream of the signaling pathways previously described. Among the most important ones are POU class 3 Homeobox 2 (POU3F2, also known as Brain-2, BRN2), FOXD3, SNAI1 and 2, Tumor protein 53 (TP53), SOX10, PAX3 and MITF. POU3F2is an early marker of the NCC and is thought to have a role in melanocyte differentiation. Cell cultures of melanoblasts in partial precursor state were shown to express POU3F2at a high level, while pigmented melanocytes had low level ofPOU3F2. FOXD3 is involved in NCC formation and represses melanoblast formation, thus suggesting that its overexpression leads to reduced numbers of melanoblasts (Alkhateeb et al., 2005). SNAI1 (also known as SNAIL) and SNAI2 (SLUG) are zing-finger TFs from the Snai family of proteins that are thought to be involved in the EMT of the NCC, but also in cell migration (Acloque et al., 2009; Barrallo-Gimeno and Nieto, 2005; Carver et al., 2001). SNAI1 is a transcription repressor that has a role in organogenesis during development by repressing mesectodermal and ectodermal genes in the mesoderm (Smith et al., 1992) and is crucial for mouse development (Sefton et al., 1998). The role of SNAI2 is explained in chapter 1.3.3. and MITF, which represents the main focus of this project will be detailed in chapter 1.4.

1.3 Phenotypes associated with defective melanocytes

Alterations in survival, migration and differentiation during melanoblast development results in phenotypes that can be sorted into three main types: vitiligo, albinism and white spotting.

1.3.1 Albinism and white spotting

Albinism and white spotting are the two major pigmentation phenotypes. Albinism affects a key functional role of melanocytes which is to produce melanin while white spotting concerns melanocyte development. Albinism is characterized by the reduction or absence of melanin production by the melanocytes but delivery to the receiving cells can also be involved. On the other hand, white spotting is the complete congenital absence of melanocytes on some part of the body where they are supposed to be present, due to the dysfunction of genes crucial for melanocyte development. The different coat colors or patterns, caused either by albinism or white spotting in mice can be explained by multiple factors of which the mutated genes are involved in. White spotting can be caused by mutations in genes important for the specification of the NCC into melanocytes precursors and EMT, proliferation and survival throughout development, invasion of the epidermis, homing in the hair follicles, differentiation, and the timing of the stage development that the mutated protein is active. Albinism can be caused by mutations in genes involved in mechanisms such as the proteins producing the matrix for melanosomes or the enzymes producing the pigment, control of the internal environment of the melanosomes and their transportation. The coat color phenotypes observed are thus caused by a failure of the melanocytes to develop in the case of white spotting or caused by a defect in the melanosome/melanin production or delivery process in the case of albinism.

Mutations in numerous genes, in both humans and mice, have been shown to lead to an abnormal coat color phenotype, mostly in heterozygous conditions as homozygotes are often lethal. These genes include *Pax3, Sox10, Ednrb, Edn3, Kit, Kitlg, Snai2, Adamts20, Mcoln3* and *Mitf* (Baxter et al., 2004). Many of these genes result in white spotting in heterozygous condition as they are dominant like PAX3 and SOX10; in the homozygous condition these cases are lethal. These genes have been studied to address how they impact the development of the melanocytes. For example, a team in the UK performed chimaeric analysis using WT embryos carrying the Dct::LacZ reporter which is expressed in melanoblasts from E10, thus allowing the staining of melanoblasts during development (Wilkie et al., 2002). They compared stained Dct::LacZ embryos with an aggregation chimaera of Dct::LacZ <-> WT. This experiment showed that the chimaeras display first (E12.5-E13.5) an overall dilution of the labelled cells, and then (E15.5-E16.5) the appearance of stripes and discrete patches, unlike the Dct::LacZ which has a more spread arrangement of the melanoblasts. They also used a modified Dct::LacZ reporter by creating a duplication in its coding region with an in-frame stop

codon leading to a non-functional protein. This duplicated sequence can be removed by homologous recombination at low frequency, which results in the restoration of the function of the LacZ protein, and therefore allowing the labelling of the founder cell and its progeny. They used this reporter to create Dct::LaacZ <-> Dct::LacZ chimaeras to generate mosaic embryos with a single-marked melanoblast clone (founder and descendants) whose expansion can be visualized. From this work, they suggested that the cervical region, the head and the face of mouse embryos is populated with a large pool of melanoblasts whereas fewer melanoblasts reside in the trunk (Wilkie et al., 2002). This was later confirmed by tracking single melanoblasts clones and mathematical modeling. Random migration and density-related dispersion of the melanoblasts showed that the trunk is populated by fewer melanoblasts. Thus, it is likely to be the first phenotype displayed in the case of motility/proliferation defect (Mort et al., 2016). *In situ* hybridization studies performed using probes directed against *Dct* (Opdecamp et al., 1997), *Kit* (Keshet et al., 1991), *Mitf* (Nakayama et al., 1998), *Solute carrier family 45 member 2 (Slc45a2)* (Baxter and Pavan, 2002) and *Premelanosome protein* (*Pmel)* (Baxter and Pavan, 2003) have revealed that the first cells expressing these melanoblast markers are located in the head and cervical regions from E10.5, and later in the trunk and the rump region at E11.5. Importantly, the authors also noticed fewer melanoblasts in the trunk. Additionally, there is one specific type of white spotting due to mutations in the *Ednrb* gene, called piebald (and often referred as piebaldism) that is due to a reduced number of melanocytes in specific areas, most often with the pigmented areas close to head and tail regions, and the non-pigmented areas in the trunk. The *piebald* phenotype in the mouse is caused by the absence or the non-functional version of the gene *Ednrb* (Hosoda et al., 1994). However, numerous questions still remain regarding melanocyte development and the specific roles of the genes involved in this process.

1.3.2 Progressive graying (mouse vitiligo)

Vitiligo is a disease that displays skin depigmentation in humans due to the loss of melanocytes in some parts of the skin. The pathogenesis is complex and is most likely multifactorial with environmental background, oxidative stress (Schallreuter and Physiology, 1999), genetic predispositions and auto-immunity (Spritz, 2010). These factors lead to the apoptosis of the melanocytes, even if the mechanism by which this happens remains unclear. Mouse models of vitiligo cannot reflect completely the human disease as, unlike humans, most of the melanocytes are distributed in the hair follicles and not in the interfollicular epidermis. Vitiligo in mice would therefore be envisioned as progressive hair graying, as the coat progressively loses its pigment concomitantly with the loss of melanocytes (Lerner et al., 1986). Melanocyte stem cells replenish melanocytes during each hair cycle in mice. An example of a mouse model of vitiligo is the *Microphthalmia vitiligo* ($Mitf^{Mi\text{-}vit}$) mouse (Steingrimsson et al., 2004), which will be discussed in chapter 1.6.

1.3.3 White spotting mouse models

In this chapter we will detail a few mouse models that have been used to determine how melanocytes are established during development. As we have already seen, many of the genes that are involved in the previously described signaling pathways are crucial for the establishment of the melanocytic lineage from the NCC. That is the case for the gene *Pax3,* as mice heterozygous for a mutation in the gene exhibit the *Splotch* phenotype; homozygous knock-out of *Pax3* is lethal (Machado et al., 2001). The *Splotch* mice display neural-tube defects with a large white spot on the belly and a tiny white spot on the forehead (Vogan et al., 1993). *Mitf* is among the first genes expressed after the specification of the NCC into melanoblasts. Another gene involved in melanocyte development is *Sox10*. Heterozygous mutations in this gene result in the *Dominant Megacolon* (*Dom*) mouse. Similar to *Splotch*, *Dom* mutations are dominant and exhibit a megacolon and a white belly spot with white feet and tail in heterozygous condition; homozygotes are lethal (Brizzolara et al., 2004). The Piebaldism phenotype can be due to mutations in *Snai2* and is similar to the *White* phenotype associated with heterozygous mutations in *Kit,* which is explained by the fact that KIT mutated cells do not express SNAI2, suggesting that SNAI2 is a downstream target of Kit signaling (Sánchez-Martín et al., 2003). SNAI2 is a zinc-finger TF, closely related to SNAI1, and has been shown to be activated through the KIT pathway both *in vitro* and *in vivo (Pérez-Losada et al., 2002)* and is expressed during development in migratory NCC but not in the pre-migratory cells (Jiang et al., 1998). SNAI2 has been shown to be important for both melanoblast survival and migration but not for the formation of NCC (Sánchez-Martín et al., 2003). Also, SNAI2 has been reported to be regulated by MITF. In humans, SNAI2 mutations cause Piebaldism and Waardenburg Syndrome type 2 (Sánchez-Martín et al., 2003).

Some other genes are important for melanoblast migration. The RTK *Kit* and its ligand *Kitlg* are amongst the most important genes for this process. Many alleles of these two genes have been identified, respectively termed *White (W)* and *Steel (Sl)* when discovered (Copeland et al., 1990; Geissler et al., 1988), which result in dominant white spotting phenotypes in heterozygous condition and exhibit white spots on the head and trunk, depending on how severe the mutation is. Similarly, mutations in the *Ednrb* and *Edn3* genes result in the *Piebald (S)* and *Lethal spotting (Ls)* mice. *Piebald (Baynash et al., 1994)* and *Lethal spotting (Hosoda et al., 1994)* mice have a white coat with occasional pigmentation on the head and the rump, together with a megacolon (Lee et al., 2003).

All of these phenotypes have been closely studied as they give important and valuable insights into the role of the different genes in melanocyte development, and also the timing of their activity. Mutations which result in severe phenotypic effects provide information about the importance of the gene in the respective cells. At the same time, severe effects on a particular cell type may limit the information provided on what role the gene plays during development.

1.3.4 Pigmentary mosaicism

Pigmentary mosaicism, also called patterned dyspigmentation, has been characterized as a patchwork of pigmentation that is caused by genetic heterogeneity in the melanocytes delivering melanin to the hair (Lombillo and Sybert, 2005). In 1967, Mintz et al. created somatic mosaic mice by mixing several combinations of two genetically distinct populations of cells together at the morula stage, with one population with the presence of gene required for pigment production and therefore called "black", and the other one without and termed as "white" or albino. These mice were then called allophenic mice and more recently aggregation chimaeras. Postzygotic mutations, in embryonic or fetal development, or in postnatal life, would also result in somatic mosaicism, with all the daughter cells carrying the mutation of the mother cell, thus creating a somewhat different population of cells in genetic terms. If this event happens early, it is likely to affect larger areas than if it happens at later stages, thus only affecting few cells or tissues. An example of this is the X-chromosome where females need to inactivate, randomly, one of the two X-chromosome during the late blastocyst stage, a process called Lyonization (Lyon, 1961). This phenomenon is crucial as some genes would be lethal if expressed from the two X-chromosomes. This process is important for pigmentation too as it causes chimerism for heterozygous alleles located on the X-chromosome or hemizygous transgenes. An elegant study using an X-linked LacZ transgene showed that the X inactivation in individual cells happens at different stages in different somatic tissues and is progressive (Tan 1993). The cases of the calico and tortoiseshell cats is a very good example of this process. Indeed, the gene coding for the yellow phenotype (due to pheomelanin, known commonly as red in cats) in heterozygotes will be inactivated in some early melanoblasts, and thus all their clonal descendants (Mintz, 1967) will resulti in the tortoiseshell coat. Calico phenotypes are also tortoiseshell phenotypes but combined with white spotting that is not X-linked. However, it is important to note that not all chimerism phenotypes are linked to the X-chromosome inactivation but can also be due to the expression of a mutated gene at a specific stage of development that in the end also results in chimerism. There are also chimeric patterns that are not related to X-inactivation nor mutations, but rather controlled the genotype of the dermis. An example is the *Agouti*-locus which results in tabby stripes in the cat or zebras, or the spots in giraffes and leopard. Briefly, the *Agouti* gene, encoding the ASIP protein, results in the agouti pattern at the hair level (Aberdam et al., 1998), which consists in a banding pattern of the hair with eumelanin and pheomelanin, which involves the pigment switching through MC1R (Lamoreux and Mayer, 1975). This process can be very precisely located, and thus result in the banding/spotting pattern of the fur of tabby cats or leopard for example. Another example that has been shown to be responsible for the establishment of the pattern of tabby cats is through the *Dkk4* gene that affects the patterning process (Kaelin et al., 2021).

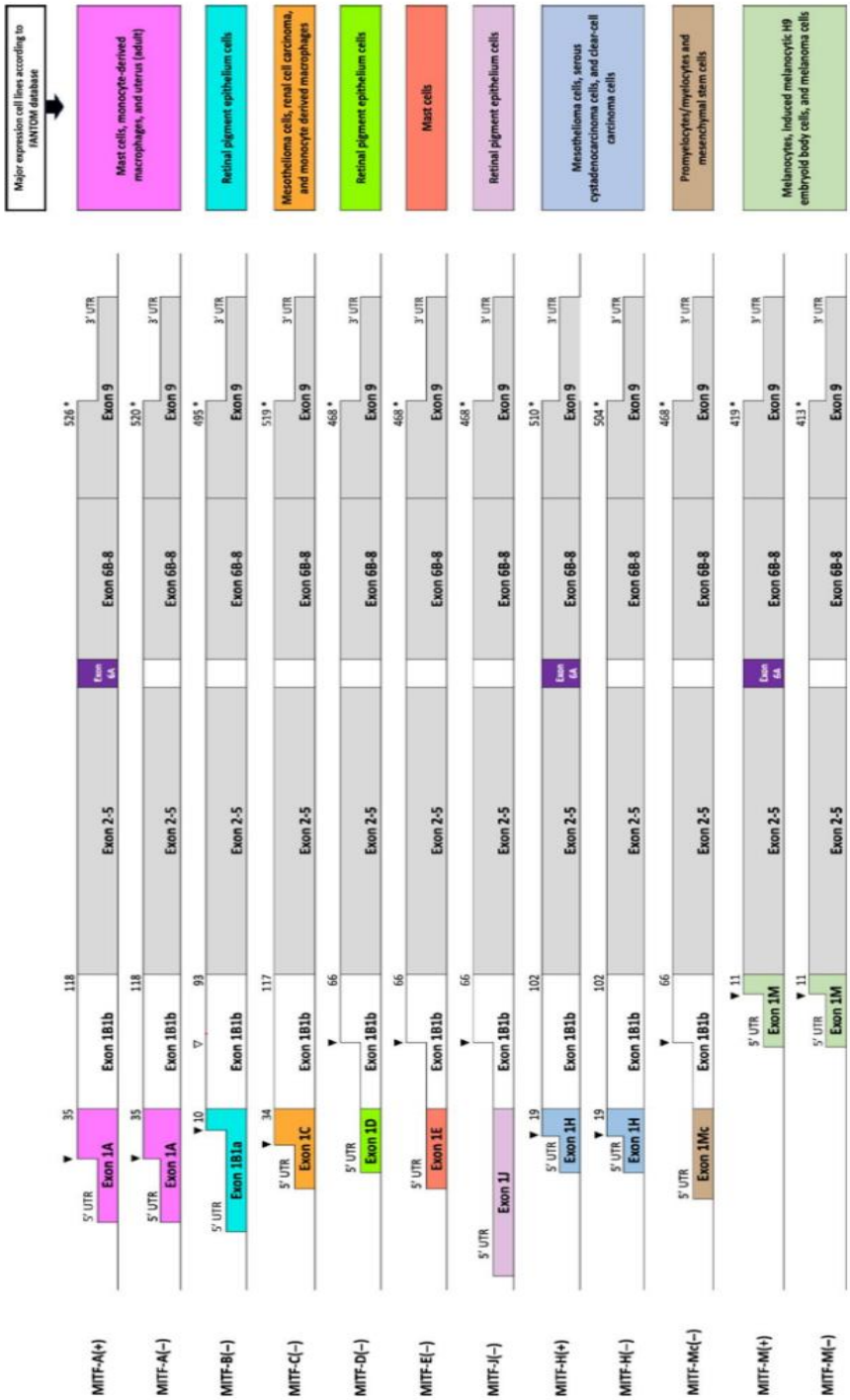

Figure 4. MITF mouse isoforms. Figure obtained with permission from Pigment Cell & Melanoma Research journal, according to permit number TBD (Vu et al., 2020).

Finally, epigenetic mosaicism describes the role of the environmental mechanisms which eventually change the genetic information through epigenetic modifications. A good example of this process are the Transposable elements, such as retrotransposons, that have been shown to regulate genomic expression of surrounding genes involved in melanocytes development or pigment production by methylation or demethylation (Happle, 2002), resulting in the skin lines of Blaschko. Recent findings have shown that some Transposons are involved in the pigmentation pattern of orchids (Hsu et al., 2019) or medaka fish (Koga et al., 2006). More interestingly, acetylation states, and in general chemical modifications, can also inhibit gene expression (Jiang et al., 2004), even though these mechanisms are poorly understood.

1.4 Microphthalmia-associated Transcription Factor

Amongst the many genes involved in development of melanoblasts and in the biology of melanocytes is the *Microphthalmia-associated Transcription Factor* (*Mitf*). *Mitf* was first discovered in 1942 by Paula Hertwig, who discovered white mice with microphthalmic eyes amongst the progeny of normally pigmented mice that had been irradiated by X-rays (Hertwig, 1942). She called this mutation *microphthalmia* (abbreviated *mi*) and these mice are still available today. Many additional mutations in *Mitf* have been discovered since then. The gene was cloned in 1993 (Hodgkinson et al., 1993) and shown to encode a basic Helix-Loop-Helix-Zipper (bHLHZip) transcription factor and many of the mutations have been characterized (Steingrimsson et al., 2004). The different *Mitf* mutations have in common defects of NCC-derived melanocytes, resulting in complete or partial loss of coat color pigmentation (Steingrímsson et al., 1994) often associated with deafness (Tachibana et al., 1992) and microphthalmia. MITF was thus considered as one of the most important transcription factors (TF) for melanocyte development as the absence or reduced activity of MITF leads to severe phenotypic traits. Phenotypes other than coat color defects show the importance of MITF in many other cell-types such as mast cells (Morii et al., 1996), retinal pigment epithelium (Yasumoto et al., 1997), osteoclasts (Weilbaecher et al., 2001) and olfactory bulb (Atacho et al., 2020; Ohba et al., 2015). Finally, recently MITF has been identified as axonal damage sensor in Schwann cells where its activation leads to nuclear translocation and induces DNA repair (Daboussi et al., 2023).

MITF is highly conserved in many species like human, mouse, rat, hamster and chicken, with the basic domain even conserved in both vertebrates and invertebrates (Baranowska Körberg et al., 2014; Gyoja, 2014; Hauswirth et al., 2012; Simionato et al., 2007). This TF can bind to DNA as homodimer or as heterodimer with other members of the microphthalmia/transcription factor E (MiT/TFE) family. The MiT/TFE family members have in common the bHLH-Zip motif that allows them to dimerize and bind to DNA. This family contains TF like Transcription factors EB (TFEB), E3 (TFE3), and EC (TFEC) which MITF can dimerize with. There are also other TFs like Myc-associated factor X (MAX), MYC and Upstream stimulatory factor (USF), but MITF cannot

dimerize with them due to the absence of a three-residue sequence EQQ[260-262] (based on MITF-M amino acids numbering) in the zipper-domain of MITF (Hemesath et al., 1994; Pogenberg et al., 2020; Pogenberg et al., 2012). Dimers of MITF can bind to DNA motifs known as E-box (CACGTG) and M-box (TCATGTG) (Aksan et al., 1998; Lowings et al., 1992).

1.4.1 Isoforms and Post-Translational Modifications of MITF

Interestingly, MITF is expressed in many different isoforms due to alternative splicing. A total of 14 isoforms of MITF have been described in the mouse, with many also conserved in humans (reviewed in (Vu et al., 2021). Most of the isoforms are due to the use of alternative first exons whereas exons 2 to 9 are common to most isoforms. In the mouse, the alternative first exons are: 1A, 1B, 1C, 1D, 1E, 1J, 1H, 1M and 1Mc (Figure 4). On top of these different isoforms, exon 6A is included in about 50% of transcripts but this exon contains 18 bp resulting in proteins containing a 6 amino acid sequence termed MITF(+) or lacking it, termed MITF(-). The isoforms are expressed in a tissue-specific manner (reviewed in (Vu et al., 2021) such that for example MITF-M is mostly expressed in melanocytes (Hershey and Fisher, 2005; Hodgkinson et al., 1993; Yasumoto et al., 1997), but MITF-A has also been detected in these cells (Flesher et al., 2020). The other isoforms have been shown to be present in other tissues. For example, MITF-E is expressed in mastocytoma cells, MITF-D in the RPE, mast cells and osteoclasts. The MITF-A, MITF-B, MITF-H and MITF-J isoforms are present in many tissues whereas MITF-H is mostly expressed in the heart, and MITF-A and MITF-J in the RPE. However, most of studies on MITF have focused on the melanocyte and melanoma-abundant isoform MITF-M, and so is the case for this thesis.

The MITF protein is also regulated through post-translational modifications (PTMs) to tune MITF activity. Such PTMs include phosphorylation, ubiquitination, SUMOylation and acetylation (reviewed in (Vu et al., 2021). This thesis focuses on the MITF-M(+) isoform and all residue numbers are based on this. Briefly, phosphorylation of MITF has been shown to be important for transcriptional activity, subcellular localization, and stability of the protein (reviewed in (Goding and Arnheiter, 2019). For example, phosphorylation of Ser73 allows MITF to interact with p300 as a cofactor and this enhances MITF transcriptional activity (Hemesath et al., 1998; Sato et al., 1997). Consistently, mutating Ser73 to Ala decreased MITF transcriptional activity (Wu et al., 2000). The Ser73 amino-acid is also involved in ubiquitin-mediated degradation of MITF (Wu et al., 2000; Xu et al., 2000). Phosphorylation of Ser73 has also been shown to mediate MITF subcellular location (Hemesath et al., 1998; Ngeow et al., 2018). MITF-M(+) can be SUMOylated on Lys182 and Lys316 and mutations to Arg in both of these PTM enhances the transcriptional activity of MITF from promoters containing multiple MITF-binding sites, but does not change its stability or localization (Murakami and Arnheiter, 2005). Finally, little is known about ubiquitination of MITF, except that MITF can be deubiquitinated by Ubiquitin-specific protease 13 (USP13)

which increases its expression and thus eventually increases the expression of genes regulating proliferation of melanoma cell lines (Zhao et al., 2011). Also, the ubiquitin ligase UCHL1 has been suggested to negatively affect MITF stability (Seo et al., 2017). The potential ubiquitination sites are thought to be Lys21, Lys91, Lys 201 and Lys265. MITF is also acetylated. It has been shown to interact with the lysine acetyl transferases CREB binding protein (CREB) and E1A Binding Protein P300 (EP300) complex which acetylate MITF (Louphrasitthiphol et al., 2023; Louphrasitthiphol et al., 2020).

1.4.2 MITF mutations in humans

Waardenburg Syndrome (WS) is a group of genetic conditions that all lead to abnormal distribution of melanocytes (Waardenburg, 1951). It is an autosomal dominant disease that can be caused by multiple mutations in genes that play a role in NCC development. There are four different types of WS, with similar general phenotypes but with some differences. Mutations in PAX3 cause WS type 1 and 3 while mutations in EDNRB or EDN3 cause type 4 (Read and Newton, 1997). Germline mutations in MITF in humans have been associated with Waardenburg syndrome type 2A (WSA2), with people affected showing hypopigmentation of skin, eyes, and hair as well as hearing loss (Tassabehji et al., 1994). A more severe kind of WS2A is called Tietz syndrome, and is characterized by albinism and congenital deafness (Tietz, 1963). Tietz syndrome is associated with deletion of R217 of MITF, a residue located in the basic domain and involved in DNA-binding; the same mutation was found in mice carrying the *Mitf*^{mi} mutation (Amiel et al., 1998; Smith et al., 2000). The phenotype of individuals carrying biallelic mutations of MITF is called COMMAD syndrome as it is associated with Coloboma, Osteopetrosis, Microphthalmia, Macrocephaly, Albinism and Deafness (George et al., 2016). This is a severe and lethal condition in humans and is similar to *Mitf*^{mi}, the most severe mutation in the mouse. In addition to the link to WS, the germline mutation E318K (Bertolotto et al., 2011) and the somatic mutations E87R, L135V, L142F, G244R, and D380N (Cronin et al., 2009) have been found in melanoma patients. The E318K mutation has been shown to predispose to melanoma in European populations (Bertolotto et al., 2011). In total, more than 18 mutations in MITF have been associated with one of the human syndromes described above. Most of the WS, Tietz and COMMAD mutations are located in the DNA-binding bHLH-Zip domain of MITF, which lead to a loss of DNA binding ability and thus, to the loss of the regulation of MITF of its target genes (Cronin et al., 2009; Grill et al., 2013). in contrast, the mutations associated with melanoma are outside these regions.

1.4.3 *Mitf* mutations in mice

In the mouse, many *Mitf* alleles have been characterized and all affect melanocytes and coat color. Some alleles also affect other structures including the Retinal Pigment Epithelium (RPE) resulting in small eyes with little to no pigmentation. Osteopetrosis or hyperosteosis can also result from MITF mutations. Approximately half of the mutations

are recessive, and the rest are semi-dominant, exhibiting a mild phenotype such as white spotting or a coat color dilution. The phenotypes of *Mitf* mutations have been reviewed previously (Moore, 1995; Steingrímsson et al., 1994). Here we will summarize the phenotypes briefly. The first *Mitf* allele that was discovered is the $Mitf^{mi}$ allele which, as explained earlier, is a semi-dominant mutation resulting from a deletion of 3 bp in the basic region of *Mitf* (del217). In homozygous condition, the mice exhibit microphthalmia, white coat, osteopetrosis and hearing loss. Heterozygous $Mitf^{mi}$ mice only show a white spot on the head or belly. The mutation associated with $Mitf^{Mi\text{-}OR}$ is a change from an Arginine to a lysine (R216K). Homozygotes have similar traits as $Mitf^{mi}$ without the hearing loss. Heterozygotes display spots on the head, the belly and the tail, with a less pigmented iris (Steingrímsson et al., 2003). The $Mitf^{Mi\text{-}Wh}$ mutation is characterized by a substitution of isoleucine 212 to aspargine (I212N); homozygous mice exhibit white coat color with intermediate microphthalmia and hearing loss. Heterozygotes show diluted coat color, hearing loss and white spots on the head, toes and tail. Interestingly, these three mutant MITF proteins do not bind to DNA. However, these mutant proteins can heterodimerize with the MITF relatives TFE3 and TFEB, and this might explain why these mutations are dominant negative. A mutation in MITF that changes the aspartic acid into an aspargine in position 222 in the first helix domain results in mice that have white areas on the belly and thorax, and that with age progressively lose its coat pigmentation and have retinal degeneration. This allele has thus been called $Mitf^{Mi\text{-}vit}$, for *vitiligo*, as progressive graying is the similar phenomenon that happens in vitiligo patients. Surprisingly, this mutation did not appear to change *Mitf* DNA binding. The many other Mitf alleles have been described in detail in previous reviews (Moore, 1995; Steingrimsson et al., 2004) and will not be detailed further here.

Interestingly, to add to the complexity of MITF, some *Mitf* alleles are able to complement the phenotypes of each other with respect to each allele in homozygous condition. In these cases, the phenotype when two different alleles are combined is less severe than each homozygote alone (Steingrímsson et al., 2003). Phenotypes associated with *Mitf* mutations can be arranged in an allelic series, ranging from completely white coat color due to the complete absence of melanocytes, to various degrees of spotting and hair graying, to completely black (no or very mild phenotype with a normal development of melanocytes as seen in the $Mitf^{mi\text{-}sp}$ allele) (Steingrimsson et al., 2004). The first interallelic complementation was shown in 1968, when it was shown that a cross of $Mitf^{mi}$ mice to mice carrying the $Mitf^{Mi\text{-}Wh}$ mutation resulted in mice that have no microphthalmia whereas homozygotes for each mutation ($Mitf^{mi/mi}$ and $Mitf^{Mi\text{-}Wh/Mi\text{-}Wh}$) have severe and intermediate microphthalmia, respectively (Konyukhov and Osipov, 1968). More recently, systematic matings of many *Mitf* mutations showed that this phenomenon is restricted to the $Mitf^{Mi\text{-}Wh}$ allele but is observed in combination with all other mutations at the locus. A model was proposed to explain the interallelic complementation associated with the $Mitf^{Mi\text{-}Wh}$ allele (Steingrímsson et al., 2003). This

model involves the alternative 6 amino acids that differentiate between the (+) and (-) versions of MITF, with the MITF(+) isoform having 20% more DNA binding ability for M and E-boxes than the MITF(-) isoform (Hemesath et al., 1994). In the wild-type situation, both isoforms go above a threshold of normal MITF activity. For *Mitf*$^{Mi\text{-}Wh}$ mutants, only the MITF$^{Mi\text{-}Wh}$ (+) isoform normally binds to DNA as heterodimer while the MITF$^{Mi\text{-}Wh}$ (-) isoform cannot, either as hetero- or homodimers. Moreover, the (-) isoform does not reach a threshold of activity where the protein has a phenotype-negative neomorphic effect, that could be explained by the regulation of new off-target genes, and thus explain the severe phenotype. Interestingly, interallelic complementation reduces the neomorphic effects of the MITF$^{Mi\text{-}wh}$ (-) isoform, resulting in more normal development and less severe phenotype. For example, the *Mitf* mutation called *Mitf*$^{Mi\text{-}vga9}$ has a severe phenotype, resulting in completely white mice with severe microphthalmia and with the stria vascularis of the cochlea lacking melanocytes (Tachibana et al., 1992). This allele results from a transgene insertion associated with a 882-bp deletion in the *Mitf* promoter (Hodgkinson et al., 1993). When *Mitf*$^{Mi\text{-}vga9}$ mice were crossed with *Mitf*$^{Mi\text{-}Wh}$ mice, the interallelic complementation was sufficient to rescue the size of the eyes, meaning that this combination was enough to reduce the neomorphic effect of MITF$^{Mi\text{-}Wh}$ (-) below the threshold of the negative effects.

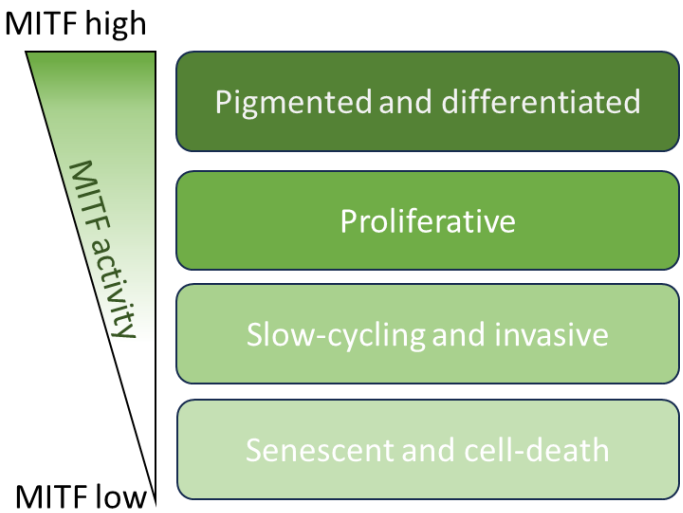

Figure 5. MITF rheostat model. This model shows what cell state the level of MITF activity is associated with. Adapted from Carreira et al., 2006, TBD.

As a conclusion, the range of phenotypes associated with *Mitf* mutations shows how important and central in melanocyte development this TF is. *Mitf* is required at many different stages of development of the pigment-producing cell, from the specification of NCC into melanoblasts (Opdecamp et al., 1997), to their migration for example (Nakayama et al., 1998), and the wide diversity of the impact of the different *Mitf* alleles that gives many different phenotypes depending on the *Mitf* mutation and stage of development underline the key role that *Mitf* plays for melanocyte development.

1.4.4 Role of MITF

MITF has been shown to regulate the expression of a vast panel of target genes involved in many processes like differentiation, proliferation, DNA-damage repair, metabolism, lysosome biogenesis, survival, senescence and invasion (Goding and Arnheiter, 2019). One of the mechanisms that *Mitf* regulates is pigment biosynthesis, a pathway that includes *Tyrosinase, Tyrosinase related protein 1 (Tyrp1)* and *Dct* by activating them through the M-box motif in their promoters (Lowings et al., 1992). These three genes encode enzymes that are directly involved in the production of melanin. However, MITF is not only involved in melanin production, but also in the many processes regulating melanosome biogenesis, transport, and ionic equilibrium. Indeed, MITF has been shown to directly regulate the expression of target genes such as *Pmel* (Baxter and Pavan, 2003) and *Melanoma antigen recognized by T cells 1* (*Mlana)* (Du et al., 2003) which code for proteins involved in melanosome maturation and structure. Interestingly, the small GTP-binding protein RAB27A involved in the transport of melanosomes has also been shown to be a direct target of MITF (Chiaverini et al., 2008).

The promoters of the anti-apoptotic proteins B-cell leukemia/lymphoma 2 protein (BCL2) (McGill et al., 2002) and Baculoviral IAP Repeat Containing 7 (BIRC7) (Dynek et al., 2008) have also been shown to be direct targets of MITF, suggesting that MITF also has an effect on regulation of apoptosis and survival of melanocytes. Moreover, cell-based work on melanoma and melanocytes have revealed that suppression of MITF leads to a reduction of the autophagy induced by starvation, and overexpression of MITF increased the number of autophagosomes (Moller et al., 2019). Thus, these results revealed that MITF is involved in regulating the starvation-induced autophagy and lysosomal activity.

Also, MITF has recently been shown to be a repressor of ECM and focal adhesion as the suppression of MITF lead to increased expression of genes involved in these processes (Dilshat et al., 2021). Moreover, MITF has also been linked to cell invasion. Indeed, when MITF was depleted in melanoma cells it promoted invasion (Carreira et al., 2006; Cheli et al., 2010). However, another study showed the opposite with MITF depletion not inducing invasion, which is suggested to be due to translational reprogramming that drives expression of genes involved in invasiveness (Falletta et al., 2017).

MITF has been shown to be positively regulating DNA repair through BRCA1, AURKB and TERT (Strub 2011). Interestingly, depletion of MITF in melanoma cell lines lead to cell cycle arrest as well as senescence (Giuliano et al., 2010; Strub et al., 2011; Wellbrock and Marais, 2005). The cell cycle arrest induced by MITF depletion can be explained by the fact that MITF has been shown to regulate the expression of many of the cell cycle regulators called Cyclins and their targets, the Cyclin-Dependent Kinases. Amongst the most important cell cycle genes that are regulated by MITF are the Cyclin-Dependent Kinase 2 (CDK2) and 4 (CDK4) (Garraway et al., 2005; Wellbrock and Arozarena, 2015). Regulation of CDK2 by MITF is important for the transition from G1 to S-phase of the cell cycle (Du et al., 2004). MITF also regulates the expression of CDK4, a critical factor for the cell cycle to progress (Loercher et al., 2005). During this progression of the cell cycle from G1 to the replication phase, Cyclin-D1 (CCND1) is required and forms a complex with CDK4 (Malumbres and Barbacid, 2009; Sherr et al., 2004). Interestingly, CCND1 has been associated as a key prognosis factor in melanoma patients and is a potential target for melanoma therapy (González-Ruiz et al., 2020). MITF was also shown to indirectly reduce the expression of CDKN2B (Carreira et al., 2006) or activate CDKN1A in cooperation with Retinoblastoma protein (RB1) (Carreira et al., 2005). This data suggests that MITF is a major regulator of the cell cycle, but MITF seems to be able to promote both cell cycle progression and its repression.

The rheostat model of MITF was suggested by Carreira et al (2006) to explain this contradiction as it explains the dual role of MITF in cell cycle but also the different states that a melanocyte cell can go through (Figure 5). In this model, high activity of MITF is associated with differentiation, but progressive reduction of this activity leads first to proliferation, then to dedifferentiation and increased invasiveness and finally to senescence and eventually cell death. Indeed, with all the evidence that has been gathered so far about the many roles of MITF in the broad processes that have been discussed above, MITF activity seems to be a key and major player in the biological phenotype of melanocytes and for their development. *Mitf* expression and activity is thus crucial for the expression of the previously cited genes and processes. Many of the direct target genes of MITF in the different biological processes and its physiological role that have been enumerated come from studies performed in melanoma tissue and melanoma cell lines, but less is known about its role during melanocyte development.

1.4.5 Melanoma and MITF

Melanoma is the deadliest form of skin cancer and arises from melanocytes. There are three types of melanomas based on localization in the body: uveal melanoma if it is located in the ocular stroma, mucosal melanoma if arising from melanocytes of the mucous membrane and cutaneous melanoma if it originates from melanocytes located in the epidermis of the skin. Cutaneous melanoma represents the largest proportion of these three types (Chang et al., 1998) and is related to UV exposure from the sun that

humans are continuously exposed to (Koh et al., 1996). Somatic mutations involved in melanoma appearance are mainly in the gene *V-raf murine sarcoma viral oncogene homolog B1* (*BRAF*), *Neuroblastoma ras viral oncogene homolog* (*NRAS*) and *Neurofibromin 1* (*NF1*). *BRAF* somatic mutations represent the vast majority of mutations occurring in melanomas with more than 50% of patients carrying a somatic *BRAF* mutation (Davies et al., 2002). BRAF is part of the MAPK/ Extracellular signal-regulated kinase (ERK) signaling pathway that has been shown to be important for cell growth regulation (Wan et al., 2004). The specific mutation of Glutamic Acid in position 600 to Valine ($BRAF^{V600E}$) represents almost 90% of all *BRAF* mutations in melanoma and leads to the hyperactivation of the ERK pathway as compared to WT BRAF (Wan et al., 2004). This mutation results in the constitutive activation of BRAF and thus, inducing melanoma progression by reducing MITF expression (Wellbrock and Marais, 2005), but also by acting as an oncogene by stimulating proliferation and survival of melanoma cells (Hingorani et al., 2003; Karasarides et al., 2004). *NRAS* mutations are found in approximately 10% of melanoma patients and activate the same pathway. Mutations in *NF1* also activate the MAPK pathway (Papp et al., 1999). Finally, somatic mutations in some of the cell cycle genes previously described including RB1, CDK4, CCND1 have been found in acral (on hands and feet) or mucosal melanomas (Kong et al., 2017; Sauter et al., 2002).

Germline mutations are found in a number of genes, mostly genes involved in regulation of the cell cycle. For example, mutations in *Cyclin Dependent Kinase Inhibitor 2A (CDKN2A)* represent around 40% of familial melanoma cases (Goldstein et al., 2007; Petronzelli et al., 2001). *CDKN2A* codes for the two proteins $p16^{INK4a}$ and $p14^{ARF}$ that play a role respectively in the G1 to S-phase transition (Fountain et al., 1992; Koh et al., 1995) and degradation of p53 (Stott et al., 1998), have shown to be at risk of forming melanoma. There are also other genes involved in familial melanomas such as CDK4, a cell cycle regulator, and in the *TERT, POT1, ACD*, and *TERF2IP* genes but the proteins encoded by these genes are all involved in telomere length control. Similarly, rare familial cases have been found harboring mutations in *BAP1, RAD51B* and *POLE* genes, all of which encode DNA repair proteins (Bertrand et al., 2020).

Genome-Wide Association Studies (GWAS) using Single Nucleotide Polymorphism (SNP) arrays have shown that MITF copy number is amplified in 20% of melanomas, which suggests that MITF is involved in the promotion/maintenance of the melanoma tumor and in its metastases (Garraway et al., 2005). Suppression of MITF in melanoma cells led to reduced tumor growth and delayed formation of melanoma (Hoek et al., 2008). MITF has thus been proposed first as a lineage specific "survival oncogene" (Garraway et al., 2005) and now as full-scale oncogene as MITF has been shown to be involved in other cancer types like Renal Carcinoma (Bertolotto et al., 2011) and gastrointestinal tumor growth (Proaño-Pérez et al., 2023). However, MITF has also been shown to have an opposite role in the case of development of metastases. The oncogenic $BRAF^{V600E}$ mutation activates the MAPK/ERK signaling pathway, and is

thought to reduce MITF levels and thus being an important factor for the progression of BRAF-positive melanoma into metastatic cells (Wellbrock and Marais, 2005). This data fit the previously mentioned rheostat model (Carreira et al., 2006) where high MITF activity leads to proliferation or differentiated state and so to maintenance of melanoma cells, whereas low MITF activity leads to invasive and thus metastatic-like melanoma cells. A recent study confirmed that this state would more likely be a de-differentiated state of the cell (Vlčková et al., 2018) and then another study also showed that this dedifferentiated state can be split in two different states depending on MITF and other factors (Rambow et al., 2018). These other factors, such as AXL and POU3F2, are also important in this process. Indeed, POU3F2which is often expressed in melanoma cells and is a direct target of $BRAF^{V600E}$, has been shown to reduce MITF levels (Thomson et al., 1995; Thurber et al., 2011). Also, highly invasive and drug resistant melanomas have been characterized with high AXL, thus with an expression inversely correlated to MITF, suggesting the role of AXL in the invasive state of melanoma (Boshuizen et al., 2018; Müller et al., 2014).

1.4.6 Role of *Mitf* during development

As one of the most important key regulators of melanocyte development, *Mitf* plays a crucial role in the establishment of the pigment-producing cells. *Mitf* is first expressed around E10.5, first in the head region and later in the tail region and drives the expression of *Dct* a few hours later when cells have already started migrating (Nakayama et al., 1998). MITF has been often called the master regulator of melanocytes development. The coat color defects, microphthalmia and osteopetrosis show that *Mitf* is necessary for the establishment of melanocytes and function of both RPE cells and osteoclasts (Steingrimsson et al., 2004). Indeed, MITF is present throughout the development of melanocytes, from the initiation of the specification of melanoblasts, to their migration and later in the pigment-producing process in the formation of the first hair.

During development, MITFhas also been specifically shown to be important for the growth and survival of melanoblasts. For example, MITF is involved in cell survival through regulation of BCL2, a protein that inhibits apoptosis (McGill et al., 2002; Veis et al., 1993). In melanoblasts, MITF has been shown to regulate the expression of important genes like *Cdk2* (Du et al., 2004), *Cdk4* (Loercher et al., 2005), *Cdkn1a* (Šestáková et al., 2010) and *Ccnd1* (Strub et al., 2011). Indeed, depletion of MITF induced cell cycle arrest in melanoblasts (Carreira et al., 2005), and this can be explained by regulation of MITF to the promoter of these cell cycle genes. However, even though MITFseems to be a crucial and key regulator of the development of melanoblasts, some other key players, interacting with MITFmight be of importance in this process and need to be unraveled.

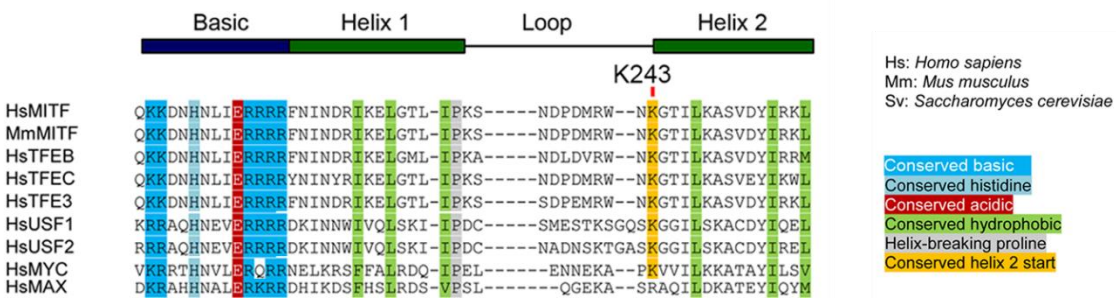

Figure 6. The *Mitf*^{K243} amino acid is highly conserved between bHLH transcription factor and species. Figure obtained with permission from Molecular Cell journal, according to permit number TBD (Louphrasitthiphol et al., 2020)

1.4.7 Regulation of *Mitf* expression

The expression of *Mitf* needs to be tightly regulated by different signaling pathways and other transcription factors. Some transcription factors such as SOX10, PAX3, LEF1, CAMP Responsive Element Binding Protein 1 (CREB1) and ONECUT2have been shown to positively regulate *Mitf* expression. In chapter 1.3.3. we explained that SOX10 has a crucial role during the specification of NCC to melanoblasts (Hou et al., 2006). SOX10 is also required for the formation, growth and maintenance of melanoma (Shakhova et al., 2012). Moreover, SOX10 has been shown to directly bind the *Mitf* promoter, in collaboration with PAX3 and leads to increased MITF expression (Lee et al., 2000); SOX10 is highly expressed in melanoma where it is involved in initiation and maintenance of the tumor (Cronin et al., 2013). ERK-mediated phosphorylation inhibits activation of SOX10 transcription (Han et al., 2018). On the other hand, POMC signaling uses the Cyclic adenosine monophosphate (cAMP) and cooperates with SOX10 to activate expression of MITF (Huber et al., 2003). PAX3 has been shown to regulate both expression and activity of *Mitf* during melanocyte development (Galibert et al., 1999), but also plays a role in maintenance of the undifferentiated state of the melanocyte stem cells by competing with MITF for binding to an enhancer region of *Dct* (Lang et al., 2005). Interestingly, PAX3 and SOX10 were shown to cooperate by synergistically activating MITF expression (Bondurand et al., 2000). The WNT/β-catenin signaling pathway is important for the transition from NCC to melanoblasts during development, through activation of the *Mitf* promoter by LEF1 binding (Dorsky et al., 2000). Finally, MITF can cooperate with LEF1 to bind to its own promoter to autoregulate its expression (Saito et al., 2002).

A few TFs have been reported to repress MITF expression, including the Glioma associated oncogene family member 2 (GLI2), Activating Transcription Factor 4 (ATF4) and FOXD3. GLI2, a TF target downstream by the Hedgehog signaling pathway (Javelaud et al., 2011) that can also be regulated by the TGF-β signaling pathway (Dennler et al., 2007), is involved in the inhibition of *Mitf* transcription (Pierrat et al.,

2012). Interestingly, high levels of GLI2 have been correlated with increased invasive and metastatic melanoma, with expression levels inversed to that of MITF (Javelaud et al., 2011). ATF4 is another TF that has also shown to inhibit *Mitf* expression through direct transcriptional repression (Falletta et al., 2017). Also, FOXD3 can repress the transcription of PAX3, a transcription activator of *Mitf* expression, and thus indirectly the expression of *Mitf* (Thomas and Erickson, 2009). This repression has been shown to happen when the NCC develops along a neurogenic fate through the ventral pathway. Additionally, FOXD3 might be involved, partially, in BRAF resistance by inhibiting *Mitf* expression (Abel et al., 2013).

1.5 Acetylation and *Mitf*^{K243R} mutation

A recent study by Louphrasitthiphol et al. (2020) showed that the presence of either CBP or p300 increased MITF acetylation. Moreover, they showed that activation of MAPK signaling results in increased MITF acetylation. Also, they performed mass spectrometry to show that residues Lys21, Lys33, Lys43, Lys243 and Lys248 (Louphrasitthiphol et al., 2023; Louphrasitthiphol et al., 2020) were all acetylated. They focused on Lysine in position 243 (*Mitf*^{K243}) of MITF-M as its molecular modelling showed the high probability of its acetylation affecting the interaction between MITF and the phosphate backbone. This residue is a highly conserved residue of both MITF and other bHLH motif family members (Figure 6). They proposed that acetylation of *Mitf*^{K243} plays a role in affecting the affinity of MITF to DNA. They mutated *Mitf*^{K243} into either Arginine that cannot be acetylated, or Glutamine that may be used as a mimic of acetylatable Lysine, (Fujimoto et al., 2012; Kim et al., 2006) and then used *in vitro* fluorescence anisotropy to show that this Lysine is indeed involved in DNA binding. Each mutation resulted in reduced DNA binding affinity to M and E-boxes, with the *Mitf*^{K243Q} mutant even less effective than the *Mitf*^{K243R} mutation. However, the in *vivo* study they performed in zebrafish revealed that, inversely to their in *vitro* study, zebrafish expressing the *Mitf*^{K243Q} mutation developed melanocytes whereas the *Mitf*^{K243R} mutant did not. Interestingly, all subcutaneous-inoculated grafts of melanoma cell lines in athymic nude mice with the *Mitf*^{K243Q} mutation resulted in tumor formation while none did with the *Mitf*^{K243R} mutant cell lines, suggesting the important role of *Mitf*^{K243} acetylation in melanoma formation. ChiP-seq data on 501mel melanoma cell lines expressing the wild type and mutant versions of MITF revealed that cells carrying the *Mitf*^{K243R} mutation exhibit less binding to known MITF target genes. Therefore, the results suggest that *Mitf*^{K243} of MITF is involved in the binding to DNA (Louphrasitthiphol et al., 2020). The fact that MAPK signaling regulates p300 activity and that WT MITF and MITF with *Mitf*^{K243Q} mutation can form tumors strongly suggests that acetylation is an important mechanism in melanoma formation. Moreover, although WT MITF and MITF with the K243Q mutation were involved in developing melanocytes and forming melanoma tumors, this was not the case with MITF carrying the K243R mutation. Also, the *Mitf*^{K243R} mutant has been shown to bind to low-affinity binding sites and the authors

of the paper suggested that this would also result in reduced availability of MITF to bind to its key regulatory elements.

However, these results on the binding capacity of the $MITF^{K243R}$ protein do not inform about the effects on the target genes, or the phenotype that such a mutation would result in a living organism such as cells or mice. The goal of this project was thus to create and characterize this mutation both *in vivo* and in an *in vitro* system to get more insights into the effect of this mutation.

2 Aims

2.1 Characterization of an inducible *Mitf*^{K243R} mutant mouse model

1. Generation of the *Mitf*^{K243R} mouse model with the Tyr::Cre or the Tyr::CreER^{T2} induction systems to activate the constitutive and hypomorphic mutation in melanocytes

2. Characterize the phenotype of the *Mitf*^{K243R} mutation in mice

2.2 Effects of the *Mitf*^{K243R} mutation in primary melanocyte cell lines *in vitro*

3. Generation and characterization of primary melanocytes carrying the inducible *Mitf*^{K243R} mutation

4. Investigating the effects of the inducible *Mitf*^{K243R} mutation on function and gene expression.

3 Materials and Methods

3.1 Generation of mice carrying the *Mitf*^{K243R} mutation

The mouse *Mitf*^{K243R} mutation was created in collaboration with Lionel Larue's lab at the Institut Curie, Paris, France. Briefly, the mutation was created by changing the adenosine in position 728 of the MITF-M cDNA into a guanosine (c.728A>G). This mutation is located in exon 8 of MITF in a cassette containing both exons 8 and 9 of the *Mitf-m* transcript. This mutation changes the 243rd codon of MITF-M from AAG (Lysine) to AGG (Arginine) (Figure 7A). The cassette was then introduced into the *Mitf* genetic locus in ES cells, right after the wild-type exons 8 and 9 (Figure 7A). The cassette is also flanked by two LoxP sites. The resulting ES cells were used to generate mice and the mutant mouse strain was crossed with either C57BL6/J Tyr::Cre mice (Delmas et al., 2003) to induce the mutation in all melanocytes or with Tyr::CreER^{T2} mice to induce the mutation only in presence of Tamoxifen. In both cases, when the Cre enzyme is expressed or activated the wild-type exons will be removed and all remaining transcripts will contain the *Mitf*^{K243R} mutation (Figure 7A). As the mutation can only occur in cells expressing *Tyrosinase,* the mutation is conditional or constitutive in melanocytes only. The *Mitf*$^{K243R/K243R}$ mice were also crossed with C57BL/6J- Dct::LacZ mice (Mackenzie et al., 1997) in order to trace the fate of melanocytes upon MITF loss. Dct::LacZ mice express β-galactosidase only in melanocytes since the Dct promoter only drives expression in these cells.

3.2 Genotyping of the transgenic mice

All mouse work was performed in the animal facility of ArcticLAS in Reykjavik in compliance with relevant laws and regulations about animal care standards. We adhered to National regulation nr. 460/2017 about protection of animals used for scientific purpose, which are based on the national law on animal welfare nr.55/2013. The Icelandic regulation on animal experiments is based on the European directive 2010/63/EU. Experiments were previously approved by MAST under the license number 2018-05-02 for general use of mice and case 2108488, Oct 4, 2021 for experiments on mice with Tamoxifen.

Animals were genotyped using samples collected from ear clips from newborn animals and from the yolk sacs of embryos. DNA was extracted from the samples in a digestion mix containing 16 mM of Ammonium Sulfate ($[NH_4]_2 SO_4$), 67 mM of Tris-HCl pH 8,8, 0,05% [v/v] of Tween-20 and 200 ng of Proteinase K (NEB, #P8017S) in deionized

water. After digestion at 55°C for at least 3 hours Proteinase K was inactivated by incubating at 95°C for 20 minutes after which the samples were cooled down on ice.

The oligonucleotide primers used for genotyping of the mice are listed in Table 1. The protocol used was previously described for the following transgenes: Dct::Lacz (Mackenzie et al., 1997), Tyr::Cre (Delmas et al., 2003), the X-chromosome without the Tyr::Cre transgene (Colombo et al., 2007), Tyr::CreER^{T2} (Yajima et al., 2006) and sex determination (Lambert et al., 2000). Primers were designed for genotyping of the *Mitf*^{K243R} mutated animals and cells.

Table 1: Primers used for PCR amplification of genomic DNA

Target gene	*Primer name*	*Sequence (5'-3')*	*Tm (°C)*	*Amplicon size*
Mitf ^{K243R}	*Mitf*Lf39-F *Mitf*Lr39-R	CCAGTGACTAAGTCTTTATAGTTCCAGG CAATTAGTGCTCACCCCACATTGGC	58 63	WT = 257 bp *Mitf* $^{+/+}$ =337 bp *Mitf* $^{K243R/K243R}$ = 350 bp
Dct::LacZ	DctLacZ-F DctLacZ-R	CAGGACACGGCTTGTCATCATGGTGT CATTCATCGTCTCTCAGGAATTCA	66 56	450 bp
Tyr::Cre	TyrCre-F TyrCre-R	GTCACTCCAGGGGTTGCTGG CCGCCGCATAACCAGTGA	64 61	473 bp
Tyr::CreER^{T2}	TyrCreER^{T2}-F TyrCreER^{T2}-R	GAAGCA ACTCATCGATTG TGAAGGGTCTGGTAGGATCA	50 57	411 bp
X-chr	LL1433 LL1441	TTCTGTTTGTGAATACCTGCAA TTGAGGGACTTC TGATATTGTAAG	59 60	1172 bp
Sry *Il3*	mSryF mSryR mIl3F mIl3R	TGGGACTGGTGACAATTGTC GAGTACAGGTGTGCAGCTCT GGGACTCCAAGCTTCAATCA TGGAGGAGGAAGAAAAGCAA	69 56 60 60	544 bp 402 bp

3.3 Hair preparation

Hair from Tyr::CreER^{T2}/0, Dct::LacZ/0 and from black, grey and white areas of *Mitf*$^{K243R/K243R}$; Tyr::Cre mice were harvested. They were placed on microscopy slides that had previously been covered in white egg and dried at RT for 2 hours. The slides were then placed in successive baths of ethanol, 50% [v/v] methanol and 50% [v/v] xylene, and pure xylene for 24 hours each. The slides were finally covered with mounting medium and a cover slide. Pictures were taken using the EVOS imaging system.

3.4 Quantification of the optical absorbance of melanin in mouse hairs

Hairs were plucked from dorsal parts of Dct::LacZ/0 (positive control), *Mitf*$^{Mi\text{-}Wh/Mi\text{-}Wh}$ (negative control) and the black, grey and white areas of *Mitf*$^{K243R/K243R}$; Tyr::Cre/Y (or

Tyr::Cre/Tyr::Cre for females) mice. For each genotype, three mg of hairs were weighed and solubilized in one mL NaOH for three hours at 85°C with slight shaking. After centrifugation at 12,000 rpm for 5 min, absorbance at 470 nm was measured in 96-well plates.

3.5 Whole mount β-galactosidase staining of embryos and melanoblast quantification

We harvested embryos from *Mitf*$^{K243R/K2432R}$; Tyr::Cre; Dct::LacZ/0 mice at E13.5, E14.5 and E15.5. The timing was done by checking for vaginal plugs every morning after the matings were set up (Behringer, 2016). Vaginal copulation plugs indicate that the mating has occurred during the previous night, and that most likely a pregnancy will be a result. Observation of morning plugs were considered at 12 hours after fertilization or day E0.5. The embryos were allowed to develop until the desired stage. The embryos were then surgically removed from their mother. After a brief wash in ice cold PBS, the embryos were fixed in fresh 4% [w/v] PFA on ice for 40 min and rinsed for 10 min in ice-cold PBS. Then the embryos were placed in permeabilization buffer (2mM of $MgCL_2$, 0.01% [w/v] of sodium deoxycholate and 0.02% of NP-40) two times for 30 min each with ice-cold PBS washes in between. We then placed the embryos in X-gal staining solution (2mM of $MgCL_2$, 0.01% [w/v] sodium deoxycholate, 0.02% [v/v] NP-40, 5 mM $K_4[Fe(CN)]_6$, 5 mM $K3[Fe(CN)]_6$, and 0.04% [w/v] X-gal) overnight at 30°C. After post-fixation in 4% [w/v] PFA and several washes in PBS, we took pictures under a stereoscopic microscope. Finally, the number of melanoblasts were quantified as follows: on each embryo, an area 400x1000 pixels in size, extending from the back to the belly on the side of the embryo, and parallel to the front limb, was drawn and cropped. The number of melanoblasts was manually counted by hand using the Cell Counting tool in ImageJ and their numbers plotted using the Prism GraphPad software.

3.6 Cryopreservation and sectioning of embryos

Embryos were collected from the desired matings and then fixed in 4% [w/v] PFA overnight at 4°C. After three washes in fresh PBS for 5 minutes each, the embryos were placed in 30% [w/v] sucrose in PBS solution (to preserve the tissues when freezing) at 4°C until they sank to the bottom of the 15 mL tube. They were then transferred to a mixture of 30% [w/v] sucrose and 50% [v/v] Optimal Cutting Temperature solution (OCT) compound for 16 hours at 4°C. Finally, after a quick bath in 100% OCT to remove the remaining sucrose, the embryos were transferred to a plastic cassette filled with OCT and frozen for a few minutes in dry ice. The frozen blocks of OCT were stored in a -80°C freezer before sectioning. Embryos embedded in frozen OCT were put in a -20°C freezer a few hours before sectioning on a cryostat at a 10 µm thickness. The sections were placed on SuperFrost adhesive slides and dried overnight and then stored at -80°C or used immediately for immunostaining or imaging in the case of the

β-galactosidase-stained embryos. Pictures were taken using the EVOS imaging system and analyzed using the ImageJ software.

3.7 Primary cell line generation and cell culture

Melanocyte cell cultures were generated from 1–3-day old pups, sacrificed according to the ethical protocol by decapitation, as previously described (Berlin et al., 2012). Briefly, a skin sample was taken from the trunk region and washed in 70% [v/v] ethanol before moving the sample to ice cold PBS. The skin samples were cut into small pieces and then incubated in a 1:1 mixture of collagenase I and IV (Gibco, USA) in PBS at 37°C for 25-50 minutes. The skin samples were then washed in Washing Buffer composed of Hank's Balanced Salt Solution [HBSS] supplemented with calcium and magnesium (Gibco, USA), 0.005% [v/v] DNase I and 20% [v/v] Fetal Bovine Serum (FBS). The skin samples were dissolved in Disassociation Buffer (Gibco, USA), transferred to a 6 well plate and incubated at 37°C for 10 minutes. The cells were then disassociated by passing first through 18G and then 20G needles. The cells were washed in Washing Buffer. Then 10^6 cells were plated per well in 6 well plates and cultured in Ham's F12 media (Gibco, USA) supplemented with 10% [v/v] FBS, 100 U/mL Penicillin-Streptomycin (Gibco, USA) and 200 nM 12-O-tetra-decanoylphorbol-13-acetate (TPA, Sigma-Aldrich, USA) at 37°C and 5% CO_2. The media was changed every day for the next two days and then three times per week. The selection of melanocytes from fibroblasts was done by adding 25 µg/mL G418 (Gibco, USA) to the media on day 2 after plating and culturing the cells in its presence for approximately 5 weeks. It took approximately 16 weeks for melanocytes to start proliferating. When reaching between 90 to 100% confluency, the cells were detached from the flasks with 1X trypsin for 5 min at 37°C. After addition of Ham's F12 medium with FBS to inactivate the trypsin, the cells were counted on a glass hemocytometer and were then ready for further experiment. The newly generated cell lines and the animals they were derived from are listed in Table 3 in chapter 4.2.1.

3.8 Induction of the *Mitf*$^{K243R/K2432R}$ mutation

Induction of the mutation was performed in the newly generated melanocyte cell lines which carry the *Mitf*$^{K243R/K2432R}$; Tyr::CreER^{T2}/0 genotype. These cells express the Cre recombinase fused to the ligand binding domain of the estrogen receptor. The fusion protein is inactive until the estrogen-mimic Tamoxifen is added which then leads to an active Cre recombinase. Cre activity can be stimulated by adding 4-Hydroxytamoxifen (4-OHT), the active metabolite of Tamoxifen which normally is activated *in vivo* through metabolism in the liver. For inducing the mutation in melanocytes, the cells were cultured in Ham's F12 medium containing 5 µg/ml of 4-OHT, added from a 10 mg/ml stock solution (solubilized in methanol). As mock vehicle control, medium with the same volume of methanol was added to the cells. To assess if the recombination had occurred, the primers for genotyping the *Mitf*^{K243R} mutation in mice were used (Table 1).

The PCR products were run on a 3% [w/v] agarose gel for 90 min to ensure separation of the fragments as the difference of base pairs between the *Mitf*^{K243R} mutant and WT is only 13 bp (see below).

3.9 Sanger sequencing

PCR amplicons generated as described in chapter 3.8 were purified with a GeneJET PCR purification kit (#K0701). Briefly, 1:1 volume of Binding Buffer was added to the PCR product mix and then a 1:2 volume of isopropanol. The mix was then transferred into a GeneJET purification column and centrifuged. Then, 700 µl of Wash Buffer were added into the column and centrifuged two times. Finally, the purified DNA was eluted with 50 µl of Elution Buffer into an Eppendorf tube. All centrifuge steps were performed at 14,000 g for 1 minute. The purified DNA samples were then shipped to GENEWIZ for Sanger sequencing.

3.10 Growth assay

Cells were seeded in a 96 well plate at a confluency of 10,000 cells per well in triplicates and were allowed to settle overnight. The day after, the cells were treated with either 4-OHT to induce the *Mitf*^{K243R} mutation or Methanol as a control. Cells were also treated with TPA or Methanol to assess the effect of TPA on the growth of the cells. The cells were incubated in the Incucyte imaging system in a cell culture incubator and pictures of the cells taken every 2 hours for a week. The Incucyte software was then used to measure cell confluency by using masks that allow the software to designate what is a cell and what is not. Growth curves were then generated and the time necessary for cells to double was calculated between 48 and 96 hours when the change of the growth phenotype was in a log-phase. The formula used to calculate the doubling time was the following: Duration x ln(2) / ln(Final Confluency – Initial Confluency).

3.11 Apoptosis assay

Cells were seeded in a 96-well plate with 5,000 cells per well in triplicate. The cells were allowed to settle for two hours with fresh Ham's F12 with 10% [v/v] FBS and 200 nM TPA, and then incubated in the same medium supplemented with Incucyte Caspase-3/7 Green reagent (Essen BioScience) at 1:1,000 dilution with a final concentration of 5 µM, and either 5 µM of Methanol (control) or 5 µM 4-OHT. The Incucyte imaging system then took pictures every two hours for 96h, both bright-field and fluorescent. The Incucyte software was used to generate masks to measure the number of fluorescent objects corresponding to the number of apoptotic cells. Finally, the Apoptotic Index was calculated by dividing the number of apoptotic cells by the confluency and compared between the conditions.

3.12 Immunostaining

The cells were seeded in 8-chamber tissue culture slides (Falcon) with 5,000 WT MITF (3922) treated for methanol or 4-OHT or *Mitf*^{K243R} treated with methanol. For the *Mitf*^{K243R} cells induced by 4-OHT, 20,000 were seeded to compensate for cell death. Treatment duration for both methanol and 4-OHT was 96h. After the media was removed, cells were incubated with 4% [w/v] PFA for 10 min to fix them and then with 0,1% [v/v] Triton X-100 for permeabilization. Cells were then incubated in blocking buffer made of 3% [w/v] BSA diluted in PBS for 30 min and then stained for 2h at RT with the primary antibody directed against Vimentin (rabbit, Cell Signaling, dilution 1/250) in antibody buffer (3% [w/v] BSA + 0,3% [v/v] Triton X-100 in PBS). After three washes in PBS, the cells were stained with the secondary goat anti-rabbit IgG antibody coupled with Alexa Fluor 488nm (Invitrogen, dilution 1/1,000) followed by 0.5 µg/ml Dapi in PBS for 5 min. After a last wash, the slides were mounted with Fluoromount-G (ThermoFischer Scientific) and covered with a coverslide and imaged on the EVOS imaging system.

3.13 Single cell migration assay

Cells were seeded in 6-well plates coated with fibronectin (20 µg/mL, overnight at 4°C and washing with PBS two times), at a low density of 5,000 cells per well to allow them to have space for single-cell migration. The cells were allowed to settle overnight in Ham's F12 with 200 nM TPA and 10% [v/v] FBS. The day after, the media was changed with fresh Ham's F12 with 10% [v/v] FBS but no TPA, and with either 5 µM of 4-OHT (1/2,000 of a 10 mM stock solution) or with Methanol (1/2,000 as a control). The plates were then placed in the Incucyte imaging system and pictures were taken every 30 min for 48h with a 10X objective. The pictures were transferred to the software ImageJ, and the Manual Tracking plugin used to generate trajectories of the cells. The coordinates of each cell and each time point were then used in the "Chemotaxis and Migration Tool" provided by Ibidi. In this software, we were able to create the cell's trajectory spider plot and get the following metrics out of every cell's migration: velocity (speed), Euclidean distance (distance between starting to end point) and accumulated distance (total distance).

3.14 Transwell invasion assay

Plates, with inserts containing a membrane of 8 µm pore size, were coated with the ECM-based hydrogel Matrigel (Corning) for one hour on top of the membrane. Then 10,000 cells were resuspended in Ham's F12 without FBS and seeded in the upper chamber of the insert. Ham's F12 medium with 10% [v/v] FBS was then added to the lower chamber of the plate and was used as the chemoattractant. The plates were incubated for 48h at 37°C and 5% CO_2. Both upper and lower chambers also contained either methanol as control or 5 µg/ml 4-OHT. Cells that migrated to the other side of the membrane were fixed in cold methanol and stained in 300 µl of 0,2% [w/v]

crystal violet solution for 20 min. Then, cells on the top of the membrane were removed with a cotton swab and the inserts washed as many times as needed to remove all the remaining crystal violet. The remaining stained cells located in the lower part of the membrane were allowed to dry for 30 min. Finally, pictures of the stained cell were taken using the EVOS imaging system, and the cells counted manually.

3.15 Flow cytometry

Approximately 50,000 WT or *Mitf*^{K243R} mutant cells were seeded in 6-well plates and treated with methanol. As the *Mitf*^{K243R} mutant cell lines tend to die after 4-OHT treatment, approximately 3 times more cells (150,000) were seeded in order to compensate for cell death after the 4-OHT treatment and seeding 50,000 cells was not enough for reliable results. After the cells were allowed to attach overnight, they were treated with either methanol or 4-OHT for 120h (5 days). After treatment, we collected the medium from every well to harvest floating and adherent cells. After centrifugation at 300 g for 5 min, the supernatant was removed, and the cells were washed and resuspended in PBS. These steps were repeated a second time. After a final centrifugation at 300 g for 5 min, the cells were resuspended in 1 mL of Vindelöf/7-AAD solution (20 mM of Tris pH 7,6, 100 mM NaCl and 0,1% [v/v] NP-40 filter sterilized before adding 20 µg/mL RNAse and 1 µg/mL of 7-AAD). 7-aminoactinomycin D (7-AAD) is a fluorescent intercalator of DNA that can be excited at 488 nm and has an emission peak of 647 nm under flow cytometer. The cells were incubated in this solution at 37°C for 30 min and protected from the light. After incubation, the samples were stored on ice until they were loaded on the flow cytometer (Attune NxT from Invitrogen). The cells were characterized using visible light diffraction either the Forward-scattered (FSC), detected along the path of the laser to analyze the size of the cells, and on the side for the Side-Scatter (SSC), detected at 90° angle relative to the laser, to analyze the granularity of the cells. The cells were also excited by a laser at 488 nm and the emission light analyzed was 647 nm. Analysis of the results was done using the software FlowJo. By using the FSC on the X-axis and the SSC on the Y-axis, we were able to remove the debris and focus only on the cells. Then, we used the FSC-Area on the X-axis and the FSC-Height on the Y-axis to keep only single cells. Finally, the intensity of the 7-AAD staining was set-up on the X-axis and presented as histogram for the Y-axis. This last graph is the one presented in the results sections.

3.16 RNA extraction for sequencing

We selected three cell lines carrying the *Mitf*$^{K243R/K2432R}$ mutation (#4774, #4775 and #4776) and one Tyr::CreER^{T2}/0 (#3922) cell line as a control (Table 2) to use for RNA sequencing. The cells were seeded at a density of 100,000 per well in triplicate and allowed to settle overnight. The following day, the first time point was harvested for each of the four different cell lines and was considered as the 0 hour time-point and did not receive any treatment. The remaining wells were treated with 5 µg/ml of 4-OHT

for 48 hours (second time-point) or 72 hours (third time-point) before being harvested. RNA extraction was done using the Quick-RNA Miniprep extraction kit (Zymo Research, R1055). Briefly, cells from each well were harvested in 600 µl RNA Lysis Buffer and centrifuged through the Spin-Away Filter and the flow-through saved for the next step. Then 600 µl of 100% [v/v] ethanol were added and then centrifuged into a Zymo-Spin IIICG column. The column containing the RNA was then washed with RNA Wash Buffer and centrifuged. Then, the columns were incubated with 5 µl DNase I (1 U/µl) into 75 µl of DNA Digestion Buffer at room temperature for 15 minutes. Following this, 400 µl of RNA Prep Buffer were added and centrifuged. Then 700 µl of RNA wash buffer were added and centrifuged and this step was repeated with 400 µl of RNA Wash Buffer. Finally, RNA was eluted from the column by centrifuging the column with 50 µl of DNase/RNase-free Water. All the centrifugation steps were performed at 15,000 g. All the samples had an RNA Integrity (RIN) score above 9. The RIN score indicates intactness of the RNA, with 1 being very degraded and 10 fully intact RNA. The RIN score is calculated by the ratio of the 18S to the 28S ribosomal RNA concentrations. The samples were then shipped to the sequencing company Novogene, UK, for sequencing.

3.17 RNA sequencing analysis

First, Trimmomatic (Bolger et al., 2014) version 0.39 was used to clean the obtained FASTQ files. Then, quantification of gene expression was done with Kallisto (Bray et al., 2016; Pimentel et al., 2017) version 0.46.1 using default parameters, the human transcriptome annotation GRCh38 from Ensembl as the reference and the cleaned FASTQ files as input. Next, we used DESeq2 (Love et al., 2014) to determine statistically significant differentially expressed genes (DEGs) across experimental conditions using cutoffs of Log2FC>1 and adjusted P-value (P-adjust)<0.05. From downstream analysis with the significant DEGs, we performed Gene Set Enrichment Analysis (GSEA), a method that assesses for the statistical difference of the DEGs according to defined set of genes, and between different biological phenotypes or states.

We also performed an Interaction model analysis using first sleuth (Love et al., 2014) version 0.30.0 to determine statistically significant differentially expressed genes (DEGs) across experimental conditions ($P < 0.05$ and Benjamini-Hochberg correction $\alpha = 0.1$ adjusted $P < 0.1$). Differentially Expressed Genes (DEGs) were filtered out using the following conditions: (i) low expression (< 2 TPM), (ii) relatively small fold-change (FC) differences (abs log2 FC < 1), and (iii) highly variable expression across biological replicates (relative standard error of the mean > 1/2). This filter resulted in a set of 193 response genes across all treatments and conditions, that we used as input for downstream analysis. Finally, a custom Python script was used to identify the genes responding specifically to a particular factor. All computational tools used for the RNA-seq data analysis are available in the GitHub repository https://github.com/adelomana/reynisfjara.

4 Results

4.1 Characterization of the *Mitf*^{K243R} mutant mice

4.1.1 Generation of the constructs

The many mutations in the *Mitf* gene in mice have firmly shown how crucial this gene is for melanocyte development. As an example, the loss-of-function mutation of *Mitf* (Steingrímsson et al., 1994) leads to white mice due to lack of melanocytes and microphthalmia due to effects on cells of the retinal pigment epithelium. Heterozygotes carrying dominant-negative mutations of *Mitf* affecting the DNA-binding domain such as *Mitf*^{mi}, *Mitf*^{OR} and *Mitf*^{Wh} (Steingrímsson et al., 1994; Steingrímsson et al., 1996) exhibit various degrees of pigment spotting or coat color dilution whereas homozygotes are completely white with varying degrees of microphthalmia. Thus, MITF is necessary for the establishment of the melanocyte lineage and is expressed early in the development of this cell type. However, what role MITF plays in subsequent steps of melanocyte development is not clear. Indeed, like other TFs, the affinity to DNA as well as the expression level of the MITF protein are crucial for gene regulation, meaning that any change in MITF expression, regulation or affinity could generate dramatic effects (Goding and Arnheiter, 2019). As described above, many PTMs have been mapped in MITF but their role in *vivo* is largely uncharted. Most of our knowledge of MITF function has been obtained using melanoma cells and so far, very little information has been generated on the role of MITF during melanocyte development. Here, we generate an inducible mutation in MITF to investigate this and particularly the role of the acetylation site K243.

The genomic structure of MITF shows that the K243 amino acid is located in exon 8 of *Mitf*-M (Figure 7A, top). We designed a conditional mutation that introduces the *Mitf*^{K243R} mutation in exon 8 of *Mitf*. To do this, a mini-cassette containing exons 8 and 9 of the wild-type *Mitf* cDNA were placed in the genomic sequence of MITF, in an intron between exons 7 and 8 (Figure 7A, middle), thus allowing the production of the normal *Mitf* transcript and MITF protein. The *Mitf*^{K243R} mutation was created in the endogenous exon 8 by introducing the c.728A>G mutation (Figure 7B – numbers refer to the mouse Mitf-M cDNA) thus changing the lysine in position 243 to arginine (p.Lys243Arg – number referred to the mouse MITF-M protein). This Lysine is located just before the second helix of the helix-loop-helix leucine zipper motif of MITF (which starts with the Glycine

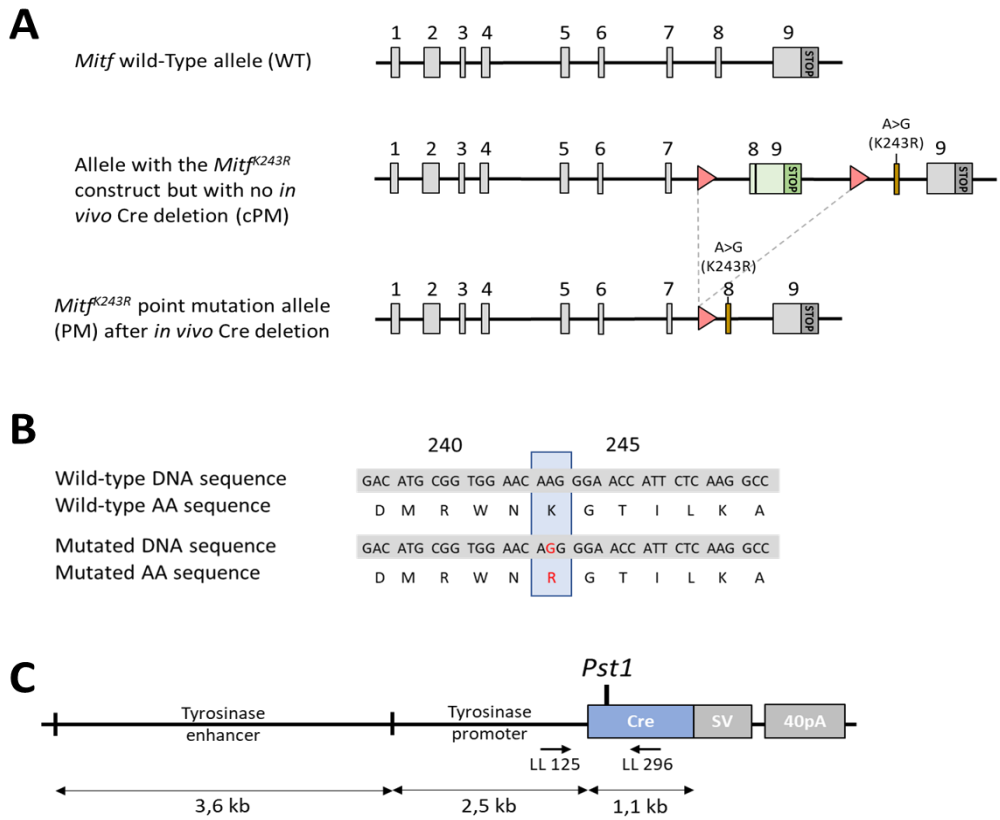

Figure 7. Knockout and transgenic constructs used in this work and the strategy of inducing the *Mitf*^{K243R} mutation *in vivo*. (A) Wild type (WT, top) and mutant *Mitf*^{K243R} alleles before (cPM, middle) and after *in vivo* induction (PM, bottom) of the conditional mutation. Light grey boxes represent WT exons, green boxes represent the minigene cassette containing wild type exons 8 and 9, inserted between the two LoxP sites (red triangles) and the blue exon represents exon 8 of Mitf with a substitution of A to G corresponding to the K243R mutation. (B) WT MITF and MITF^{K243R} mutant DNA and amino-acid (AA) sequences. The substitution of A to G and its resulting change in the amino acid sequence is shown in red. (C) Schematic of the Tyr::Cre transgene construct. It consists of the fusion of an enhancer (3.6 kb) and promoter (2.5 kb) of the Tyrosinase gene with the Cre recombinase gene (1.1 kb). Following the 3' end of is the SV40 small T intron-exon sequence (SV) and a polyadenylation signal (40pA). Primers LL 125 (forward) and LL 296 (reverse) are displayed. The restriction site Pst1 is within the PCR amplicon produced with the two primers previously described.

in position 244), at the junction between the loop and HLH domains. This position is highly conserved in MITF in different species and in basic helix-loop-helix Leucine Zipper domains of different bHLH-LZ proteins (Figure 6)(Goding and Arnheiter, 2019) and is expected to make contact with the DNA phosphate backbone but not with a

DNA base (Pogenberg et al., 2012). Unlike Lysine, Arginine cannot be acetylated, thus most likely this is expected to affect DNA binding (Louphrasitthiphol et al., 2020).

The technique of generating a conditional knock-out mutation in mice using the Cre recombinase has been used for a few decades. This is a powerful tool that has been used to study specific gene function in mice, adults and embryos by inactivating or reducing its expression or activity. The general mechanism and the design of this valuable technique has been reviewed (Friedel et al., 2011). For generating a construct containing an inducible *Mitf*^{K243R} mutation, a mini-cassette containing fused exons 8 and 9 of Mitf preceded by a splice-acceptor and followed by a polyA signal was inserted between two LoxP sites in the intron located between exons 7 and 8 of the Mitf locus. LoxP is a 34 bp sequence that can be recognized by a specific integrase, the Cre recombinase, which mediates homologous recombination. Thus, in the absence of Cre, the wild type *Mitf* gene will be produced from the minigene. However, upon Cre introduction into cells that contain this construct, the mini-cassette is removed, leaving only one LoxP-site (Figure 7A, bottom). The *Mitf*^{K243R} mutation was inserted into exon 8 after the mini-cassette and will be the only *Mitf* gene that can be produced from this chromosome after Cre has been allowed to remove the mini-cassette. This Cre/LoxP-system thus allows tissue-specific recombination if the Cre recombinase is expressed in a tissue-specific manner. Before application of the Cre recombinase, the cells express wild type MITF with the codon in position 243 of MITF being translated to a Lysine as in wild type (Figure 7B, top). After the Cre recombinase treatment, only the mutant version will be expressed, and the mutant codon AGG thus translated into an Arginine instead of Lysine (Figure 7B, bottom).

To study the effect of this *Mitf* mutation only in melanoblasts/melanocytes, we crossed mice carrying the *Mitf*^{K243R} construct system to transgenic mice expressing the Cre recombinase under regulation of the melanocyte-specific *Tyrosinase* promoter (Delmas et al., 2003) as this gene is expressed early during the development of melanoblasts (Ferguson and Kidson, 1997). The size of the Tyrosinase promoter used in this construct is 6.1 kb (Figure 7C) and is composed of the immediate region upstream the first exon of the Tyrosinase gene and a 3.6 kb enhancer region located 15 kb upstream of the first exon which contains important and essential transcriptional regulatory elements. These regulatory sequences are located upstream of the Cre recombinase sequence (Cre sequence length is 1134 bp) followed by the SV40 small T intron-exon sequence together with a polyadenylation signal at the 3′ end. Importantly, the Tyr::Cre transgene was incorporated into the X chromosome in the transgenic mice meaning that females can have one or two copies of the transgene whereas males can only have one (Delmas et al., 2003).

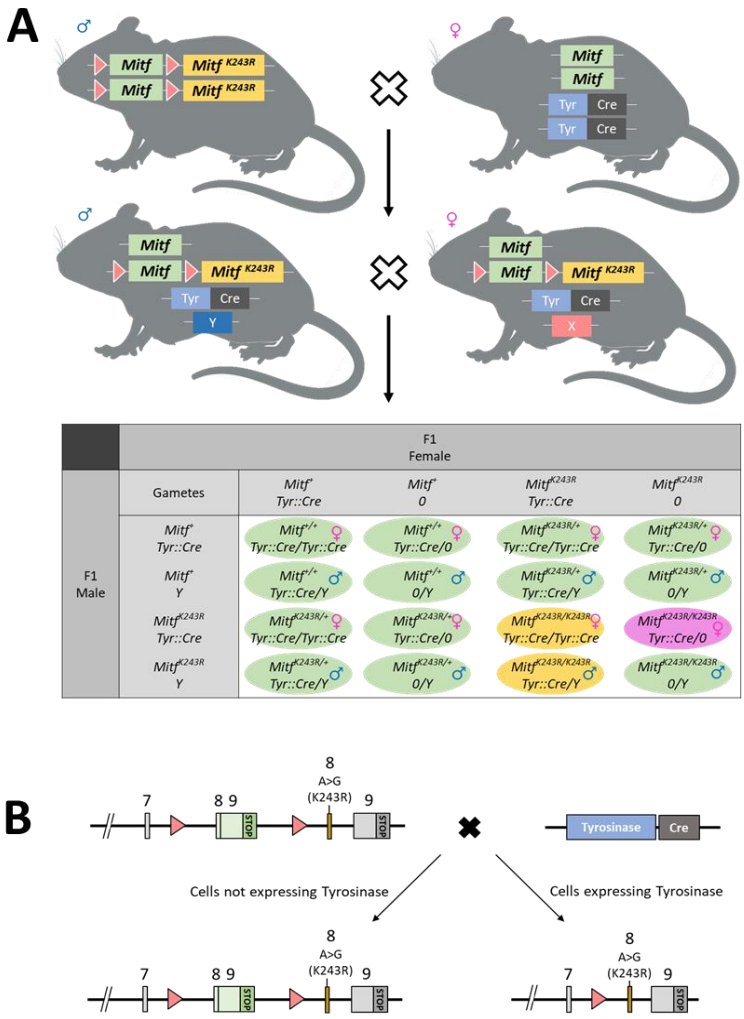

Figure 8. Generation of the *Mitf*^{K243R} mutant mice *in vivo*. (A) Mating scheme used to generate the *Mitf*$^{K243R/K243R}$; Tyr::Cre/Y or Tyr::Cre mice. First mating is with a homozgyous parent carrying the MitfK243R allele, crossed with the other parent having the Tyr::Cre construct (homozygous for the female). The resulting F1 offspring carrying both the *Mitf*^{K243R} and the Tyr::Cre constructs were then intercrossed. The outcomes of the possible genotypes are listed in the Punnett square: each parent can give four types of gametes and 16 outcomes. Allelic combinations leading to the WT phenotype are indicated in green whereas combinations leading to possible phenotypes are indicated in purple and yellow based on sex and number of Tyr::Cre alleles. (B) Schematic of the strategy used to constitutively induce the MitfK243R mutation in melanocytes by using the Cre-LoxP system with activation of the Cre recombinase using the melanocytic Tyrosinase promoter.

4.1.2 Generation of the *Mitf*^{K243R} mouse

To generate mice where the mutation can be constitutively induced in melanoblasts and thus in melanocytes, the two transgenic strains carrying the *Mitf*^{K243R} construct system and the Tyr::Cre driver were mated (Figure 8A). The aim was to generate both sexes of mice homozygous for the *Mitf*^{K243R} mutation and at least hemizygous for the Tyr::Cre transgene. First, mice homozygous for the *Mitf*^{K243R} construct were mated with mice homozygous for the Tyr::Cre transgene but carrying WT *Mitf* (Figure 8A, top). The resulting F1 generation should be carrying WT *Mitf* on one allele and the *Mitf*^{K243R} construct on the other allele, and one allele only of the Tyr::Cre transgene. The Tyr::Cre transgene is located on the X-chromosome so the genotype of hemizygous females is written as Tyr::Cre/X and homozygous Tyr::Cre/Tyr::Cre as they have two X-chromosomes, whereas the genotype of males is written as Tyr::Cre/Y as they can have only one X-chromosome. The F1 mice resulting from this first mating were intercrossed (Figure 8A, middle) resulting in an F2 generation that can have 12 different outcomes, representing 8 different genotypes. In the Punnett square presented in Figure 8A the four different types of gametes that the F1 female and male mice produce are represented. The resulting genotype outcome is shown with gender and phenotype indicated: green for WT animals, purple for females with one copy of the Tyr::Cre transgene, and yellow for *Mitf*^{K243R} homozygotes that are also homo- or hemizygous for the Tyr::Cre transgene. The resulting phenotypes will be detailed further in the following chapter. In the *Mitf*^{K243R} mutant mice, cells expressing Tyrosinase will also express Cre recombinase which will then remove the wild-type cassette of exons 8 and 9 of *Mitf* located between the two LoxP sites, thus resulting in expression of transcripts from exon 8 carrying the c.728A>G mutation leading to an MITF protein with the *Mitf*^{K243R} mutation (Figure 8B, right arrow). Cells that do not express Tyrosinase will not have the cassette sequence removed and will therefore express wild-type *Mitf* mRNA and protein (Figure 8B, left arrow).

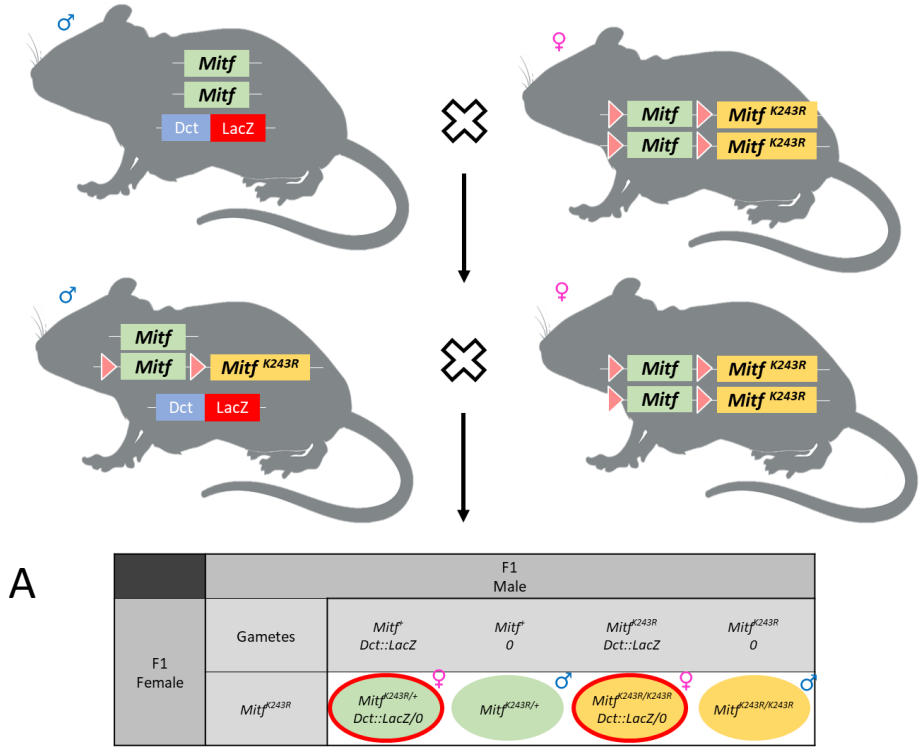

Figure 9. The Dct::LacZ transgene, principle and integration into the *Mitf*^{K243R} model. (A) Male expressing the Dct::LacZ transgene was mated with a female homozygous for the *Mitf*^{K243R} construct with half of the offspring inheriting the Dct::LacZ reporter. (B) The resulting F1 (in the figure is shown the case of a male) with the Dct::LacZ reporter, also heterozygous for the *Mitf*^{K243R} construct, was backcrossed with a female *Mitf*$^{K243R/K243R}$. (C) The male in this case can give four different gametes, and the female only one. Thus, the possible resulting genotypes are displayed in the Punnett square: mice heterozygous for the *Mitf*^{K243R} construct are shown in a green circle whereas - homozygotes are in yellow. Half the offspring will also carry the Dct::LacZ reporter (circled by a redline) and will be used for further experiments.

4.1.3 Generation of triple transgenic mice also carrying the Dct::LacZ reporter

In order to track the fate of the melanoblasts, we crossed the newly generated *Mitf*$^{K243R/K243R}$; Tyr::Cre mice with the Dct::LacZ reporter (Mackenzie et al., 1997). LacZ, an *Escherichia coli* gene, codes for the β-galactosidase protein but in the Dct::LacZ construct its expression is controlled by the regulatory elements of the pigmentation gene Dct. As a marker for early melanoblasts, the Dct::LacZ transgene is a powerful tool to track the fate of melanoblasts (Mackenzie et al., 1997). β-galactosidase is an enzyme that can hydrolyze -galactosides such as X-gal (molecular formula: 5-bromo-4-chloro-3-indolyl β-D-galactopyranoside) into a single monosaccharide of galactose and a molecule of 5-bromo-4-chloro-3-hydroxyindole. This last molecule can, in presence of oxygen, dimerize to give 5,5′-dibromo-4,4′-dichloro-indigo that becomes blue in

presence of ferri- and ferro-cyanide solution. Thus, all cells expressing Dct, when exposed to X-gal staining (detailed earlier in chapter 3.5) become blue, allowing us to track this specific cell type, from stage E9,5 and onward (Steel et al., 1992).

The mating scheme used to generate the animals is shown in Figure 5A. A *Mitf*$^{K243R/K243R}$ mouse resulting from the matings presented in chapter 4.1.2. was mated to a mouse carrying the Dct::LacZ reporter. To simplify the mating schemes, we removed the Tyr::Cre transgene to only focus on the principle of how to integrate the Dct::LacZ reporter and getting back to the *Mitf*^{K243R} homozygous. All the resulting F1 generation of this first mating will carry one allele of the *Mitf*^{K243R} construct and half of them will also have one copy of the Dct::LacZ (Figure 9B). A male mouse coming from this F1 (*Mitf*$^{K243R/+}$; Dct::LacZ/0) was backcrossed (Figure 9B) with a *Mitf*$^{K243R/K243R}$ female. The four different genotypes of gametes that the male can give rise to are listed in the Punnett square presented in Figure 9C. The female can only give one type of gametes (left side of the Punnett square). This cross is thus supposed to result in 50% *Mitf*^{K243R} heterozygous mice (green circles in Figure 9C) with 50% of those expressing the Dct::LacZ reporter (red borders around green circles). The other 50% of the mice generated by this cross will be *Mitf*$^{K243R/K243R}$ females or males (yellow circles) where 50% carry the Dct::LacZ reporter (red border around the yellow circles). Briefly, within two generations of mice, we were able to maximize the odds of ¼ chance to obtain *Mitf*^{K243R} mutant mice also carrying the Dct::LacZ reporter.

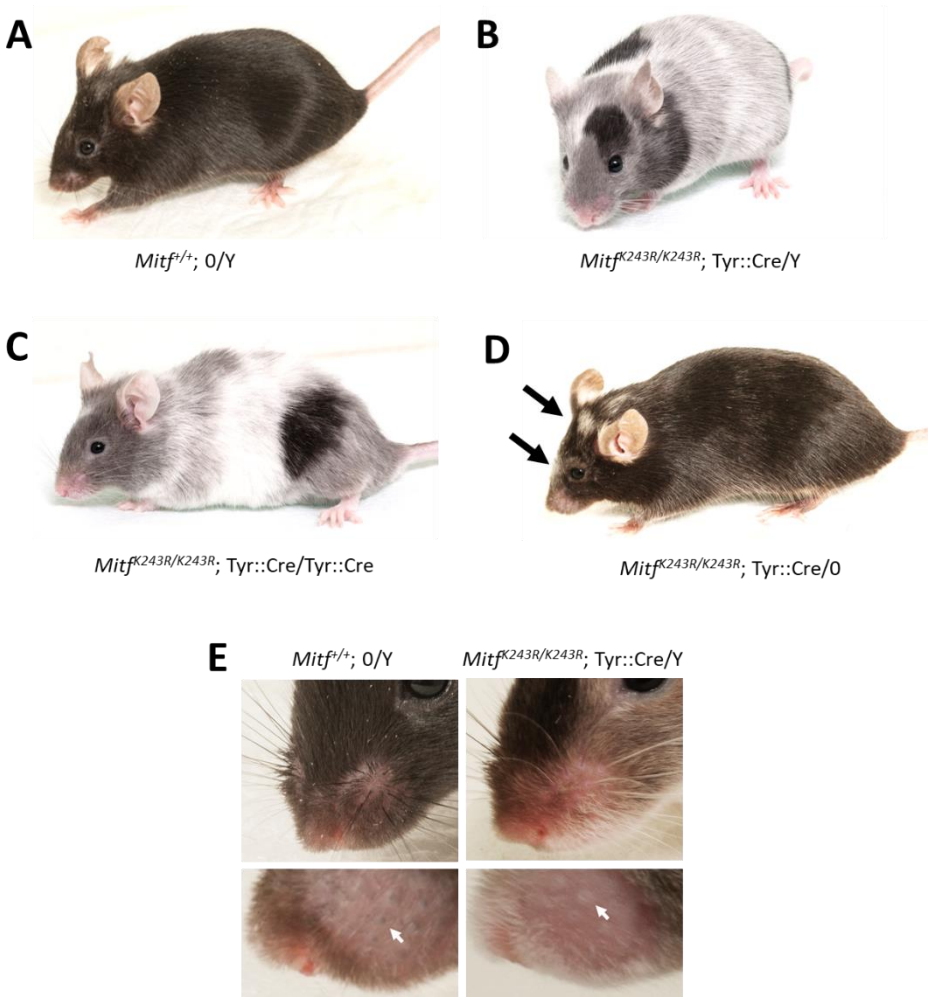

Figure 10. The effects of the *Mitf*^{K243R} mutation on mouse phenotype. (A) Phenotype of a male mouse carrying the conditional *Mitf*^{K243R} construct but not the Tyr::Cre transgene resulting in WT Mitf phenotype. (B) Phenotype of a male mouse homozygous for the *Mitf*^{K243R} mutation and hemizygous for the Tyr::Cre transgene. (C) Phenotype of a mouse homozygous for the *Mitf*^{K243R} mutation and the Tyr::Cre transgene (on both X chromosomes). (D) Phenotype of a female mouse homozygous for the *Mitf*^{K243R} construct but hemizygous for the Tyr::Cre transgene. Notice the white spot on the head (upper arrow) as the only visible phenotype with a lighter snout (lower arrow). (E) Enlarged pictures of snouts of WT *Mitf* (left panel) and *Mitf*^{K243R} mutant (right panel). One dermal papilla is indicated by an arrow for each phenotype.

4.1.4 *Mitf*^{K243R} mice have altered coat color

The matings of mice carrying the transgenes discussed in 4.1.1 result in different coat color phenotypes based on genotype (as examples presented in Figures 10A to E). More pictures for all the possible genotypes are displayed in Appendix A, Supplementary Figure 35. Mice homozygous for the *Mitf*^{K243R} construct but which do not carry the Tyr::Cre transgene driver are black and undistinguishable from WT mice of the C57BL/6J genetic background. Males homozygous for the *Mitf*^{K243R} mutation and hemizygous for the Tyr::Cre transgene driver show a different coat color phenotype where the coat alternates between white areas, areas of "salt and pepper" grey coat color and areas with apparently normal black coat color (Figure 10B). Females that are homozygous for both the *Mitf*^{K243R} mutation and the Tyr::Cre transgene have the same phenotype with interchanging areas of white, "salt and pepper" and black coat color (Figure 10C). Interestingly, females homozygous for the *Mitf*^{K243R} construct but carrying only one allele of the Tyr::Cre driver are almost fully black like WT MITF mice, except they have small white spots on the head between the ears and their snouts are often lighter in color (Figure 10D, arrow showing the white spot). Whereas WT mice have black whiskers with clearly black hair bulbs (Figure 6E, left panel) the *Mitf*$^{K243R/K243R}$; Tyr::Cre/Y animals have white whiskers and no coloration of the hair bulb (Figure 1E, right panel). Altogether, this suggests that the *Mitf*^{K243R} mutation results in a partial phenotype in melanocytes upon activation of the mutation using the Tyr::Cre transgene. As the Tyr::Cre transgene is on the X-chromosome it is possible that the differences observed between hetero- and homozygotes for the transgene reflect consequences of X-chromosome inactivation. As the same phenotype is observed in both sexes where X-chromosomes contain the transgene, it is likely that the observed phenotype is du23e to the induced *Mitf*^{K243R} mutation. The white areas reflect early and complete loss of MITF activity in melanoblasts/melanocytes, the "salt and pepper" areas may indicate partial loss whereas black areas probably reflect failure of Cre-induced homologous recombination events in melanoblasts/melanocytes. Tyr::Cre is expressed at stage E11.5, when MITF expression has already started (Tyr is actually dependent on MITF) meaning that the timing of the event can also be partially responsible for this phenotype. These results show that the *Mitf*^{K243R} mutation can be induced constitutively in melanocytes by activating the expression of the Cre recombinase (which removes the cassette of WT *Mitf*) through the *Tyrosinase* promoter, and results in a new white spotting phenotype.

4.1.5 Genotyping strategy of the *Mitf*^{K243R} mutant mice

The strategy for determining the genotype of the mice is shown in Figure 11A. The top panel represents the wild-type version of *Mitf* from exon 7 to the stop codon. The primers called Lf39 and Lr39 were designed to hybridize to the intronic region between exons 7 and 8 to amplify a 257 bp fragment in wild type mice (Figure 11A, top, labelled WT). The same set of primers will amplify a 337 fragment when the LoxP-cassette is present, but recombination has not taken place, e.g. in cells not expressing Tyrosinase. The size difference is due to the LoxP site (34 base pair) and an additional 46 base pair fragment which is present resulting from the integration of the cassette when designing the construct (Figure 11A, middle, cPM). A total of 80bp thus explains the difference between the 257 bp and 337 bp PCR products. When Cre removes the cassette and one LoxP-site (Figure 11A, bottom lane, PM), this results in a 350 bp band in cells where the recombination has taken place. The size difference is explained by an additional 13 bp sequence, shown as a blue box in Figure 11A, which is located between the second LoxP site and the sequence that the reverse Lr39 primers hybridizes to.

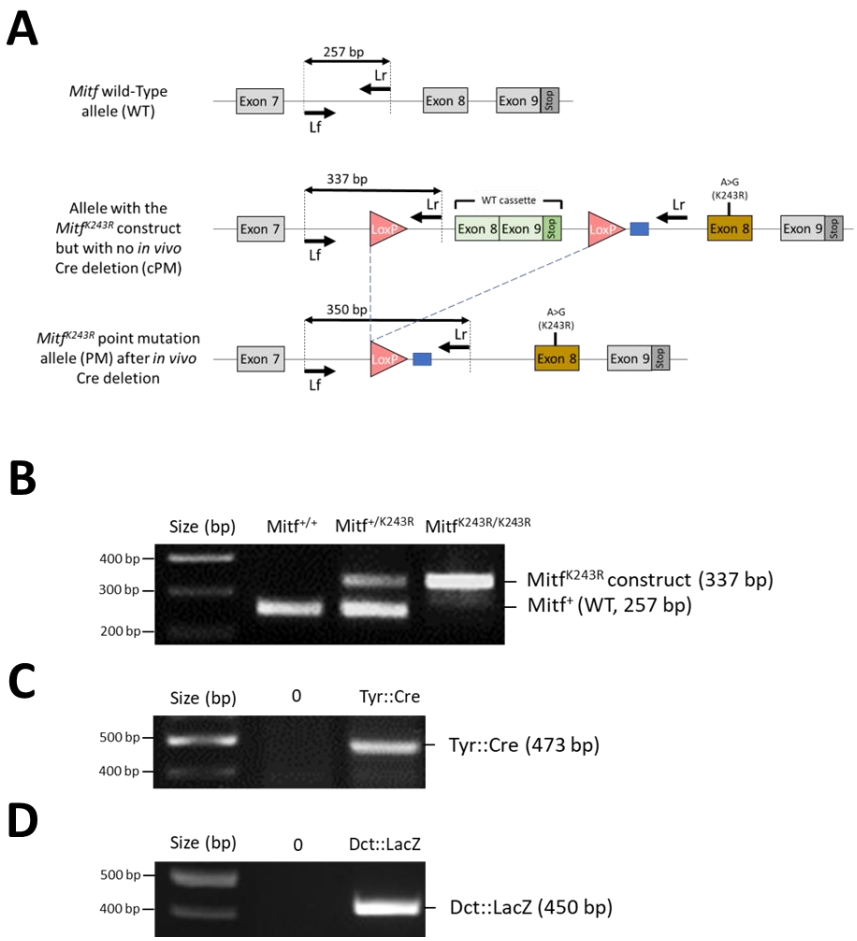

Figure 11. Genotyping of the MitfK243R mutant mice and of the Tyr::Cre and Dct::LacZ transgenes. (A) Schematic representation of the genotyping strategy used for animals and embryos to determine the status of the K243R mutation. The expected size of PCR amplicons by using the forward (Lf) and reverse (Lr) primers are shown for Wild-type (WT, top), the non-induced mutation (cPM, middle) and for the in vivo induced *Mitf*^{K243R} mutation (PM, bottom). Red triangles represent LoxP-sites, green boxes the WT exons, the blue rectangle the additional 13 bp located between the second LoxP site and the reverse primer Lr and the yellow box exon 8 carrying the *Mitf*^{K243R} mutation. The distances between the Lf and Lr primers are indicated in every case. (B-D) PCR results for the genotyping strategy. (B) Gel electrophoresis of the PCR products from the indicated genotypes. (C) Gel electrophoresis of mice without (0, second lane, no band) or with the Tyr::Cre transgene (third lane, band at 473 bp). The DNA size ladder is in the first lane. (D) Gel electrophoresis of mice without (0, second lane, no band) or with the Dct::LacZ transgene (third lane with a band at 450 bp). On the gel, the DNA size ladder is located in the first lane.

Typical results of the genotyping strategy are shown in Figure 11B, C and D. We performed the PCR on DNA extracted from ear clips of animals. Based on the genotyping strategy shown in Figure 11A, we were able to genotype the mice carrying the *Mitf*^{K243R} construct (Figure 11B). As expected, following the genotyping strategy with the Lf39 and Lr39 primers, we distinguished homozygous WT (*Mitf*$^{+/+}$) mice from hemizygous (*Mitf*$^{K243R/+}$) and homozygous mutants (*Mitf*$^{K243R/K243R}$). Indeed, after running the PCR products on a 2% agarose gel, the *Mitf*$^{+/+}$ mice showed a band at 257 bp whereas the *Mitf*$^{K243R/K243R}$ mutant showed a band at 337 bp. The reason for this is that the vast majority of cells in the ears (the DNA was isolated from ear clips) do not express tyrosinase. Consistent with that, heterozygous *Mitf*$^{K243R/+}$ mice show two bands, at 257 and 337 bp. We were also able to determine which animals were carrying the Tyr::Cre transgene and which were not (Figure 11C) by using a set of previously described primers (Delmas et al., 2003). Mice that carry the transgene showed a band at 473 bp but if not, no DNA product was produced by PCR and no band was displayed on the agarose gel. After this method was used for confirming the relationship between genotype and phenotype in a number of generations, eventually genotyping was done by visual inspection as mice carrying the *Mitf*^{K243R} transgene were either with no phenotype (*Mitf*$^{K243R/K243R}$; X/X), with a white spot on the head and a lighter snout (*Mitf*$^{K243R\ /K243R,}$; Tyr::Cre/X) or with the white, black and grey spots (*Mitf*$^{K243R\ /K243R}$; Tyr::Cre/Tyr::Cre and *Mitf*$^{K243R\ /K243R}$; Tyr::Cre/Y). We were also able to design primers that allowed the separation of the Dct::LacZ carriers from the non-carrier mice (Figure 11D). Similar to the Tyr::Cre transgene, mice without the Dct::LacZ transgene did not show a band whereas the carriers showed a 450 bp band on an agarose gel. We have also optimized the protocols that allow us to genotype the mice for the Tyr::Cre and Dct::LacZ transgenes, and for the status of the *Mitf*^{K243R} mutation on both alleles. To simplify the discussion, as the *Mitf*$^{K243R/K243R*}$; Tyr::Cre/Y males and the *Mitf*$^{K243R/K243R*}$; Tyr::Cre/Tyr::Cre female have the same phenotype, we will only speak about the males in the dissertation, unless stated otherwise.

4.1.6 Characterization of hair from the differently pigmented areas

As previously explained, the *Mitf*$^{K243R/K243R}$ mutant mice display a clear coat color phenotype. To investigate the pigmentation in more detail, the distribution of pigmentation in the hairs and the production of melanin were characterized. We first plucked hairs for investigating distribution of pigmentation in individual hairs from the three differently pigmented areas. Figures 12A and B show the areas where hairs were plucked from WT (*Mitf*$^{+/+}$; 0/Y, solid line) and mutant mice (*Mitf*$^{K243R/K243R}$; Tyr::Cre/Y). For the mutant mice, the three different coat color areas are delimited by either a solid line (black areas), broken line ("salt and pepper" grey areas) or dotted line (white areas). Pictures of the hairs from the differently pigmented areas from *WT MITF* or *Mitf*$^{K243R/K243R}$ mutant mice are displayed in Figure 12C. The figure shows a ladder-type two-row auriferous hair medulla filled with melanin consistent with previous observations (Chernova, 2003). The outside of the hair is called the cuticle and the

medullar cells are located in the area where the pigment granules are located (darkest part of the hair in the *WT MITF* hair). The space between each medullar cell is called cavity and the layer between the medullar cells and the cuticle is called cortex. The WT hair shows the most melanin in the medullary segments and nice dense packing of the pigmented stacks. Hair from black areas of the *Mitf*$^{K243R/K243R}$ mutant mice show almost the same amount of melanin in each medullar cell as observed in *WT MITF*. Hairs from the "salt and pepper" area are divided into individual hairs with grey or no pigmentation. The grey hair shows less melanin than the hair from the black areas as we can observe less pigment in each stack. The white hair from the grey "salt and pepper" areas are devoid of melanin. The presence of these two different hair colors explains this "salt and pepper" grey-like color where gray and white hair alternates. Finally, like for the white hair in the grey area, the hairs from the white areas are also not filled with any pigment granules. In order to quantitate melanin in hair from the black, "salt and pepper" grey and white areas of the *Mitf* $^{K243R/K243R}$ mutant mice, hair was digested in NaOH to release the eumelanin and the absorbance, directly related to the quantity of eumelanin (Hu et al., 1995), was measured at 470 nm wavelength (Figure 12D). As controls, hair from Dct::LacZ/0 (positive control) and *Mitf*$^{Mi\text{-}Wh/Mi\text{-}Wh}$ (negative control, no melanin) was also analyzed. The relative absorbance of hair from wild type mice was set at 100% (Figure 12E). The relative absorbance of the black hairs of the *Mitf*$^{K243R/K243R}$ mutant was 93% of that of wild type. The negative control *Mitf*$^{Mi\text{-}Wh/Mi\text{-}Wh}$ showed only 2% relative absorbance of WT control, meaning that the pigment is almost non-existent in the hair stacks of these animals. The "salt and pepper" grey areas of the *Mitf*$^{K243R/K243R}$ mutant shows 37% absorbance relative to that of WT. This is consistent with the fact that only grey and white hair is present in this area. Finally, for the white areas of the *Mitf*$^{K243R/K243R}$ mutant, the relative absorbance was only 5% of that of WT hair, similar to the *Mitf*$^{Mi\text{-}Wh/Mi\text{-}Wh}$ negative control. This shows that hair from this area does not contain melanin.

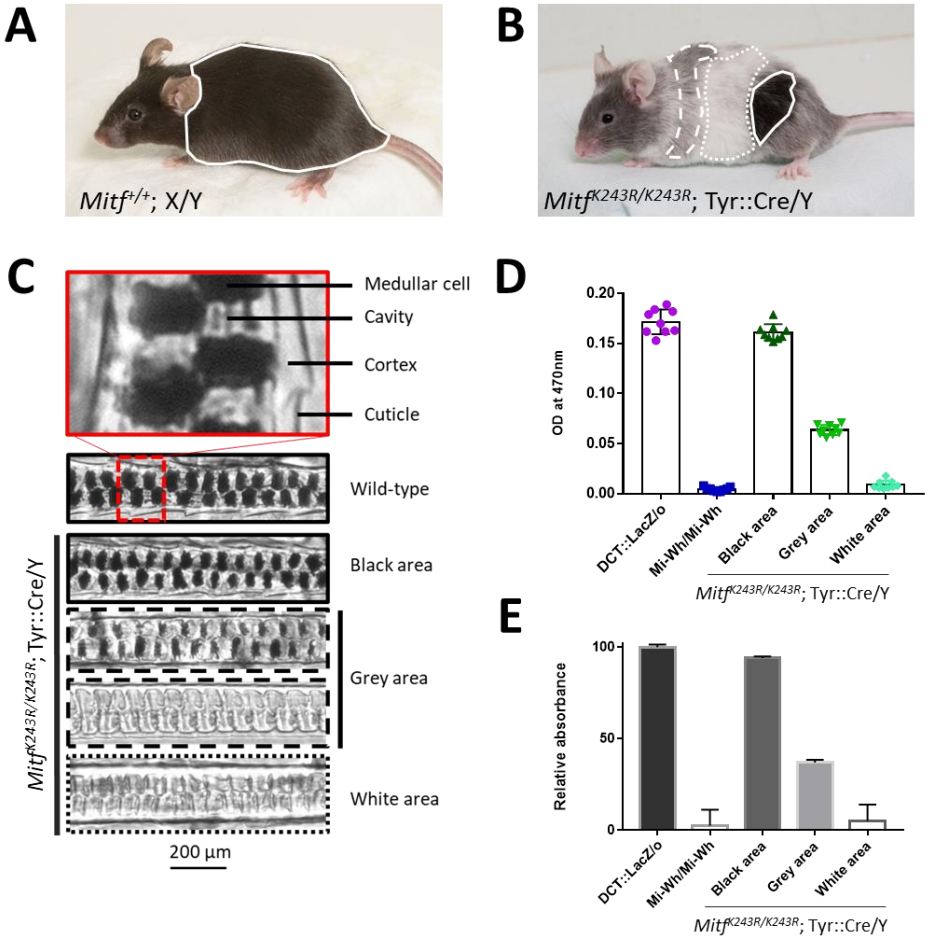

Figure 12. Mouse hair from grey areas have less eumelanin and white areas none. (A) Phenotype of WT *Mitf* mouse (*Mitf*$^{K243R/K243R}$; 0/Y). The solid line represents the location of the plucked hairs. (B) Phenotype of the *Mitf*^{K243R} mutant mouse (*Mitf*$^{K243R/K243R}$; Tyr::Cre/Y). The solid line represents the location of the plucked hair from the black area, the broken line the hair from the "salt and pepper" grey area, and the dotted line from the white area. (C) Pictures of hair from the different coat color regions of the WT *Mitf* and mutant mice. Outlines of each picture corresponds to the area of the mouse in B that they are plucked from. (D) Optical density (OD) measured at 470 nm from the extraction of pigment from hair of the different coat color regions shown in Figure 8B and C and compared to positive (WT mice hair) and negative (Mi-White mutant mice) controls. Each dot represents the optical absorbance for n=3 animals in triplicate. (E) Same data as presented in Figure 10D but with the relative absorbance (on Y axis) compared to the OD of Dct::LacZ/0 hair.

4.1.7 Effects of the *Mitf*^{K243R} mutation on melanocyte development

4.1.7.1 Mitf^{K243R} *mice have fewer melanoblasts*

At day E13.5 of mouse embryonic development, melanoblasts are proliferating and migrating through the dorso-lateral pathway. To track melanocyte development in wild type and mutant mice we used the Dct::LacZ transgene. *Dct* is expressed from day E9 in the eye and can be detected in the RPE at E10.5. *Dct* is then expressed in caudal regions of the neural tube from E9,5. It is also expressed in the telencephalon from E12.5 (Mackenzie et al., 1997). Caudal nerves, dorsal root ganglia and the optic stalk are also stained but this staining seems to be independent from the expression of *Dct* as *Dct* RNA probes failed to detect *Dct* expression in these developing parts of the embryo at these stages (Pavan and Tilghman, 1994a). This might be explained, as proposed previously (Mackenzie et al., 1997), by the lack of the complete regulatory elements of *Dct* from the DCT::LacZ construct leading to reduced inhibition of *Dct* expression or by an unexpected cooperation of the *Dct* promoter and *LacZ* gene which may result in ectopic expression of the *Dct* RNA and protein. Thus, by using this method, it is possible to detect melanoblasts from as early as E10.5.

We used β-galactosidase staining to track the development and migration of melanoblasts at three different stages of their development: E13.5, E14.5 and E15.5. Figure 13 shows WT and *Mitf*$^{K243R/K243R}$; Tyr::Cre mutant embryos also carrying the Dct::LacZ reporter after staining for β-galactosidase activity using Xgal. In each figure, WT embryos are depicted on the left panel and *Mitf*$^{K243R/K243R}$ mutants on the right panel. Developmental stages are E13.5 (Figure 13A), E14.5 (Figure 13B) and E15.5 (Figure 13C). As can be seen from Figure 13A, there is a difference in the number of melanocytes between the wild type and mutant embryos at E13.5. Indeed, if we zoom in on the belly region of the embryo (white square marked with broken line), we can see a greater density of melanoblasts in the wild type embryos than in the mutant embryos. To quantitate this difference, the melanoblasts were counted manually by hand (using the "Cell counter" tool in ImageJ) in 82 embryos (14 *WT MITF* and 68 *Mitf*$^{K243R/K243R}$ mutant) in an area indicated in the boxed region, as shown in Figure 13. The average number of melanoblasts in E13.5 embryos is displayed on the graph of Figure 13D which compares melanoblast numbers in all the embryos. At embryonic stage E13.5, there are fewer melanoblasts in the *Mitf*$^{K243R/K243R}$ mutants than in the *WT MITF* embryo. The *WT MITF* embryos have a mean of 526 melanoblasts in the indicated square (±51, n=8) whereas *Mitf*$^{K243R/K243R}$ mutant embryos had a mean of 213 melanoblasts (±14, n=34). One day later, at E14.5 (Figure 13E), the number of *WT MITF* melanoblasts has almost doubled to a mean of 933 (±78, n=6) whereas the number of *Mitf*$^{K243R/K243R}$ mutant melanoblasts barely increased to 247 (±17, n=34). To summarize, the number of melanoblasts in the *Mitf*$^{K243R/K243R}$ mutants represents half of the number of melanoblasts observed in *WT MITF* at E13.5 and a quarter of the melanoblasts observed in wild type at E14.5. At E15.5, the number of melanoblasts in

wild type embryos had increased significantly and many are visible (Figure 13C, darker blue dots) in the hair placodes that will subsequently invaginate and give rise to the future hair bulb. In the *Mitf*$^{K243R/K243R}$ mutants, in addition to the reduced number of melanoblasts at this stage, the melanoblasts seem also not to cluster into the hair placodes as fewer dark blue dots were observed.

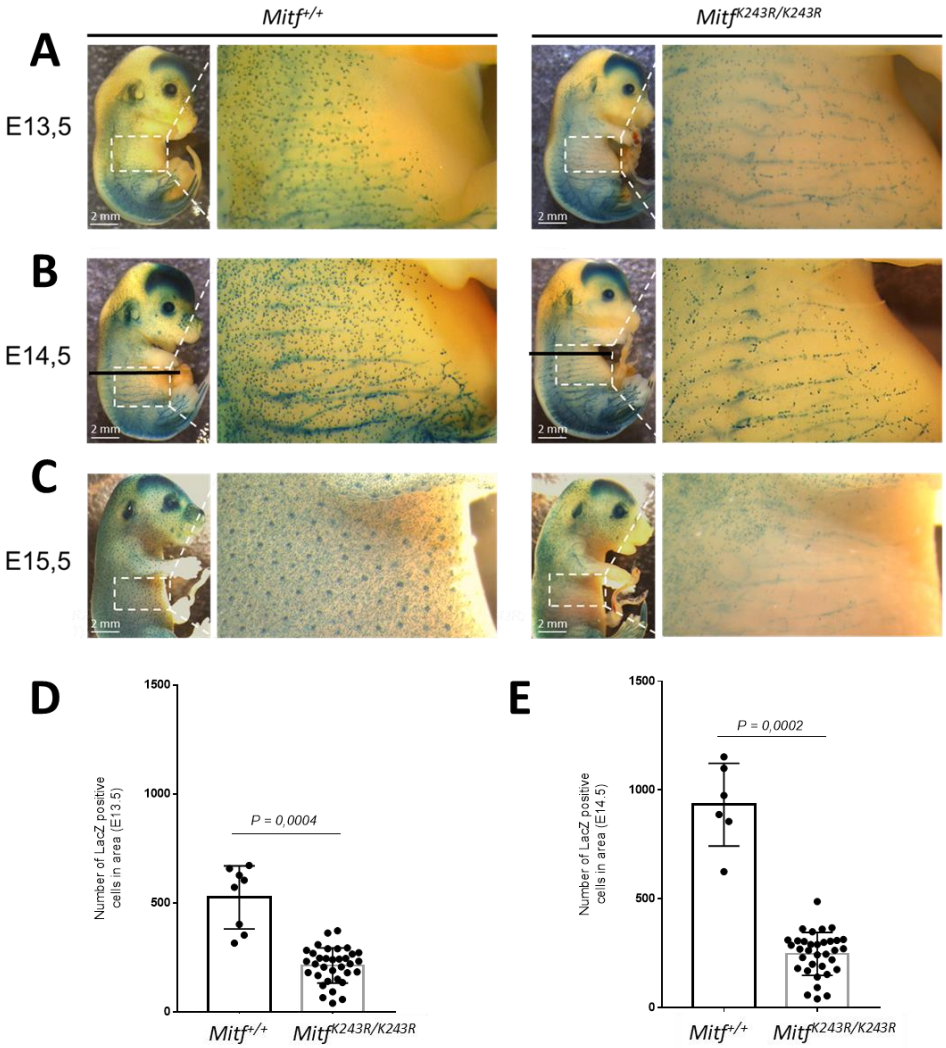

Figure 13. The *Mitf*^{K243R} mutation reduces melanoblast numbers. (A) Whole-mount preparations of WT *Mitf* (*Mitf*$^{+/+}$; X/Y left) and *Mitf*^{K243R} mutant (*Mitf*$^{K243R/K243R}$; Tyr::Cre/Y, right) embryos stained with Xgal at the embryonic stages E13.5. The rectangle delimited by the white broken line is enlarged on the right side of each picture. (B) Embryonic stage E14.5. The black lines shown on both WT *Mitf* and *Mitf*^{K243R} mutant embryos indicates the location of the sections presented in Figure 10A. (C) Embryonic stage E15.5. Hair placodes are indicated with a yellow arrow. (D) Quantification of the number of Dct::lacZ positive cells in the indicated squares at E13.5. Each dot represents the number of melanoblasts in the square of one embryo. Unpaired T-test with Welch's correction was used for statistical analysis WT *Mitf* (n=8) and MITF^{K243R} mutant (n=34) embryos at E13.5. (E) Quantification of the number of Dct::lacZ positive cells in the indicated squares at E14.5. Same statistical analysis was used for WT *Mitf* embryos (n=6) and MITF^{K243R} mutant (n=34) as explained for Figure 9D.

4.1.7.2 The phenotype of MITF^{K243R} *mutant mice can be seen early in development*

In adult mice the whiskers of the *Mitf*^{K243R} mutant are white (Figure 10E). In WT embryos at E14.5, we can see that there are already nicely formed whisker hair follicles, (Figure 14, white arrow), meaning that many melanoblasts have already clustered together in this place. On the contrary, in the *Mitf*^{K243R} mutant embryo, at this stage, the melanoblasts have not clustered in an organized way (Figure 14A). In the *Mitf*^{K243R} mutants (Fig 14A, right), a high density of melanoblasts is observed in the region where the whiskers would normally form (black arrow) but those do not seem to cluster normally in the hair follicles. Thus, the white color of the whiskers of *Mitf*^{K243R} mutant mice can explained by the fact that the melanoblasts are not able to cluster in the forming hair placodes (Figure 10E) that is normally happening in WT MITF melanocytes. In approximately 20% of mice homozygous for the *Mitf*^{K243R} mutation a black spot is visible on the head (*Mitf*^{K243R} mutant of Figure 14C, black arrow, 14D), (Figure 14D). This may be due to the fact that the melanoblasts first form in the head region and may already have formed when MITF was replace by *Mitf*^{K243R} mutant, thus leading to normally pigmented melanocytes at E14.5. In Figure 14A (red arrow), it can be seen that the *Mitf*^{K243R} mutant embryo shows a patch of high density melanoblasts on the neck, similar to the melanoblast density seen in wild type (Figure 14C, red arrow).

Although it is not possible to say for sure that the phenotype seen in E14.5 embryos reflects the phenotype seen in the adult mouse, the previously discussed investigation suggests a direct link. We have determined the percentage of mice that had common phenotypic features, both in the *Mitf* mutant embryos (Figure 14B) and adults (Figure 14D), only considering in this case the head/neck and the rump regions. As indicated in Fig. 14D, all (n=20) of the *Mitf*^{K243R} mutant mice showed solid grey on the face, always with a white spot on the forehead (Figure 14C, purple arrow) with an occasional (20%) black spot (Figure 14C, black arrow). The neck region showed a black spot in a majority of mice (55%). Finally, 75% of the *Mitf*^{K243R} mutant mice also carry a black spot in the rump region (Figure 14C, blue arrow). In the embryos (n=17), we observed that all the mutant embryos but one (94%) had a high density of melanoblasts around the eyes and nose. Also, 76% of the embryos showed a high density of melanoblasts on the back and on the rump. These numbers show that the high density of melanoblasts that we observe in the face of most of the developing embryos (94%) will give rise to grey solid color face (100%) that can even be with a black spot in some cases (20%). Interestingly, all the *Mitf*^{K243R} mutant mice display a white spot on the forehead, suggesting that this specific area might be more complicated for the melanoblasts to reach. We also observed similar rates in *Mitf*^{K243R} mutant adult mice and embryos in the neck (respectively 55% and 76%) and in the rump (respectively 75% and 76%). Together, these data from both embryos and adult mice suggest that establishment of the adult phenotype is already visible at E14.5 of development and is reflected in the number of developing melanoblasts.

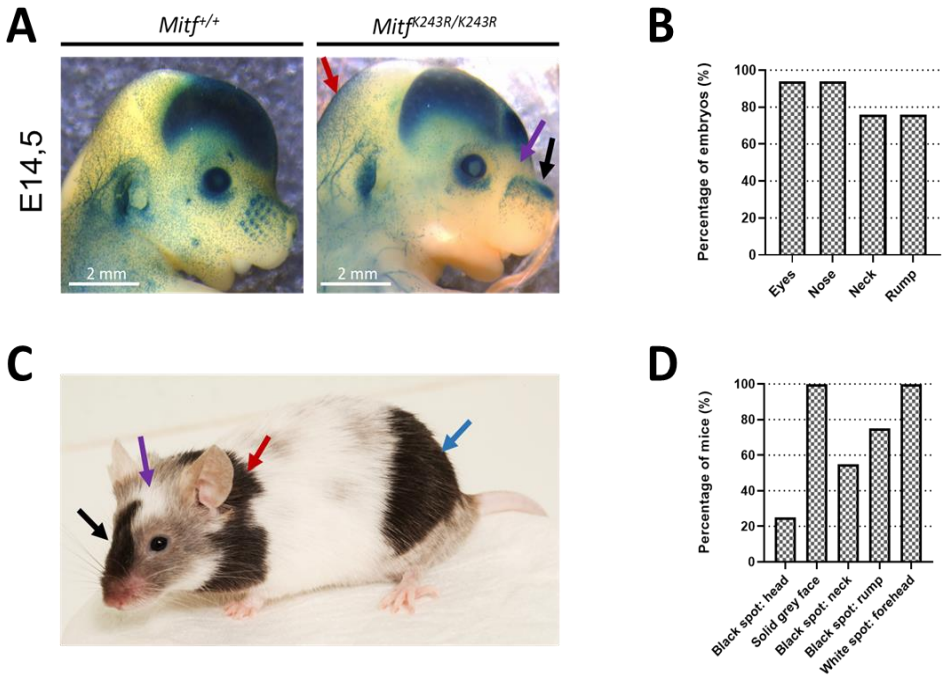

Figure 14. Pattern of melanoblast distribution in *Mitf*^{K243R} mice at developmental stage E14.5. (A) Photo of the heads of WT *Mitf* (*Mitf*$^{+/+}$; 0/Y, left) and two *Mitf*^{K243R} mutant (*Mitf*$^{K243R/K243R}$; Tyr::Cre/Y, right) embryos at E14.5. The white arrow is localizing the forming hair follicles for the whisker hairs of WT *Mitf* embryo. The black arrow indicate the high density of melanoblast in the nose of the *Mitf*^{K243R} mutant embryos. Notice that almost no (middle) hair follicles are forming or they are disorganized (right). Red arrows indicate areas with high numbers of melanoblasts on the neck of the embryo. Purple arrow show a hole in melanoblasts density on the forehead (B) Percentage of embryos showing a high density of melanoblasts at the location indicated on the X-axis (n=17). (C) Picture of a *Mitf*^{K243R} mutant mouse with areas of interest indicated with arrows of the same colors as for the embryos in 12A. (D) Percentage of adult mice showing the features indicated on the X-axis (n=20).

4.1.7.3 *Mitf*^{K243R} mutant melanoblasts fail to invade the epidermis.

To look closer at the developing melanoblasts, the β-galactosidase-stained E14.5 embryos shown in Figure 13 were cryopreserved and sectioned at 10 µm-thickness transverse sections on a cryostat. The sections are presented in Figure 15A and the region they are from is indicated in Figure 13B by a black line in the E14.5 embryo. Some of the recognizable structures such as the caudal nerves are indicated in Figure 15A. As can be seen from the sections, WT melanoblasts are located close to the periphery of the embryo, in the epidermis. However, in the *Mitf*$^{K243R/K243R}$ embryos, the melanoblasts are further away from the periphery, in the dermis, and very few, if any, make it into the epidermis. To quantitate this, Dct-positive cells in the different locations were counted (Figure 15B) along the periphery of the embryo. The mean number of melanoblasts in the epidermis of *WT MITF* embryos was 38±9 (n=5), whereas it was 2±2 (n=11), in the *Mitf*$^{K243R/K243R}$ embryos. This difference is significant (on-way ANOVA P value < 0.0001, P-value < 0,0001, Tukey's multiple comparisons test). The mean number of melanoblasts in the dermis of WT embryos was 24±12 (n=5 sections), whereas it was 27±5 (n=11 sections), in the dermis of *Mitf*$^{K243R/K243R}$ mutant embryos; no significant difference was observed between these two mean values (p-value = 0,88, Tukey's multiple comparisons test). To put these numbers in perspective, we have calculated the ratio of epidermal melanoblasts at E14.5 (Figure 15C). The ratio of WT melanoblasts in the epidermis is 61.8±6% (n=5), whereas it is 7.2±2% (n=11) in the epidermis of *Mitf*$^{K243R/K243R}$ embryos, and the difference is significant (P-value < 0,0001, unpaired T test). The majority of WT melanoblasts are therefore able to go through the basement membrane at E14.5 to populate the epidermis, but only a small portion of *Mitf*$^{K243R/K243R}$ melanoblasts undergo the same process. This shows that the reduced total number of melanoblasts observed in these embryos is due to the number of epidermal melanoblasts, that is almost null in *Mitf*^{K243R} mutant embryos, and not to dermal melanoblasts. It thus shows that very few melanoblasts invade the epidermis by traversing the basement membrane.

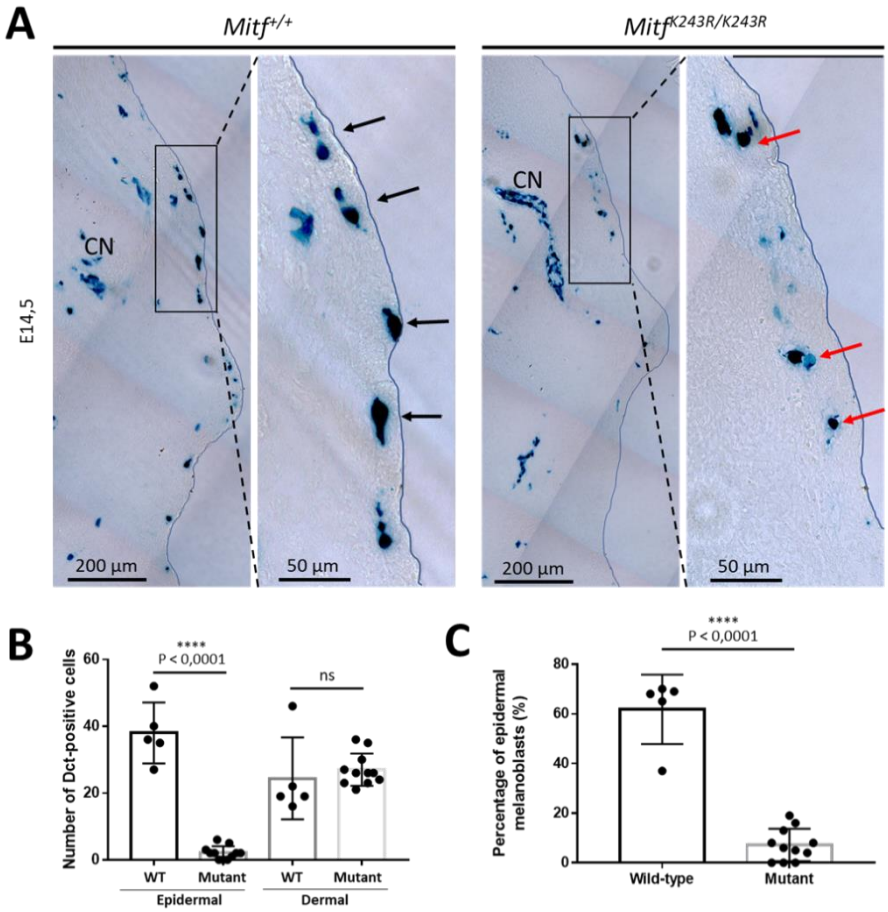

Figure 15. The *Mitf*^{K243R} mutation affects invasion of melanoblast into the epidermis. (A) Cryosections of WT *Mitf* (left panel) or *Mitf*^{K243R} mutant (right panel) embryos stained for β-galactosidase activity. LacZ positive cells in the dermis or the epidermis are considered as melanoblasts. Embryos are oriented such that dorsal as at the top and ventral is oriented to the bottom of the picture. The full blue line represents the periphery of the embryo. The right panel in each case is a higher magnification of the area indicated by a black square in each of the left panels. Caudal nerves (CN) are also stained in blue and are as indicated on the top left picture of the WT *Mitf* sectioned embryo. Melanoblasts that have gone through the basal membrane are shown by the black arrows, and melanoblasts that are still in the dermis are indicated with the red arrows. The light squares in the background are the result of the tiling of high magnification pictures together in order to increase picture quality. (B) The number of LacZ positive cells in the epidermis or the dermis of WT *Mitf* or *Mitf*^{K243R} mutant embryos. Each dot represents the number of melanoblasts on one section. Statistical analysis was performed by using the Tukey's multiple comparisons test. (C) Ratio of epidermal melanoblasts for WT *Mitf* or *Mitf*^{K243R} mutant. Stastistical analysis was performed using an unpaired T test with the P-value calculated under 0,0001.

4.1.8 Generation of the 4-OHT inducible *Mitf*$^{K243R/K243R}$ mutation mouse strain

As previously mentioned, animals carrying both the *Mitf*$^{K243R/K243R}$ mutant construct and the Tyr::Cre transgene constitutively activate the *Mitf*^{K243R} mutation in tyrosinase-expressing melanoblasts during development, and later, in fully developed melanocytes. The recombinase from the Tyr::Cre transgene is constitutively activated in melanoblasts from around day 10.5 of in *utero* development (Delmas et al., 2003). To be able to induce the mutation at different time points, we introduced a different transgene into our *Mitf*^{K243R} mutant strain. In this system the CreER^{T2} transgene was used where Cre recombinase is fused to a mutated ligand binding domain of the human estrogen receptor (Indra et al., 1999). The structure of the construct is similar to the Tyr::Cre construct except the Cre coding sequence has been replaced with the CreER^{T2} sequence. This mouse model has been previously generated and described (Yajima et al., 2006) and its construct is shown in Figure 16A. Like before, expression of the recombinase from this construct is limited to melanocytes using the same *Tyrosinase* regulatory elements as for the Tyr::Cre transgene. However, the recombinase is inactive until it is induced by 4-Hydroxytamoxifen (4-OHT), a metabolite of Tamoxifen. Using such a mechanism is useful to temporally control the activation of the Cre recombinase in melanocytes. The principle of the induction will be explained in chapter 4.2.2.

As a genotyping strategy of the Tyr::CreER^{T2} transgene, we used the same method as previously described (Yajima et al., 2006) with primers LL148 and LL 622 (localized on the construct shown in Figure 12A). The expected size of the PCR amplicons is 411 bp for mice carrying the transgene, whereas no band was expected for non-carriers (Figure 16B). To introduce the Tyr::CreER^{T2} transgene into mice also carrying the *Mitf*^{K243R} and Dct::LacZ constructs, we performed the matings shown in Figure 16C (first mating step) and 16D (second mating step). We only depict here the matings with the *Mitf*^{K243R} construct and the Tyr::CreER^{T2} transgene. First, we needed to breed a mouse carrying the Tyr::CreER^{T2} transgene alone with one carrying the *Mitf*^{K243R} construct homozygously as well as the Tyr::Cre transgene that we wanted to replace (Figure 16C) and crossed the animals with the desired phenotype (*Mitf*$^{K243R/+}$; Tyr::CreER^{T2}/0, yellow circle) to *Mitf*^{K243R} homozygotes to obtain the desired offspring (Figure 16D). However, when replacing the Tyr::Cre transgene by the Tyr::CreER^{T2} (Figure 16C), the fact that the Tyr::Cre and Tyr::CreER^{T2} transgenes carry similar sequences was problematic for genotyping. By using a restriction enzyme genotyping strategy (Supplementary Figure 36D, appendix A), it was possible to determine if the mice carried only the Tyr::CreER^{T2} or Tyr::Cre constructs, or both, which was necessary for the next steps of this study.

We needed to make sure that only one allele of Tyr::CreER^{T2} transgene was delivered to the offspring as Tyr::CreER^{T2} is lethal in homozygous condition (Le Coz et al., 2021; Yajima et al., 2006). Thus, we used a homozygous *Mitf*$^{K243R/K243R}$ male that also carries the Tyr::CreER^{T2} transgene such that half of the offspring will get the Tyr::CreER^{T2}

transgene and all will be heterozygous for the *Mitf*^{K243R} mutation. Similarly, the female used for this mating carries one copy of the Dct::LacZ transgene, meaning that half of the resulting pups also carry the Dct::LacZ transgene. As a result, we were able to use the mice with the genotype circled in yellow for further experiments and use them for further breeding to generate more animals of the desired genotype. It also allows us to create primary melanocyte cell lines where we can induce the *Mitf*^{K243R} mutation and study its effects over time (detailed in chapter 4.2.3).

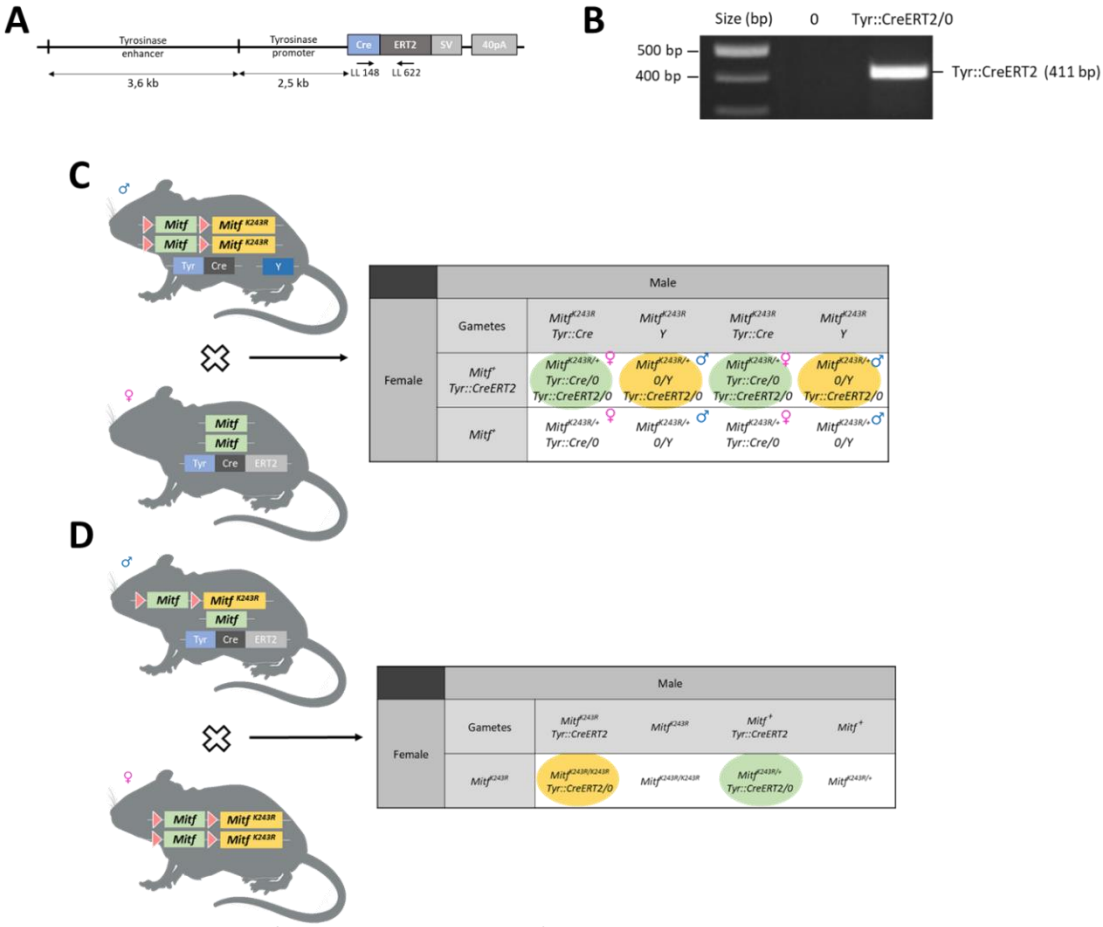

Figure 16. Generation of mice carrying the *Mitf*^{K243R} construct with Dct::LacZ and Tyr::CreER^{T2} transgenes. (A) Structure of the Tyr::CreER^{T2} transgene. It consists of a fusion of the Tyrosinase enhancer (3.6 kb) and promoter (5.5 kb) sequences with the CreER^{T2} recombinase, with SV40 and polyadenylation sequences at the end. The link sequence between the Tyrosinase enhancer and promoter is a β-globin intervening sequence. Primers LL 148 (forward) and LL 622 (reverse) that we have used for genotyping are displayed. (B) PCR genotyping agarose gel were used to check for the Tyr::CreER^{T2} status of the animals. Primers used are LL 148 and LL 622 as shown in Figure 12A. (C) The mating scheme used for introducing the Tyr::CreER^{T2} transgene into mice also carrying the *Mitf*^{K243R} construct. Punnett square representing the possible genotypes (8 in total) resulting from the cross. Only mice that carry the Tyr::CreER^{T2} transgene but not the Tyr::Cre transgene, shown in yellow circles, were selected for further matings. (D) Mating used to obtain the desired genotype, indicated in yellow circles. Male is heterozygous for the *Mitf*^{K243R} construct and the Tyr::CreER^{T2} transgene, whereas the female is homozygous for the *Mitf*^{K243R} construct. Mice having the phenotype indicated in green circle was used for further matings.

4.2 Effects of the *Mitf*$^{K243R/K243R}$ mutation in *vitro*

4.2.1 Generation of the primary melanocyte cell lines

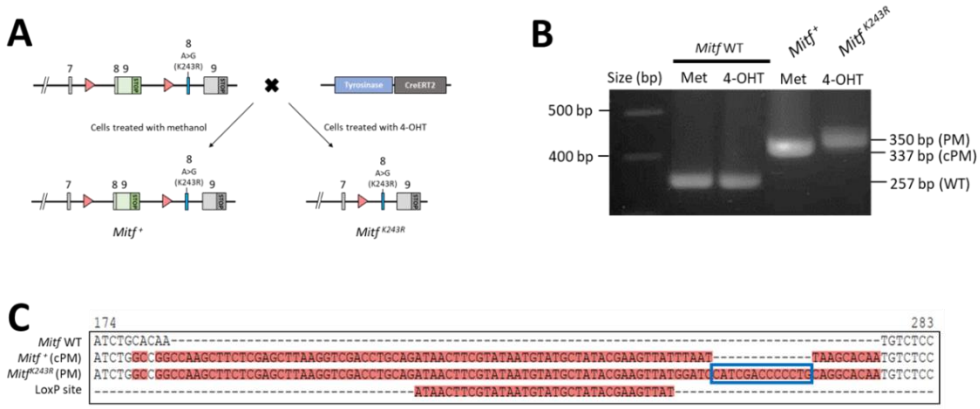

Figure 17. Genetic construct and strategy of the conditional induction of the *Mitf*^{K243R} mutation in *vitro* through the *Tyr::CreER*^{T2} *system*. (A) Schematic of the strategy used to induce the *Mitf*^{K243R} mutation by using the CreER^{T2}-LoxP system with activation of the CreER^{T2} recombinase from the Tyrosinase promoter and upon activation of the CreER^{T2} recombinase by 4-Hydroxytamoxifen (4-OHT) treatment. Methanol is used as a control as it does not activate CreER^{T2} recombinase. The end results are either *Mitf*$^{+}$ (CreER^{T2} not activated) or *Mitf*^{K243R} (CreER^{T2} activated by 4-OHT). (B) Agarose gel showing results of the PCR used to determine the *Mitf*^{K243R} status of the cells. The results of the PCR amplicons are shown for WT cells (WT *Mitf*), cells carrying the *Mitf*^{K243R} construct but not induced (*Mitf*$^{+}$, resulting in a WT *Mitf* phenotype) or induced by 4-OHT (*Mitf*^{K243R}). (C) Sanger sequencing results of the amplicons shown in Figure 14D. Bases highlighted in red are different from the WT *Mitf* sequence. Bases boxed in blue are the 13 additional bases located after the second LoxP site.

To better understand the role of the *Mitf*^{K243R} mutation in melanocytes *in vitro*, we isolated melanocytes from the skin of newborn pups (1 to 3 days old) from WT and *Mitf*$^{K243R/K243R}$; Tyr::CreER^{T2}/0 mice and cultured them *in vitro* to obtain primary melanocyte cell lines. Briefly, we dissected skin from newborn pups derived from matings of the mice in Figure 16D (yellow circles). The culture medium was supplemented with TPA at all times to stimulate cell growth (Arita et al., 1992), and also with G418 (Geneticin) for a few days to positively select melanocytes from fibroblasts (Halaban and Alfano, 1984). After a couple of months of changing the medium three times a week, the cell lines started to grow, reached 90% confluency and were ready to be split. We used the first four passages to expand the cell line and saved them in freezing medium for long term conservation in liquid nitrogen. The cell lines generated are detailed in Table 2. The table lists the following information: cell line number (from the number of the newborn pup from which the cell line was generated), date of generation (first month of culture), if the cells carry the *Mitf*^{K243R} construct and/or the Tyr::CreER^{T2} and Dct::LacZ transgenes.

Table 2. Primary melanocytes cell lines generated. * tg = transgene, ** = HG is Hilmar Gunnlaugsson, RL is Romain Lasseur.

Cell line #	Date of generation	*Mitf*^{K243R}	Tyr::CreER^{T2}	Dct::LacZ	Generated by
3477	February_2018	tg/tg*	tg/0	0/0	HG**
3478	February_2018	tg/tg	tg/0	0/0	HG
3597	May_2018	tg/tg	0/0	0/0	HG
3598	May_2018	tg/tg	tg/0	tg/0	HG
3600	May_2018	tg/tg	0/0	tg/0	HG
3601	May_2018	tg/tg	0/0	0/0	HG
3602	May_2018	tg/tg	tg/0	0/0	HG
3916	December_2018	0/0	tg/0	0/0	HG
3917	December_2018	0/0	tg/0	0/0	HG
3918	December_2018	0/0	0/0	0/0	HG
3919	December_2018	0/0	0/0	0/0	HG
3920	December_2018	0/0	tg/0	0/0	HG
3921	December_2018	0/0	0/0	0/0	HG
3922	**December_2018**	**0/0**	**tg/0**	**0/0**	HG
4229	October_2019	0/0	tg/0	0/0	RL**
4230	**October_2019**	**0/0**	**0/0**	**0/0**	RL
4231	October_2019	0/0	tg/0	0/0	RL
4244	October_2019	0/0	tg/0	0/0	RL
4248	October_2019	0/0	tg/0	0/0	RL
4249	October_2019	0/0	tg/0	0/0	RL
4250	October_2019	0/0	0/0	0/0	RL
4251	December_2019	0/0	0/0	0/0	RL
4252	December_2019	0/0	0/0	0/0	RL
4253	December_2019	0/0	0/0	0/0	RL
4256	December_2019	0/0	tg/0	0/0	RL
4774	**July_2021**	**tg/tg**	**tg/0**	**tg/0**	RL
4775	**July_2021**	**tg/tg**	**tg/0**	**tg/0**	RL
4776	**July_2021**	**tg/tg**	**tg/0**	**tg/0**	RL
4777	July_2021	tg/tg	tg/0	tg/0	RL

For our experiments we used cell lines number 4230 (*WT MITF*, no transgene) and 3922 (*WT MITF*, Tyr::CreER^{T2}/0) as control cell lines. We used cell lines 4774, 4775 and 4776 as *Mitf*^{K243R} 4OHT-inducible cell lines (genotype: *Mitf*$^{K243R/K243R}$; Tyr::CreER^{T2}/0; Dct::LacZ). The cell lines we have generated are valuable *in vitro* models as we can induce the *Mitf*^{K243R} mutation at will and then study the change in phenotype due to this mutation.

4.2.2 Induction of the *Mitf*^{K243R} mutation in the cell lines

Figure 17A shows the cells carrying both the *Mitf*^{K243R} construct (homozygous) and the Tyr::CreER^{T2} transgene (hemizygous) and how the Cre recombinase deflox the cassette containing the WT exon 8 and 9 in presence of 4-OHT. On the contrary, if the cells are treated only with methanol, the diluent of 4-OHT, Cre recombination is not activated, and the cells express *Mitf* from the cassette containing wild type exons 8 and 9 (*Mitf*$^{+/+}$). Figure 17B is an illustration of the genotyping strategy used to determine whether the *Mitf*^{K243R} mutation was induced upon 4-OHT treatment. The three different genotypes possible for the cells are: *Mitf* Wild-Type allele (*WT MITF*), *Mitf* with the uninduced *Mitf*^{K243R} construct (cPM, *Mitf*^{K243R} non-floxed) or after Cre-induced deletion of *Mitf* leading to the *Mitf*^{K243R} construct (PM, *Mitf*^{K243R} floxed). The genotyping strategy is based on the DNA sequences of three different alleles (Figure 17A): before treatment or after treatment by methanol or 4-OHT. To verify the status of *Mitf in* the cells in culture, we genotyped the cells as previously described in Figure 11A. Additionally, when the cells were treated with 4-OHT it resulted in a band of 350 bp in size (PM, *Mitf*^{K243R} floxed). Thus, we have an important and simple tool to determine whether the *Mitf*^{K243R} mutation has been induced. To confirm that the DNA amplicons produced by PCR were of correct size and sequence (e.g., for the cassette insertion and the LoxP site), the three different PCR amplicons (*WT MITF*, *Mitf*^{K243R} non-floxed and *Mitf*^{K243R} floxed) from Figure 17B were Sanger sequenced (Figure 17C). The Sanger sequencing showed that after 4-OHT treatment the 13 additional base pairs expected upon inducing the mutation are present, showing that the recombination actually occurred. The sequence of the LoxP site that was inserted is only present in the *Mitf*^{K243R} non-floxed and the *Mitf*^{K243R} floxed alleles. Moreover, the 13 bp difference between the *Mitf*^{K243R} non-floxed and the *Mitf*^{K243R} floxed allele sequences allow us to track the induction of the *Mitf*^{K243R} mutation in the mutant cells and thus to make sure that the phenotype is associated with the *Mitf*^{K243R} mutation status.

4.2.3 Phenotypic characterization of the *Mitf*^{K243R} mutant cell lines

4.2.3.1 The Mitf^{K243R} *mutation affects melanocyte proliferation*

We have previously shown (in part 4.1.7.1) that *Mitf*^{K243R} mutant melanoblasts *in vivo* are fewer than the WT melanoblasts during embryonic development. Thus, we wanted to determine the effects of the *Mitf*^{K243R} mutation on proliferation *in vitro*. The first assay we

performed to assess this effect was to measure the growth of the cells using the Incucyte Imaging System (Figure 18). For this experiment we used cell lines 4230 (*WT MITF*, no transgene) and 3922 (*WT MITF*, Tyr::CreER^{T2}/0) as control cell lines. We also used three independently derived *Mitf*$^{K243R/K243R}$; Tyr::CreER^{T2}/0 cell lines (4774, 4775 and 4776) where the *Mitf*^{K243R} mutation can be induced by 4-OHT. After the cells were seeded in culture medium in 96-well plates, they were treated either with methanol (control) or 4-OHT for seven days. We set up the Incucyte system to take pictures every two hours for 168 hours. In Figure 18, we display representative pictures for every cell line at 0 hour (beginning of the experiment), at 96 hours (half of the experiment) and 168 hours (end of experiment). As the contrast of the images was not sufficient, we added a mask (created through the Incucyte software) that highlights the area that the cells cover, and then allows the calculation of the cell confluency. Pictures representative for both *WT MITF* cell lines (4230 and 3922) are shown in Figure 18A. For both wild type cell lines, the confluency of cells treated with methanol looks similar to the ones treated with 4-OHT after 96 hours and 168 hours of treatment. On the other hand, representative pictures of cell lines carrying both the *Mitf*^{K243R} construct and the Tyr::CreER^{T2} transgene (4774, 4775 and 4776) are displayed in Figure 18B. Contrary to the *WT MITF* cells, when all three mutant cell lines were treated with 4-OHT, the confluency did not seem to increase compared to when treated with methanol at 96 and 168 hours. This suggests major effects of the mutation on cell growth.

We also looked at the difference of growth of the WT MITF cells with and without TPA, an activator of PKC (photomicrographs not shown), and graphed their growth curve (Figure 19A). As expected from the literature, TPA is necessary for the cells to grow as after 72h growth curves of both 3922 and 4230 cell lines were flat, showing the cells do not proliferate after this amount of time without TPA. The cells still growing for 72h are most likely explained by the fact that before the experiments the cells were treated with TPA and that it still has some long-lasting effects in the cell, as suggested previously (Krasagakis et al., 1993). Figures 19B and C display the evolution of the confluency on graphs with the time on the X-axis (in hours) and the percentage of confluency of the entire well on the Y-axis (range from 0 to 100%). The *WT MITF* cell line 4230 (Figure 19B) shows a very slight difference of confluency between the two treatments at 96 hours: the cells treated with methanol reached 55% confluency whereas those treated with 4-OHT reached 48%. At 168 hours, methanol-treated cells had reached 75% confluency when 4-OHT-treated cells had reached 66%. However, the slope of both growth curves seems parallel, though with slightly fewer cells in those treated by 4-OHT. The percentage of confluency of the *WT MITF* cell line 3922 (Tyr::CreER^{T2}/0, Figure 19B) did not change when treated with 4-OHT; both reached 60% at 168 hours. Upon methanol treatment the three *Mitf*$^{K243R/K243R}$ mutant cell lines with the Tyr::CreER^{T2} transgene (light purple curves) grew in the following manner (Figure 19C): the 4774 cell line went from 7% confluency at 0 hour to 34% at 168 hours, 4775 went from 9% confluency at 0 hour to 39% at 168 hours for and the 4776 cell line went

from 6% at 0 hour to 42% (168 hours). However, the same cell lines, when treated with 4-OHT to induce the *Mitf*^{K243R} mutation, did not follow the same curve. Indeed, 24 hours after the beginning of 4-OHT treatment, the 4774 cell line reached its maximum confluency (14%) and then decreased to 6%. For the 4775 cell line, the confluency reached its maximum (17%) at 48 hours and then decreased slowly to 13%. The cell line 4776 reached 11% confluency at 72 hours and then stayed at this value until 168 hours. Unlike the two first cell lines, the confluency of cell line 4776 did not decrease after reaching its maximum.

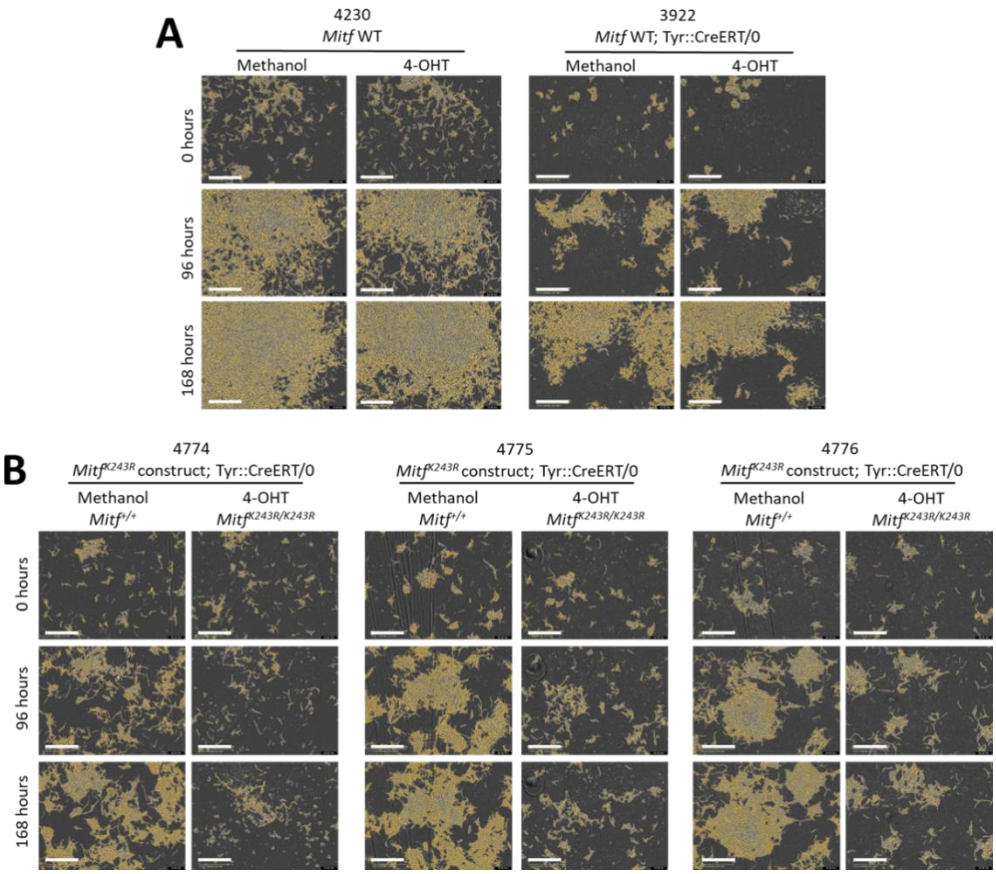

Figure 18. *Mitf*^{K243R} mutant cells fail to grow. Images of cultured cells taken by the Incucyte imaging system at 0, 96 and 168h. Confluency, representing the coverage of the well by the cells, is displayed in a yellow mask on the pictures and was measured by the Incucyte software. The scale bar in the bottom left of every picture represents 400 µM. (A) Images of control cells wild-type for *Mitf* with no transgene (4230, *Mitf*$^{+/+}$) or with the inducible Tyr::CreER^{T2}/0 transgene without the *Mitf*^{K243R} construct (3922, *Mitf*$^{+/+}$). Both were treated with either methanol or 4-OHT for 168h. (B) Images of cells carrying the *Mitf*$^{K243R/K243R}$ construct and the Tyr::CreER^{T2}/0 transgene (4774, 4775 and 4776) treated with either methanol (control, *Mitf*$^{K243R/K243R}$ non-floxed) or 4-OHT (mutation induced, *Mitf*$^{K243R/K243R}$ floxed).

To determine effects of the MITF mutation on doubling time, we evaluated the time that cells need to double between 48 and 96 hours (Figure 19D), which is the time window located in the log phase of the cells (when the cells are in a logarithmic growth phase). The graph shows the number of hours necessary for the cells to double within the time window shown between the blue discontinued lines on Figures 19B,C. For positive values, the higher the value, the longer it takes for the cells to double. In contrast, negative values represent a decreasing population of cells representing dying cells. The first observation is that the doubling times of the *WT MITF* cells (67±12 hours for 4230 and 44±13 hours for 3922) and cells carrying the *Mitf*^{K243R} construct (*Mitf*^{K243R} non-floxed) (67±9 hours for 4774, 60±4 hours for 4775 and 50±9 hours for 4776) are not statistically different upon methanol treatment (P-value > 0,05). This means that in the presence of wild type MITF control-treated, no differences are observed in growth rate of melanocytes. Upon 4-OHT treatment, the two *WT MITF* cell lines (3922 and 4230), showed no statistical differences in the doubling times: for the *WT MITF* 4230 cells, doubling time was 67±12 hours when treated with the control and 85±15 hours when treated with 4-OHT (P-value = 0,72). For the *WT MITF* 3922 (Tyr::CreER^{T2}/0) cells, the doubling time was 44±13 hours with the control and 46±6 hours upon 4-OHT treatment (P-value > 0,99). In contrast, the cells carrying the *Mitf*^{K243R} construct showed a significant difference when treated with 4-OHT. Indeed, the control-treated 4774 cells exhibited a doubling time of 67±9 hours whereas when treated with 4-OHT they had a negative value of -62±8 hours, indicating that 50% of the cells are lost. Similarly, the 4775 cells treated with the control had a doubling time of 60±4 hours whereas it was -251±99 upon 4-OHT treatment. Finally, the *Mitf*^{K243R} cell line 4776 had a doubling time of 50±9 hours when treated with the control whereas it was 227±90 hours upon 4-OHT treatment. This indicates that this cell line, when treated with 4-OHT, still grows but at a much slower rate.

These results show a severely reduced growth of the primary melanocytes induced with the *Mitf*^{K243R} mutation. Indeed, for two of the three mutant cell lines (4774 and 4775), the cells show a negative growth rate indicating cell death on top of reduced proliferation. This double effect on growth of the cells, due to suppressed proliferation and defect in survival might explain the fewer melanoblasts observed in *vivo* in developing embryos. Interestingly, the third *Mitf*^{K243R} mutant 4776 cell line showed a smaller proportion of dying cells, compared to 4774 and 4775. Taken together, these results show that the *Mitf*^{K243R} mutation severely affects proliferation and possibly survival of melanocytes. However, this assay does not inform us of the proportion of cells proliferating versus proportion of cells dying.

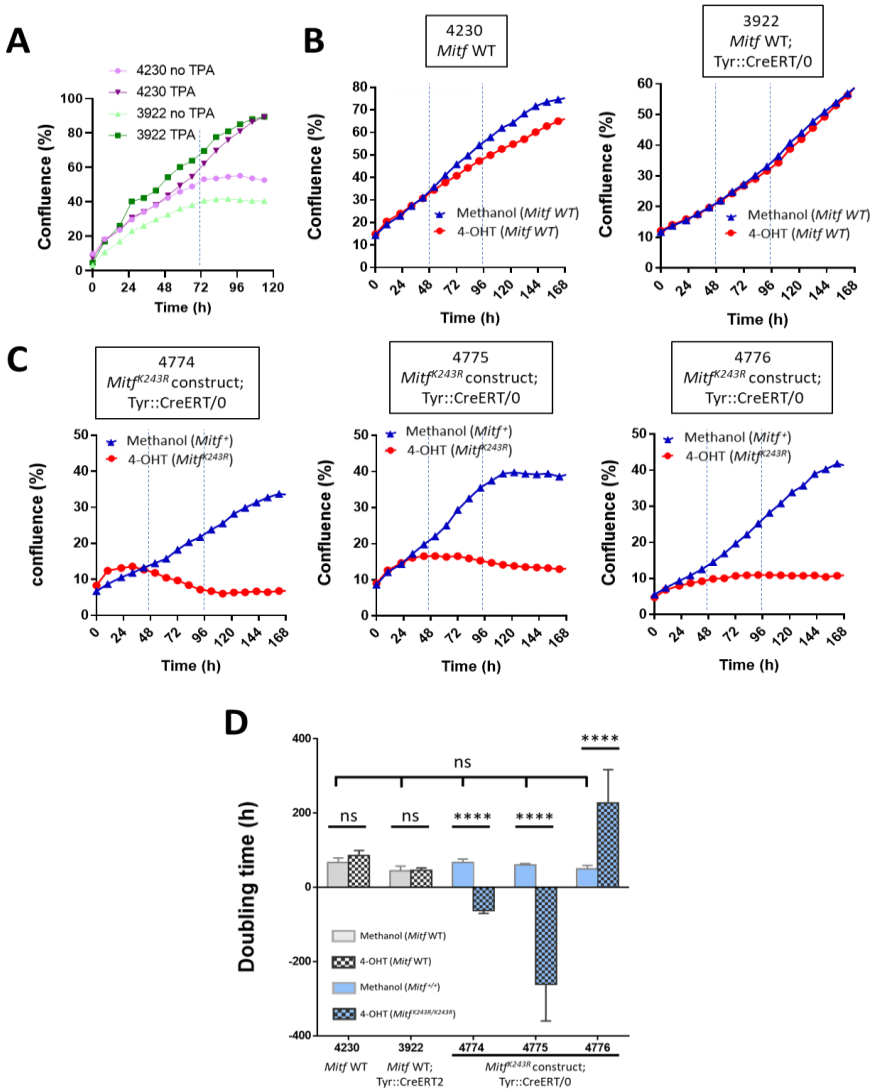

Figure 19. *Mitf*^{K243R} mutant cell population stops to grow and start dying. (A) and (B) Confluency (in percentages) of each indicated WT cell lines from 0 to 168h treated with methanol (control, blue) or 4-OHT (red). (C) The growth curves of the three cell lines carrying the Mitf^{K243R} inducible construct (Mitf^{K243R}; Tyr::CreER^{T2}/0). Cells were treated with either methanol (blue) or 4-OHT (red) to induce the mutation. The blue vertical lines show the time window between 48h and 96h used to calculate the doubling times. (D) Doubling time of the cells based on the confluency in A and B. Statistical analysis was performed by a Tukey's multiple comparison test and P-values are evaluated as follows: P > 0,05 = ns and P < 0,0001 = ****.

4.2.3.2 *Mitf*^{K243R} mutation affects the cell cycle by increasing the number of cells in Sub G1 phase

To assess the effect of the *Mitf*^{K243R} mutation on the proportion of cells proliferating and in apoptosis, we performed a cell cycle analysis experiment using a the 7-AAD fluorescent DNA intercalator (Figure 21). The intensity of the fluorescence of 7-AAD is directly correlated with the concentration of intact DNA. Thus, by looking at the intensity of 7-AAD staining, we were able to determine the percentage of cells in each step of the cell cycle. Cells have 2n DNA in G1 phase (cells can also be in the G0 resting phase), between 2n and 4n in S-phase and 4n in G2/M phase. If the DNA content is below 2n due to DNA fragmentation, the cells are in a sub-G1 state and considered apoptotic. In contrast, if the cells have DNA content greater than 4n, they are considered polyploid. Figure 20 represents the cell cycle profile from flow cytometry in graphs where the intensity of the 7-AAD fluorescence is on the X-axis and the unit area (percentage of cells at a certain intensity) on the Y-axis. For this experiment, we used cell line number 3922 as *WT MITF* and the three *Mitf*^{K243R} inducible cell lines (4774, 4775, and 4776) as the experimental cells. Red curves represent the cells treated for 72h with methanol as control, and blue cells represent cells treated with 4-OHT. We defined gates for grouping cells at the same cell cycle step. Briefly, to set up the gates for each phase we used the peak where the highest fluorescence intensity was observed in the methanol treated cells as the reference gate. This value represents the cells in G1-phase with 2n DNA and we adjusted the zone to both sides of the peak. We then did the same with the peak located at twice the value of the G1 peak: this situates the G2/M-phase peak. The zone in between the G1 and G2/M peaks is then defined as the S-phase gate. All the cells located before the G1 gate are defined in the sub G1 gate whereas all the cells located after the G2/M gate are defined as the Polynuclear gate. Gates are displayed in increasing shades of grey with increased intensity of the fluorescence.

In Figure 21, the percentage of cells of Figure 20 is represented by the value of the area under the curve in the gate. Based on this, we calculated the percentage of cells in every cell cycle step using the area under the curve in every gate and plotted the values in bar plots (Figure 21A to E). There is one graph for each cell cycle stage, with every cell line treated with methanol or 4-OHT labelled on the X-axis while the Y-axis stands for the percentage of cells. The percentages shown represent the total number of cells in all the cell cycle steps: Sub G1 (Figure 21A), G1 (Figure 21B), S (Figure 21C), G2/M (Figure 21D) phases and Polynuclear cells (Figure 21E). The WT cells did not show any differences upon treatment with methanol or 4-OHT for the cell cycle phases Sub-G1, G1, S and G2/M whereas polynuclear cells had two percent more cells in this phase when the cells were treated with methanol. For the *Mitf*^{K243R} inducible cell lines, we noticed that two of the cell lines (4774 and 4775) behaved the same for all the cell cycle phases. Upon 4-OHT treatment, the Sub-G1 phase was increased from 16% to 54% for 4774 and from 11% to 45% for 4775 when compared to methanol. In contrast,

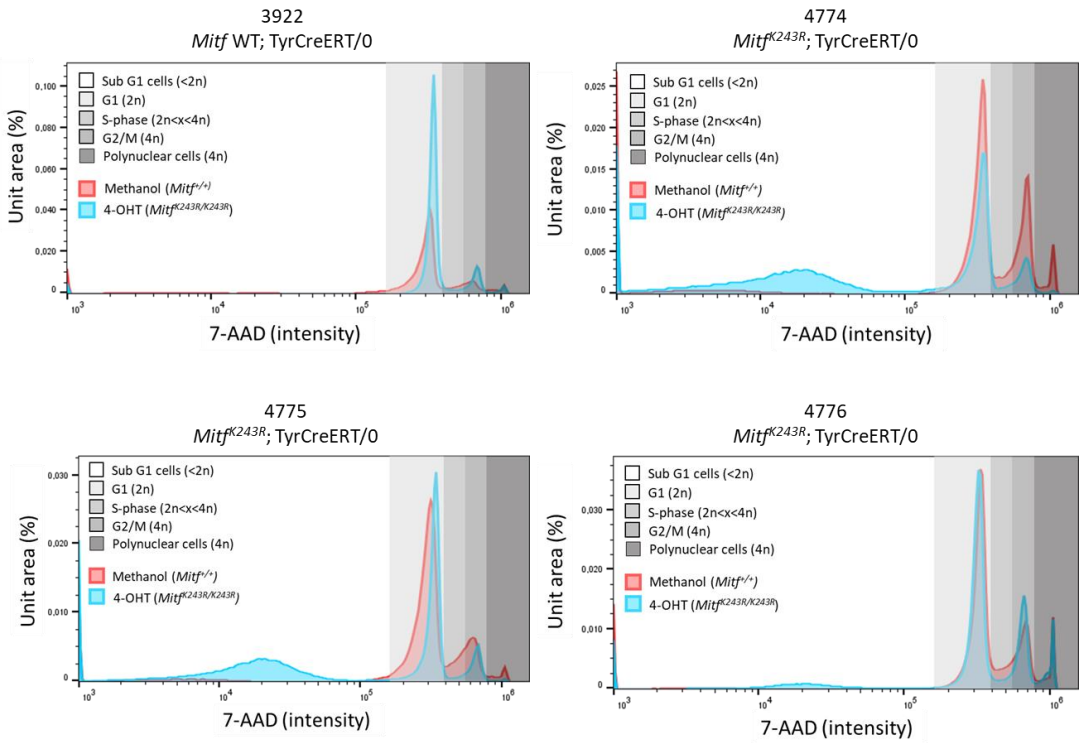

Figure 20. Cell cycle profiles of WT and *Mitf*^{K243R} mutated cells. Cell cycle profiles are shown in graphs with the fluorescence intensity of the 7-AAD (staining for the DNA) on the X-axis on a logarithmic scale and the relative value for the count of cells on the Y-axis (unit area). The WT *Mitf* (3922) or *Mitf*$^{K243R/K243R}$ (4774, 4775, 4776) cells were either treated with methanol (control, red curve and area) or 4-OHT (mutation induced, blue curve and area). Gates used to define the different cell cycle steps (G1, S-phase and G2/M), apoptotic cells (Sub G1) and polynuclear cells are displayed as different shades of grey as indicated in the legend.

when treated by 4-OHT these cells show a decrease in G1 phase from 49% to 35% for 4774 and from 64% to 44% for 4775. A similar decrease was observed in S-phase which decreased from 8% to 3% for 4774 and from 9% to 3% for 4775. For the G2/M-phase, the 4774 cell line showed a decrease from 21% with methanol to 6% with 4-OHT, and 4775 from 12% to 7%. Finally, less than 1% of the 4774 and 4775 cells are polynuclear upon 4-OHT treatment, while 6% and 4% of the methanol treated cells were polynuclear, respectively. The differences between methanol and 4-OHT treatment are all significant (p-value < 0,0001). Interestingly, the *Mitf*^{K243R} inducible cell line 4776 acted differently from the 4774 and 4775 cell lines for all the cell cycle phases except the S-phase. These cells showed no significant differences in the percentages of polynuclear cells, Sub-G1 or G1 phases, whereas the G2/M phase was significantly increased after 4-OHT treatment, but only from 16% to 18%. However, like the 4774 and 4775 cell lines, 4776 showed a reduction from 12% to 6% in the proportion of cells in S-phase when treated by 4-OHT. Thus, unlike the 4774 and 4775 cells lines, 4776 has reduced proliferation but the cell cycle does not seem to be altered as much

as the two other cell lines and does not show cell death. Stacked charts of the non-dying cells (with the Sub-G1 peak removed) and statistical tests are shown in Appendix A, Supplementary Figure 37.

Together, these results indicate that the *Mitf*^{K243R} mutation reduces the number of cells going through the S-phase of the cell cycle. It might also play a role in the progression from the G2/M phase to mitosis and might also increase cell apoptosis (the 4774 and 4775 mutant cell lines show these features). Thus, we suggest that the *Mitf*^{K243R} mutation leads to a disruption of cell cycle progression, thus explaining why there are fewer melanoblasts in developing embryos, first because of reduced proliferation and possibly due to effects on cell survival.

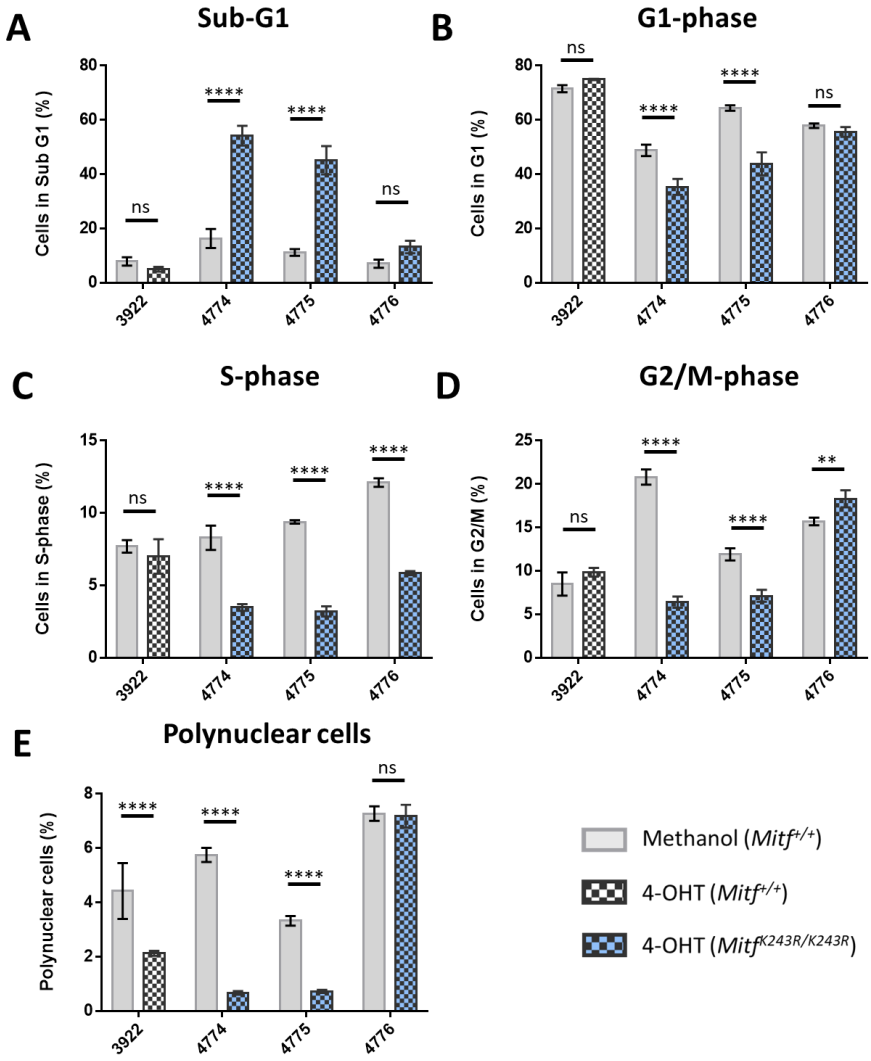

Figure 21. Quantification of cell cycle profiles exhibit a reduced number of *Mitf*^{K243R} mutant cells entering S-phase. The percentages of cells in each step of the cell cycle are presented in bar plots: (A) for Sub-G1, (B) for G1-phase, (C) for S-phase, (D) for G2/M-phase and (E) for the polynuclear cells. Each bar represents the mean (with the standard error) for each of three replicates of every condition and cell type. Statistical analysis was performed using Sidak's multiple comparison test and P-values are evaluated as following: P > 0,05 = ns, P < 0,05 = *, P < 0,01 = **, P < 0,001 = *** and P < 0,0001 = ****.

4.2.3.3 *Mitf*^{K243R} mutant cells become apoptotic after 48 hours of 4-OHT treatment

To confirm the effect of the *Mitf*^{K243R} mutation on cell survival, we performed an apoptosis assay to quantify the number of cells that enter this state after induction of the mutation. To do so, we measured the fluorescence of cells incubated with the Caspase-3/7 dye in the medium. This dye can penetrate the cell only if the plasma membrane integrity is reduced, which is the case of apoptotic cells, and then bind to DNA and emit a fluorescent signal. The fluorescence was captured by the Incucyte Imaging system from just before the beginning of either methanol or 4-OHT treatment to 96h. Representative pictures of the fluorescence at 0h (before the treatment), 48h and 96h are displayed in figure 22A, with every dot representing an apoptotic cell. We did not observe any difference at 0h but observed an increased number of apoptotic cells from 48h, which increased even more at 96h. To quantify this increase, we counted the number of apoptotic cells for every picture with the Incucyte software and divided it by the percentage of confluency to obtain an apoptotic index: the lower this value is, the less apoptotic cells there are regarding the whole cell population, and the higher this value is the more apoptotic cells are. The WT cell lines 4230 and 3922 showed almost no apoptotic cells for every time point for both methanol and 4-OHT treatment (Figure 22B) with an apoptotic index being around 0,2. Similarly, the cells lines carrying the *Mitf*^{K243R} construct treated by methanol showed almost no apoptotic cells. However, these same cells treated by 4-OHT to induce the *Mitf*^{K243R} mutation showed a significant increase of apoptotic cells from 48h. Indeed, the 4774 cell line showed the largest increase with an apoptotic index of 11, 96h after the induction of the *Mitf*^{K243R} mutation. The apoptotic index value of the 4775 cell line after 96h was 7 and 4 for the 4776 cell line. This result confirms that the cells with the *Mitf*^{K243R} mutation undergo apoptosis, as suggested by the growth and the cell cycle profile assays. The 4774 cell line has the most apoptosis, and the 4776 cell line has less, which is coherent with the growth and cell cycle profile assays previously described.

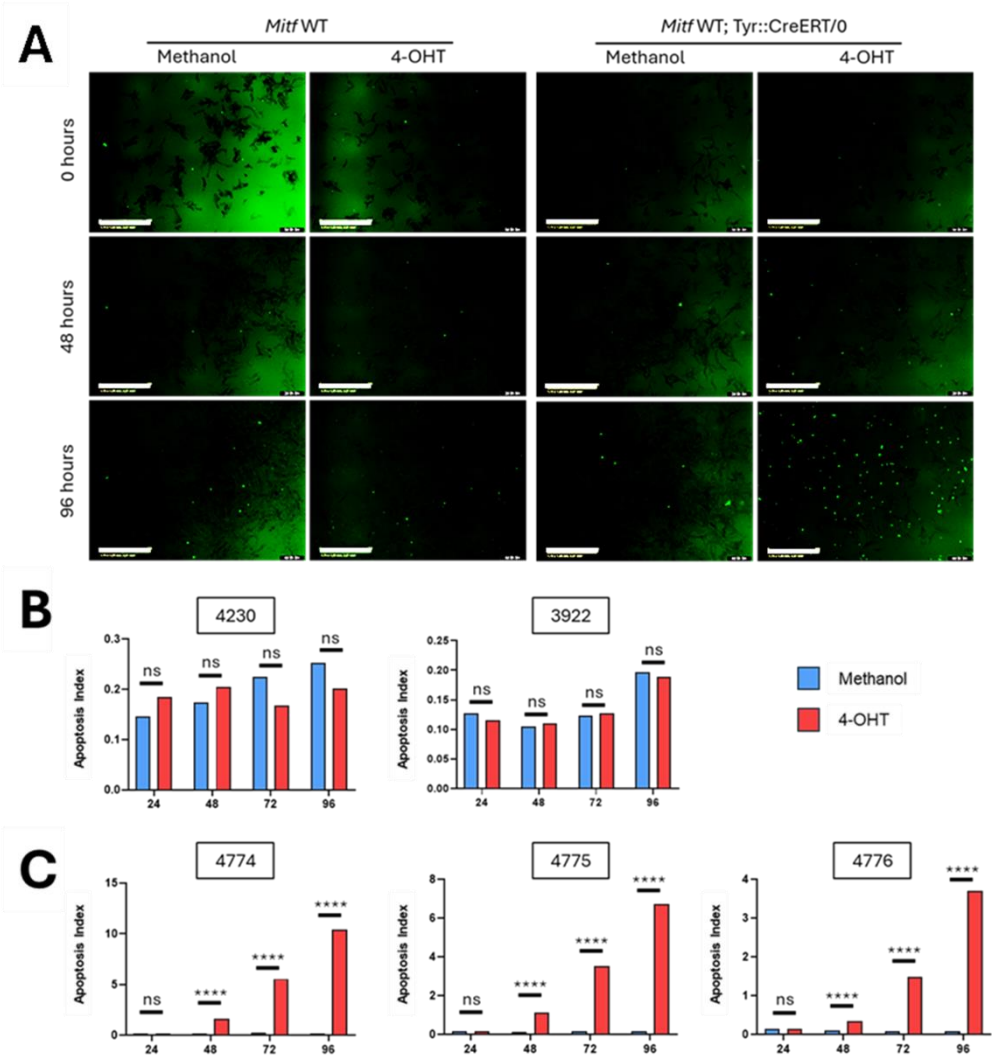

Figure 22. *Mitf*^{K243R} mutants cells die after 48h of 4-OHT treatment. (A) Representative images of the apoptosis for WT *Mitf* (3922 and 4230) or cells carrying the *Mitf*$^{K243R/K243R}$ construct and the Tyr::CreER^{T2}/0 transgene (4774, 4775 and 4776) treated with either methanol or 4-OHT, before treatment at 0h, or 48 and 96h after treatment. Green fluorescence indicates apoptotic cells. The scale bar length is 400 µm. (B) Graph of the calculated apoptosis index on the WT *Mitf* cells lines 4230 and 3922 treated with methanol (blue) or 4-OHT (red). (C) Graph of the apoptosis index of the *Mitf*$^{K243R/K243R}$; Tyr::CreER^{T2}/0 cell lines 4774, 4775 and 4776 treated with methanol (*Mitf*$^{K243R/K243R}$ no-floxed, blue) or 4-OHT (*Mitf*$^{K243R/K243R}$ floxed, red). Statistical analysis was performed by a Tukey's multiple comparison test and P-values are evaluated as follows: P > 0,05 = ns and P < 0,0001 = ****. Biological replicates: n=3.

4.2.3.4 The Mitf^{K243R} mutation seems to reduce the size of melanocytes

To further assess the state of the cells, we also looked at their morphology after 96h of induction by methanol (control) or 4-OHT in both cell types. Immunostaining of the cytoskeleton using anti-Vimentin antibodies revealed that there are no major changes in cell shape observed upon either the 4-OHT treatment or the *Mitf^{K243R}* mutation (Figure 23A, green channel), even though the 4774 cell morphology looks more shrunk. However, the size of the nuclei in the *Mitf^{K243R}* mutant cells seemed smaller compared to their control for most of the cells (Figure 23A, blue channel). We thus measure the size of the nuclei for every cell line and conditions and plotted their values in a dot plot (Figure 23B). This study revealed that the two *Mitf^{K243R}* mutant cell lines 4774 (P-value < 0,0001) and 4775 (P-value < 0,01) have a significantly reduced nuclear size upon induction of the *Mitf^{K243R}* mutation. Interestingly, increased nuclear size is thought to be important for transcription and cell cycle progression (Webster et al., 2009), and nuclear size has been shown to be relevant to cell size (Jevtić et al., 2014). Therefore, this suggests that, 96h after the induction by 4-OHT, the *Mitf^{K243R}* mutation significantly but slightly changes the morphology of the cells of the 4774 and 4775 cell lines, but not the 4776 cell lines. Again, this is consistent with the assays we previously described, confirming the changes upon *Mitf^{K243R}* mutation, with more effects on the 4774 and 4775 cell lines than in 4776.

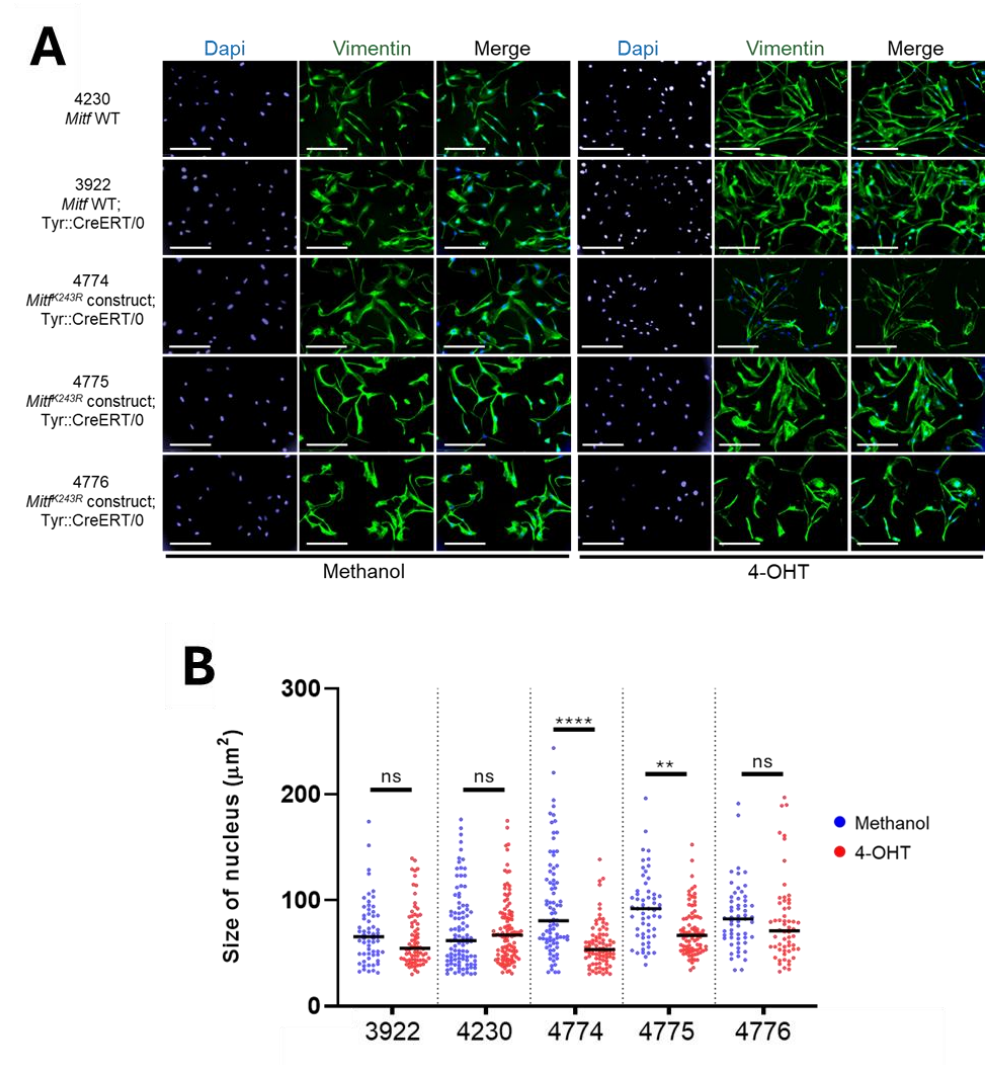

Figure 23. The *Mitf*^{K243R} mutation reduces the size of the nucleus of cell lines 4774 and 4775. (A) Representative pictures of Vimentin (cytoskeleton, green) and DAPI (nucleus, blue) fluorescent staining in WT *Mitf* or *Mitf*^{K243R} cells treated with methanol or 4-OHT. Scale bar = 100 µm. (B) Dot-plot representing the size of every nucleus in µm^2 based on quantification of Dapi staining. Statistical analysis was performed using Tukey's multiple comparison test and P-values are evaluated as follows: P > 0,05 = ns, P < 0,01 = ** and P < 0,0001 = ****. Biological replicates n=3.

4.2.3.5 Migration of single melanocytes in vitro does not change upon *Mitf*^{K243R} mutation

From observations made in embryos, *Mitf* mutant melanoblasts migrate through the dorso-lateral pathway as they can be seen in many locations distant from the neural crest. As developing melanoblasts are single cells (Figures 13A and B), we performed single-cell migration assays to test if migration of *Mitf* mutant melanoblasts is affected. Briefly, we seeded cells at low confluency (5000 cells in 6 well-plates) to be able to observe single cells. We then removed TPA from the medium to stop proliferation (TPA is inducing PKC and stimulating cell proliferation) and treated them either with methanol (control) or 4-OHT to induce the mutation. We imaged the cells every 30 minutes for 48 hours. We then tracked the cells manually using the "Chemotaxis and Migration Tool" (Ibidi) and created plots for displaying the trajectory of the cells (spider plots of Figures 24A and B). The center of these plots is the starting point of each cell's trajectory, and the black line represents their trajectories with the red dot as the ending point. Practically, the spider plots show that the area within which the cells move are up to 400 µm up, down and on each side of the starting point, representing a total area of 640 mm^2. We observe on the spider plots that neither the *WT MITF* (Figure 24A) nor *Mitf*^{K243R} inducible cells (Figure 24B), show a difference in single cell migration, regardless of treatment (methanol on the left panel and 4-OHT on the right panel). With the Ibidi tool, we were able to extract three metrics characterizing the trajectories of the cells: the velocity (speed in µm/min), the accumulated distance (total distance traveled by the cells in µm) and the Euclidean distance (distance between the starting and ending points in µm). For the *WT MITF* cell line (Figure 24C), velocity was 0,29±0,02 µm/min upon methanol treatment and 0,29±0,02 µm/min upon 4-OHT treatment (P-value = 0,95). The accumulated distance was 780±54 µm when treated with methanol and 820±55 µm when treated with 4-OHT (P-value = 0,63). Finally, the Euclidean distance was 91±9 µm when treated with methanol, and 98±19 µm when treated with 4-OHT (P-value = 0,79). Similarly, for the *Mitf*^{K243R} inducible cell lines (Figure 24D), we did not see changes in velocity, accumulated or Euclidean distances between the two treatments, suggesting that the Mitf mutation has no effect on migratory properties. Indeed, velocity was 0,27±0,01 µm/min upon methanol treatment and 0,27±0,01 µm/min upon 4-OHT treatment; this difference is not significant (P-value=0,99). The accumulated distance was 755±33 µm after methanol treatment and 752±41 µm after 4-OHT treatment and again the difference was not significant (P-value=0,96). The Euclidean distance was 143±19 µm in methanol treated cells and 180±015 µm in the 4-OHT treated cells (P-value=0,14). None of these three metrics were significantly different (P-value > 0,0001). In accordance with what we have observed on the spider plots, none of these metrics show a difference between cells treated with methanol or 4-OHT, thus reinforcing the idea that the *Mitf*^{K243R} mutation does not play a major role in the migration of the cells.

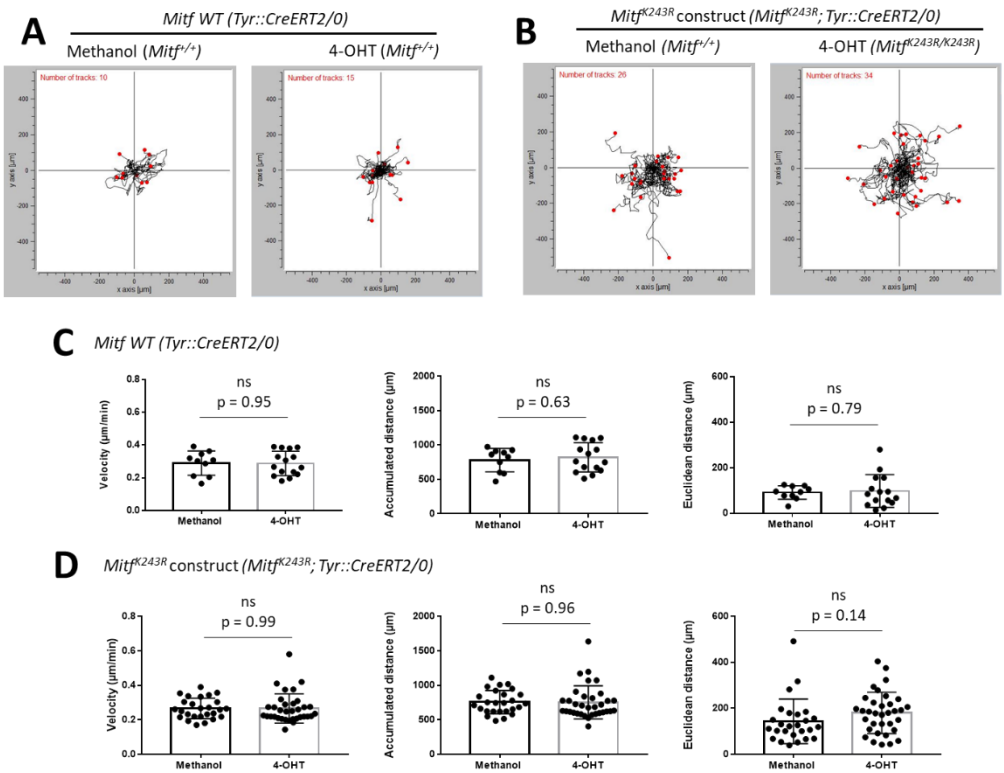

Figure 24. WT and *Mitf*^{K243R} mutant melanocytes show no difference in single-cell migration. (A) Spider plot graphs representing the trajectory of each WT *Mitf* tracked cell treated with methanol (left graph) or 4-OHT (right graph). The center of the graph is the starting point of each cell and the red dots represent the endpoint of their travel within the well. Distances are shown in µm and the number of cells tracked is shown on the top left corner of each spider plot. (B) Spider plot graphs for *Mitf*^{K243R} inducible cells treated with methanol (*Mitf*$^{K243R/K243R}$ non-floxed, left graph) or 4-OHT (*Mitf*$^{K243R/K243R}$ floxed, right graph). (C) Characteristics of the single-cell tracking for each condition of WT *Mitf* cells. Velocity represents the speed (in µm/min), accumulated distance corresponds to the total distance cells have traveled (in µm) and Euclidean distance is the direct distance between the starting point to the endpoint of the trajectory of the cells. Each dot represents the metric of a single cell. Statistical analysis was performed using the Mann-Whitney's test and P-values are evaluated as following: P > 0,05 = ns. (D) Same as (C) for the cells with the *Mitf*^{K243R} construct.

4.2.4 Effects of the *Mitf*^{K243R} mutation on gene expression

4.2.4.1 4-OHT treatment induces the Mitf^{K243R} *mutation but also affects gene expression in WT*

ChIP-seq experiments have shown that the *Mitf*^{K243R} mutant protein binds to low-affinity binding sites throughout the genome of melanoma cells but exhibits reduced DNA binding to the target genes that support melanocyte development (Louphrasitthiphol et al., 2020). We thus performed mRNA-sequencing analysis of cell lines 3922, 4774, 4775 and 4776, to see if this impaired DNA-binding of the *Mitf*^{K243R} mutant is translated into effects on gene expression in melanocytes. To do so, we extracted total RNA from both WT (Tyr::CreER^{T2}/0) and *Mitf*^{K243R} inducible cell lines (*Mitf*$^{K243R/K243R}$; Tyr::CreER^{T2}/0) at 0h time points (no treatment), as well as at the 48h and 72h time points after 4-OHT treatment. After quality control of the RNA integrity, samples were paired-end sequence by Novogene, UK. We then assessed the quality of the reads (Appendix, Figure) and cleaned them with Trimmomatic, aligned them with Kallisto to the reference GRCh38 genome from Ensembl, quantified the reads using DESeq2 and annotated them with gene IDs. Genes with lower expression than two TPMs in all the sequenced samples were cutoff.

Principal Component Analysis (PCA) was performed (Figure 25A) and showed that the largest variability displayed on the X-axis (PC1) represents 43% of the total variability between all the samples. This variability represents the difference between the 0h time point of each cell line with the 48h and 72h time points and shows that the time of treatment leads to clear differences between all the cell lines. This means that the largest variability is an effect due to the treatment by 4-OHT, regardless of the induction of the mutation itself. This information is crucial, as we need to remove this effect that might mask the effects of the *Mitf*^{K243R} mutation on gene expression. The second largest variability (PC2) representing 18% of the variability was less different for the wild type 3922 cell line between 0h, 48h and 72h than it was for the three other cell lines 4774, 4775 and 4776. This suggests that PC2 shows the variability due to the effect of the *Mitf*^{K243R} mutation. Therefore, for the rest of the analysis, we tried to exclude as much as possible of PC1 due to the non-specific effects of 4-OHT treatment. Note that the 72h time point of the 4774 mutant cell line is missing one replicate, thus reducing the significancy of the DEGs.

We also wanted to monitor the efficiency of the induction of the mutant *Mitf* transcripts. To do so, we aligned the reads obtained from the sequence data to the reference mouse genome GRCm39 from Ensembl to get the percentage of mutated A to G in position 728 of the *Mitf* gene (chr6: 98,013,686 is the position in the genome). The percentages are displayed in Figure 25B. No mutations were found for the WT cell line 3922, which is consistent with what we expected. The *Mitf*^{K243R} inducible cell lines 4774 and 4775 showed similar percentages of mutated *Mitf* transcripts at 48h (60%) and 72h

(70%) while they had less than 1% at 0h. Interestingly, the third *Mitf*^{K243R} inducible cell line expressed 85% mutant transcripts at 48h and 94% at 72h while this line only had 1% at 0h. Finally, we looked at *Mitf* isoform-related TPM expression (Figure 25C). Only the *Mitf*-M(+), -A(+), -A(-) and Mdel (a variant of MITF-M isoform) isoforms were detected in the WT and mutant cells. Interestingly, expression of the *Mitf*-M isoform did not change in quantity either the *Mitf*^{K243R} inducible cell lines or in the WT cells. Only the *Mitf*-A(+) isoform showed differential expression over time, with four times increase in the *Mitf*^{K243R} inducible cell lines after 4-OHT treatment, while it barely changed in the *WT MITF* cell line. These results suggest that the *Mitf*^{K243R} mutation is induced in the inducible cell lines with a good efficiency and that the expression of the *Mitf*-A(+) isoform increases upon activation of the *Mitf*^{K243R} mutation. This suggests that MITF-M may repress the expression of MITF-A(+) in melanocytes and that the *Mitf*^{K243R} mutation may be important for the regulation of this specific isoform.

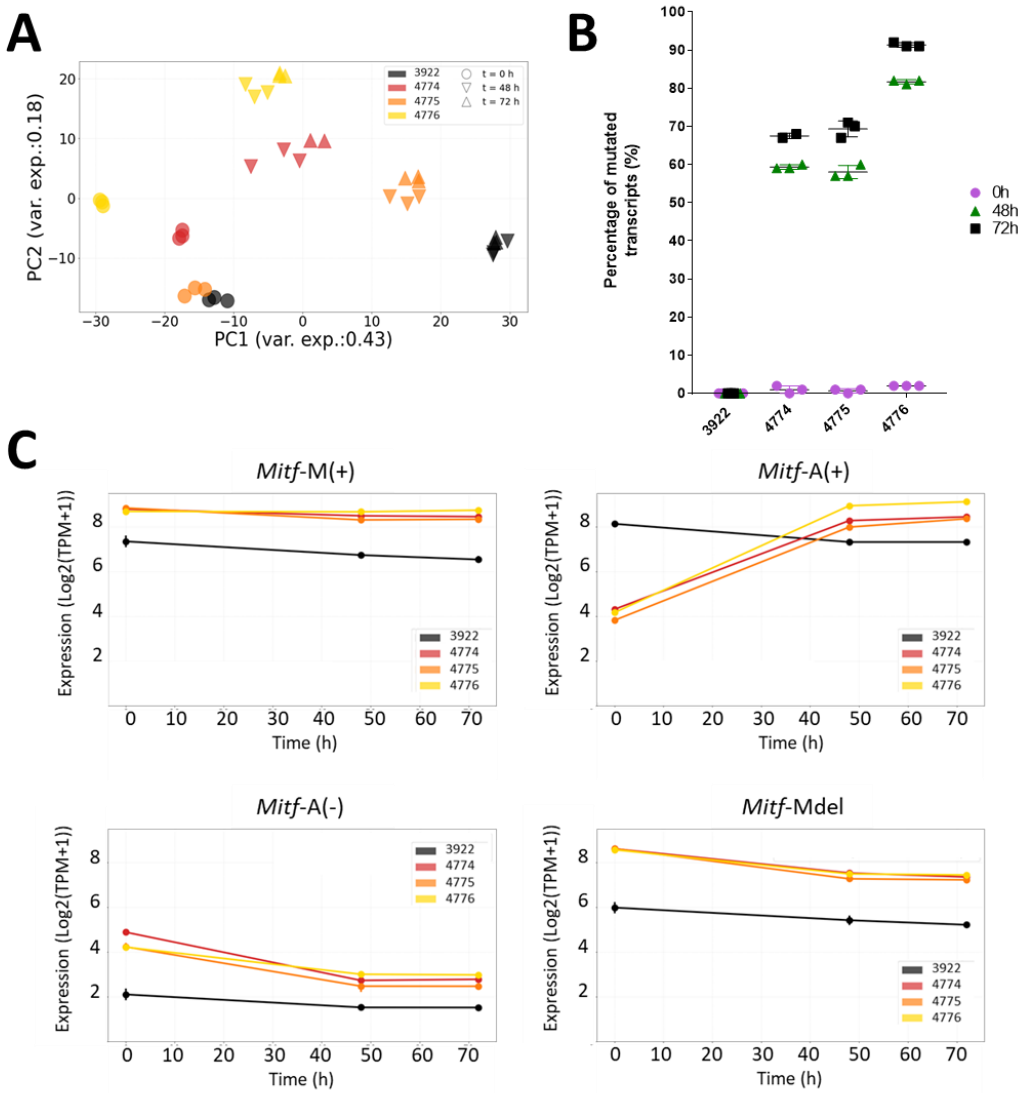

Figure 25. 4-OHT treatment affects gene expression. (A) Principal Component Analysis plot representing the variability in a 2D plot. PC1 corresponds to the largest variability, and PC2 the second largest. Each color stands for a cell line: black (3922), red (4774), orange (4775) and yellow (4776). Circles corresponds to the initial 0h time point, tip-down triangles the 48h time point and tip-up triangles the 72h time point. (B) Percentage of the mutant *Mitf* transcripts resulting from the alignment of the reads to the transcriptome on the Integrative Genomics Viewer (IGV). (C) Expression in Log2(TPM+1)) of the detected isoforms of *Mitf*-M(+), -A(+), -A(-) and -Mdel for each cell line over time.

4.2.4.2 The 4-OHT treatment masks the effects of the Mitf^{K243R} mutation

We asked the following question: "what are the differentially expressed genes upon induction of the *Mitf*^{K243R} mutation?". We thus analyzed the DEGs after 72h of 4-OHT treatment of the WT and mutant cells lines compared to the 0h time point, displayed as volcano plots (Figure 26). The cutoff for the Fold Change (FC) was 1 and the P-adjust (=adjusted P-value) shown on a -Log10 scale was 0,05. The DEGs that passed both thresholds of 1 for log2FC and 0,05 for P-adjust are shown in red dots (Figure 26). The first observation is that in the WT cell line 3922 there are two-fold fewer significant downregulated DEGs (Figure 26A) (n = 153) than DEGs that are upregulated (n = 333). In contrast, the *Mitf*^{K243R} mutant cell lines have more downregulated than upregulated genes. The 4774 cell line has 50 down- and 30 upregulated genes (Figure 26B), the 4775 has 163 down- and 123 upregulated genes (Figure 26C) and the 4776 125 down- and 71 upregulated genes (Figure 26D). To get a better overview of the effect of the *Mitf*^{K243R} mutation, we performed a Gene Set Enrichment Analysis (GSEA) which aims to gather the DEGs into group of genes that share a common biological function. The results of this analysis are displayed in the dot-plots of Figure 27. The dot-plots show the top ten categories for both activated (left panel) and suppressed (right panel) biological processes (BP) and are ranked from the top with the lowest P-adjust. Interestingly, the profiles of the dot-plots of all four cell lines 3922 WT (Figure 27A) and mutants 4774 (Figure 27B), 4775 (Figure 27C) and 4776 (Figure 27D) were quite similar. Indeed, many of the most enriched activated BPs in both WT and mutant cell lines are "mitotic cell cycle", "nuclear division", "mitotic sister chromatid segregation". On the other side, the suppressed BPs shared by all cell line involve cation and ion homeostasis, or cation and ion transmembrane transport, with the 3922 WT and 4775 and 4776 mutant cell lines sharing many more processes together than with the mutant 4774. The different behavior of 4774 is likely to be a downstream effect of the missing third replicate.

Altogether, these results confirm the results of the PCA plot, that the 4-OHT treatment has an impact on the expression of many genes. The fact that many DEGs, as well as BPs, of the *Mitf*^{K243R} mutant cell lines are also differentially expressed in the WT cell line does not explain the major effects of the mutation on proliferation of the cells. The similarity of the results between WT and *Mitf*^{K243R} mutants does not follow the dramatic difference in the growth phenotype of the cells. Therefore, we decided to perform the same analysis with a slightly different pipeline.

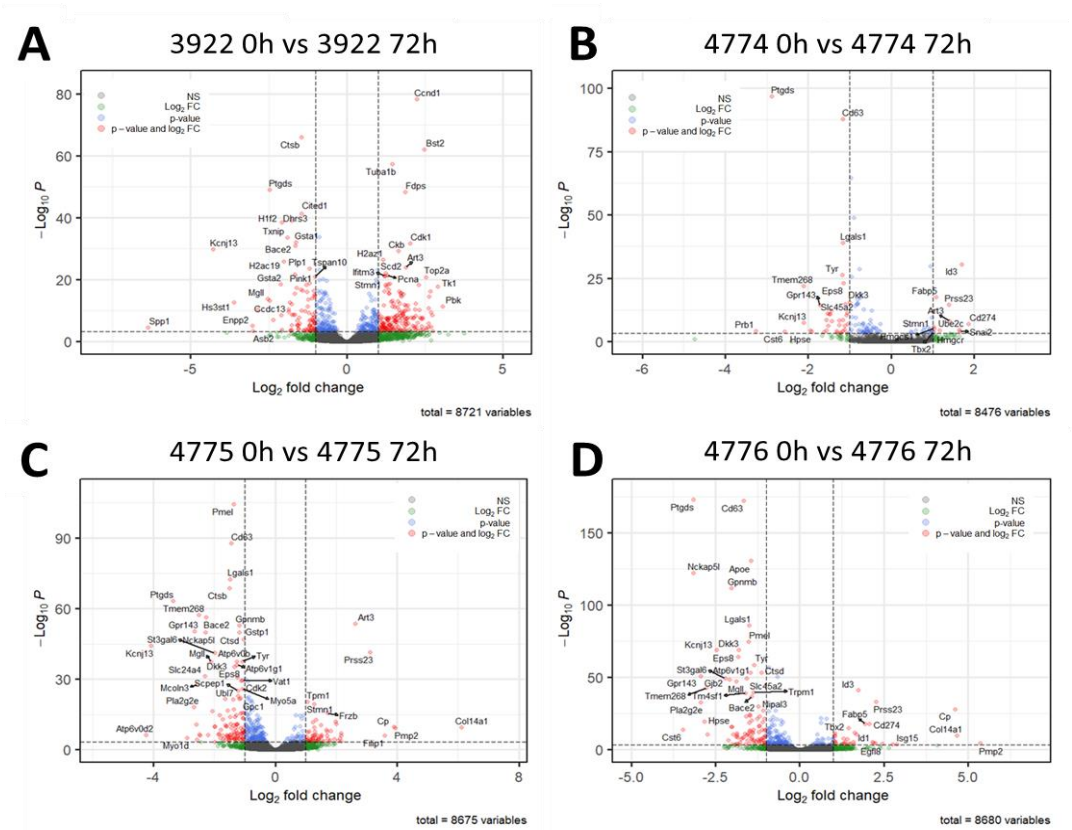

Figure 26. Gene expression profile upon 4-OHT treatment. Volcano plots representing the DEGs before and after 72h of 4-OHT treatment in (A) the 3922 WT cell line, and the *Mitf*^{K243R} mutant cell lines (B) 4774, (C) 4775 and (D) 4776. The X-axis shows the Log2FC and the Y-axis the P-adjust in -Log10. The cut-off used for Log2FC is 1 and for the P-adjust is -Log10P<0,05. Downregulated genes are shown in red dots on the left of the plot while upregulated genes are shown in red on the right.

4.2.4.3 Mitf^{K243R} mutation activates the WNT signaling pathway and regulation of transcription

To find the genes that depend on MITF, we removed the DEGs in each mutant cell line that were also differentially expressed upon 4-OHT treatment of the WT cell line. We kept all the genes that were differentially expressed in both WT and mutant cell lines but were differentially affected (upregulated in WT and downregulated in mutant, or the other way around). After this treatment, the volcano plots of the mutant cell lines 4774 (Figure 28A), 4775 (Figure 28B) and 4776 (Figure 28C) showed fewer DEGs than previously (Figures 26B, C and D). However, by doing this, we selected genes that are more likely to be differentially expressed by the effect of the mutation and are not due to the 4-OHT treatment. The mutant cell lines have 51 genes for 4774 (Figure 28A, 26 down- and 25 upregulated), 100 for 4775 (Figure 28B, 49 down- and 51 upregulated) and 92 for 4776 (Figure 28C, 30 down- and 60 upregulated). It is interesting to notice that the cell line 4776, which is the only mutant cell line of the three that did not have negative growth in our cell culture assays, has two times more upregulated genes than downregulated genes, while the two others have equivalent numbers (50% of each for 4774 and 4775). This might be one of the reasons why the 4776 mutant cell line behaves slightly different in culture.

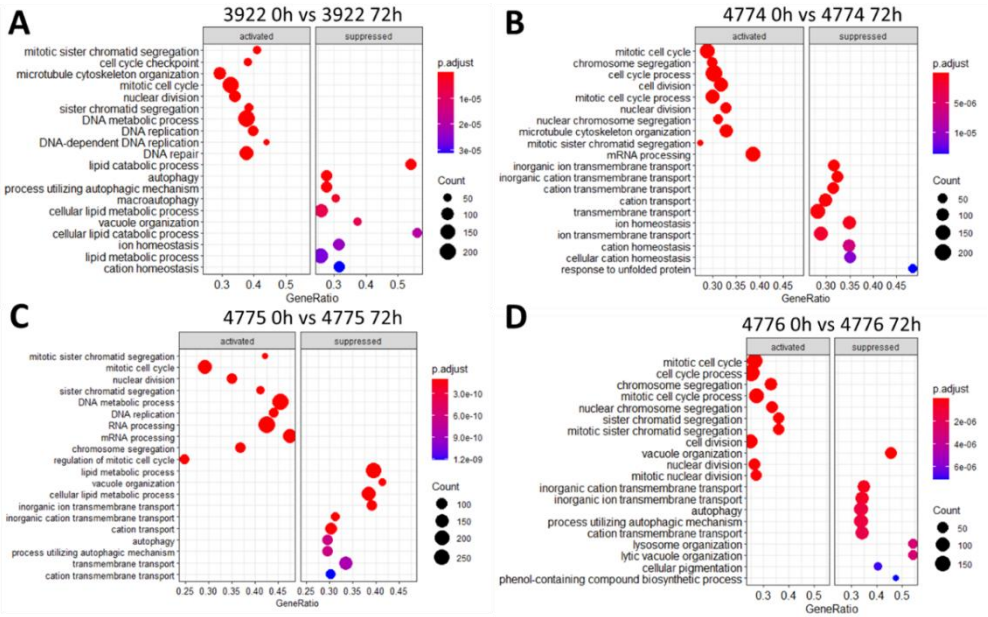

Figure 27. GSEA profiles of the cell lines upon 4-OHT induction. Dotplots representing the significantly activated (left of the plot) or suppresed (right of the plot) biological processes in each cell line: (A) 3922 WT MITF , (B) 4774 cells, (C) 4775 cells and (D) 4776 cells. Terms of the biological processes are written on the left of the plot, and the size of the dots represent the number of genes involved in the BPs, with the color indicating adjusted P-value.

GSEA analysis showed that for the 3922 WT cell line, the biological processes (BPs) activated upon 4-OHT treatment are the same as presented in Figure 27A as in that case the DEGs are the same. However, the BPs for the three *Mitf*^{K243R} mutant cell lines are completely different after we removed the DEGs that were also differentially expressed in WT MITF. The BPs activated upon treatment of the 4774 cell line included two main groups (Figure 29A): genes involved in transcription regulation, and WNT signaling. The BPs that were reduced in expression were mostly genes involved in response to unfolded or incorrect proteins, and positive regulation of DNA binding. The GSEA analysis of the 4775 mutant cell line (Figure 29B) shows that activated genes are involved in transcription and its regulation whereas suppressed genes are involved in ion and transmembrane transport. Lastly, GSEA analysis of the 4776 mutant cell (Figure 29C) showed that activated BPs categories were cell surface receptor signaling pathway involved in cell-cell signaling and canonical WNT signaling. Many of the DEGs of these two categories are the same, like *Snai2, Fgfr3, Sox4, Bcl9, Frzb* and *Fzd7*. Suppressed BPs are involved in positive regulation of DNA binding and incorrect protein and protein folding.

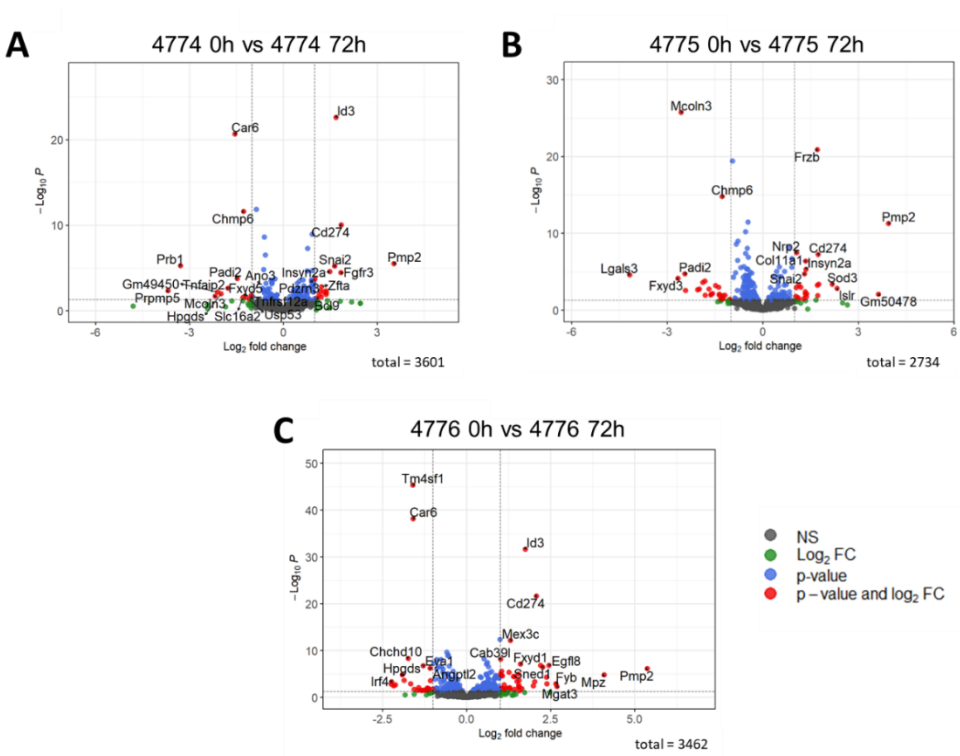

Figure 28. Gene expression profile upon 4-OHT treatment of the *Mitf*^{K243R} mutant cell lines with the DEGs of the WT MITF cell line removed. Volcano plots representing the DEGs before and after 72h of 4-OHT treatment in *Mitf*^{K243R} mutance cell lines (A) 4774, (B) 4775 and (C) 4776 but without the DEGs that are also differentially expressed in the 3922 WT MITF cell line. Parameters of the plots are the same as for Fig 26.

With the many different terms that are activated and suppressed, we wanted to see precisely how many were actually shared between these three mutant cell lines. A Venn diagram (Figure 29D) showed that five BPs are shared by all three cell lines, with four related to the WNT signaling pathway, and the fifth involved in cell surface receptor signaling pathway involved in cell-cell signaling (which include the DEGs of the four other BPs). The WNT signaling pathway is, as discussed in the introduction, crucial for melanocyte development starting from the NCC and all through migration to the epidermis (Dunn et al., 2000; Petit and Larue, 2016), and is known to activate *Mitf* gene expression (McGill et al., 2002). Our results suggest that the WNT pathway at large is a target of MITF. We plotted one of the GSEA terms, the WNT signaling pathway, using Enrichment plots for each cell line (Figure 30A). Such plots give a visual insight of the enrichment score based on a gene set and provides an Enrichment Score (ES), which reflects how much the DEGs are overrepresented (down- or upregulated) in the ranked gene set. However, this value cannot be compared between the cell lines as there are differences in DEGs dataset sizes. So, we also calculated the Normalized Enrichment Score (NES) that considers the differences in size of the datasets, meaning that these values can be compared between the different cell lines. As expected, the NES of the 3922 WT cell line showed a low NES score of -0.89 with

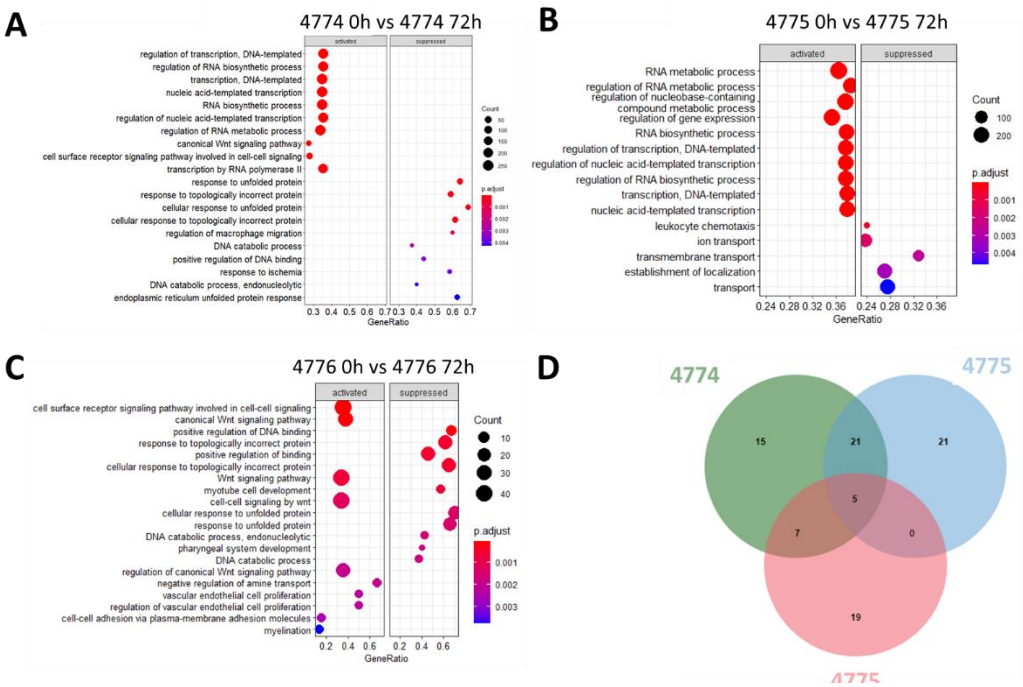

Figure 29. GSEA profiles of the *Mitf*^{K243R} cell lines after removal of the effects of the 4-OHT treatment. The dotplots representing the results of the GSEA for the *Mitf*^{K243R} mutant cell lines (A) 4774, (B) 4775 and (C) 4776 are this time done with the DEGs of the WT MITF removed, thus removing the effects of the 4-OHT treatment. Parameters are the same as for Fig 27. (D) Venn diagram representing the overlapping terms in 4774, 4775 and 4776.

a high P-value of 0,86, meaning that the gene set in the WT cells is not enriched. In contrast, the three mutant cell lines showed high NES scores of 1.68 for 4774, 2.09 for 4775 and 1.67 for 4776, with low P-values respectively of 6e-04, 4e-04 and 6e-04. This confirms that the WNT signaling pathway is repressed by MITF and thus activated in the presence of the *Mitf*^{K243R} mutation and might explain why the cells do not proliferate and die.

The three *Mitf*^{K243R} mutant cell lines 4774, 4775 and 4776 showed increased apoptosis (Figure 22) and reduced proliferation (Figure 19) upon induction of the *Mitf*^{K243R} mutation. However, the cell lines 4774 and 4775 seem to be more similar to each other than they are to the 4776 line. We therefore studied the 21 enriched BPs that are shared between them (Figure 29D). Most of those BPs are related to regulation of RNA metabolic and biosynthetic processes and transcription in general, with most of the same genes involved. We thus selected the one that had the largest number of genes involved which is transcription, DNA-templated. Enrichment plots of this BP (Figure 30B) confirmed the enrichment of the mutant cell line with NES scores of 1.55 for 4774 (P-value=2e-04), 1.83 for 4775 (P-value=4e-04) while the 3922 WT cell line has a NES score of only 1.11 (P-value=0.16). We also looked at the Enrichment plot for 4776, and, interestingly, it revealed that the NES is 1.67 (P-value=6e-04). This is explained by the fact that the cut-off used by the R package used the ES instead of the NES, with a slightly bigger number of differentially expressed genes in the dataset, thus reducing the ES compared to 4774 and 4775 where the dataset in smaller. This suggests that deregulation of the transcription processes would be one possible explanation for why the *Mitf*^{K243R} mutant cell lines die.

Lastly, we plotted some of the DEGs on a heatmap (Figure 30C) with their relative expression displayed by Z-score. The Z-score is a dimensionless value that we can use to compare the expression of a given sample to the expression of the same gene in all the other samples. Basically, a Z-score of 0 means that the expression is the same as the mean of all the samples they are compared with whereas a positive value means the expression is more than the average of all the other samples and a negative value that the expression is less. On this heatmap, we can see two trends: the first four genes are upregulated in WT MITF and downregulated in *Mitf*^{K243R} mutant, the ten others are downregulated or not changing expression in WT but upregulated in *Mitf*^{K243R} mutant. In the *Mitf*^{K243R} mutant downregulated genes, *Hes1* and *Tgfb1* are of particular interest due to their role in the survival and differentiation of the melanocytic lineage (Hitoshi et al., 2002). In addition to that, *Tgfb1* has also been shown to be important for proliferation (Chalmers et al., 2022). The *Mitf*^{K243R} mutant downregulated genes were also of interest. FZD7 is a receptor involved in WNT/β-catenin signaling (Umar et al., 2022), as well as BCL9, a co-activator for β-catenin (MacDonald et al., 2009). *Frzb* is also a gene involved in WNT signaling as an antagonist, strongly expressed in glial cells but lowly in melanocytic lineage (Jin et al., 2001), and low level of FRZB is thought to be important for *Mitf* upregulation (Thomas and Erickson, 2008). Similarly, BMP4 is an

agonist for the glial lineage instead of the melanocytic lineage (Jin et al., 2001). FGFR3 is a protein involved in melanoma progression (Li et al., 2019). Importantly, SNAI2, an important and necessary gene for NCC and melanoblast establishment (Sánchez-Martín et al., 2003) is also overexpressed in the *Mitf*^{K243R} mutant. Interestingly, *Id3* (Inhibitor of Differentiation 3), a gene from the HLH TF family ID and a BMP target, is upregulated in response to melanoma targeted therapy (Larribère et al., 2017), is inversely expressed with SOX10 and MITF and controls melanoma cells migration (Sachindra, 2018). Finally, we found that *Cd274* (coding for PD-L1) was increased. This protein acts as an immune checkpoint and is used by cancer cells to bypass immune cell tolerance. MITF has been recently been linked to *Cd274* as it reduces its expression to favorize immunosurveillance (Ballotti et al., 2020).

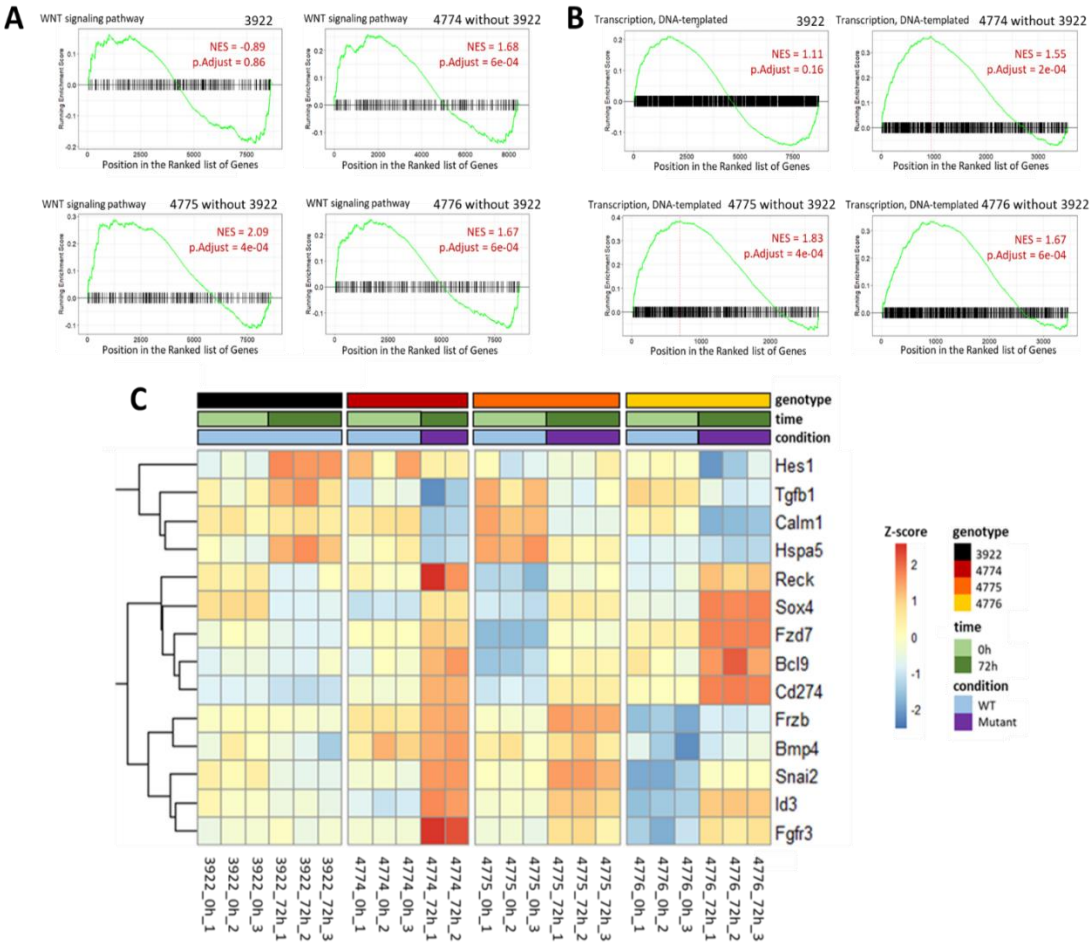

Figure 30. *Mitf*^{K243R} mutation changes expression of genes involved in WNT signaling pathway and transcription. (A) GSEA plot of genes involved in *WNT signaling pathway* in the 3922 WT MITF cell line and the *Mitf*^{K243R} mutant cell lines 4774, 4775 and 4776 after removal of 3922 DEGs. (B) GSEA plot for the BP*Transcription, DNA-templated*. (C) Heatmap of some of the DEGs in the four cell lines displayed by Z-score. Genotype, time and condition are displayed on top of the heatmap.

4.2.4.4 *Mitf*^{K243R} mutants do not activate cell cycle genes

Primary cultures of melanocytes need stimulation by the PKC pathway through TPA to grow (Prince et al., 2003). Indeed, TPA can mimic Diacylglycerol in order to induce the PKC-mediated signaling MAP kinase pathway (Magnuson et al., 1994; Seger and Krebs, 1995) as described in the introduction. TPA has also been shown to promote ERK phosphorylation of MITF S73 which enhances its transcriptional activity (Hemesath et al., 1998; Wu et al., 2000). This is crucial information in the case of this analysis, as this means that through the TPA treatment we increase MITF activity. Therefore, we also looked at genes that are not differentially expressed upon 4-OHT treatment in the mutants but are in WT. In other words, we studied the genes whose expression was differentially affected in WT MITF but not in the *Mitf*^{K243R} mutant. The assumption is that the TPA-induced role of WT MITF is impaired in the *Mitf*^{K243R} mutant. As we only did one biological replicate of the *WT MITF* cell line the power of the analysis is reduced.

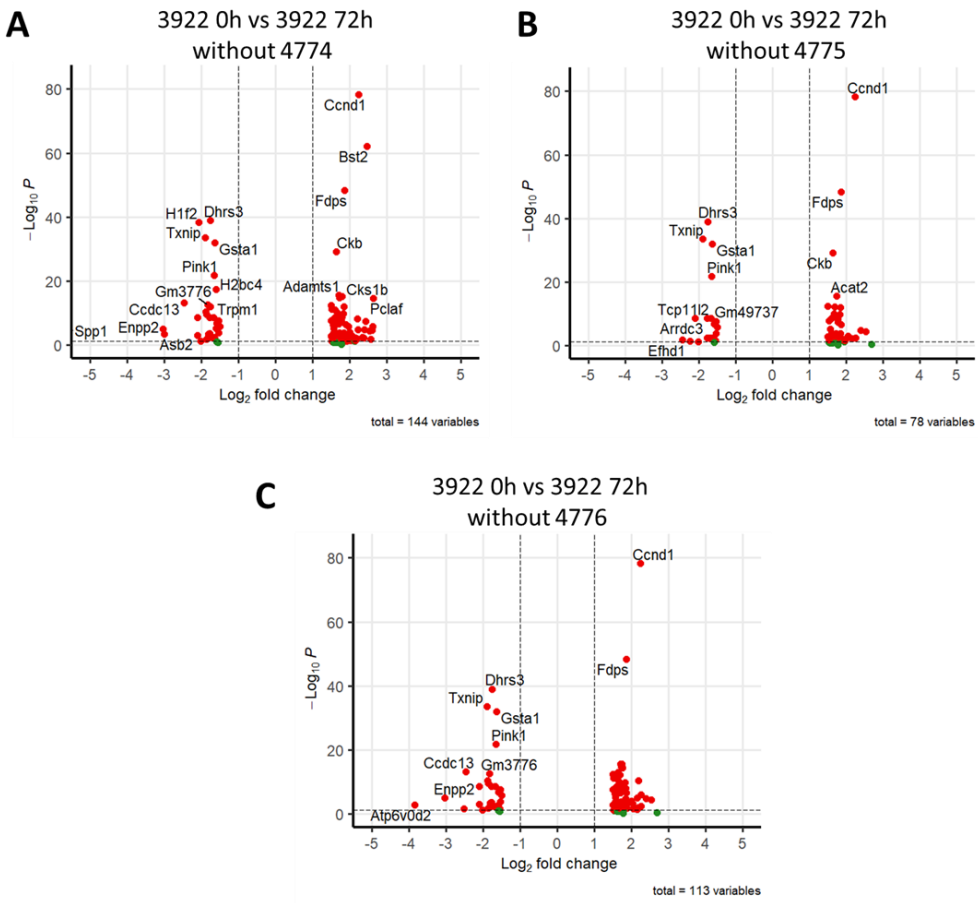

Figure 31. Many DEGs in the 3922 WT MITF cell line do not change expression in *Mitf*^{K243R} mutants. Volcano plots showing only the DEGs in the WT cell line that are not differentially expressed in the *Mitf*^{K243R} mutant cell lines (A) 4774, (B) 4775 and (C) 4776.

We selected only the DEGs that are two-fold different in FC in WT compared to the *Mitf*^{K243R} mutants: we kept only the genes that have no or very little change over time in the mutants (-0,5 < log2FC < 0,5) but change over time in WT (log2FC < -1 for downregulated or >1 for upregulated). Volcano plots show the genes that are differentially expressed in the 3922 WT cells but not in the mutant cells after 4-OHT treatment (Figure 31). The comparisons between wild type and the 4774 mutant cell line are shown in Figure 31A, the 4775 cells in Figure 31B, and 4776 in Figure 31C. The *Ccnd1* gene which codes for the Cyclin-D1 protein, seems particularly overexpressed in WT but not in the *Mitf*^{K243R} mutants. This gene has been shown to be important for the progression of the cell cycle from the G1 phase, and also for activation of gene expression (Bienvenu et al., 2010) and MITF has been shown to directly bind to the promoter region of this gene (Strub et al., 2011). Therefore, the lack of activation of the expression of *Ccnd1* by the *Mitf*^{K243R} mutant despite TPA activation makes it an interesting candidate to explain the arrested proliferation of the mutant cells.

We then performed a GSEA on the DEGs in WT that are not in the *Mitf*^{K243R} mutants to look at the BPs activated or suppressed. Dot-plots were generated with the DEGs from the WT 3922 cells that are not differentially expressed in the *Mitf*^{K243R} mutants 4774 (Figure 32A), 4775 (Figure 32B) or 4776 (Figure 32C). To get a better overview of the BPs activated or suppressed, we visualized them in a Venn diagram (Figure 32D). There are 5 terms that were shared between the three analysis and these terms are all related to cell cycle: "cell cycle", "cell cycle process", "mitotic cell cycle process", "nuclear division" and "mitotic cell cycle". This strongly suggests that WT MITF cells activate cell cycle whereas the *Mitf*^{K243R} mutant cells do not. This explains the proliferative effects *in vitro*.

As MITF is known to play a role in the regulation of cell cycle as mentioned in the introduction, we looked at some of the genes that are known to be important for the progression of the cell cycle and arranged them in a heatmap, with the DEGs displayed by Z-score. We plotted a list of 12 DEGs in this heatmap, which are genes that have been shown to be involved in cell cycle: *Ccnd1, Cdkn1a, Cdkn2a, Ccnb1, Ccna2, Ccne1, E2f1, Rbl1, Trp53, Cdkn1b, Cdk2* and *Cdk4* (Figure 32E) We also added *Brca1*, a gene that is involved in DNA repair and transcription and has been shown to be regulated by MITF (Strub 2011). Interestingly, all these cell cycle genes except *Cdkn1b*, *Cdk2* and *Cdk4* show increased expression in the WT MITF cell line upon TPA and 4-OHT treatments whereas they are not differentially expressed in the *Mitf*^{K243R} mutant cells over the same treatments. *Cdkn1b* is the only gene in this set that is downregulated in WT cells but is unchanged in *Mitf*^{K243R} mutant cells. *Cdk2* is slightly downregulated while *Cdk4* does not show any differential expression, in either WT or *Mitf*^{K243R} mutant cells. This is surprising since both CDK2 and CDK4 have been shown to be regulated by MITF in melanoma cells. *Brca1* is downregulated in WT cells, but its expression is unchanged in *Mitf*^{K243R} mutants. Together, the differential expression of these genes suggests that WT MITF regulates the expression of many important cell cycle genes.

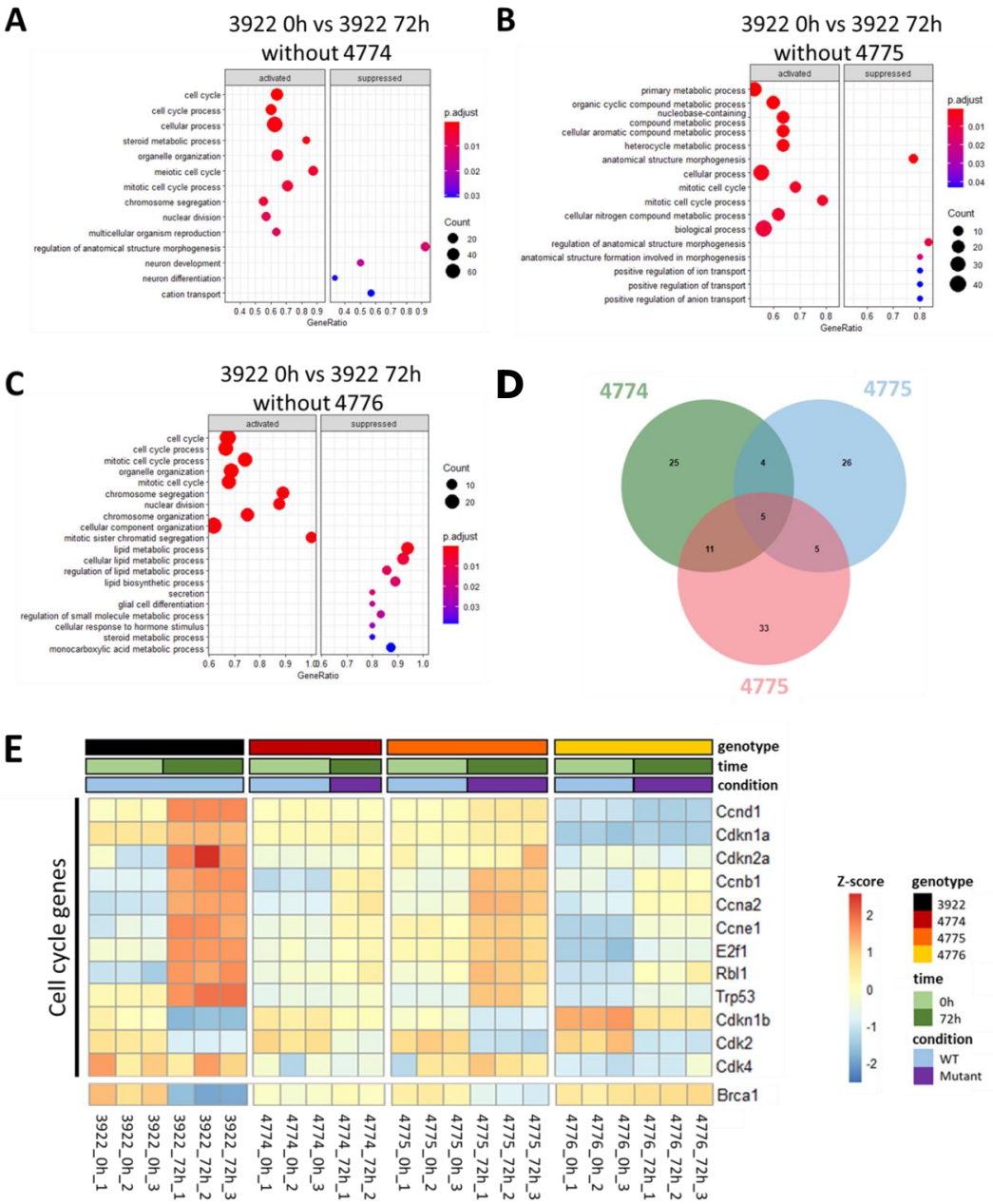

Figure 32. *Mitf*^{K243R} do not regulate cell cycle genes while WT MITF does. Dotplots representing the results of the GSEA of the 3922 WT MITF cell line for the DEGs that are not differentially expressed in the *Mitf*^{K243R} mutant cell lines (A) 4774, (B) 4775 and (C) 4776. (D) Venn diagram with the overlapping terms in the three GSEA. (E) Heatmap of some cell cycle DEGs in the four cell lines displayed by Z-score. Genotype, time and condition are displayed on top of the heatmap.

As the design of our RNA sequencing study was multifactorial, involving two different genotypes, two conditions (with and without 4-OHT treatment) and three time points, we also performed a more elaborate way to analyze it by using an interaction model analysis using DESeq2 to estimate the DEGs. This model basically consists of finding differential gene expression over time regardless of the differences in gene expression at the beginning of the experiment. This means that we are looking for genes that do not change in the same manner over time (from 0h to 48h and 72h) in WT and mutant cells. To summarize this model, instead of asking ourselves the question "what are the differentially expressed genes upon induction of the *Mitf*^{K243R} mutation?" as we previously did in a simpler manner, we instead asked "how does the expression of this gene change over time by looking at the slope regardless of the expression level at the beginning?". To do that, after filtering out the low expressed genes (<2 TPMs), we gave simple values that represent the slope of the expression of each gene over time and for every sample. Slopes were represented as follow: genes with Log2 FC from minus infinity to -1 were given the trajectory value -2 (strong negative slope), genes with Log2 FC from -1 to -Log2(1,5) were given the trajectory value -1 (soft negative slope), genes with Log2 FC from -Log2(1,5) to Log2(1,5) were given the trajectory value 0 (flat slope), genes with Log2 FC from Log(1,5) to 1 were given the trajectory value 1 (soft positive slope) and genes with the Log2 FC from 1 to positive infinity were given the trajectory value of 2 (strong positive slope). Then, we selected all the genes that have more than one unit of discrete trajectory difference between the WT and mutant, which means that their slopes were different over time. By doing this, we were able to identify 193 DEGs that have different expression trajectories over time between WT and mutant cells. A total of 66 of the DEG were downregulated (Log2 FC < -1) and 127 upregulated (Log2 FC > 1). All the up and downregulated genes are displayed on the dot plot of Figure 33A with the FC on the X-axis and the average number of TPMs on the Y-axis. Also, as the *Mitf*^{K243R} mutation has been shown to increase binding of MITF to low-affinity binding sites and decrease DNA-binding compared to WT MITF (Louphrasitthiphol et al., 2020), we wondered if it would have an effect on the binding to sites of normal target genes of MITF with a differential expression. To do so, we used a list of known high-confidence MITF target genes from the DoRothEA database, a gene regulatory network with TF-target gene interactions (Garcia-Alonso et al., 2019). The genes were also displayed in a dot plot of Figure 33B. Interestingly, only one gene, *G protein-coupled receptor 143 (Gpr143)* is reduced in expression upon Mitf knockdown, its differential response is just above the cut-off of Log2 FC(-1). This can be explained by the fact that the WT and mutant gene expression trajectories are actually quite similar but somehow did pass the filter we set up. Only one gene, *Snai2*, was upregulated, but this time the WT and mutant trajectories were significantly different. None of the other known target genes of MITF showed differential response. However, this interaction model is very complex and we realized that it was complicated to infer any hypothesis about the gene expression and its correlation with the phenotype of the cells. Moreover, GSEA and GO term analysis did not reveal any gene set enriched,

confirming the complexity of this analysis. This could also be explained by the low number of DEGs, despite the fact that we lowered the threshold filters as low as possible. However, this analysis has a lot of power, due to the three technical replicates as well as the three biological replicates. Thus, this analysis can be used as a very good study to discover gain or loss of genes upon the *Mitf*^{K243R} mutation. We plotted the gene expression trajectories for four of the most interesting genes, *Lgals1, Egfl8, Tm4sf1* and *Naglu*, based on their function and the number of TPMs (Figure 33C). Galectin-1, encoded by *Lgals1*, has been shown to be important for the regulation of immune responses in T-cells and to be expressed in cutaneaous malignant melanoma patients. Interestingly, this gene is downregulated upon inducing the *Mitf*^{K243R} mutation, showing a potential repression of this gene by the *Mitf*^{K243R} mutant as WT MITF does not change this gene expression over time. Similarly, TM4SF1 (encoded by *Tm4sf1*) does not change gene expression in WT MITF but is downregulated upon inducing the *Mitf*^{K243R} mutation. This gene has been shown to be important for cell growth, motility and metastasis in human lung cancer and is overexpressed in malignant melanomas Again, downregulation of this gene by the *Mitf*^{K243R} mutant could explain the loss of growth for mutant melanocytes. The N-acetylglucosaminidase, shortened by NAGLU (encoded by *Naglu*) is also downregulated upon inducing the *Mitf*^{K243R} mutation. This gene has been characterized by its role in neuronal differentiation from early in development (Petrova et al., 2023). Lastly, EGFL8 (encoded by *Egfl8)* was upregulated in our gene expression data. This gene has been shown to be involved in negative regulation of Notch signaling (Choi et al., 2012; Subhan et al., 2013). Thus, upregulation of this gene upon *Mitf*^{K243R} mutation is coherent with what we observed in our gene expression, as *Hes1*, a downstream target of Notch signaling, is downregulated (Figure 30C). Our data thus suggests the *Mitf*^{K243R} mutation, in cells stimulated by TPA, has a major effect on genes involved in the regulation of cell cycle as well as on WNT/β-catenin signaling.

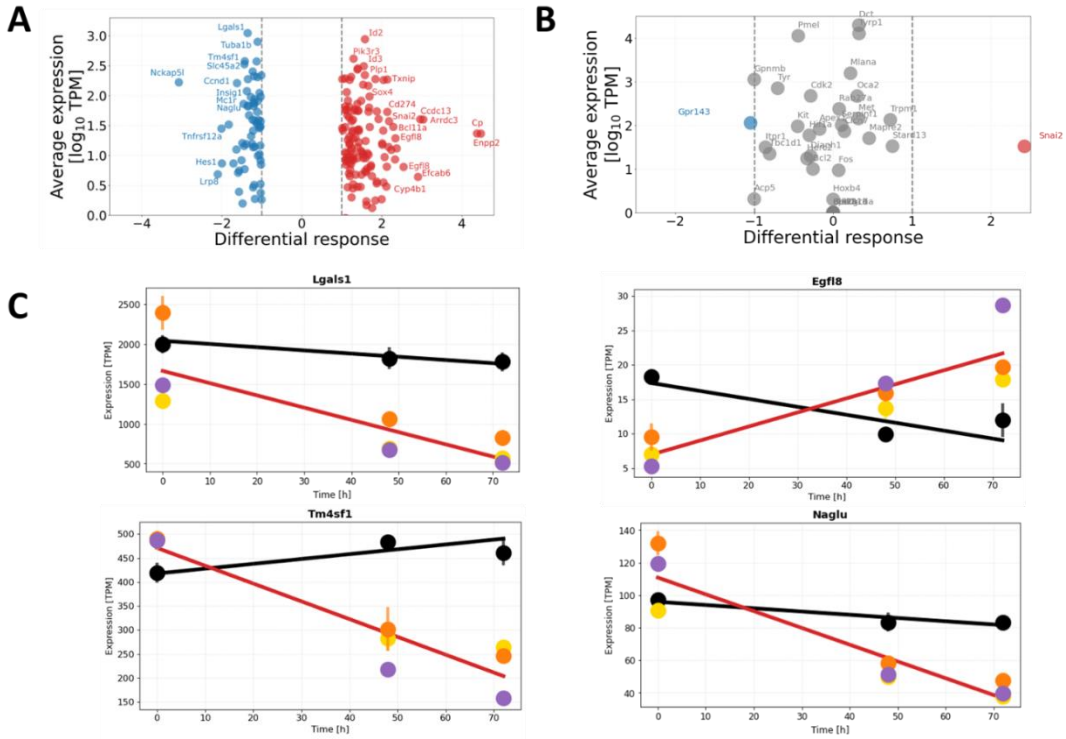

Figure 33. Effects of the *Mitf*^{K243R} mutation on gene expression. (A) Volcano plot showing the average expression (Log10 TPM, Y-axis) as a function of differential response (Log2 Fold Change, X-axis) of the Differentially Expressed Genes upon induction of the *Mitf*^{K243R} mutation over time. Upregulated genes are in red, downregulated in blue. Genes with no differential response were removed for better visualization. (B) Volcano plot showing the average expression of the highest confidence known target genes of MITF obtained from the DoRothEA database. (C) Expression trajectory plots over time for the genes *Lgals1, Egfl8, Tm4sf1* and *Naglu*. Black color indicates the WT MITF 3922 cell line, and the *Mitf*^{K243R} mutant lines are shown in yellow (4774), orange (4775) and purple (4776). Expression values are expresseed in TPM.

5 Discussion and conclusion

Most of what is known about the role of MITF comes from studying melanoma cell lines. These studies have revealed that MITF directly binds and activates expression of genes that are involved in the regulation of cell cycle (Du et al., 2004; Strub et al., 2011), proliferation (Widlund et al., 2002), (Carreira et al., 2005), differentiation (Cheli et al., 2010), cell adhesion (Dilshat et al., 2021), invasion (Carreira et al., 2006), senescence (Giuliano et al., 2010), survival (McGill et al., 2002), DNA-damage repair (Giuliano et al., 2010; Strub et al., 2011) and migration (Carreira et al., 2006; Cheli et al., 2012; Dilshat et al., 2021; Falletta et al., 2017; Giuliano et al., 2010). However, less is known about the role of MITF in these processes during melanocyte development.

In this project, we aimed to answer two questions: First, what is the role of the K243 residue in MITF, and second, what is the role of MITF during melanoblast development. We have shown that mutating K243 to lysine leads to animals with a coat color of alternating white spots with black and grey areas, suggesting that this residue plays an important role, possibly due to acetylation. We characterized the phenotype of the *Mitf*^{K243R} mutant mice in detail and studied the effects of this mutation on melanoblasts through different stages of development (E13.5, E14.5 and E15.5). To understand better the role of this mutation, we generated cell lines from mutant embryos where the *Mitf*^{K243R} mutation can be induced and subsequently assessed its effects over time by looking at proliferation, cell cycle stages and migration. Finally, we performed an RNA sequencing experiment to understand which genes are involved in the phenotype changes after induction of the mutation.

5.1 Effects of the *Mitf*^{K243R} mutation *in vivo*

To better understand the role of Mitf in development, we have created a conditional hypomorphic mouse model, where the *Mitf*^{K243R} mutation is induced only in melanocytes, using Cre driven by Tyr promoter. The mice that are constitutively induced with this mutation displayed a phenotype with coat color alternating between black, "salt-and-pepper" grey, or white areas. This phenotype thus raised the following questions: Do the white areas reflect lack of melanocytes or defective pigmentation process? Are the melanocytes in the "salt-and-pepper" grey areas fewer, or partially functional? What explains the black areas? Also, what explains the phenotype of females hemizygous for Tyr::Cre and homozygous for *Mitf*^{K243R}? In this chapter, we will try to answer these questions to explain the phenotype based on the developmental experiments we performed.

5.1.1 The *Mitf*^{K243R} mutant phenotype affects melanoblast development

We used the Dct-LacZ marker to track the melanoblasts throughout development in these mice, and the results showed that fewer melanoblasts develop in the trunk of E13.5 and E14.5 *Mitf*$^{K243R/K243R}$; Tyr::Cre/Y mutant male embryos than in *Mitf*$^{+/+}$; X/Y WT male embryos. Moreover, at stage E15.5, melanoblasts in the epidermis do not cluster in the forming hair placodes where they normally gather close to the dermal papilla and settle to form fully mature melanocytes, like they do in WT embryos. This could be explained either by the reduced number of melanoblasts which in the end fail to populate the dermal papilla or by a motility defect of the melanoblasts. Fewer cells are also consistent with the reduced proliferation we observe in the melanocyts upon removal of MITF (Figure 13). Even though melanoblasts migrate and proliferate in the dermis from E10.5, the epidermis is the major region for proliferation of melanoblasts where already half of the total number of melanoblasts are located by E12.5 (Luciani et al., 2011). After proliferation and migration in the dermis, melanoblasts need to invade the epidermis where they will perform most of their proliferation and migration and eventually populate the dermal papilla. To verify if the *Mitf*^{K243R} mutant melanoblasts were able to invade the epidermis, we sectioned the LacZ-stained embryos and counted the number of melanoblasts in both compartments, dermis and epidermis. The sections of E14.5 embryos revealed that there were fewer melanoblasts in the epidermis of *Mitf*^{K243R} mutants compared to WT. To invade the epidermis, cells need to go through an important structure, the basement membrane (BM). This membrane is composed of thin layers of Extra Cellular Matrix (ECM) proteins such as collagen IV, laminins and proteoglycans, and separates the dermis from the epidermis. BM has an important role in protecting the underlying tissues from mechanical stress and microbial invasions. The main mechanisms that have been suggested for the melanoblasts to invade the BM and reach the epidermis are that they change their shape and squeeze through the BM and/or degrade its components locally and temporarily (Luciani et al., 2011). Interestingly, even though there are fewer melanoblasts developing in E14.5 *Mitf*^{K243R} mutants overall (Figure 13B), we counted the repartition of melanoblasts in the dermis and epidermis and this revealed that, at this stage of development, there are the same number of melanoblasts in the dermis in WT and mutant embryos (Figure 15B), but almost none in the epidermis for *Mitf*^{K243R} mutant while the WT MITF has already more epidermal than dermal melanoblasts. This suggests that *Mitf*^{K243R} mutant melanoblasts struggle to cross the basement membrane to invade the epidermis and although they are fewer in total number, they accumulate in the dermis, thus altering the ratio of melanoblasts in the dermis vs epidermis. This is the first time that MITF is shown to be involved in regulating the process of BM invasion during melanoblast development, or for the motility of the cells towards the epidermis first, and second in the forming hair follicle. Therefore, we tried to produce the same conditions *in vitro* to simulate the epidermal invasion through the BM by performing a Transwell invasion assay. We used inserts with chemoattractant-supplemented medium in the lower chamber for the cells to invade Matrigel (a BM-mimic hydrogel). However, the results displayed in Supplementary Figure 38 (Appendix A) were not convincing, for two main reasons.

First, the assay is meant to be performed in a short period of time to reduce the effects of proliferation. Second, the technical replicates were very different, even when performed in the exact same way, at the same moment. Our RNA sequencing data performed on primary melanocyte cell lines did not show any major changes in the expression of genes obviously involved in invasion in the GSEA analysis. The only gene that might be involved in such a process is *Snai2*, a transcription factor involved in the EMT process. EMT is a process that cells go through to change their epithelial characteristics into invasive mesenchymal ones. This EMT process is involved in melanoma tumor progression as well as metastasis formation. During EMT the cell adhesion molecules such as the calcium-dependent proteins E- (encoded by *Cdh1*), N- (encoded by *Cdh2*) and P-cadherins play important roles. Indeed, from E11.5, dermal melanoblasts have been shown to be E- and P-cadherin negative, but then within 48h show a 200-fold increase of E-cadherin expression before their invasion of the epidermis (Nishimura et al., 1999). Melanoblasts have been shown to be E-cadherin negative and P-cadherin positive during their localization into the hair follicle. Interestingly, SNAI2 (also called SLUG or SNAIL2) has been shown to reduce E-cadherin (encoded by the *Cdh1* gene) expression and increase expression of ZEB1, another key player in the EMT (Wels et al., 2011). Moreover, *Snai2* has been shown to be upregulated by *Mitf* (Dilshat et al., 2021; Sánchez-Martín et al., 2003). In our RNA sequencing data, we show that *Snai2* is upregulated in the $Mitf^{K243R}$ mutation (see later in this discussion).

In most cases, *Mitf* mutations in mice lead to the absence of melanocytes, thus leading to a severe coat color phenotype. However, a few *Mitf* mutations show less severe phenotypes including $Mitf^{mi\text{-}vit}$ which shows large black spots in young animals which subsequently leads to progressive loss of pigmentation. Another example is $Mitf^{mi\text{-}rw}$ which in homozygotes results in white animals with black spots on the head and the rump (Steingrimsson et al., 2004). Also, some combinations of *Mitf* alleles lead to partial phenotype despite a severe phenotype if the alleles are homozygous. For example, $Mitf^{mi\text{-}Wh}$ homozygous animals are completely white with reduced eye size, but combinations with other *Mitf* alleles display either less severe coat color phenotype (diluted or with pigmented spots) or a normal eye size, or both (Steingrímsson et al., 2003). Interestingly, we generated a mouse model with a mutation ($Mitf^{K243R}$) that is constitutively induced in melanocytes early in development that has a milder phenotype than most of the previously reported *Mitf* mutated mice. This novel mouse model carrying the $Mitf^{K243R}$ mutation is therefore a unique hypomorphic inducible model to study melanocytes development. This model is quite unique because most *Mitf* mutations result in the absence of melanoblasts and thus a completely white coat color, which has suggested that *Mitf* is most important TF for melanocyte development. Using the Tyr::Cre transgene, this conditional mutation is induced after the wild-type *Mitf* gene has already been expressed and melanoblast specification has already started. Therefore, this model allows us to study the effect of the $Mitf^{K243R}$ at later stages of MITF-driven melanoblast specification.

5.1.2 Timing of the induction of the *Mitf*^{K243R} mutation creates the coat color pattern

The phenotype of *Mitf*^{K243R} mutant mice revealed that melanocytes are not completely absent. Indeed, the black areas found in all mice carrying the *Mitf*^{K243R} mutation indicate that these regions contain fully functional melanocytes which can produce melanin in these areas. This could be explained either by an incomplete recombination by Cre or because the induction of the Cre recombinase took place after at least some melanoblasts were established. It could also be that WT MITF is required for the establishment of the melanoblasts but not later as these cells will inevitably express both Tyr::Cre and, as a consequence, mutant MITF, but still having enough melanocytes in the black areas to produce enough melanin and have black hairs. The fact that the first melanoblasts are located in the head/neck and rump area during development (Baxter and Pavan, 2003) and that these areas corresponds to where the fully pigmented areas are located in the *Mitf*^{K243R} animals suggests that the second option is more likely (Figure 12B). The grey areas suggest that these areas either contain fewer or malfunctioning melanocytes. Analysis of the pigment in the hair showed areas with alternating white and grey hairs (Figure 12C-E) suggesting that some hair follicles had either completely dysfunctional melanocytes or none whereas other follicles had some or partly functional melanocytes. Each of the mice also had completely white areas either lacking melanocytes or containing dysfunctional cells. The hairs in these areas had no pigment. Tracking melanoblasts during the development revealed that there are fewer melanoblasts in the *Mitf*^{K243R} mutants and that they do not cluster in the forming hair follicles. It is most likely that in the white areas, no melanoblasts, and thus later no melanocytes, have developed. Interestingly, in "salt-and-pepper" grey areas, there might be few melanoblasts that have developed and clustered in the forming hair follicle and these few would be able to produce enough melanin for some hairs to be gray. This also could be explained by a failure of melanoblasts to cluster in the hair follicle, as suggested by the lack of melanoblasts gathering in the forming whisker hair follicle of the *Mitf*^{K243R} mutants (Figure 14A). Moreover, the "salt-and-pepper" means that a few white hairs are located in this area, suggesting that melanoblasts may not be equally spread. Therefore, our hypothesis is that only very few melanoblasts are located in the epidermis of *Mitf*^{K243R} mutants, where they are supposed to primarily locate around E14.5. Thus, the few melanoblasts in the epidermis are only present in some hair follicles and are not sufficient in number to produce adequate melanin in the hair resulting in grey hair.

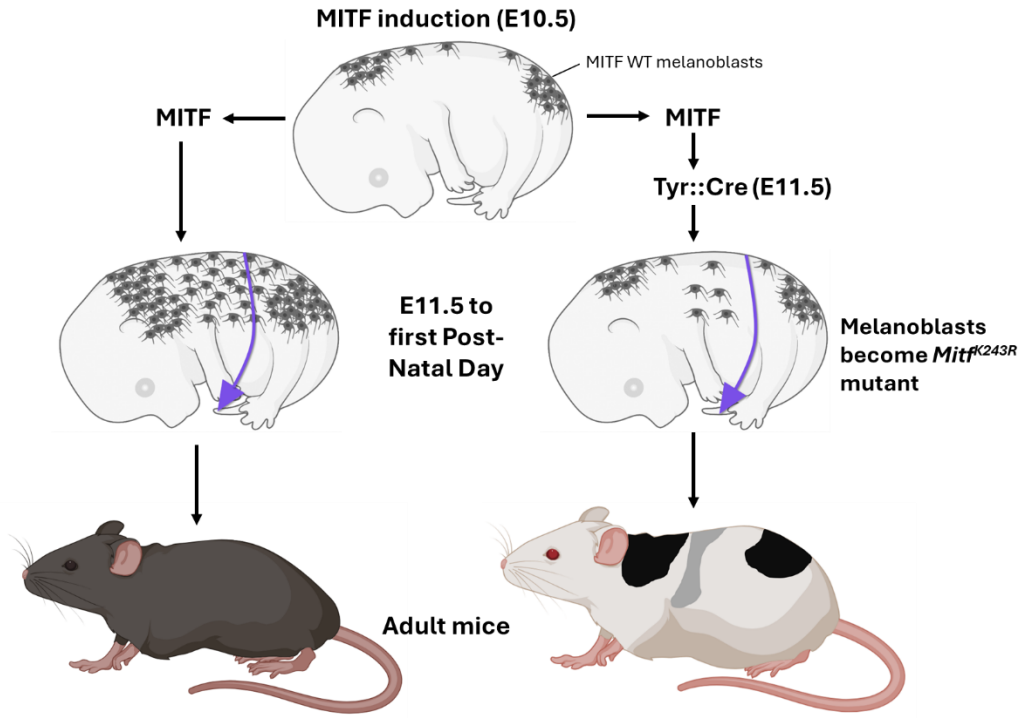

Mintz et al., (1967) used allophenic mice, which correspond to animals that have two or more allelic pigmentation phenotypes and studied the so called "mosaic" pattern that these mice display. The mice had a striped pattern, with alternative transverse bands

Figure 34. Model illustrating the timeline of establishment of melanocytes in WT MITF and *Mitf*^{K243R} mutant mice.

throughout the length of their body, and a clear mid-dorsal separation. From head to tail, they were able to count 17 successive bands. From these results, they theorized that melanocytes were clonally derived from 34 melanoblasts -17 on each side of the body. These melanocytes then proliferated and migrated along a lateral pathway (Mintz, 1967). However, this theory has been revised later with instead 34 progenitors per side as a correction for random clumping (West, 1975; Wolpert and Gingell, 1970). Moreover, there have been other studies showing that NCC differentiation into the melanocytic lineage happens earlier in the head than in the trunk and is more complex (Huszar et al., 1991). More recently, Wilkie et al. (2002) have revised Mintz's theory, again using mosaic and chimeric mice. They conclude that here is a larger pool of melanoblast progenitors and that there is a pool of melanoblasts in the cervical region. Moreover, they confirmed that melanoblasts in head and trunk regions disperse earlier than in the trunk. Finally, they conclude that many more progenitors are responsible for populating the head while only a few populate the trunk.

In our mouse model, the *Tyrosinase* promoter drives Cre expression. It is known that *Mitf* itself is a key regulator of *Tyrosinase* expression which may complicate our analysis.

A possibility that we cannot exclude is that there is incomplete recombination by the Cre-LoxP system in melanoblasts during development. Indeed, incomplete excision can lead to different kinds of phenotypes such as mosaicism. This can be caused by either cells that fail to express Cre or if Cre is expressed but fails in recombining the LoxP sites. However, it is unlikely that this phenomenon happens in our case as the mosaicism seems to follow a set of rules that are consistent with the temporal development of melanocytes (grey and black head or rump, "salt and pepper" grey and white trunk, white spot on the forehead) and does not seem to be completely random.

To summarize this first part of the thesis, we suggest as explanation for the phenotype of the *Mitf*^{K243R} mutant mice two main points, shown in Figure 34. The first is that the timing of the induction of the *Mitf*^{K243R} mutation takes place after *Mitf* is activated during development, which most likely explains the black spots on the rump and the back, meaning that *Mitf*^{K243R} activation is delayed after melanoblasts specification. The second main point we suggest is that the *Mitf*^{K243R} mutation considerably reduces the number of melanoblasts developing, causing the lack of pigmentation. Finally, our results show that melanoblasts struggle to cross the basement membrane as they normally require, and this would suggest for the first time a new role for MITF in allowing melanoblasts to invade the epidermis to reach their final location in the hair follicle.

5.2 Effects of the *Mitf*^{K243R} mutation in *vitro*

5.2.1 The *Mitf*^{K243R} mutation has a strong effect on the phenotype of the *Mitf*^{K243R} mutant cells

To investigate the effects of the *Mitf*^{K243R} mutation in *vitro*, we generated primary melanocyte cell lines where we can induce the *Mitf*^{K243R} mutation at will and study its effects over time. Growth assay revealed that 48h after induction, treating the *Mitf*^{K243R} mutant cells with 4-OHT stopped growth (Figure 19) and FACS analysis showed that the cells are stuck in G1-phase (Figure 21B) and have less cells going through S-phase (Figure 21C). In addition, the cells have increased apoptosis (Figure 22) and slightly changed morphology (Figure 23). However, we observed that in all the phenotypic assays we performed the 4776 cell line behaved slightly different from the 4774 and 4775 cells. Indeed, the 4776 cell line has a growth curve that is flat whereas the 4774 and 4775 growth curves suggest cell death. Line 4776 has less cells in the Sub-G1 peak and has an apoptotic index that was 1/4 and 1/2 smaller than that of 4774 and 4775, respectively. In addition, this cell line does not show a significant change in morphology whereas the 4774 and 4775 do. Importantly, RNA sequencing analysis (Figure 25B) also revealed that the 4776 had more mutant transcripts (94%) than the 4774 (68%) and 4775 (70%) lines after 72h of treatment. We suspect that most likely a difference in the Cre-mediated induction of the *Mitf*^{K243R} mutation would explain the difference between the 4774 and 4775 cells on the one hand from 4776 on the other

hand Thus, this emphasized that the biological replicates (4774, 4775 and 4776) of the *Mitf*^{K243R} inducible cell lines still have differences, thus warranting separate studies of the RNA sequencing data.

In vivo, melanoblasts induced to express the *Mitf*^{K243R} mutation do not seem to be able to reach distant positions such as the ventral part of the embryo from their initial development in the dorsal part. They might be slower to migrate and thus reach distal parts of the embryos later than WT MITF, or not at all, and in lower numbers. Thus, we performed a single-cell migration assay to study if the cells would also have slower migration *in vitro*. The assay showed no changes in migration for neither *WT MITF* nor the *Mitf*^{K243R} mutated cell, regardless of induction by 4-OHT, suggesting that the *Mitf*^{K243R} mutation does not have any effect on migration of melanoblasts. However, we did observe reduced invasion of the melanoblasts into the epidermis in *Mitf*^{K243R} mutant embryos at E14.5. This result might be of crucial importance, suggesting that MITF is essential for melanoblasts getting through the basement membrane to enter the epidermis. The basement membrane separates the dermis from the epidermis and melanoblasts need to actively go through this membrane to reach the hair follicle. These would need to be confirmed with later stages embryos from E15.5 and sectioned to get the ratio of dermal/epidermal melanoblasts in order to confirm these results. The basement membrane is rich in many components such as collagens, laminins and proteoglycans and plays an important role to protect the underlying tissues. Therefore, cells have to develop mechanisms to go through the basement membrane and, often, this involves degrading the BM with the help of matrix metalloproteases for example. However, unlike melanoma cells that use invadopodia to invade the basement membrane to go to the dermis from the epidermis and creates metastases (Li et al., 2010), it seems that melanoblasts do not degrade the BM at E13.5, but rather go through a more permissive BM at this stage of development, similarly to lymphatic endothelial BM and dendritic cells (Pflicke and Sixt, 2009). This also suggests that the mechanisms involved in melanoblasts invasion of the epidermis are different from the ones involved in melanoma cells invasiveness. This is the first time that *Mitf* has been implicated in this process. As previously explained, using a Transwell invasion assay was not successful in showing effects on migration *in vitro*. Further investigation using a different set-up for the Transwell invasion assay or using a different set of experiments is necessary to answer the important question of the role of MITF in the invasion of the epidermis during development. There are a lot fewer melanoblasts that have the ability to cross the BM in the *Mitf*^{K243R} mutant and that the melanoblasts do not gather in the hair placodes as we observed in the *Mitf*^{K243R} mutant embryos at E15.5 (Figure 13C) and in the whiskers (14A). This could explain that the few melanoblasts that have made it through the BM will not be enough to deliver sufficient melanin for full hair coloration, either in the whiskers or in the "salt-and-pepper" grey areas.

5.2.2 The *Mitf*^{K243R} mutation affects gene expression

Finally, we performed an RNA sequencing experiment to study the gene expression changes upon the induction of the *Mitf*^{K243R} mutation. Surprisingly, the PCA revealed that the 4-OHT treatment has a large impact on gene expression (Figure 24A). We did not expect this based on our phenotypic assays, as the WT cell lines did not show differences in any of the phenotypes we assayed upon treatment with 4-OHT. Indeed, the largest variability observed on the PCA plot is due to the 4-OHT treatment. However, the second largest variability is mostly observed in the *Mitf*^{K243R} mutant cell lines, and very little in the WT, strongly suggesting that this is due to the mutation. This effect of 4-OHT needs to be considered during our analysis. We were able to get rid of the DEGs that are due to the 4-OHT treatment by excluding all the genes that were similarly affected upon treatment of both WT and *Mitf*^{K243R} mutants. At the same time, we kept the genes that were differently affected upon 4-OHT treatment in WT and *Mitf*^{K243R} mutants: the genes that were differentially expressed in mutants but not in WT, and vice versa. Even though this way to analyze the data is not perfect, as bias may be introduced by removing some of the genes that might actually be differentially expressed by the mutation, we are confident with the DEGs we found. They were found in the three biological replicates giving significant power to the analysis. However, knowing that the 4-OHT treatment has such an impact on gene expression we would in the future include more than one WT cell line as a control as we cannot exclude the possibility that the cell line used here acts strangely for some reason.

Interestingly, we found in our RNAseq data that the *Mitf-A* isoform was dysregulated over time after the induction of the *Mitf*^{K243R} mutation. This suggests that the *Mitf*^{K243R} mutation has a regulatory effect on the MITF-A isoform, either through directly affecting transcription of the A isoform or indirectly through other factors. As the different isoforms use different promoters, this suggests that the *Mitf*^{K243R} mutation is important to bind to the promoter for the transcription of the *Mitf-A* isoform, but not for the *Mitf-M* isoform. However, the *Mitf*^{K243R} mutation seems not to influence the regulation of the MITF-F isoform.

The analysis revealed that the *Mitf*^{K243R} mutation has an effect on target genes that do not show differential expression over time in WT MITF but are different upon inducing the *Mitf*^{K243R} mutation. The data revealed a few genes that are differentially affected in *Mitf*^{K243R} mutant cell lines compared to WT MITF. Some genes were overexpressed upon induction of the *Mitf*^{K243R} mutation including *Snai2, Fzd7, Frzb, Fgfr3, Bmp4* and *Cd274* (coding for PD-L1), while they were not changed in the WT MITF cell line. Other genes such as *Hes1* and *Tgfb1* (coding for TGF-β) were increased upon 4-OHT treatment of the WT MITF cell line but were reduced upon treatment of the *Mitf*^{K243R} mutant cells. Interestingly, most of these genes are involved in WNT and Notch signaling pathways, two signaling pathways crucial for melanoblasts and melanocytes at various steps in their development. As a result, this suggests that MITF is necessary to maintain the WNT

signaling pathway when the cells are stimulated by TPA. The WNT signaling pathway is evolutionary conserved and is not specific for the melanocytic lineage, but necessary for embryonic development, as it regulates many important processes such as cell proliferation and migration as well as body axing and establishment of pre-migratory NCC. In the case of the melanocytic lineage, this pathway is also important, as mice that are deficient for this pathway show abnormal pigmentation. Moreover, β-catenin, one of the key components of the WNT signaling, has been shown to control MITF expression and function (Schepsky et al., 2006). . Alterations of β-catenin lead to reduced numbers of melanoblast development *in vivo* (Luciani et al., 2011), and interestingly, overexpression of β-catenin also reduces the number of melanoblasts (Delmas et al., 2007), suggesting the dose-dependent role of this pathway. Interestingly, in melanoma, WNT signaling has been shown to be a better prognosis marker, with reduced proliferation and invasiveness of the tumors (Chien et al., 2009; Katkat et al., 2023; Uka et al., 2020). In WNT signaling, WNT proteins bind to their receptors called frizzled, like FZD7, and induce a cascade of activation in the cell resulting in the expression of β-catenin which will itself induce the expression of many genes such as *Mitf* or *Ccnd1*. FZD7 has been recently shown to be important for the development of carcinogenesis including in melanoma (Larasati et al., 2022; Tiwary and Xu, 2016). Similarly, upregulation of the *Fgfr3* gene, one of the four FGF receptors, has been linked to melanoma growth and malignancy (Li et al., 2019), suggesting a potential role in melanocyte development. FRZB is a secreted protein that competes with frizzled receptors for WNT binding and has been shown to promote glial and neuronal lineage during development and not the melanocytic lineage (Jin et al., 2001). Similarly, BMP4, a protein involved in BMP signaling, also favors the glial/neuronal lineage (Jin et al., 2001). These two upregulated genes are thus involved in signaling pathways which aim to favor the development of glial cells and neurons instead of melanocytes, and thus might also explain the lack of melanocytes developing in the *Mitf*^{K243R} mutants. The Notch signaling pathway also seems to be induced upon the *Mitf*^{K243R} mutation. This pathway has been shown to be important for the initiation and delamination of NCCs (Hari et al., 2002) and in the survival of melanoblasts and melanocyte stem cells (Moriyama et al., 2006). The *Hes1* and *Tgfb1* genes are downregulated upon the *Mitf*^{K243R} mutation. HES1 (Hairy/Enhancer of Split 1), a bHLH transcription factor, is one of the main downstream target of this pathway and has been shown to promote maintenance of stem-cells and melanoblasts by inhibiting apoptosis (Aubin-Houzelstein et al., 2008; Kageyama et al., 2000). Moriyama et al. (2002) have rescued severe pigmentation defects in mice by ablating Notch signaling by overexpressing HES1. This suggests the important role of this gene in the melanocytic lineage and its potential regulation by MITF. Moreover, HES1 has been shown to synergically function with TGF-β signaling, a signaling pathway that was reported as important for NCC development (Delannet and Duband, 1992). Finally, MITF has been shown to be important for melanocyte survival through its effects on BCL2 (McGill et al., 2002) and the Melanoma Inhibitor of Apoptosis (ML-IAP) (Dynek et al., 2008).

Neither of these two proposed MITF targets were observed to be differentially expressed in our RNA sequencing analysis. However, *Hes1* expression, downstream of *Tgfb1*, has been associated with inhibition of apoptosis so the downregulation of *Hes1* and *Tgfb1* expression that we observed in *Mitf*^{K243R} mutant cells can explain the increased apoptosis (Figure 22).

The expression of the *Snai2* and *Cd274* genes was increased in the *Mitf*^{K243R} mutants compared to WT MITF. SNAI2 is a protein that has been shown to be involved in the EMT process of the NCCs, but also in the maintenance of MSCs in the hair follicle (Pérez-Losada et al., 2002). SNAI2 is necessary for the establishment of NCCs, and has been shown to be important for the migration and survival of melanoblasts (Sánchez-Martín et al., 2003). Interestingly, upregulation of *Snai2* would be expected to increase the ability of melanoblasts to traverse the BM which is opposite to what we observed. SNAI2 has been implicated in EMT (Dilshat et al., 2021) and might be expected to lead to the ability to traverse the BM. Perhaps SNAI2 is not sufficient for this to take place or perhaps our cell lines do not properly replicate the true nature of melanoblasts. Alternatively, as a E-cadherin repressor, increase in SNAI2 could explain why invasion of the epidermis by the melanoblasts is not possible, as increase in E-cadherin seems to be important for the EMT switch as previously shown by Nishimura in 1999. The *Cd274* gene (coding for PD-L1, an immune checkpoint inhibitor) has been shown to be implicated in immune invasion of melanoma (Juneja et al., 2017). What exact role it has in melanocytes is not clear at this point. However, a study has shown that MITF acts in favor of immunosurveillance, thus against the development of melanoma, by repressing the expression of PD-L1 (Ballotti et al., 2020). Moreover, in addition to its well-known role as a checkpoint inhibitor, PD-L1 has been shown to be a marker for G0-quiescent cell-state (Palmer et al., 2022), thus suggesting an anti-proliferative effect after its activation by the *MITF*^{K243R} mutant protein.

TPA is thought to stimulate the Mitogen-Activated Protein (MAP) kinase by mimicking Diacylglycerol (DAG), activating RAF through the Protein Kinase C (PKC). RAF then activates the MAPK, an important pathway in eukaryotes which regulates many processes including proliferation, differentiation, death and migration (Wilkinson and Millar, 2000). The cultured melanocytes stopped growing upon removal of TPA from the culture medium after 72h (Figure 19A). This could be explained by the fact that TPA-induced changes in the cells persist longer, even after TPA-removal, as Krasagakis et al. (1993) showed to be the case for human melanocytes. Primary mouse melanocytes cell lines like we have generated were shown to be dendritic (Bennett et al., 1987; Krasagakis et al., 1993) in presence of TPA like we observed in Figure 23A by immunostaining of the cytoskeleton.

We thus studied the RNA sequencing data in a different way, by analyzing the genes whose expression was differentially affected in WT MITF but not in the *Mitf*^{K243R} mutant. By analyzing the RNA sequencing data this way, we revealed genes that are

differentially expressed in the WT over time, but that are not in the case of *Mitf*^{K243R} mutant, suggesting the loss of regulation of these genes with the mutation upon stimulation of growth by TPA. That is the case of *Cyclin-D1* (*Ccnd1*), which has been shown to be crucial for cell cycle progression, specifically for the progression from the G1 phase to the S-phase of replication (Fu et al., 2004). Studies performed in melanoma cells have shown that the MITF-M isoform is important and crucial for cell cycle progression as its inhibition leads to cell cycle arrest in G0/1 phase (Giuliano et al., 2010; Koh et al., 1995). The flow cytometry data showed that in melanocytes MITF is essential for proliferation in *vitro*. Indeed, the three *Mitf*^{K243R} mutant cell lines showed a severely reduced number of cells in S-phase, and a blockade in G1 phase for the two mutant cell lines 4774 and 4775. A study revealed that MITF indirectly activates *Ccnd1* transcription (Pan et al., 2015) through TBX2 from the T-box TF family (Carreira et al., 2000). Our RNAseq data suggests the same mechanism happens in WT MITF cells with MITF stimulation resulting in the upregulated transcription of *Ccnd1*. However, we did not see any changes in expression of TBX2, meaning that the regulation of *Ccnd1* by MITF is rather direct as suggested by Carreira et al. (2006), in cooperation with *Rbl1*. In contrast, cells with the *Mitf*^{K243R} mutation did not activate the transcription of *Ccnd1*, despite stimulation by TPA.

Despite its importance in cell cycle, *Ccnd1* is not the only cell cycle gene that is upregulated in WT MITF cell line but not in *Mitf*^{K243R} mutant cells. In fact, *Cdkn1a* (p21), *Cdkn2a* (coding for both p16 and p14), *Ccnb1* (Cyclin-B1), *Ccna2* (Cyclin-A2), *Ccne1* (Cyclin-E1), *E2f1* (E2F transcription factor 1), *Rbl1* (Retinoblastoma-like protein 1) and *Trp53* (p53) show increased expression in wild type but not in the mutant. This finding is crucial as depletion of MITF in melanoma cell lines has similarly been shown to lead to cell cycle arrest (Carreira et al., 2005; Carreira et al., 2006; Giuliano et al., 2010; Strub et al., 2011; Wellbrock and Marais, 2005). Therefore, the *Mitf*^{K243R} mutation seems to act as a knockdown for the cell cycle progression genes. The Cyclin-Dependent Kinases 2 (CDK2) and 4 (CDK4) did not show differential expression between WT MITF and the *Mitf*^{K243R} mutant cell lines, which is in contrast to the previous literature (Du et al., 2004; Loercher et al., 2005) where MITF has been shown to be important for maintaining CDK2 at the transcriptional level. This suggests that the *Mitf*^{K243R} mutation is not important for regulating CDK2 transcription in melanocytes. As a conclusion, the results suggest that TPA induces growth by activatingMITF through the MAPK pathway and that the *Mitf*^{K243R} mutation leads to the removal of MITF regulation of cell cycle progression genes. The downregulation of anti-apoptotic genes might explain the induction of apoptosis due to the *Mitf*^{K243R} mutation. The phenotypic assays confirmed that the *Mitf*^{K243R} mutant cells could not grow as they are stuck in the G1 or G0 and S-phase of the cell cycle, but also die by getting in apoptosis.

These results are coherent and might explain why there are less melanoblasts developing in the embryos, regardless of the timing of the induction of the mutation. Together, these results have revealed that Lys243 of MITF plays an important role in

gene regulation and mutation of this amino-acid into a non-acetylatable residue affects its regulation of important genes including genes involved in WNT/ β -catenin signaling as well as genes involved in cell cycle regulation. Louphrasitthiphol et al. (2023) have shown that the *Mitf*^{K243R} mutation increases DNA-binding to low-affinity binding sites. They also suggest that this increased binding for low-affinity binding sites would therefore reduce the concentration of MITF that will bind to its target genes. Our RNA sequencing results seem to be consistent with that. Indeed, first, we observed new DEGs upon *Mitf*^{K243R} mutation. Second, there is a loss of regulation of WT MITF target genes after induction of the *Mitf*^{K243R} mutation in the cells. This work is therefore bringing new insights into the role of MITF during melanocyte development and the timing of induction of crucial genes necessary for this.

To summarize, we generated an *in vitro* model where we can induce the *Mitf*^{K243R} mutation in primary mouse melanocytes and observe its effects over time. With this model, we can at least partially explain some of the phenotype features we observed *in vitro* and link them to the genes that are differentially expressed after activation of the *Mitf*^{K243R} mutation.

Despite the new insights we found for the role of MITF during melanocyte development with our *in vivo* and *in vitro* experiments, there are still many questions remaining to answer. It would be interesting to confirm that *Mitf*^{K243R} mutant melanoblasts do not invade the epidermis as WT MITF do. This could be done by sectioning β-galactosidase stained embryos at later stages from E15.5 and compare the number of epidermal and dermal melanoblasts at this stages. Also, we came with an innovative way to induce the *Mitf*^{K243R} *in vitro* by using the *Mitf*^{K243R}; Tyr::CreERT^{2}mouse model and generating the inducible melanocytes out of these animals. However, as the 4-OHT treatment induced the biggest variation of gene expression in the case of the RNA sequencing, maybe using a different approach of induction of the mutation could be interesting in order to confirm our RNA sequencing results. We could for example generate a cell model with low MITF expression, induce the *Mitf*^{K243R} mutant and observe the effects of the mutation. These experiments would be of a particular interest to characterize even more the role of the *Mitf*^{K243R} mutation and therefore of MITF in general in melanocyte development, and also about the target genes involved during the establishment of the pigment-producing cells.

References

<Porter&Meyer_1994 - A distal tyrosinase upstream element stimulates gene expression in neural-crest-derived melanocytes of transgenic mice, position-independent and mosaic expression.pdf>.

Abdel-Malek, Z.A., Scott, M.C., Furumura, M., Lamoreux, M.L., Ollmann, M., Barsh, G.S., and Hearing, V.J.J.J.o.c.s. (2001). The melanocortin 1 receptor is the principal mediator of the effects of agouti signaling protein on mammalian melanocytes. *114*, 1019-1024.

Abdel-Malek, Z.A., and Supp, D. (2008). β-Defensin 3: a novel and unexpected key that unlocks the melanocortin 1 receptor (Wiley Online Library).

Abel, E.V., Basile, K.J., Kugel, C.H., Witkiewicz, A.K., Le, K., Amaravadi, R.K., Karakousis, G.C., Xu, X., Xu, W., and Schuchter, L.M.J.T.J.o.c.i. (2013). Melanoma adapts to RAF/MEK inhibitors through FOXD3-mediated upregulation of ERBB3. *123*, 2155-2168.

Aberdam, E., Bertolotto, C., Sviderskaya, E.V., de Thillot, V., Hemesath, T.J., Fisher, D.E., Bennett, D.C., Ortonne, J.-P., and Ballotti, R.J.J.o.B.C. (1998). Involvement of microphthalmia in the inhibition of melanocyte lineage differentiation and of melanogenesis by agouti signal protein. *273*, 19560-19565.

Acloque, H., Adams, M.S., Fishwick, K., Bronner-Fraser, M., and Nieto, M.A.J.T.J.o.c.i. (2009). Epithelial-mesenchymal transitions: the importance of changing cell state in development and disease. *119*, 1438-1449.

Adameyko, I., Lallemend, F., Aquino, J.B., Pereira, J.A., Topilko, P., Müller, T., Fritz, N., Beljajeva, A., Mochii, M., and Liste, I.J.C. (2009). Schwann cell precursors from nerve innervation are a cellular origin of melanocytes in skin. *139*, 366-379.

Aksan, I., Goding, C.J.M., and biology, c. (1998). Targeting the microphthalmia basic helix-loop-helix–leucine zipper transcription factor to a subset of E-box elements in vitro and in vivo. *18*, 6930-6938.

Alberts, B. (2017). Molecular biology of the cell (Garland science).

Alkhateeb, A., Fain, P.R., and Spritz, R.A.J.J.o.G.I.M. (2005). Candidate functional promoter variant in the FOXD3 melanoblast developmental regulator gene in autosomal dominant vitiligo. *20*, 388-391.

Alonso, L., and Fuchs, E.J.J.o.c.s. (2006). The hair cycle. *119*, 391-393.

Amiel, J., Watkin, P.M., Tassabehji, M., Read, A.P., and Winter, R.M.J.C.d. (1998). Mutation of the MITF gene in albinism-deafness syndrome (Tietz syndrome). *7*, 17-20.

Arita, Y., O'Driscoll, K.R., and Weinstein, I.B.J.C.R. (1992). Growth of human melanocyte cultures supported by 12-O-tetradecanoylphorbol-13-acetate is mediated through protein kinase C activation. *52*, 4514-4521.

Atacho, D.A., Reynisson, H., Petursdottir, A.T., Eysteinsson, T., Steingrimsson, E., and Petersen, P.H.J.E. (2020). Mitf links neuronal activity and long-term homeostatic intrinsic plasticity. *7*.

Aubin-Houzelstein, G., Djian-Zaouche, J., Bernex, F., Gadin, S., Delmas, V., Larue, L., and Panthier, J.J. (2008). Melanoblasts' proper location and timed differentiation depend on Notch/RBP-J signaling in postnatal hair follicles. J Invest Dermatol *128*, 2686-2695.

Ballotti, R., Cheli, Y., and Bertolotto, C.J.M.c. (2020). The complex relationship between MITF and the immune system: a Melanoma ImmunoTherapy (response) Factor? *19*, 1-12.

Baranowska Körberg, I., Sundström, E., Meadows, J.R., Rosengren Pielberg, G., Gustafson, U., Hedhammar, Å., Karlsson, E.K., Seddon, J., Söderberg, A., and Vilà, C.J.P.O. (2014). A simple repeat polymorphism in the MITF-M promoter is a key regulator of white spotting in dogs. *9*, e104363.

Barrallo-Gimeno, A., and Nieto, M.A. (2005). The Snail genes as inducers of cell movement and survival: implications in development and cancer.

Baxter, L.L., Hou, L., Loftus, S.K., and Pavan, W.J. (2004). Spotlight on spotted mice: a review of white spotting mouse mutants and associated human pigmentation disorders. Pigment Cell Res *17*, 215-224.

Baxter, L.L., Moreland, R.T., Nguyen, A.-D., Wolfsberg, T.G., and Pavan, W.J.J.D. (2010). A curated online resource for SOX10 and pigment cell molecular genetic pathways. *2010*, baq025.

Baxter, L.L., and Pavan, W.J.J.G.E.P. (2003). Pmel17 expression is Mitf-dependent and reveals cranial melanoblast migration during murine development. *3*, 703-707.

Baxter, L.L., and Pavan, W.J.J.M.o.d. (2002). The oculocutaneous albinism type IV gene Matp is a new marker of pigment cell precursors during mouse embryonic development. *116*, 209-212.

Baynash, A.G., Hosoda, K., Giaid, A., Richardson, J.A., Emoto, N., Hammer, R.E., and Yanagisawa, M.J.C. (1994). Interaction of endothelin-3 with endothelin-B receptor is essential for development of epidermal melanocytes and enteric neurons. *79*, 1277-1285.

Belmadani, A., Jung, H., Ren, D., and Miller, R.J.J.D. (2009). The chemokine SDF-1/CXCL12 regulates the migration of melanocyte progenitors in mouse hair follicles. *77*, 395-411.

Bennett, D.C., Cooper, P.J., and Hart, I.R.J.I.j.o.c. (1987). A line of non-tumorigenic mouse melanocytes, syngeneic with the B16 melanoma and requiring a tumour promoter for growth. *39*, 414-418.

Bertolotto, C., Lesueur, F., Giuliano, S., Strub, T., De Lichy, M., Bille, K., Dessen, P., d'Hayer, B., Mohamdi, H., and Remenieras, A.J.N. (2011). A SUMOylation-defective MITF germline mutation predisposes to melanoma and renal carcinoma. *480*, 94-98.

Bertrand, J.U., Steingrimsson, E., Jouenne, F., Bressac-de Paillerets, B., and Larue, L. (2020). Melanoma Risk and Melanocyte Biology. Acta Derm Venereol *100*, adv00139.

Bienvenu, F., Jirawatnotai, S., Elias, J.E., Meyer, C.A., Mizeracka, K., Marson, A., Frampton, G.M., Cole, M.F., Odom, D.T., and Odajima, J.J.N. (2010). Transcriptional role of cyclin D1 in development revealed by a genetic—proteomic screen. *463*, 374-378.

Bolger, A.M., Lohse, M., and Usadel, B.J.B. (2014). Trimmomatic: a flexible trimmer for Illumina sequence data. *30*, 2114-2120.

Bondurand, N., Pingault, V., Goerich, D.E., Lemort, N., Sock, E., Caignec, C.L., Wegner, M., and Goossens, M.J.H.m.g. (2000). Interaction among SOX10, PAX3 and MITF, three genes altered in Waardenburg syndrome. *9*, 1907-1917.

Boshuizen, J., Koopman, L.A., Krijgsman, O., Shahrabi, A., van den Heuvel, E.G., Ligtenberg, M.A., Vredevoogd, D.W., Kemper, K., Kuilman, T., and Song, J.-Y.J.N.m. (2018). Cooperative targeting of melanoma heterogeneity with an AXL antibody-drug conjugate and BRAF/MEK inhibitors. *24*, 203-212.

Bray, N.L., Pimentel, H., Melsted, P., and Pachter, L.J.N.b. (2016). Near-optimal probabilistic RNA-seq quantification. *34*, 525-527.

Brizzolara, A., Torre, M., Favre, A., Prato, A.P., Bocciardi, R., and Martucciello, G.J.J.o.p.s. (2004). Histochemical study of Dom mouse: a model for Waardenburg-Hirschsprung's phenotype. *39*, 1098-1103.

Carreira, S., Goodall, J., Aksan, I., La Rocca, S.A., Galibert, M.-D., Denat, L., Larue, L., and Goding, C.R.J.N. (2005). Mitf cooperates with Rb1 and activates p21 Cip1 expression to regulate cell cycle progression. *433*, 764-769.

Carreira, S., Goodall, J., Denat, L., Rodriguez, M., Nuciforo, P., Hoek, K.S., Testori, A., Larue, L., Goding, C.R.J.G., and development (2006). Mitf regulation of Dia1 controls melanoma proliferation and invasiveness. *20*, 3426-3439.

Carreira, S., Liu, B., and Goding, C.R.J.J.o.B.C. (2000). The gene encoding the T-box factor Tbx2 is a target for the microphthalmia-associated transcription factor in melanocytes. *275*, 21920-21927.

Carver, E.A., Jiang, R., Lan, Y., Oram, K.F., Gridley, T.J.M., and biology, c. (2001). The mouse snail gene encodes a key regulator of the epithelial-mesenchymal transition. *21*, 8184-8188.

Chalmers, F.E., Dusold, J.E., Shaik, J.A., Walsh, H.A., and Glick, A.B. (2022). Targeted deletion of TGFbeta1 in basal keratinocytes causes profound defects in stratified squamous epithelia and aberrant melanocyte migration. Dev Biol *485*, 9-23.

Chang, A.E., Karnell, L.H., and Menck, H.R.J.C.I.I.J.o.t.A.C.S. (1998). The National Cancer Data Base report on cutaneous and noncutaneous melanoma: a summary of 84,836 cases from the past decade. *83*, 1664-1678.

Cheli, Y., Giuliano, S., Fenouille, N., Allegra, M., Hofman, V., Hofman, P., Bahadoran, P., Lacour, J., Tartare-Deckert, S., and Bertolotto, C.J.O. (2012). Hypoxia and MITF control metastatic behaviour in mouse and human melanoma cells. *31*, 2461-2470.

Cheli, Y., Ohanna, M., Ballotti, R., and Bertolotto, C. (2010). Fifteen-year quest for microphthalmia-associated transcription factor target genes. Pigment Cell Melanoma Res *23*, 27-40.

Chernova, O.J.B.B.o.t.R.A.o.S. (2003). Architectonic and diagnostic significance of hair cortex and medulla. *30*, 53-62.

Chiaverini, C., Beuret, L., Flori, E., Abbe, P., Bille, K., Bahadoran, P., Ortonne, J.-P., Bertolotto, C., and Ballotti, R.J.J.o.B.C. (2008). Microphthalmia-associated transcription factor regulates RAB27A gene expression and controls melanosome transport. *283*, 12635-12642.

Chien, A.J., Moore, E.C., Lonsdorf, A.S., Kulikauskas, R.M., Rothberg, B.G., Berger, A.J., Major, M.B., Hwang, S.T., Rimm, D.L., and Moon, R.T.J.P.o.t.N.A.o.S. (2009). Activated Wnt/ß-catenin signaling in melanoma is associated with decreased proliferation in patient tumors and a murine melanoma model. *106*, 1193-1198.

Choi, H.-J., Yoon, T.-D., Muhammad, I., Jeong, M.-H., Lee, J., Baek, S.-Y., Kim, B.-S., Yoon, S.J.B., and communications, b.r. (2012). Regulatory role of mouse epidermal growth factor-like protein 8 in thymic epithelial cells. *425*, 250-255.

Cichorek, M., Wachulska, M., Stasiewicz, A., and Tyminska, A. (2013). Skin melanocytes: biology and development. Postepy Dermatol Alergol *30*, 30-41.

Colombo, S., Berlin, I., Delmas, V., Larue, L.J.M., melanosomes: biosynthesis, b., physiological,, and functions, p. (2011). Classical and nonclassical melanocytes in vertebrates. 21-61.

Colombo, S., Petit, V., Kumasaka, M., Delmas, V., and Larue, L.J.P.c.r. (2007). Flanking genomic region of Tyr:: Cre mice, rapid genotyping for homozygous mice. *20*, 305-306.

Copeland, N.G., Gilbert, D.J., Cho, B.C., Donovan, P.J., Jenkins, N.A., Cosman, D., Anderson, D., Lyman, S.D., and Williams, D.E.J.C. (1990). Mast cell growth factor maps near the steel locus on mouse chromosome 10 and is deleted in a number of steel alleles. *63*, 175-183.

Costin, G.-E., Valencia, J.C., Vieira, W.D., Lamoreux, M.L., and Hearing, V.J.J.J.o.c.s. (2003). Tyrosinase processing and intracellular trafficking is disrupted in mouse primary melanocytes carrying the underwhite (uw) mutation. A model for oculocutaneous albinism (OCA) type 4. *116*, 3203-3212.

Cronin, J.C., Watkins-Chow, D.E., Incao, A., Hasskamp, J.H., Schönewolf, N., Aoude, L.G., Hayward, N.K., Bastian, B.C., Dummer, R., and Loftus, S.K.J.C.r. (2013). SOX10 ablation arrests cell cycle, induces senescence, and suppresses melanomagenesis. *73*, 5709-5718.

Cronin, J.C., Wunderlich, J., Loftus, S.K., Prickett, T.D., Wei, X., Ridd, K., Vemula, S., Burrell, A.S., Agrawal, N.S., Lin, J.C., *et al.* (2009). Frequent mutations in the MITF pathway in melanoma. Pigment Cell Melanoma Res *22*, 435-444.

Daboussi, L., Costaguta, G., Gullo, M., Jasinski, N., Pessino, V., O'Leary, B., Lettieri, K., Driscoll, S., and Pfaff, S.L.J.C.R. (2023). Mitf is a Schwann cell sensor of axonal integrity that drives nerve repair. *42*.

Davies, H., Bignell, G.R., Cox, C., Stephens, P., Edkins, S., Clegg, S., Teague, J., Woffendin, H., Garnett, M.J., and Bottomley, W.J.N. (2002). Mutations of the BRAF gene in human cancer. *417*, 949-954.

De Strooper, B., and Annaert, W.J.T.J.o.c.b. (2001). Where Notch and Wnt signaling meet: the presenilin hub. *152*, F17-F20.

Delannet, M., and Duband, J.-L.J.D. (1992). Transforming growth factor-β control of cell-substratum adhesion during avian neural crest cell emigration in vitro. *116*, 275-287.

Delmas, V., Beermann, F., Martinozzi, S., Carreira, S., Ackermann, J., Kumasaka, M., Denat, L., Goodall, J., Luciani, F., Viros, A.J.G., *et al.* (2007). β-Catenin induces immortalization of melanocytes by suppressing p16INK4a expression and cooperates with N-Ras in melanoma development. *21*, 2923-2935.

Delmas, V., Martinozzi, S., Bourgeois, Y., Holzenberger, M., and Larue, L. (2003). Cre-mediated recombination in the skin melanocyte lineage. Genesis *36*, 73-80.

Dennler, S., André, J., Alexaki, I., Li, A., Magnaldo, T., Ten Dijke, P., Wang, X.-J., Verrecchia, F., and Mauviel, A.J.C.r. (2007). Induction of sonic hedgehog mediators by transforming growth factor-β: Smad3-dependent activation of Gli2 and Gli1 expression in vitro and in vivo. *67*, 6981-6986.

Dilshat, R., Fock, V., Kenny, C., Gerritsen, I., Lasseur, R.M.J., Travnickova, J., Eichhoff, O.M., Cerny, P., Moller, K., Sigurbjornsdottir, S., *et al.* (2021). MITF reprograms the extracellular matrix and focal adhesion in melanoma. Elife *10*.

Dorsky, R.I., Raible, D.W., Moon, R.T.J.G., and development (2000). Direct regulation of nacre, a zebrafish MITF homolog required for pigment cell formation, by the Wnt pathway. *14*, 158-162.

Du, J., Miller, A.J., Widlund, H.R., Horstmann, M.A., Ramaswamy, S., and Fisher, D.E.J.T.A.j.o.p. (2003). MLANA/MART1 and SILV/PMEL17/GP100 are transcriptionally regulated by MITF in melanocytes and melanoma. *163*, 333-343.

Du, J., Widlund, H.R., Horstmann, M.A., Ramaswamy, S., Ross, K., Huber, W.E., Nishimura, E.K., Golub, T.R., and Fisher, D.E.J.C.c. (2004). Critical role of CDK2 for melanoma growth linked to its melanocyte-specific transcriptional regulation by MITF. *6*, 565-576.

Dunn, K.J., Brady, M., Ochsenbauer-Jambor, C., Snyder, S., Incao, A., and Pavan, W.J.J.P.c.r. (2005). WNT1 and WNT3a promote expansion of melanocytes through distinct modes of action. *18*, 167-180.

Dunn, K.J., Williams, B.O., Li, Y., and Pavan, W.J.J.P.o.t.N.A.o.S. (2000). Neural crest-directed gene transfer demonstrates Wnt1 role in melanocyte expansion and differentiation during mouse development. *97*, 10050-10055.

Dupin, E., Real, C., Glavieux-Pardanaud, C., Vaigot, P., and Le Douarin, N.M.J.P.o.t.N.A.o.S. (2003). Reversal of developmental restrictions in neural crest lineages: transition from Schwann cells to glial-melanocytic precursors in vitro. *100*, 5229-5233.

Dynek, J.N., Chan, S.M., Liu, J., Zha, J., Fairbrother, W.J., and Vucic, D.J.C.R. (2008). Microphthalmia-associated transcription factor is a critical transcriptional regulator of melanoma inhibitor of apoptosis in melanomas. *68*, 3124-3132.

Ellis, R.A., MONTAGNA, W.J.J.o.H., and Cytochemistry (1958). Histology and cytochemistry of human skin. XV. Sites of phosphorylase and amylo-1, 6-glucosidase activity. *6*, 201-207.

Erickson, C.A., Duong, T., and Tosney, K.W.J.D.b. (1992). Descriptive and experimental analysis of the dispersion of neural crest cells along the dorsolateral path and their entry into ectoderm in the chick embryo. *151*, 251-272.

Ernfors, P.J.E.c.r. (2010). Cellular origin and developmental mechanisms during the formation of skin melanocytes. *316*, 1397-1407.

Falletta, P., Sanchez-del-Campo, L., Chauhan, J., Effern, M., Kenyon, A., Kershaw, C.J., Siddaway, R., Lisle, R., Freter, R., Daniels, M.J.J.G., *et al.* (2017). Translation reprogramming is an evolutionarily conserved driver of phenotypic plasticity and therapeutic resistance in melanoma. *31*, 18-33.

Fenouille, N., Tichet, M., Dufies, M., Pottier, A., Mogha, A., Soo, J.K., Rocchi, S., Mallavialle, A., Galibert, M.-D., and Khammari, A.J.P.o. (2012). The epithelial-mesenchymal transition (EMT) regulatory factor SLUG (SNAI2) is a downstream target of SPARC and AKT in promoting melanoma cell invasion. *7*, e40378.

Ferguson, C.A., and Kidson, S.H. (1997). The regulation of tyrosinase gene transcription. Pigment Cell Res *10*, 127-138.

Fitch, K.R., McGowan, K.A., Van Raamsdonk, C.D., Fuchs, H., Lee, D., Puech, A., Hérault, Y., Threadgill, D.W., De Angelis, M.H., Barsh, G.S.J.G., *et al.* (2003). Genetics of dark skin in mice. *17*, 214-228.

Flesher, J.L., Paterson-Coleman, E.K., Vasudeva, P., Ruiz-Vega, R., Marshall, M., Pearlman, E., MacGregor, G.R., Neumann, J., Ganesan, A.K.J.P.c., and research, m. (2020). Delineating the role of MITF isoforms in pigmentation and tissue homeostasis. *33*, 279-292.

Fountain, J.W., Karayiorgou, M., Ernstoff, M.S., Kirkwood, J.M., Vlock, D.R., Titus-Ernstoff, L., Bouchard, B., Vijayasaradhi, S., Houghton, A.N., and Lahti, J.J.P.o.t.N.A.o.S. (1992). Homozygous deletions within human chromosome band 9p21 in melanoma. *89*, 10557-10561.

Friedel, R.H., Wurst, W., Wefers, B., Kühn, R.J.T.M.M., and Protocols (2011). Generating conditional knockout mice. 205-231.

Fu, M., Wang, C., Li, Z., Sakamaki, T., and Pestell, R.G.J.E. (2004). Minireview: Cyclin D1: normal and abnormal functions. *145*, 5439-5447.

Fujimoto, H., Higuchi, M., Koike, M., Ode, H., Pinak, M., Bunta, J.K., Nemoto, T., Sakudoh, T., Honda, N., and Maekawa, H.J.J.o.c.c. (2012). A possible overestimation of the effect of acetylation on lysine residues in KQ mutant analysis. *33*, 239-246.

Galibert, M.-D., Dexter, T.J., Goding, C.R., and Yavuzer, U.J.J.o.B.C. (1999). Pax3 and regulation of the melanocyte-specific tyrosinase-related protein-1 promoter. *274*, 26894-26900.

Garcia-Alonso, L., Holland, C.H., Ibrahim, M.M., Turei, D., and Saez-Rodriguez, J.J.G.r. (2019). Benchmark and integration of resources for the estimation of human transcription factor activities. *29*, 1363-1375.

Garraway, L.A., Widlund, H.R., Rubin, M.A., Getz, G., Berger, A.J., Ramaswamy, S., Beroukhim, R., Milner, D.A., Granter, S.R., and Du, J.J.N. (2005). Integrative genomic analyses identify MITF as a lineage survival oncogene amplified in malignant melanoma. *436*, 117-122.

Geissler, E.N., Ryan, M.A., and Housman, D.E.J.C. (1988). The dominant-white spotting (W) locus of the mouse encodes the c-kit proto-oncogene. *55*, 185-192.

George, A., Zand, D.J., Hufnagel, R.B., Sharma, R., Sergeev, Y.V., Legare, J.M., Rice, G.M., Schwoerer, J.A.S., Rius, M., and Tetri, L.J.T.A.J.o.H.G. (2016). Biallelic mutations in MITF cause coloboma, osteopetrosis, microphthalmia, macrocephaly, albinism, and deafness. *99*, 1388-1394.

Giuliano, S., Cheli, Y., Ohanna, M., Bonet, C., Beuret, L., Bille, K., Loubat, A., Hofman, V., Hofman, P., and Ponzio, G.J.C.r. (2010). Microphthalmia-associated transcription factor controls the DNA damage response and a lineage-specific senescence program in melanomas. *70*, 3813-3822.

Goding, C.R., and Arnheiter, H. (2019). MITF-the first 25 years. Genes Dev *33*, 983-1007.

Goldstein, A.M., Brewer, K.C., Doyle, A.M., Nagy, N., and Roberts, D.J.J.M.o.d. (2005). BMP signaling is necessary for neural crest cell migration and ganglion formation in the enteric nervous system. *122*, 821-833.

Goldstein, A.M., Chan, M., Harland, M., Hayward, N.K., Demenais, F., Bishop, D.T., Azizi, E., Bergman, W., Bianchi-Scarra, G., and Bruno, W.J.J.o.m.g. (2007). Features associated with germline CDKN2A mutations: a GenoMEL study of melanoma-prone families from three continents. *44*, 99-106.

González-Ruiz, L., González-Moles, M.Á., González-Ruiz, I., Ruiz-Ávila, I., Ayén, Á., Ramos-García, P.J.P.c., and research, m. (2020). An update on the implications of cyclin D1 in melanomas. *33*, 788-805.

Grill, C., Bergsteinsdottir, K., Ogmundsdottir, M.H., Pogenberg, V., Schepsky, A., Wilmanns, M., Pingault, V., and Steingrimsson, E. (2013). MITF mutations associated with pigment deficiency syndromes and melanoma have different effects on protein function. Hum Mol Genet *22*, 4357-4367.

Gyoja, F. (2014). A genome-wide survey of bHLH transcription factors in the Placozoan Trichoplax adhaerens reveals the ancient repertoire of this gene family in metazoan. *542*, 29-37.

Halaban, R., and Alfano, F.D.J.I.v. (1984). Selective elimination of fibroblasts from cultures of normal human melanocytes. *20*, 447-450.

Halaban, R., Ghosh, S., Baird, A.J.I.v.c., and biology, d. (1987). bFGF is the putative natural growth factor for human melanocytes. *23*, 47-52.

Han, S., Ren, Y., He, W., Liu, H., Zhi, Z., Zhu, X., Yang, T., Rong, Y., Ma, B., and Purwin, T.J.J.N.c. (2018). ERK-mediated phosphorylation regulates SOX10 sumoylation and targets expression in mutant BRAF melanoma. *9*, 28.

Happle, R.J.D. (2002). Transposable elements and the lines of Blaschko: a new perspective. *204*, 4-7.

Hari, L., Brault, V., Kléber, M., Lee, H.-Y., Ille, F., Leimeroth, R., Paratore, C., Suter, U., Kemler, R., and Sommer, L.J.T.J.o.c.b. (2002). Lineage-specific requirements of β-catenin in neural crest development. *159*, 867-880.

Harper, D.C., Theos, A.C., Herman, K.E., Tenza, D., Raposo, G., and Marks, M.S.J.J.o.B.C. (2008). Premelanosome amyloid-like fibrils are composed of only golgi-processed forms of Pmel17 that have been proteolytically processed in endosomes. *283*, 2307-2322.

Hauswirth, R., Haase, B., Blatter, M., Brooks, S.A., Burger, D., Drögemüller, C., Gerber, V., Henke, D., Janda, J., and Jude, R.J.P.g. (2012). Mutations in MITF and PAX3 cause "splashed white" and other white spotting phenotypes in horses. *8*, e1002653.

Hemesath, T.J., Price, E.R., Takemoto, C., Badalian, T., and Fisher, D.E.J.N. (1998). MAP kinase links the transcription factor Microphthalmia to c-Kit signalling in melanocytes. *391*, 298-301.

Hemesath, T.J., Steingrímsson, E., McGill, G., Hansen, M.J., Vaught, J., Hodgkinson, C.A., Arnheiter, H., Copeland, N.G., Jenkins, N.A., Fisher, D.E.J.G., *et al.* (1994). Microphthalmia, a critical factor in melanocyte development, defines a discrete transcription factor family. *8*, 2770-2780.

Hemmings, B.A., and Restuccia, D.F.J.C.S.H.p.i.b. (2012). Pi3k-pkb/akt pathway. *4*, a011189.

Henion, P.D., and Weston, J.A.J.D. (1997). Timing and pattern of cell fate restrictions in the neural crest lineage. *124*, 4351-4359.

Herraiz, C., Garcia-Borron, J.C., Jiménez-Cervantes, C., and Olivares, C.J.B.e.B.A.-M.B.o.D. (2017). MC1R signaling. Intracellular partners and pathophysiological implications. *1863*, 2448-2461.

Hershey, C.L., and Fisher, D.E.J.G. (2005). Genomic analysis of the Microphthalmia locus and identification of the MITF-J/Mitf-J isoform. *347*, 73-82.

Hertwig, P.J.Z.f.I.A.-u.V. (1942). Neue mutationen und koppelungsgruppen bei der hausmaus. *80*, 220-246.

Hingorani, S.R., Jacobetz, M.A., Robertson, G.P., Herlyn, M., and Tuveson, D.A.J.C.r. (2003). Suppression of BRAFV599E in human melanoma abrogates transformation. *63*, 5198-5202.

Hirobe, T.J.T.A.R. (1984). Histochemical survey of the distribution of the epidermal melanoblasts and melanocytes in the mouse during fetal and postnatal periods. *208*, 589-594.

Hitoshi, S., Alexson, T., Tropepe, V., Donoviel, D., Elia, A.J., Nye, J.S., Conlon, R.A., Mak, T.W., Bernstein, A., Van Der Kooy, D.J.G., *et al.* (2002). Notch pathway molecules are essential for the maintenance, but not the generation, of mammalian neural stem cells. *16*, 846-858.

Hodgkinson, C.A., Moore, K.J., Nakayama, A., Steingrímsson, E., Copeland, N.G., Jenkins, N.A., and Arnheiter, H.J.C. (1993). Mutations at the mouse microphthalmia locus are associated with defects in a gene encoding a novel basic-helix-loop-helix-zipper protein. *74*, 395-404.

Hoek, K.S., Eichhoff, O.M., Schlegel, N.C., Döbbeling, U., Kobert, N., Schaerer, L., Hemmi, S., and Dummer, R.J.C.r. (2008). In vivo switching of human melanoma cells between proliferative and invasive states. *68*, 650-656.

Hosoda, K., Hammer, R.E., Richardson, J.A., Baynash, A.G., Cheung, J.C., Giaid, A., and Yanagisawa, M.J.C. (1994). Targeted and natural (piebald-lethal) mutations of endothelin-B receptor gene produce megacolon associated with spotted coat color in mice. *79*, 1267-1276.

Hou, L., Arnheiter, H., and Pavan, W.J.J.P.o.t.N.A.o.S. (2006). Interspecies difference in the regulation of melanocyte development by SOX10 and MITF. *103*, 9081-9085.

Hsu, C.-C., Su, C.-J., Jeng, M.-F., Chen, W.-H., and Chen, H.-H.J.P.p. (2019). A HORT1 retrotransposon insertion in the PeMYB11 promoter causes harlequin/black flowers in Phalaenopsis orchids. *180*, 1535-1548.

Hu, D.-N., McCormick, S.A., Orlow, S.J., Rosemblat, S., Lin, A.Y., Wo, K.J.I.o., and science, v. (1995). Melanogenesis by human uveal melanocytes in vitro. *36*, 931-938.

Huber, W.E., Price, E.R., Widlund, H.R., Du, J., Davis, I.J., Wegner, M., and Fisher, D.E.J.J.o.B.C. (2003). A tissue-restricted cAMP transcriptional response: SOX10 modulates α-melanocyte-stimulating hormone-triggered expression of microphthalmia-associated transcription factor in melanocytes. *278*, 45224-45230.

Huszar, D., Sharpe, A., Hashmi, S., Bouchard, B., Houghton, A., and Jaenisch, R.J.D. (1991). Generation of pigmented stripes in albino mice by retroviral marking of neural crest melanoblasts. *113*, 653-660.

Ikeya, M., Lee, S.M., Johnson, J.E., McMahon, A.P., and Takada, S.J.N. (1997). Wnt signalling required for expansion of neural crest and CNS progenitors. *389*, 966-970.

Indra, A.K., Warot, X., Brocard, J., Bornert, J.-M., Xiao, J.-H., Chambon, P., and Metzger, D.J.N.a.r. (1999). Temporally-controlled site-specific mutagenesis in the basal layer of the epidermis: comparison of the recombinase activity of the tamoxifen-inducible Cre-ERT and Cre-ERT2 recombinases. *27*, 4324-4327.

Javelaud, D., Alexaki, V.I., Pierrat, M.J., Hoek, K.S., Dennler, S., Van Kempen, L., Bertolotto, C., Ballotti, R., Saule, S., Delmas, V.J.P.c., *et al.* (2011). GLI2 and M-MITF transcription factors control exclusive gene expression programs and inversely regulate invasion in human melanoma cells. *24*, 932-943.

Jevtić, P., Levy, D.L.J.C.b., and paradoxes, t.n.e.r.a.m.e.p. (2014). Mechanisms of nuclear size regulation in model systems and cancer. 537-569.

Jiang, R., Lan, Y., Norton, C.R., Sundberg, J.P., and Gridley, T.J.D.b. (1998). The Slug gene is not essential for mesoderm or neural crest development in mice. *198*, 277-285.

Jiang, Y.-h., Bressler, J., and Beaudet, A.L.J.A.R.G.H.G. (2004). Epigenetics and human disease. *5*, 479-510.

Jin, E.-J., Erickson, C.A., Takada, S., and Burrus, L.W.J.D.b. (2001). Wnt and BMP signaling govern lineage segregation of melanocytes in the avian embryo. *233*, 22-37.

Jordan, S.A., and Jackson, I.J.J.M.o.d. (2000). A late wave of melanoblast differentiation and rostrocaudal migration revealed in patch and rump-white embryos. *92*, 135-143.

Juneja, V.R., McGuire, K.A., Manguso, R.T., LaFleur, M.W., Collins, N., Haining, W.N., Freeman, G.J., and Sharpe, A.H.J.J.o.E.M. (2017). PD-L1 on tumor cells is sufficient for immune evasion in immunogenic tumors and inhibits CD8 T cell cytotoxicity. *214*, 895-904.

Kaelin, C.B., McGowan, K.A., and Barsh, G.S.J.N.c. (2021). Developmental genetics of color pattern establishment in cats. *12*, 5127.

Kageyama, R., Ohtsuka, T., Tomita, K.J.M., and cells (2000). The bHLH gene Hes1 regulates differentiation of multiple cell types. *10*, 1-7.

Karasarides, M., Chiloeches, A., Hayward, R., Niculescu-Duvaz, D., Scanlon, I., Friedlos, F., Ogilvie, L., Hedley, D., Martin, J., and Marshall, C.J.J.O. (2004). B-RAF is a therapeutic target in melanoma. *23*, 6292-6298.

Katkat, E., Demirci, Y., Heger, G., Karagulle, D., Papatheodorou, I., Brazma, A., Ozhan, G.J.F.i.C., and Biology, D. (2023). Canonical Wnt and TGF-β/BMP signaling enhance melanocyte regeneration but suppress invasiveness, migration, and proliferation of melanoma cells. *11*, 1297910.

Keshet, E., Lyman, S.D., Williams, D.E., Anderson, D.M., Jenkins, N., Copeland, N., and Parada, L.F.J.T.E.J. (1991). Embryonic RNA expression patterns of the c-kit receptor and its cognate ligand suggest multiple functional roles in mouse development. *10*, 2425-2435.

Kim, S.C., Sprung, R., Chen, Y., Xu, Y., Ball, H., Pei, J., Cheng, T., Kho, Y., Xiao, H., and Xiao, L.J.M.c. (2006). Substrate and functional diversity of lysine acetylation revealed by a proteomics survey. *23*, 607-618.

Koga, A., Iida, A., Hori, H., Shimada, A., Shima, A.J.M.b., and evolution (2006). Vertebrate DNA transposon as a natural mutator: the medaka fish Tol2 element contributes to genetic variation without recognizable traces. *23*, 1414-1419.

Koh, H.K., Geller, A.C., Miller, D.R., Grossbart, T.A., and Lew, R.A.J.A.o.d. (1996). Prevention and early detection strategies for melanoma and skin cancer: current status. *132*, 436-443.

Koh, J., Enders, G.H., David Dynlacht, B., and Harlow, E.J.N. (1995). Tumour-derived p16 alleles encoding proteins defective in cell-cycle inhibition. *375*, 506-510.

Kong, Y., Sheng, X., Wu, X., Yan, J., Ma, M., Yu, J., Si, L., Chi, Z., Cui, C., and Dai, J.J.C.C.R. (2017). Frequent genetic aberrations in the CDK4 pathway in acral melanoma indicate the potential for CDK4/6 inhibitors in targeted therapy. *23*, 6946-6957.

Konyukhov, B., and Osipov, V. (1968). Interallelic complementation of microphthalmia and white genes in mice.

Krasagakis, K., Garbe, C., Krüger-Krasagakes, S., and Orfanos, C.E.J.J.o.i.d. (1993). 12-O-tetradecanoylphorbol-13-acetate not only modulates proliferation rates, but also alters antigen expression and LAK-cell susceptibility of normal human melanocytes in vitro. *100*, 653-659.

Lambert, J.-F., Benoit, B.O., Colvin, G.A., Carlson, J., Delville, Y., and Quesenberry, P.J.J.J.o.n.m. (2000). Quick sex determination of mouse fetuses. *95*, 127-132.

Lamoreux, M.L., Delmas, V., Larue, L., and Bennett, D. (2010). The colors of mice: a model genetic network (John Wiley & Sons).

Lamoreux, M.L., and Mayer, T.C.J.D.B. (1975). Site of gene action in the development of hair pigment in recessive yellow (ee) mice. *46*, 160-166.

Lang, D., Lu, M.M., Huang, L., Engleka, K.A., Zhang, M., Chu, E.Y., Lipner, S., Skoultchi, A., Millar, S.E., and Epstein, J.A.J.N. (2005). Pax3 functions at a nodal point in melanocyte stem cell differentiation. *433*, 884-887.

Larasati, Y., Boudou, C., Koval, A., and Katanaev, V.L.J.D.d.t. (2022). Unlocking the Wnt pathway: therapeutic potential of selective targeting FZD7 in cancer. *27*, 777-792.

Larribère, L., Novak, D., Wu, H., Hüser, L., Granados, K., Orouji, E., and Utikal, J.J.O. (2017). New role of ID3 in melanoma adaptive drug-resistance. *8*, 110166.

Larue, L., de Vuyst, F., and Delmas, V. (2013). Modeling melanoblast development. Cell Mol Life Sci *70*, 1067-1079.

Lavker, R.M., Sun, T.-T., Oshima, H., Barrandon, Y., Akiyama, M., Ferraris, C., Chevalier, G., Favier, B., Jahoda, C.A., and Dhouailly, D. (2003). Hair follicle stem cells. Paper presented at: Journal of Investigative Dermatology Symposium Proceedings (Elsevier).

Le Coz, M., Aktary, Z., Watanabe, N., Yajima, I., Pouteaux, M., Charoenchon, N., Motohashi, T., Kunisada, T., Corvelo, A., and Larue, L. (2021). Targeted Knockout of beta-Catenin in Adult Melanocyte Stem Cells Using a Mouse Line, Dct::CreER(T2), Results in Disrupted Stem Cell Renewal and Pigmentation Defects. J Invest Dermatol *141*, 1363-1366 e1369.

Lee, H.O., Levorse, J.M., and Shin, M.K. (2003). The endothelin receptor-B is required for the migration of neural crest-derived melanocyte and enteric neuron precursors. Dev Biol *259*, 162-175.

Lee, M., Goodall, J., Goding, C.R., Verastegui, C., and Ballotti, R.J.J.o.B.C. (2000). Direct regulation of the Microphthalmia promoter by Sox10 links Waardenburg-Shah syndrome (WS4)-associated hypopigmentation and deafness to WS2. *275*, 37978-37983.

Lerner, A.B., Shiohara, T., Boissy, R.E., Jacobson, K.A., Lamoreux, M.L., and Moellmann, G.E.J.J.o.i.d. (1986). A mouse model for vitiligo. *87*.

Li, A., Dawson, J.C., Forero-Vargas, M., Spence, H.J., Yu, X., König, I., Anderson, K., and Machesky, L.M.J.C.b. (2010). The actin-bundling protein fascin stabilizes actin in invadopodia and potentiates protrusive invasion. *20*, 339-345.

Li, A., Ma, Y., Yu, X., Mort, R.L., Lindsay, C.R., Stevenson, D., Strathdee, D., Insall, R.H., Chernoff, J., and Snapper, S.B.J.D.c. (2011). Rac1 drives melanoblast organization during mouse development by orchestrating pseudopod-driven motility and cell-cycle progression. *21*, 722-734.

Li, L., Zhang, S., Li, H., and Chou, H.J.B.c. (2019). FGFR3 promotes the growth and malignancy of melanoma by influencing EMT and the phosphorylation of ERK, AKT, and EGFR. *19*, 1-12.

Lindner, G., Botchkarev, V.A., Botchkareva, N.V., Ling, G., van der Veen, C., and Paus, R.J.T.A.j.o.p. (1997). Analysis of apoptosis during hair follicle regression (catagen). *151*, 1601.

Loercher, A.E., Tank, E.M., Delston, R.B., and Harbour, J.W.J.T.J.o.c.b. (2005). MITF links differentiation with cell cycle arrest in melanocytes by transcriptional activation of INK4A. *168*, 35-40.

Lombillo, V.A., and Sybert, V.P.J.C.o.i.p. (2005). Mosaicism in cutaneous pigmentation. *17*, 494-500.

Louphrasitthiphol, P., Loffreda, A., Pogenberg, V., Picaud, S., Schepsky, A., Friedrichsen, H., Zeng, Z., Lashgari, A., Thomas, B., and Patton, E.E.J.N.C. (2023). Acetylation reprograms MITF target selectivity and residence time. *14*, 6051.

Louphrasitthiphol, P., Siddaway, R., Loffreda, A., Pogenberg, V., Friedrichsen, H., Schepsky, A., Zeng, Z., Lu, M., Strub, T., Freter, R., *et al.* (2020). Tuning Transcription Factor Availability through Acetylation-Mediated Genomic Redistribution. Mol Cell *79*, 472-487 e410.

Love, M.I., Huber, W., and Anders, S.J.G.b. (2014). Moderated estimation of fold change and dispersion for RNA-seq data with DESeq2. *15*, 1-21.

Lowings, P., Yavuzer, U., Goding, C.J.M., and Biology, C. (1992). Positive and negative elements regulate a melanocyte-specific promoter. *12*, 3653-3662.

Luciani, F., Champeval, D., Herbette, A., Denat, L., Aylaj, B., Martinozzi, S., Ballotti, R., Kemler, R., Goding, C.R., De Vuyst, F., *et al.* (2011). Biological and mathematical modeling of melanocyte development. Development *138*, 3943-3954.

Lyon, M.F.J.n. (1961). Gene action in the X-chromosome of the mouse (Mus musculus L.). *190*, 372-373.

MacDonald, B.T., Tamai, K., and He, X.J.D.c. (2009). Wnt/β-catenin signaling: components, mechanisms, and diseases. *17*, 9-26.

Machado, A.F., Martin, L.J., and Collins, M.D.J.C.p.d. (2001). Pax3 and the splotch mutations: structure, function, and relationship to teratogenesis, including gene-chemical interactions. *7*, 751-785.

Mackenzie, M.A., Jordan, S.A., Budd, P.S., and Jackson, I.J.J.D.b. (1997). Activation of the receptor tyrosine kinase Kit is required for the proliferation of melanoblasts in the mouse embryo. *192*, 99-107.

Magnuson, N., Beck, T., Vahidi, H., Hahn, H., Smola, U., and Rapp, U. (1994). The Raf-1 serine/threonine protein kinase. Paper presented at: Seminars in cancer biology.

Malumbres, M., and Barbacid, M.J.N.r.c. (2009). Cell cycle, CDKs and cancer: a changing paradigm. *9*, 153-166.

McGill, G.G., Horstmann, M., Widlund, H.R., Du, J., Motyckova, G., Nishimura, E.K., Lin, Y.-L., Ramaswamy, S., Avery, W., and Ding, H.-F.J.C. (2002). Bcl2 regulation by the melanocyte master regulator Mitf modulates lineage survival and melanoma cell viability. *109*, 707-718.

Mercer, J.J.T.A.j.o.c.n. (1998). Menkes syndrome and animal models. *67*, S1022-S1028.

Mintz, B.J.P.o.t.N.A.o.S. (1967). Gene control of mammalian pigmentary differentiation. I. Clonal origin of melanocytes. *58*, 344-351.

Moller, K., Sigurbjornsdottir, S., Arnthorsson, A.O., Pogenberg, V., Dilshat, R., Fock, V., Brynjolfsdottir, S.H., Bindesboll, C., Bessadottir, M., Ogmundsdottir, H.M., *et al.* (2019). MITF has a central role in regulating starvation-induced autophagy in melanoma. Sci Rep *9*, 1055.

Moore, K.J.J.T.i.G. (1995). Insight into the microphthalmia gene. *11*, 442-448.

Morii, E., Tsujimura, T., Jippo, T., Hashimoto, K., Takebayashi, K., Tsujino, K., Nomura, S., Yamamoto, M., and Kitamura, Y. (1996). Regulation of mouse mast cell protease 6 gene expression by transcription factor encoded by the mi locus.

Moriyama, M., Osawa, M., Mak, S.-S., Ohtsuka, T., Yamamoto, N., Han, H., Delmas, V., Kageyama, R., Beermann, F., and Larue, L.J.T.J.o.c.b. (2006). Notch signaling via Hes1 transcription factor maintains survival of melanoblasts and melanocyte stem cells. *173*, 333-339.

Mort, R.L., Ross, R.J., Hainey, K.J., Harrison, O.J., Keighren, M.A., Landini, G., Baker, R.E., Painter, K.J., Jackson, I.J., and Yates, C.A.J.N.c. (2016). Reconciling diverse mammalian pigmentation patterns with a fundamental mathematical model. *7*, 10288.

Müller-Röver, S., Foitzik, K., Paus, R., Handjiski, B., van der Veen, C., Eichmüller, S., McKay, I.A., and Stenn, K.S.J.J.o.i.d. (2001). A comprehensive guide for the accurate classification of murine hair follicles in distinct hair cycle stages. *117*, 3-15.

Müller, J., Krijgsman, O., Tsoi, J., Robert, L., Hugo, W., Song, C., Kong, X., Possik, P.A., Cornelissen-Steijger, P.D., and Foppen, M.H.G.J.N.c. (2014). Low MITF/AXL ratio predicts early resistance to multiple targeted drugs in melanoma. *5*, 5712.

Murakami, H., and Arnheiter, H.J.P.c.r. (2005). Sumoylation modulates transcriptional activity of MITF in a promoter-specific manner. *18*, 265-277.

Nakayama, A., Nguyen, M.-T.T., Chen, C.C., Opdecamp, K., Hodgkinson, C.A., and Arnheiter, H.J.M.o.d. (1998). Mutations in microphthalmia, the mouse homolog of the human deafness gene MITF, affect neuroepithelial and neural crest-derived melanocytes differently. *70*, 155-166.

Newton, A.C.J.C.r. (2001). Protein kinase C: structural and spatial regulation by phosphorylation, cofactors, and macromolecular interactions. *101*, 2353-2364.

Ngeow, K.C., Friedrichsen, H.J., Li, L., Zeng, Z., Andrews, S., Volpon, L., Brunsdon, H., Berridge, G., Picaud, S., Fischer, R., *et al.* (2018). BRAF/MAPK and GSK3 signaling converges to control MITF nuclear export. Proc Natl Acad Sci U S A *115*, E8668-E8677.

Nishikawa, S., Kusakabe, M., Yoshinaga, K., Ogawa, M., Hayashi, S., Kunisada, T., Era, T., Sakakura, T., and Nishikawa, S.-I.J.T.E.j. (1991). In utero manipulation of coat color formation by a monoclonal anti-c-kit antibody: two distinct waves of c-kit-dependency during melanocyte development. *10*, 2111-2118.

Nishimura, E.K., Granter, S.R., and Fisher, D.E.J.S. (2005). Mechanisms of hair graying: incomplete melanocyte stem cell maintenance in the niche. *307*, 720-724.

Nishimura, E.K., Jordan, S.A., Oshima, H., Yoshida, H., Osawa, M., Moriyama, M., Jackson, I.J., Barrandon, Y., Miyachi, Y., and Nishikawa, S.-I.J.N. (2002). Dominant role of the niche in melanocyte stem-cell fate determination. *416*, 854-860.

Nishimura, E.K., Yoshida, H., Kunisada, T., and Nishikawa, S.-I.J.D.b. (1999). Regulation of E-and P-cadherin expression correlated with melanocyte migration and diversification. *215*, 155-166.

Nishizuka, Y.J.S. (1992). Intracellular signaling by hydrolysis of phospholipids and activation of protein kinase C. *258*, 607-614.

Ohba, K., Takeda, K., Yamamoto, H., and Shibahara, S.J.G.t.C. (2015). Microphthalmia-associated transcription factor is expressed in projection neurons of the mouse olfactory bulb. *20*, 1088-1102.

Opdecamp, K., Nakayama, A., Nguyen, M., Hodgkinson, C.A., Pavan, W.J., and Arnheiter, H.J.D. (1997). Melanocyte development in vivo and in neural crest cell cultures: crucial dependence on the Mitf basic-helix-loop-helix-zipper transcription factor. *124*, 2377-2386.

Ozeki, H., Wakamatsu, K., Ito, S., and Ishiguro, I.J.A.b. (1997). Chemical characterization of eumelanins with special emphasis on 5, 6-dihydroxyindole-2-carboxylic acid content and molecular size. *248*, 149-157.

Palmer, J.W., Villavicencio, K.M., Idris, M., Weddle, D., Filipp, F.V., Program, N.C.S., Pavan, W.J., and Harris, M.L.J.b. (2022). The relationship between PD-L1 and quiescence in melanocyte stem cell aging. 2022.2009. 2022.508528.

Pan, L., Ma, X., Wen, B., Su, Z., Zheng, X., Liu, Y., Li, H., Chen, Y., Wang, J., and Lu, F.J.C.p. (2015). Microphthalmia-associated transcription factor/T-box factor-2 axis acts through Cyclin D1 to regulate melanocyte proliferation. *48*, 631-642.

Papp, T., Pemsel, H., Zimmermann, R., Bastrop, R., Weiss, D.G., and Schiffmann, D.J.J.o.m.g. (1999). Mutational analysis of the N-ras, p53, p16INK4a, CDK4, and MC1R genes in human congenital melanocytic naevi. *36*, 610-614.

Paulsson, M. (1992). Basement membrane proteins: structure, assembly, and cellular interactions. Critical reviews in biochemistry and molecular biology *27*, 93-127.

Pavan, W.J., and Tilghman, S.M. (1994a). Piebald lethal (sl) acts early to disrupt the development of neural crest-derived melanocytes. Proceedings of the National Academy of Sciences *91*, 7159-7163.

Pavan, W.J., and Tilghman, S.M.J.P.o.t.N.A.o.S. (1994b). Piebald lethal (sl) acts early to disrupt the development of neural crest-derived melanocytes. *91*, 7159-7163.

Pérez-Losada, J., Sánchez-Martın, M., Rodrıguez-Garcıa, A., Sánchez, M.L., Orfao, A., Flores, T., and Sánchez-Garcıa, I.J.B., The Journal of the American Society of Hematology (2002). Zinc-finger transcription factor Slug contributes to the function of the stem cell factor c-kit signaling pathway. *100*, 1274-1286.

Petit, V., and Larue, L.J.E.D. (2016). Any route for melanoblasts to colonize the skin! *25*, 669-673.

Petronzelli, F., Sollima, D., Coppola, G., Martini-Neri, M.E., Neri, G., Genuardi, M.J.G., Chromosomes, and Cancer (2001). CDKN2A germline splicing mutation affecting both P16INK4 and P14ARF RNA processing in a melanoma/neurofibroma kindred. *31*, 398-401.

Petrova, R., Patil, A.R., Trinh, V., McElroy, K.E., Bhakta, M., Tien, J., Wilson, D.S., Warren, L., and Stratton, J.R.J.S.R. (2023). Disease pathology signatures in a mouse model of Mucopolysaccharidosis type IIIB. *13*, 16699.

Pflicke, H., and Sixt, M.J.J.o.E.M. (2009). Preformed portals facilitate dendritic cell entry into afferent lymphatic vessels. *206*, 2925-2935.

Pierrat, M.-J., Marsaud, V., Mauviel, A., and Javelaud, D.J.J.o.B.C. (2012). Expression of microphthalmia-associated transcription factor (MITF), which is critical for melanoma progression, is inhibited by both transcription factor GLI2 and transforming growth factor-β. *287*, 17996-18004.

Pimentel, H., Bray, N.L., Puente, S., Melsted, P., and Pachter, L.J.N.m. (2017). Differential analysis of RNA-seq incorporating quantification uncertainty. *14*, 687-690.

Pla, P., and Larue, L.J.I.J.o.D.B. (2003). Involvement of endothelin receptors in normal and pathological development of neural crest cells. *47*, 315-325.

Pogenberg, V., Ballesteros-Álvarez, J., Schober, R., Sigvaldadóttir, I., Obarska-Kosinska, A., Milewski, M., Schindl, R., Ögmundsdóttir, M.H., Steingrímsson, E., and Wilmanns, M.J.N.A.R. (2020). Mechanism of conditional partner selectivity in MITF/TFE family transcription factors with a conserved coiled coil stammer motif. *48*, 934-948.

Pogenberg, V., Ogmundsdottir, M.H., Bergsteinsdottir, K., Schepsky, A., Phung, B., Deineko, V., Milewski, M., Steingrimsson, E., and Wilmanns, M. (2012). Restricted leucine zipper dimerization and specificity of DNA recognition of the melanocyte master regulator MITF. Genes Dev *26*, 2647-2658.

Potterf, S.B., Furumura, M., Dunn, K.J., Arnheiter, H., and Pavan, W.J.J.H.g. (2000). Transcription factor hierarchy in Waardenburg syndrome: regulation of MITF expression by SOX10 and PAX3. *107*, 1-6.

Potterf, S.B., Furumura, M., Sviderskaya, E.V., Santis, C., Bennett, D.C., and Hearing, V.J.J.E.C.R. (1998). Normal Tyrosine Transport and Abnormal Tyrosinase Routing inPink-Eyed DilutionMelanocytes. *244*, 319-326.

Price, E.R., Ding, H.-F., Badalian, T., Bhattacharya, S., Takemoto, C., Yao, T.-P., Hemesath, T.J., and Fisher, D.E.J.J.o.B.C. (1998). Lineage-specific signaling in melanocytes: c-kit stimulation recruits p300/CBP to microphthalmia. *273*, 17983-17986.

Prince, S., Wiggins, T., Hulley, P., and Kidson, S.J.P.c.r. (2003). Stimulation of melanogenesis by tetradecanoylphorbol 13-acetate (TPA) in mouse melanocytes and neural crest cells. *16*, 26-34.

Proaño-Pérez, E., Serrano-Candelas, E., García-Valverde, A., Rosell, J., Gómez-Peregrina, D., Navinés-Ferrer, A., Guerrero, M., Serrano, C., and Martín, M.J.C.G.T. (2023). The microphthalmia-associated transcription factor is involved in gastrointestinal stromal tumor growth. *30*, 245-255.

Rambow, F., Rogiers, A., Marin-Bejar, O., Aibar, S., Femel, J., Dewaele, M., Karras, P., Brown, D., Chang, Y.H., Debiec-Rychter, M., *et al.* (2018). Toward Minimal Residual Disease-Directed Therapy in Melanoma. Cell *174*, 843-855 e819.

Read, A.P., and Newton, V.E.J.J.o.m.g. (1997). Waardenburg syndrome. *34*, 656-665.

Sachindra, S. (2018). Role of Id3 in melanoma dedifferentiation and resistance to targeted therapy.

Saito, H., Yasumoto, K.-i., Takeda, K., Takahashi, K., Fukuzaki, A., Orikasa, S., and Shibahara, S.J.J.o.B.C. (2002). Melanocyte-specific microphthalmia-associated transcription factor isoform activates its own gene promoter through physical interaction with lymphoid-enhancing factor 1. *277*, 28787-28794.

Sánchez-Martín, M., Pérez-Losada, J., Rodríguez-García, A., González-Sánchez, B., Korf, B.R., Kuster, W., Moss, C., Spritz, R.A., and Sánchez-García, I.J.A.J.o.M.G.P.A. (2003). Deletion of the SLUG (SNAI2) gene results in human piebaldism. *122*, 125-132.

Sato, S., Roberts, K., Gambino, G., Cook, A., Kouzarides, T., and Goding, C.J.O. (1997). CBP/p300 as a co-factor for the Microphthalmia transcription factor. *14*, 3083-3092.

Sauter, E.R., Yeo, U.-C., von Stemm, A., Zhu, W., Litwin, S., Tichansky, D.S., Pistritto, G., Nesbit, M., Pinkel, D., and Herlyn, M.J.C.r. (2002). Cyclin D1 is a candidate oncogene in cutaneous melanoma. *62*, 3200-3206.

Schallreuter, K.J.S.P., and Physiology (1999). Successful treatment of oxidative stress in vitiligo. *12*, 132-138.

Schepsky, A., Bruser, K., Gunnarsson, G.J., Goodall, J., Hallsson, J.H., Goding, C.R., Steingrimsson, E., Hecht, A.J.M., and biology, c. (2006). The microphthalmia-associated transcription factor Mitf interacts with β-catenin to determine target gene expression. *26*, 8914-8927.

Schiaffino, M.V., and Tacchetti, C.J.P.c.r. (2005). The ocular albinism type 1 (OA1) protein and the evidence for an intracellular signal transduction system involved in melanosome biogenesis. *18*, 227-233.

Schouwey, K., Delmas, V., Larue, L., Zimber-Strobl, U., Strobl, L.J., Radtke, F., and Beermann, F. (2007). Notch1 and Notch2 receptors influence progressive hair graying in a dose-dependent manner. Dev Dyn *236*, 282-289.

Sefton, M., Sánchez, S., and Nieto, M.A.J.D. (1998). Conserved and divergent roles for members of the Snail family of transcription factors in the chick and mouse embryo. *125*, 3111-3121.

Seger, R., and Krebs, E.G.J.T.F.j. (1995). The MAPK signaling cascade. *9*, 726-735.

Seo, E.Y., Jin, S.-P., Sohn, K.-C., Park, C.-H., Lee, D.H., and Chung, J.H.J.J.o.I.D. (2017). UCHL1 regulates melanogenesis through controlling MITF stability in human melanocytes. *137*, 1757-1765.

Šestáková, B., Ondrušová, L., Vachtenheim, J.J.P.c., and research, m. (2010). Cell cycle inhibitor p21/WAF1/CIP1 as a cofactor of MITF expression in melanoma cells. *23*, 238-251.

Shakhova, O., Zingg, D., Schaefer, S.M., Hari, L., Civenni, G., Blunschi, J., Claudinot, S., Okoniewski, M., Beermann, F., and Mihic-Probst, D.J.N.c.b. (2012). Sox10 promotes the formation and maintenance of giant congenital naevi and melanoma. *14*, 882-890.

Sherr, C.J., Roberts, J.M.J.G., and development (2004). Living with or without cyclins and cyclin-dependent kinases. *18*, 2699-2711.

Shin, M.K., Levorse, J.M., Ingram, R.S., and Tilghman, S.M.J.N. (1999). The temporal requirement for endothelin receptor-B signalling during neural crest development. *402*, 496-501.

Simionato, E., Ledent, V., Richards, G., Thomas-Chollier, M., Kerner, P., Coornaert, D., Degnan, B.M., and Vervoort, M.J.B.e.b. (2007). Origin and diversification of the basic helix-loop-helix gene family in metazoans: insights from comparative genomics. *7*, 1-18.

Smith, D.E., Amo, F.F.D., and Gridley, T.J.D. (1992). Isolation of Sna, a mouse gene homologous to the Drosophila genes snail and escargot: its expression pattern suggests multiple roles during postimplantation development. *116*, 1033-1039.

Smith, S.D., Kelley, P.M., Kenyon, J.B., and Hoover, D.J.J.o.m.g. (2000). Tietz syndrome (hypopigmentation/deafness) caused by mutation ofMITF. *37*, 446-448.

Spritz, R.A.J.G.m. (2010). The genetics of generalized vitiligo: autoimmune pathways and an inverse relationship with malignant melanoma. *2*, 1-5.

Steel, K.P., Davidson, D.R., and Jackson, I.J.D. (1992). TRP-2/DT, a new early melanoblast marker, shows that steel growth factor (c-kit ligand) is a survival factor. *115*, 1111-1119.

Steingrímsson, E., Arnheiter, H., Hallsson, J.H., Lamoreux, M.L., Copeland, N.G., and Jenkins, N.A.J.G. (2003). Interallelic complementation at the mouse Mitf locus. *163*, 267-276.

Steingrimsson, E., Copeland, N.G., and Jenkins, N.A. (2004). Melanocytes and the microphthalmia transcription factor network. Annu Rev Genet *38*, 365-411.

Steingrímsson, E., Moore, K.J., Lamoreux, M.L., Ferré-D'Amaré, A.R., Burley, S.K., Sanders Zimring, D.C., Skow, L.C., Hodgkinson, C.A., Arnheiter, H., and Copeland, N.G.J.N.g. (1994). Molecular basis of mouse microphthalmia (mi) mutations helps explain their developmental and phenotypic consequences. *8*, 256-263.

Steingrímsson, E., Nii, A., Fisher, D.E., Ferré-D'Amaré, A.R., McCormick, R.J., Russell, L.B., Burley, S.K., Ward, J.M., Jenkins, N.A., and Copeland, N.G.J.T.E.j. (1996). The semidominant Mi (b) mutation identifies a role for the HLH domain in DNA binding in addition to its role in protein dimerization. *15*, 6280-6289.

Stott, F.J., Bates, S., James, M.C., McConnell, B.B., Starborg, M., Brookes, S., Palmero, I., Ryan, K., Hara, E., and Vousden, K.H.J.T.E.j. (1998). The alternative product from the human CDKN2A locus, p14ARF, participates in a regulatory feedback loop with p53 and MDM2. *17*, 5001-5014.

Strub, T., Giuliano, S., Ye, T., Bonet, C., Keime, C., Kobi, D., Le Gras, S., Cormont, M., Ballotti, R., and Bertolotto, C.J.O. (2011). Essential role of microphthalmia transcription factor for DNA replication, mitosis and genomic stability in melanoma. *30*, 2319-2332.

Subhan, F., Yoon, T.-D., Choi, H.J., Muhammad, I., Lee, J., Hong, C., Oh, S.-O., Baek, S.-Y., Kim, B.-S., and Yoon, S.J.I.j.o.m.m. (2013). Epidermal growth factor-like domain 8 inhibits the survival and proliferation of mouse thymocytes. *32*, 952-958.

Suzuki, I., Cone, R.D., Im, S., Nordlund, J., and Abdel-Malek, Z.A.J.E. (1996). Binding of melanotropic hormones to the melanocortin receptor MC1R on human melanocytes stimulates proliferation and melanogenesis. *137*, 1627-1633.

Sviderskaya, E.V., Wakeling, W.F., and Bennett, D.C.J.D. (1995). A cloned, immortal line of murine melanoblasts inducible to differentiate to melanocytes. *121*, 1547-1557.

Tachibana, M., Hara, Y., Vyas, D., Hodgkinson, C., Fex, J., Grundfast, K., Arnheiter, H.J.M., and Neuroscience, C. (1992). Cochlear disorder associated with melanocyte anomaly in mice with a transgenic insertional mutation. *3*, 433-445.

Takeda, K., Yasumoto, K.-i., Takada, R., Takada, S., Watanabe, K.-i., Udono, T., Saito, H., Takahashi, K., and Shibahara, S.J.J.o.B.C. (2000). Induction of melanocyte-specific microphthalmia-associated transcription factor by Wnt-3a. *275*, 14013-14016.

Tassabehji, M., Newton, V.E., and Read, A.P.J.N.g. (1994). Waardenburg syndrome type 2 caused by mutations in the human microphthalmia (MITF) gene. *8*, 251-255.

Thomas, A.J., and Erickson, C.A. (2008). The making of a melanocyte: the specification of melanoblasts from the neural crest. Pigment Cell Melanoma Res *21*, 598-610.

Thomas, A.J., and Erickson, C.A. (2009). FOXD3 regulates the lineage switch between neural crest-derived glial cells and pigment cells by repressing MITF through a non-canonical mechanism.

Thomson, J., Murphy, K., Baker, E., Sutherland, G.R., Parsons, P.G., Sturm, R.A., and Thomson, F.J.O. (1995). The brn-2 gene regulates the melanocytic phenotype and tumorigenic potential of human melanoma cells. *11*, 691-700.

Thurber, A., Douglas, G., Sturm, E., Zabierowski, S., Smit, D., Ramakrishnan, S., Hacker, E., Leonard, J., Herlyn, M., and Sturm, R.J.O. (2011). Inverse expression states of the BRN2 and MITF transcription factors in melanoma spheres and tumour xenografts regulate the NOTCH pathway. *30*, 3036-3048.

Tietz, W.J.A.j.o.h.g. (1963). A syndrome of deaf-mutism associated with albinism showing dominant autosomal inheritance. *15*, 259.

Tiwary, S., and Xu, L.J.P.o. (2016). FRIZZLED7 is required for tumor inititation and metastatic growth of melanoma cells. *11*, e0147638.

Tobin, D.J., Hagen, E., Botchkarev, V.A., and Paus, R.J.J.o.i.d. (1998). Do hair bulb melanocytes undergo apotosis during hair follicle regression (catagen)? *111*, 941-947.

Uka, R., Britschgi, C., Krättli, A., Matter, C., Mihic, D., Okoniewski, M.J., Gualandi, M., Stupp, R., Cinelli, P., and Dummer, R.J.O. (2020). Temporal activation of WNT/β-catenin signaling is sufficient to inhibit SOX10 expression and block melanoma growth. *39*, 4132-4154.

Umar, S.A., Dong, B., Nihal, M., and Chang, H.J.F.i.O. (2022). Frizzled receptors in melanomagenesis: From molecular interactions to target identification. *12*, 1096134.

Veis, D.J., Sorenson, C.M., Shutter, J.R., and Korsmeyer, S.J.J.C. (1993). Bcl-2-deficient mice demonstrate fulminant lymphoid apoptosis, polycystic kidneys, and hypopigmented hair. *75*, 229-240.

Vlčková, K., Vachtenheim, J., Réda, J., Horák, P., Ondrušová, L.J.J.o.c., and medicine, m. (2018). Inducibly decreased MITF levels do not affect proliferation and phenotype switching but reduce differentiation of melanoma cells. *22*, 2240-2251.

Vogan, K.J., Epstein, D.J., Trasler, D.G., and Gros, P.J.G. (1993). The splotch-delayed (Spd) mouse mutant carries a point mutation within the paired box of the Pax-3 gene. *17*, 364-369.

Vu, H.N., Dilshat, R., Fock, V., and Steingrimsson, E. (2021). User guide to MiT-TFE isoforms and post-translational modifications. Pigment Cell Melanoma Res *34*, 13-27.

Waardenburg, P.J.J.A.j.o.h.g. (1951). A new syndrome combining developmental anomalies of the eyelids, eyebrows and noseroot with pigmentary anomalies of the iris and head hair and with congenital deafness; Dystopia canthi medialis et punctorum lacrimalium lateroversa, hyperplasia supercilii medialis et radicis nasi, heterochromia iridum totaliis sive partialis, albinismus circumscriptus (leucismus, polioss) et surditas congenita (surdimutitas). *3*, 195.

Wan, P.T., Garnett, M.J., Roe, S.M., Lee, S., Niculescu-Duvaz, D., Good, V.M., Jones, C.M., Marshall, C.J., Springer, C.J., and Barford, D.J.C. (2004). Mechanism of activation of the RAF-ERK signaling pathway by oncogenic mutations of B-RAF. *116*, 855-867.

Watanabe, K.i., Takeda, K., Yasumoto, K.i., Udono, T., Saito, H., Ikeda, K., Takasaka, T., Takahashi, K., Kobayashi, T., and Tachibana, M.J.P.c.r. (2002). Identification of a distal enhancer for the melanocyte-specific promoter of the MITF gene. *15*, 201-211.

Webster, M., Witkin, K.L., and Cohen-Fix, O.J.J.o.c.s. (2009). Sizing up the nucleus: nuclear shape, size and nuclear-envelope assembly. *122*, 1477-1486.

Wehrle-Haller, B., Morrison-Graham, K., and Weston, J.A.J.D.b. (1996). Ectopic c-kit Expression Affects the Fate of Melanocyte Precursors inPatchMutant Embryos. *177*, 463-474.

Wehrle-Haller, B., and Weston, J.A.J.D. (1995). Soluble and cell-bound forms of steel factor activity play distinct roles in melanocyte precursor dispersal and survival on the lateral neural crest migration pathway. *121*, 731-742.

Weilbaecher, K.N., Motyckova, G., Huber, W.E., Takemoto, C.M., Hemesath, T.J., Xu, Y., Hershey, C.L., Dowland, N.R., Wells, A.G., and Fisher, D.E.J.M.c. (2001). Linkage of M-CSF signaling to Mitf, TFE3, and the osteoclast defect in Mitfmi/mi mice. *8*, 749-758.

Wellbrock, C., and Arozarena, I. (2015). Microphthalmia-associated transcription factor in melanoma development and MAP-kinase pathway targeted therapy. Pigment Cell Melanoma Res *28*, 390-406.

Wellbrock, C., and Marais, R.J.T.J.o.c.b. (2005). Elevated expression of MITF counteracts B-RAF–stimulated melanocyte and melanoma cell proliferation. *170*, 703-708.

Wels, C., Joshi, S., Koefinger, P., Bergler, H., and Schaider, H.J.J.o.i.d. (2011). Transcriptional activation of ZEB1 by Slug leads to cooperative regulation of the epithelial–mesenchymal transition-like phenotype in melanoma. *131*, 1877-1885.

West, J.J.J.o.t.b. (1975). A theoretical approach to the relation between patch size and clone size in chimaeric tissue. *50*, 153-160.

Widlund, H.R., Horstmann, M.A., Price, E.R., Cui, J., Lessnick, S.L., Wu, M., He, X., and Fisher, D.E.J.T.J.o.c.b. (2002). β-Catenin–induced melanoma growth requires the downstream target Microphthalmia-associated transcription factor. *158*, 1079-1087.

Wilkie, A.L., Jordan, S.A., and Jackson, I.J. (2002). Neural crest progenitors of the melanocyte lineage: coat colour patterns revisited.

Wilkinson, M.G., and Millar, J.B.J.T.F.J. (2000). Control of the eukaryotic cell cycle by MAP kinase signaling pathways. *14*, 2147-2157.

Wolpert, L., and Gingell, D. (1970). Striping and the pattern of melanocyte cells in chimaeric mice.

Wu, M., Hemesath, T.J., Takemoto, C.M., Horstmann, M.A., Wells, A.G., Price, E.R., Fisher, D.Z., Fisher, D.E.J.G., and development (2000). c-Kit triggers dual phosphorylations, which couple activation and degradation of the essential melanocyte factor Mi. *14*, 301-312.

Xu, W., Gong, L., Haddad, M.M., Bischof, O., Campisi, J., Yeh, E.T., and Medrano, E.E.J.E.c.r. (2000). Regulation of microphthalmia-associated transcription factor MITF protein levels by association with the ubiquitin-conjugating enzyme hUBC9. *255*, 135-143.

Yajima, I., Belloir, E., Bourgeois, Y., Kumasaka, M., Delmas, V., and Larue, L. (2006). Spatiotemporal gene control by the Cre-ERT2 system in melanocytes. Genesis *44*, 34-43.

Yasumoto, K.-i., Watabe, H., Valencia, J.C., Kushimoto, T., Kobayashi, T., Appella, E., and Hearing, V.J.J.J.o.B.C. (2004). Epitope mapping of the melanosomal matrix protein gp100 (PMEL17): rapid processing in the endoplasmic reticulum and glycosylation in the early Golgi compartment. *279*, 28330-28338.

Yasumoto, K.-i., Yokoyama, K., Takahashi, K., Tomita, Y., and Shibahara, S.J.J.o.B.C. (1997). Functional analysis of microphthalmia-associated transcription factor in pigment cell-specific transcription of the human tyrosinase family genes. *272*, 503-509.

Zhao, X., Fiske, B., Kawakami, A., Li, J., and Fisher, D.E.J.N.c. (2011). Regulation of MITF stability by the USP13 deubiquitinase. *2*, 414.

Appendix A

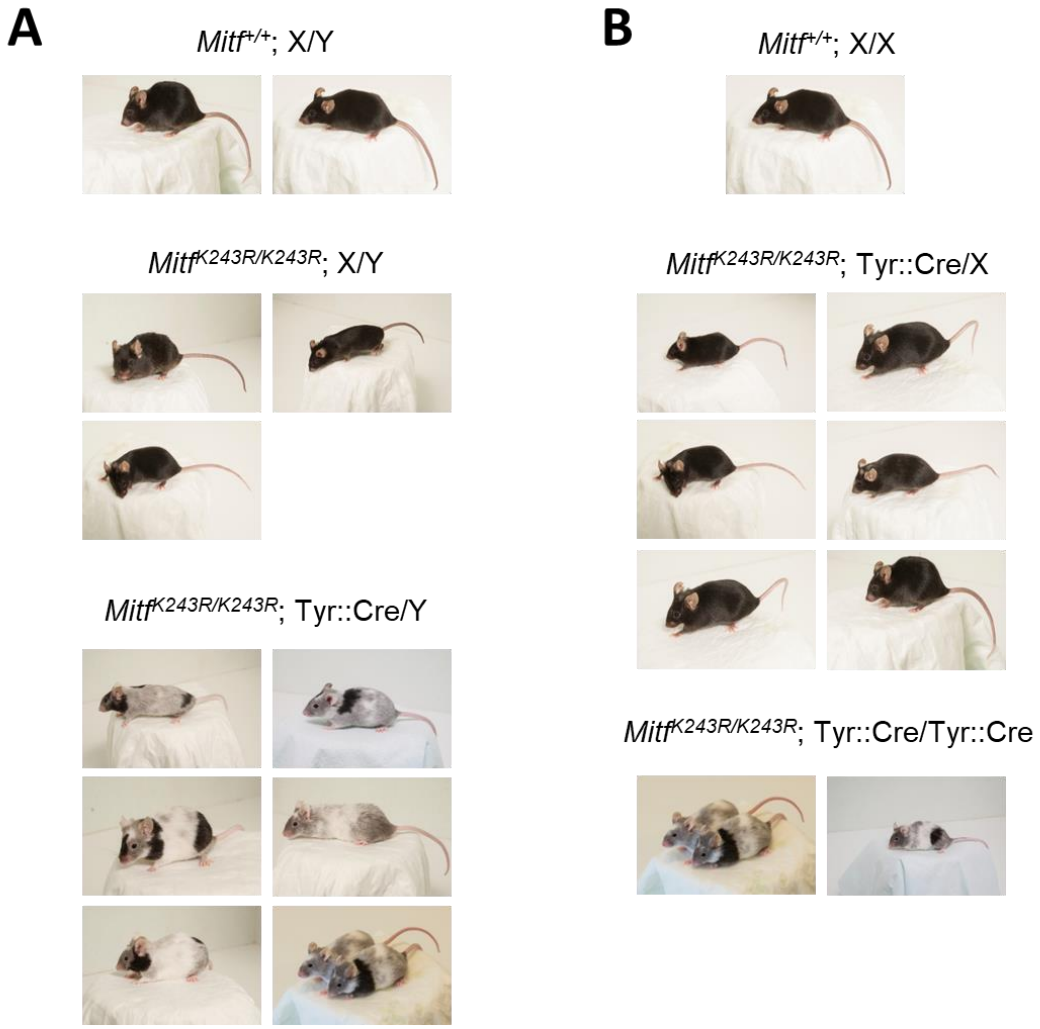

Figure 35. Montage of *Mitf*^{K243R} phenotype and WT MITF mice. Pictures of mice with the different possible genotypes for the *Mitf*^{K243R} and Tyr::Cre transgenes. (A) Males are displayed on the left panel with WT MITF (either *Mitf*$^{+/+}$; X/Y or *Mitf*$^{K243R/K243R}$; X/Y) or *Mitf*^{K243R} mutant (*Mitf*$^{K243R/K243R}$; Tyr::Cre/Y). (B) Females are displayed on the right panel with WT MITF (*Mitf*$^{+/+}$; X/X), mild intermediate phenotype of hemizygous (*Mitf*$^{K243R/K243R}$; Tyr::Cre/X) and full *Mitf*^{K243R} mutant phenotype (*Mitf*$^{K243R/K243R}$; Tyr::Cre/Tyr::Cre).

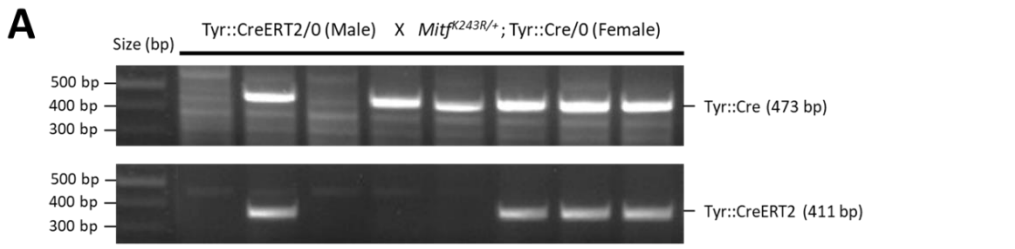

B

Gametes	X	Tyr::Cre
Theoritical ratio	50 %	50 %
Observed ratio	87 %	13 %

C

Gametes	+	Tyr::CreERT2
Theoritical ratio	50 %	50 %
Observed ratio	56 %	44 %

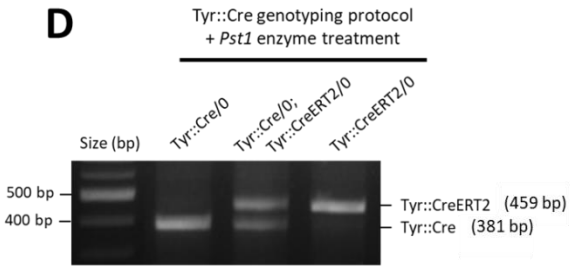

Figure 36. Genotyping strategy to separate Tyr::CreER^{T2} positive mice from Tyr::Cre. (A) Agarose gel with amplicons produced from PCR with Tyr::Cre (top gel, band at 473 bp) or Tyr::CreER^{T2} (bottom gel, band at 411 bp) primers as previously described respectively in Figures 4C and 8B. PCR genotyping was done on DNA extracted from resulting pups of the breeding shown in Figure 9C, between a WT *Mitf* male with the Tyr::CreER^{T2} driver and a MitfK243R/+ ; Tyr::Cre/0; Dct::LacZ female. To simplify, only the Tyr::Cre and Tyr::CreER^{T2} transgenes are shown. The first lane on the left is the ladder for the size of the amplicons. (B) Punnett square showing both theoretical and observed ratios of Tyr::Cre positive and negative mice. The number of mice used to compute this ratio is n=46. (C) Punnett square of both theoretical and observed ratios of positive and negative Tyr::CreER^{T2} mice. The number of mice used to compute this ratio is n=46. (D) Agarose gel of Tyr::Cre PCR that were also treated with the restriction enzyme Pst1. This gel shows the three possible outcomes which are Tyr::Cre (381 bp) or Tyr::CreER^{T2} (459 bp) alone, or both of them (one band at 381 and one at 459).

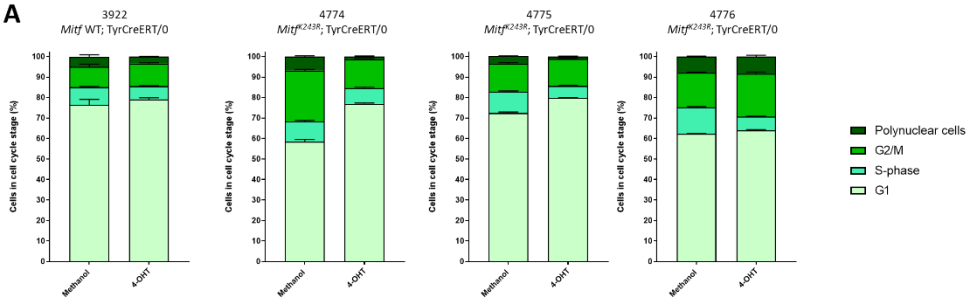

B

	G1	S-phase	G2/M	Polynuclear
3922	* 0.04	Ns 0.11	Ns 0.72	Ns 0.45
4774	**** <0.0001	** 0.001	**** <0.0001	**** <0.0001
4775	**** <0.0001	** 0.001	Ns 0.63	**** <0.0001
4776	*** 0.0008	**** <0.0001	**** <0.0001	Ns 0.59

Figure 37. Non-dying cells do not cycle normally. (A) Stacked charts of non-dying cells (cells from sub-G1 peak removed) in percentages for the WT MITF 3922 and the *Mitf*^{K243R} mutant cells 4774, 4775 and 4776. (B) Statistical significance for the difference of percentage of cells for each cell cycle phase treated with either methanol or 4-OHT in each cell line. Test performed is two-way ANOVA (P value < 0.0001), and multiple comparisons test is the Sidak's Multiple comparisons test with the values displayed in the table.

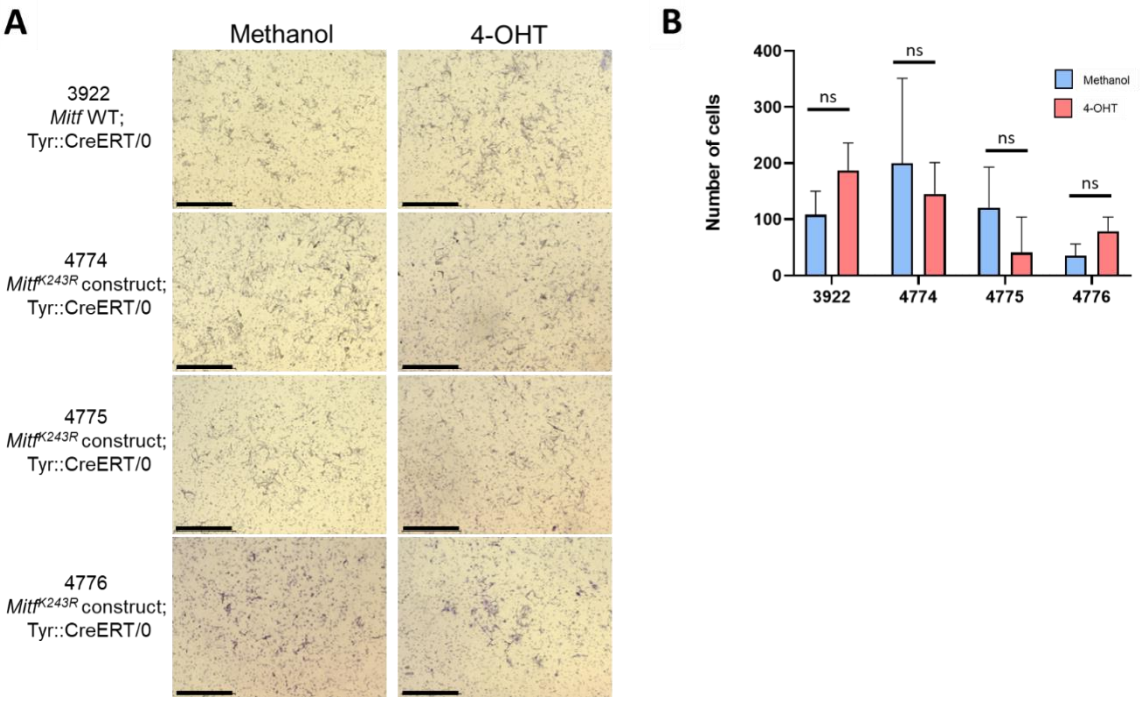

Figure 38. Transwell invasion assay. (A) Representative pictures of the cells that have invade through the Matrigel and stained with crystal violet, either treated with methanol (control) or 4-OHT on WT MITF cells (3922) or *Mitf*^{K243R} inducible cell lines (4774, 4775 and 4776). Pictures were taken on the EVOS imaging system after 48h of treatment and subsequent stainign steps. Scale bar represents 100 µm. (B) Barplot displaying the quantification of the number of stained cells that have invade the Matrigel.

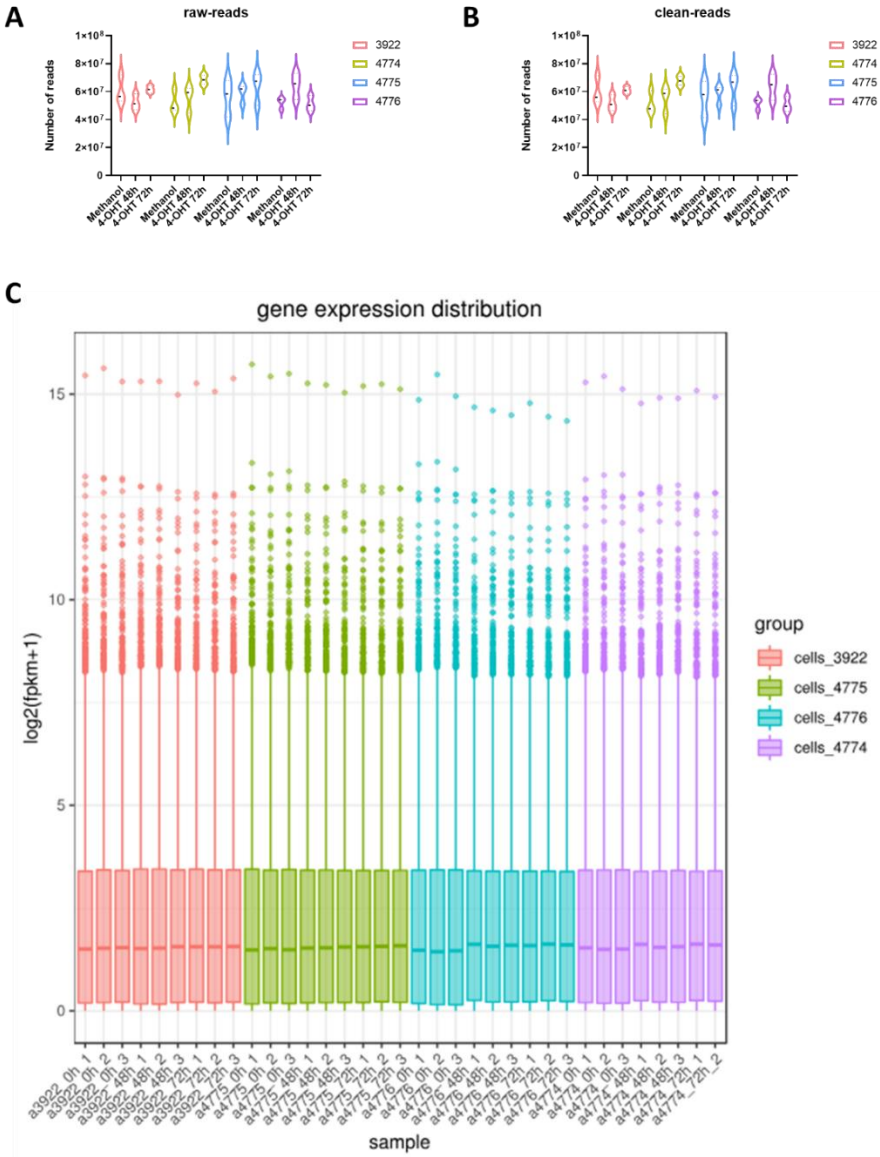

Figure 39. Quality control for the RNA sequencing. (A) Library size for each cell line after 0H (no treatment), 48H or 72h (4-OHT treatment). Raw-reads numbers are displayed in millions. (B) Numbers of reads after cleaning with Trimmomatic. All the raw-reads were 99.97% clean, with the remaining 0.03% removed. (C) Gene expression distribution before analysis. The expression for each sample is expressed in Log2(FPKM+1).